The classified or limited status of this document applies to each page thereof unless otherwise marked. Separate page printouts MUST be marked accordingly.

MSFC MPR-___-FE-70-1

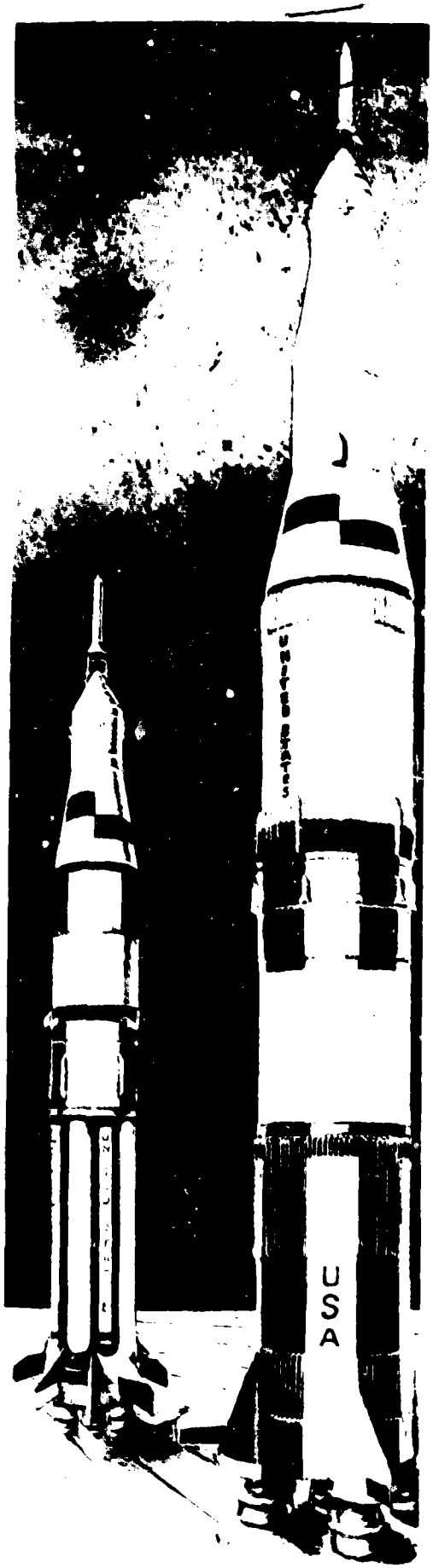

GEORGE C. MARSHALL SPACE FLIGHT CENTER

SATURN

MPR-SAT-FE-70-1

JANUARY 30, 1970

SATURN V LAUNCH VEHICLE FLIGHT EVALUATION REPORT AS-507 APOLLO 12 MISSION

PREPARED BY
SATURN FLIGHT EVALUATION WORKING GROUP

NASA

31

GEORGE C. MARSHALL SPACE FLIGHT CENTER

MPR-SAT-FE-70-1

SATURN V LAUNCH VEHICLE
FLIGHT EVALUATION REPORT - AS-507
APOLLO 12 MISSION

PREPARED BY

SATURN FLIGHT EVALUATION WORKING GROUP

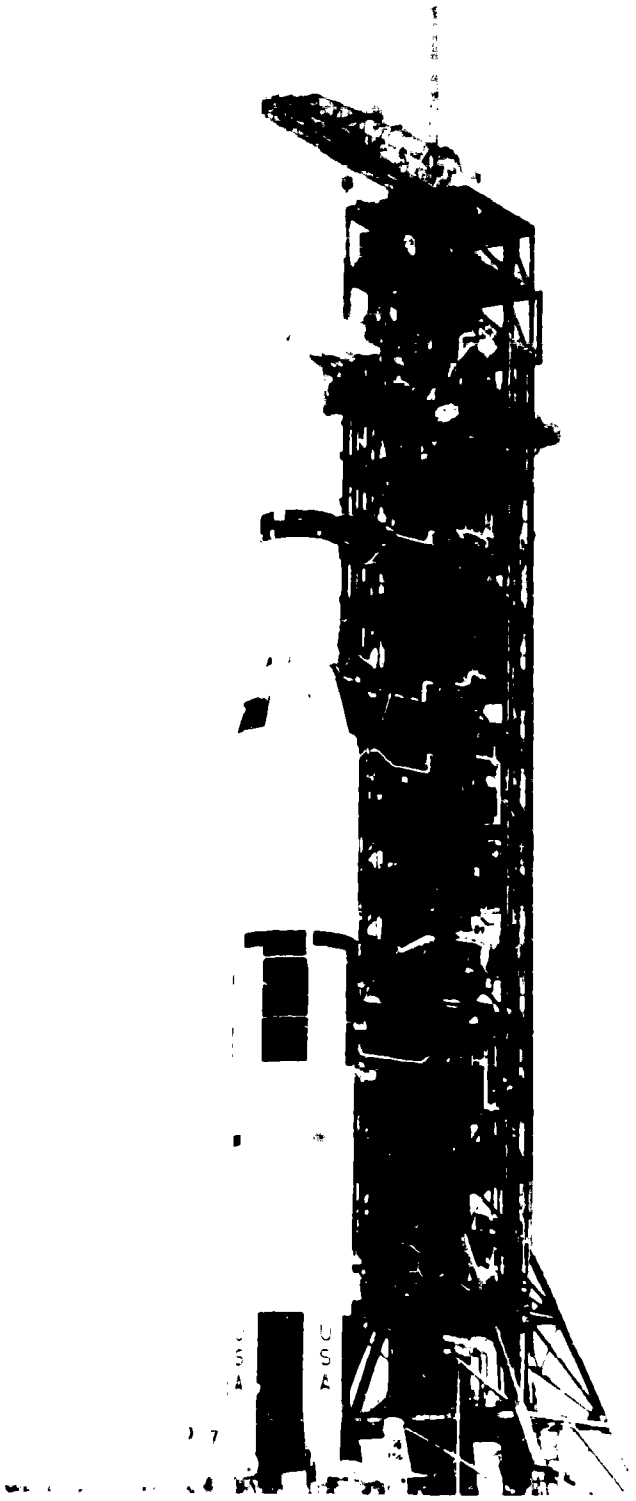

AS-507 LAUNCH VEHICLE

MPR-SAT-FE-70-1

SATURN V LAUNCH VEHICLE FLIGHT EVALUATION REPORT - AS-507

APOLLO 12 MISSION

BY

Saturn Flight Evaluation Working Group
George C. Marshall Space Flight Center

ABSTRACT

Saturn V AS-507 (Apollo 12 Mission) was launched at 11:22:00.00 Eastern Standard Time on November 14, 1969, from Kennedy Space Center, Complex 39, Pad A. The vehicle lifted off on schedule on a launch azimuth of 90 degrees east of north and rolled to a flight azimuth of 72.029 degrees east of north. The launch vehicle successfully placed the manned spacecraft in the planned translunar injection coast mode.

The Mandatory and Desirable Objectives of this mission were accomplished with the exception of inserting the S-IVB/IU into a slingshot trajectory on the first pass of the moon. No failures, anomalies, or deviations occurred that seriously affected the flight or mission.

Any questions or comments pertaining to the information contained in this report are invited and should be directed to:

Director, George C. Marshall Space Flight Center
Huntsville, Alabama 35812
Attention: Chairman, Saturn Flight Evaluation Working Group, S&E-CSE-LF (Phone 453-2575)

TABLE OF CONTENTS

TABLE OF CONTENTS (CONTINUED)

TABLE OF CONTENTS (CONTINUED)

TABLE OF CONTENTS (CONTINUED)

TABLE OF CONTENTS (CONTINUED)

TABLE OF CONTENTS (CONTINUED)

TABLE OF CONTENTS (CONTINUED)

LIST OF ILLUSTRATIONS

LIST OF ILLUSTRATIONS (CONTINUED)

LIST OF ILLUSTRATIONS (CONTINUED)

LIST OF ILLUSTRATIONS (CONTINUED)

LIST OF ILLUSTRATIONS (CONTINUED)

LIST OF ILLUSTRATIONS (CONTINUED)

LIST OF TABLES

LIST OF TABLES (CONTINUED)

LIST OF TABLES (CONTINUED)

LIST OF TABLES (CONTINUED)

ACKNOWLEDGEMENT

This report is published by the Saturn Flight Evaluation Working Group--composed of representatives of Marshall Space Flight Center, John F. Kennedy Space Center, and MSFC's prime contractors--and in cooperation with the Manned Spacecraft Center. Significant contributions to the evaluation have been made by:

George C. Marshall Space Flight Center

Science and Engineering

Central Systems Engineering
Aero-Astrodynamics Laboratory
Astrionics Laboratory
Computation Laboratory
Astronautics Laboratory

Program Management

John F. Kennedy Space Center

Manned Spacecraft Center

The Boeing Company

McDonnell Douglas Astronautics Company

International Business Machines Corporation

North American Rockwell/Space Division

North American Rockwell/Rocketdyne Division

ABBREVIATIONS

AOS	Acquisition of Signal
APS	Auxi Propulsion System
ARIA	Apollo Range Instrument Aircraft
ASI	Augmented Spark Igniter
AVP	Address Verification Pulse
BDA	Bermuda
CCS	Command and Communications System
CDDT	Countdown Demonstration Test
CECO	Center Engine Cutoff
CG	Center of Gravity
CM	Command Module
CNV	Cape Kennedy
CRO	Carnarvon
CRP	Computer Reset Pulse
CSM	Command and Service Module
CVS	Continuous Vent System
CYI	Grand Canary Island
DEE	Digital Events Evaluator
DO	Desirable Objective
DTS	Data Transmission System
EBW	Exploding Bridge Wire
ECO	Engine Cutoff
ECS	Environmental Control System
EDS	Emergency Detection System
EMR	Engine Mixture Ratio
EPO	Earth Parking Orbit
ESC	Engine Start Command
EST	Eastern Standard Time
ETW	Error Time Word
EVA	Extra-Vehicular Activity
FCC	Flight Control Computer
FM/FM	Frequency Modulation/ Frequency Modulation
FRT	Flight Readiness Test
GBS	Gas Bearing System
GFCV	GOX Flow Control Valve
GDSX	Goldstone Wing Station
GG	Gas Generator
GOX	Gaseous Oxygen
G	Guidance Reference Release
GSE	Ground Support Equipment
GSCU	Ground Support Cooling Unit
GTK	Grand Turk Island
GYM	Guaymas
HAW	Hawaii
HDA	Holddown Arm
HFCV	Helium Flow Control Valve
HSK	Honeysuckle (Canberra)
IGM	Iterative Guidance Mode

ABBREVIATIONS (CONTINUED)

IMU	Inertial Measurement Unit
IU	Instrument Unit
KSC	Kennedy Space Center
LET	Launch Escape Tower
LH_2	Liquid Hydrogen
LM	Lunar Module
LOI	Lunar Orbit Insertion
LOS	Loss of Signal
LOX	Liquid Oxygen
LV	Launch Vehicle
LVDA	Launch Vehicle Data Adapter
LVDC	Launch Vehicle Digital Computer
LVGSE	Launch Vehicle Ground Support Equipment
MCC-H	Mission Control Center - Houston
MILA	Merritt Island Launch Area
ML	Mobile Launcher
MMH	Monomethyl Hydrazine
MO	Mandatory Objective
MOV	Main Oxidizer Valve
MR	Mixture Ratio
MSC	Manned Spacecraft Center
MSFC	Marshall Space Flight Center
MSFN	Manned Space Flight Network
MSS	Mobile Service Structure
MTF	Mississippi Test Facility
M/W	Methanol Water
NPSP	Net Positive Suction Pressure
NPV	Nonpropulsive Vent
NASA	National Aeronautics and Space Administration
OAT	Overall Test
OCP	Orbital Correction Program
OECO	Outboard Engine Cutoff
OMNI	Omni Directional
OMPT	Operational Mass Point Trajectory
OT	Operational Trajectory
PAFB	Patrick Air Force Base
PCM	Pulse Code Modulation
PCM/FM	Pulse Code Modulation/ Frequency Modulation
POI	Parking Orbit Insertion
PMR	Programed Mixture Ratio
PRA	Patrick Reference Atmosphere
PTCS	Propellant Tanking Control System
PU	Propellant Utilization
RF	Radio Frequency
RFI	Radiofrequency Interference
RMS	Root Mean Square
RP-1	Designation for S-IC Stage Fuel (kerosene)
SA	Service Arm
SC	Spacecraft
SLA	Spacecraft/LM Adapter
SM	Service Module
SPS	Service Propulsion System
SRSCS	Secure Range Safety Command System
SS/FM	Single Sideband/Frequency Modulation

ABBREVIATIONS (CONTINUED)

STDV	Start Tank Discharge Valve
SV	Space Vehicle
T_1	Time Base 1
TCS	Thermal Conditioning System
TD&E	Transposition, Docking and Ejection
TEI	Transearth Injection
TEX	Corpus Christi (Texas)
TLI	Translunar Injection
TM	Telemeter, Telemetry
TMR	Triple Modular Redundant
TSM	Tail Service Mast
TVC	Thrust Vector Control
UCR	Unsatisfactory Condition Report
USB	Unified S-Band
UT	Universal Time
VAN	Vanguard (ship)
VHF	Very High Frequency

MISSION PLAN

The AS-507 flight (Apollo 12 Mission) is the seventh flight of the Apollo/Saturn V flight test program. The primary objective of the mission is to land astronauts on the lunar surface and return them safely to earth. The crew consists of Charles Conrad, Jr. (Mission Commander), Richard Gordon, Jr. (Command Module Pilot), and Alan Bean (Lunar Module Pilot).

The AS-507 flight vehicle is composed of the S-IC-7, S-II-7, and S-IVB-7N stages; Instrument Unit (IU)-7; Spacecraft/Lunar Module Adapter (SLA)-15; and Spacecraft (SC). The SC consists of Command and Service Module (CSM) -108 and Lunar Module (LM)-6.

Vehicle launch from Complex 39A at Kennedy Space Center (KSC) is along a 90 degree azimuth with a roll to a variable flight azimuth of 72 to 96 degrees measured east of true north. Vehicle mass at S-IC ignition is 6,484,620 lbm. The S-IC stage powered flight is approximately 162 seconds; the S-II stage provides powered flight for approximately 387 seconds. Following S-IVB first burn (approximately 135 seconds duration), the S-IVB/IU/SLA/LM/CSM is inserted into a circular 100 n mi altitude (referenced to the earth equatorial radius) Earth Parking Orbit (EPO). Vehicle mass at orbit insertion is 300,003 lbm.

At approximately 10 seconds after EPO insertion, the vehicle is aligned with the local horizontal. Continuous hydrogen venting is initiated shortly after EPO insertion and the Launch Vehicle (LV) and CSM systems are checked in preparation for the Translunar Injection (TLI) burn. During the second or third revolution in EPO, the S-IVB stage is reignited and burns for approximately 345 seconds. This burn injects the S-IVB/IU/SLA/LM/CSM into a free-return, translunar trajectory.

Approximately 15 minutes after TLI, the vehicle initiates an inertial attitude hold for CSM separation, docking and LM ejection. Following the attitude freeze, the CSM separates from the LV and the SLA panels are jettisoned. The CSM then transposes and docks to the LM. After docking, the CSM/LM is ejected from the S-IVB/IU. Following CSM/LM ejection, the S-IVB/IU configuration achieves a co-rotational slingshot trajectory by using propulsive venting of liquid hydrogen (LH_2), dumping of liquid oxygen (LOX) and by firing the Auxiliary Propulsion System (APS) ullage engines. The slingshot trajectory results in a solar orbit for the S-IVB/IU.

During the 3 day translunar coast, the astronauts perform star-earth landmark sightings, Inertial Measurement Unit (IMU) alignments, general lunar navigation procedures and possibly four midcourse corrections. One of these corrections will maneuver the SC into a hybrid trajectory approximately 28 hours after TLI. At approximately 83 hours and 25 minutes, a Service Propulsion System (SPS) burn (Lunar Orbit Insertion [LOI]) of approximately 342 seconds inserts the CSM/LM into a 60 by 170 n mi altitude parking orbit.

Approximately two revolutions after LOI, a 17.6-second SPS burn will adjust the orbit into a 54 by 66 n mi altitude. The LM is entered by astronauts Conrad and Bean and checkout is accomplished. During the thirteenth revolution in orbit at 108 hours, the LM separates from the CSM and prepares for the lunar descent. The LM descent propulsion system is used to brake the LM into the proper landing trajectory and maneuver the LM during descent to the lunar surface.

Following lunar landing, two 3.5 hour Extra-Vehicular Activity (EVA) time periods are scheduled during which the astronauts will explore the lunar surface, examine the LM exterior, investigate in the vicinity of the Surveyor III spacecraft, and deploy scientific instruments. The total stay time on the lunar surface is open-ended, with a planned maximum of 32 hours, depending upon the outcome of current lunar surface operations planning and of real-time operational decisions. After the EVA, the astronauts prepare the ascent propulsion system for lunar ascent.

The CSM performs a plane change approximately 19 hours before lunar ascent. At approximately 142 hours and 8 minutes, the ascent stage inserts the LM into a 9 by 45 n mi altitude lunar orbit, and rendezvous and docks with the CSM. The astronauts reenter the CSM, jettison the LM, photograph possible lunar exploration sites, and prepare for Transearth Injection (TEI). TEI is accomplished at approximately 172 hours and 23 minutes with a 129-second SPS burn. The time and duration of the SPS TEI burn is dependent upon an optional astronaut rest period.

During the 72-hour transearth coast, the astronauts perform navigation procedures, star-earth-moon sightings and possibly three midcourse corrections. The Service Module (SM) separates from the Command Module (CM) 15 minutes before reentry. Splashdown occurs in the Pacific Ocean approximately 244 hours and 35 minutes after liftoff.

After the recovery operations, a biological quarantine is imposed on the crew and CM. An incubation period of 18 days from splashdown (21 days from lunar ascent) is required for the astronauts. The hardware incubation period is the time required to analyze certain lunar samples.

FLIGHT SUMMARY

The fifth manned Saturn V Apollo space vehicle, AS-507 (Apollo 12 Mission) was launched at 11:22:00 Eastern Standard Time (EST) on November 14, 1969 from Kennedy Space Center (KSC), Complex 39, Pad A. This seventh launch of the Saturn V/Apollo successfully performed all the mandatory and desirable objectives required for successful accomplishment of the primary mission objective which basically was to perform an ALSEP lunar landing mission. The only objective not accomplished, insertion of S-IVB/IU into a solar orbit, fundamentally had no effect on the mission.

The launch countdown support systems performed well. However, several systems experienced component failures and malfunctions that required corrective action, but all repairs were accomplished in time to maintain the launch schedule. Damage to the pad, mobile launcher, and support equipment was minor.

The trajectory parameters of AS-507 from launch to Translunar Injection (TLI) were close to nominal. The vehicle was launched on an azimuth 90 degrees east of north. A roll maneuver was initiated at 12.8 seconds that placed the vehicle on a flight azimuth of 72.029 degrees east of north. The space-fixed velocity at S-IC Outboard Engine Cutoff (OECO) was 10.4 m/s (34.1 ft/s) less than nominal. The space-fixed velocity at S-II OECO was 17.3 m/s (56.8 ft/s) less than nominal. The space-fixed velocity at parking orbit insertion was 0.5 m/s (1.7 ft/s) less than nominal. The apogee was 0.2 kilometer (0.1 n mi) greater than nominal, and the perigee was 4.0 kilometers (2.2 n mi) less than nominal. The parameters at TLI were also close to nominal. The space-fixed velocity was 1.6 m/s (5.2 ft/s) less than nominal, the altitude was 1.6 kilometers (0.9 n mi) less than nominal and C_3 was 60,828 m^2/s^2 (654,747 ft^2/s^2) less than nominal. Following Lunar Module (LM) ejection, the vehicle attempted a slingshot maneuver. The S-IVB/IU closest approach of 5707 kilometers (3082 n mi) above the lunar surface did not provide sufficient energy to escape the earth-moon system. The failure to achieve slingshot was due to the application of an excessively long ullage engine burn which was calculated using the telemetered state vector rather than the vector obtained from tracking. Even though the slingshot maneuver was not achieved, the fundamental objectives of not impacting the spacecraft, the earth or the moon were achieved.

All S-IC propulsion systems performed satisfactorily and the propulsion performance level was very close to the predicted level. Stage site thrust (averaged from liftoff to OECO) was 0.55 percent higher than predicted. Total propellant consumption rate was 0.26 percent higher than predicted

with the total consumed Mixture Ratio (MR) 0.34 percent higher than predicted. Specific impulse was 0.20 percent higher than predicted. Center Engine Cutoff (CECO) was commanded by the IU as planned. OECO, initiated by the LOX low level sensors, occurred 0.74 second earlier than predicted.

The S-II propulsion system performed satisfactorily throughout the flight. The S-II stage operation time was 2.1 seconds longer than predicted. Total stage thrust at 61 seconds after S-II Engine Start Command (ESC) was 0.05 percent below predicted. Total propellant flowrate (including pressurization flow) was equal to the predicted and vehicle specific impulse was 0.05 percent below predicted at this time slice. Stage propellant MR was 0.36 percent above predicted. Low frequency low amplitude oscillations were observed on all engines during S-II boost prior to CECO; however, net engine performance levels were not affected.

The J-2 engine operated satisfactorily throughout the operational phase of S-IVB first and second burns with normal engine shutdowns. S-IVB first burn duration was 2.5 seconds longer than predicted. The engine performance during first burn, as determined from standard altitude reconstruction analysis, deviated from the predicted by +0.40 percent for thrust while the specific impulse was equal to the predicted. The Continuous Vent System (CVS) adequately regulated LH_2 tank ullage pressure during orbit, and the Oxygen/Hydrogen (O_2/H_2) burner satisfactorily achieved LH_2 and LOX tank repressurization for restart. However, the O_2/H_2 burner shutdown did not occur at the programed time due to an intermittent electrical "open" circuit. This delay in shutdown resulted in a suspected burnthrough in the O_2/H_2 burner. Engine restart conditions were within specified limits. The restart at full open Propellant Utilization (PU) valve position was successful. S-IVB second burn duration was 3.8 seconds less than predicted. The engine performance during second burn, as determined from the standard altitude reconstruction analysis, deviated from the predicted by 0.76 percent for thrust and 0.05 percent for specific impulse. Subsequent to second burn, the stage propellant tanks were safed satisfactorily, with sufficient impulse being derived from the LOX dump to impart 32.8 ft/s to stage velocity.

The S-IC, S-II, and S-IVB stage hydraulic systems performed satisfactorily. During this period all parameters were within specification limits, although the return fluid temperature of one S-IC actuator rose unexpectedly at 100 seconds.

The structural loads experienced during the S-IC boost phase were well below design values. The maximum high Q region bending moment was 37 x 10^6 lbf-in. at the S-IC LOX tank which was less than 20 percent of design value. Low level oscillations, similar to those of previous flights, were evident during each stage burn but caused no problems. The S-II stage experienced four periods of 16-hertz oscillations during S-II mainstage prior to CECO. Oscillations in the chamber pressure, LOX sump pressure, and LOX inlet pressure occurred at the same frequency as the structural vibrations. The loading resulting from these oscillations, however, caused no structural failure or degradation.

The guidance and navigation system performed satisfactorily. The parking orbit and TLI parameters were within the 3-sigma tolerance. The S-IVB/IU did not achieve heliocentric orbit due to the computed time for the APS ullage burn. This burntime computation was based on the telemetered state vector which was within the 3-sigma limit but exceeded the allowable limits for accomplishing slingshot. The state vector was in error due to a rather large space-fixed component velocity difference observed prior to the S-IVB stage second burn, which was enlarged through the second active guidance period. The LVDC, the Launch Vehicle Data Adapter (LVDA), and the ST-124M-3 inertial platform functioned satisfactorily.

The AS-507 Flight Control Computer (FCC), Thrust Vector Control (TVC) and APS satisfied all requirements for vehicle attitude control during the flight. All maneuvers were properly accomplished. All separations occurred as expected without producing significant attitude deviations.

The AS-507 launch vehicle electrical systems and Emergency Detection System (EDS) performed satisfactorily throughout all phases of flight except during S-IVB restart preparations. During this time the S-IVB stage electrical systems did not respond properly to burner LOX shutdown valve "CLOSE" and telemetry calibrate "ON" commands from the S-IVB switch selector. Both of the command failures were isolated to intermittent conditions in a bus module (404A3A29) or the associated mating connector (404A3W1P29) located in the S-IVB sequencer. Operation of the batteries, power supplies, inverters, Exploding Bridge Wire (EBW) firing units and switch selectors was normal.

Apollo 12 was the first Saturn vehicle launched in rainy weather. Shortly after 36.5 seconds into the flight, there were numerous space vehicle indications of a massive electrical disturbance, followed by a second disturbance at 52 seconds. The astronauts reported that, in their opinion, the vehicle had been hit by lightning. Camera data, telemetered data, and Launch Vehicle Data Adapter/Launch Vehicle Digital Computer (LVDA/LVDC) bit errors showed that the vehicle had been struck by lightning at 36.5 seconds. Virtually no discernible effects were noted on the launch vehicle during the 52-second disturbance. Atmospheric electrical factors and the fact that the vehicle does not have the capacitance to store sufficient energy to produce the effects noted indicate that the lightning discharge at 36.5 seconds was triggered by the vehicle. The 52-second disturbance may have been due to a lesser lightning discharge. The launch vehicle hardware and software suffered no significant effects; therefore, the mission proceeded as scheduled. There is no evidence of vehicle pyrotechnics being endangered, due to built-in protection in the circuitry. Some modification to present launch mission rules will be required to preclude launching of the vehicle when the probability of triggered lightning discharges is deemed unacceptable.

Vehicle base pressure environments were generally in good agreement with previous flight data. Base thermal environments, in general, were similar to those experienced on earlier flights.

The Environmental Control System (ECS) performed satisfactorily. There was evidence of direct incidence solar heating near IU panel 20, through the open end of the IU, after spacecraft separation. Components located in this area, cooled by the Thermal Conditioning System (TCS), showed an increase in temperature without any performance degradation through 40,000 seconds. During this period of solar heating, the gas bearing differential pressure decreased below the expected lower limit because of temperature effects of the Gas Bearing Supply (GBS) system GN_2 pressure regulator. The performance of the ST-124M-3 platform was not affected by this decrease in pressure.

All elements of the data system performed satisfactorily throughout flight except for problems with the Command and Communication System (CCS) uplink signal and omni downlink antenna system during translunar coast. Measurement performance was excellent as evidenced by 99.9 percent reliability. This reliability is the same as AS-506 when the highest reliability for any Saturn V flight was attained.

Telemetry performance was nominal. Very High Frequency (VHF) telemetry Radio Frequency (RF) propagation was generally good, though the usual problems due to flame effects and staging were experienced. VHF data were received to 25,260 seconds (07:01:00). Command systems RF performance for both the Secure Range Safety Command System (SRSCS) and CCS was nominal except for the CCS problems noted. Goldstone Wing Station (GDSX) received CCS signals to 46,070 seconds (12:47:50). Good tracking data were received from the C-Band radar, with Merritt Island Launch Area (MILA) indicating final LOS at 43,560 seconds (12:06:00). The 71 ground engineering cameras provided good data during the launch.

Evaluation of the launch vehicle data revealed no failures, five anomalies and eight deviations. These anomalies and deviations are summarized in the following tables.

Table 1. Summary of Anomalies

ITEM	ANOMALY IDENTIFICATION						RECOMMENDED CORRECTIVE ACTION			PARAGRAPH REFERENCE
	VEHICLE SYSTEM	DESCRIPTION (CAUSE)	EFFECT ON MISSION	MISSION CRITICALITY	EFFECT ON NEXT MISSION	OCCURRENCE (RANGE TIME SECONDS)	DESCRIPTION	ACTION STATUS	VEHICLE EFFECTIVITY	
1	Vehicle	Vehicle struck by triggered lightning at 36.5 seconds.	None	1	Probable change in mission rule	36.5	MSFC launch mission rule recommendation complete. Final decision to be taken by joint MSC, KSC, MSFC, & MSF action.	Closed	AS-508 and Subs	12A
2	S-II Low Frequency Oscillations	S-II stage experienced four periods of 16 hertz oscillations during S-II mainstage. (Inherent characteristic of the present configuration of the S-II stage.)	None	3	None anticipated. Similar oscillations are expected, but the vehicle can withstand 3 times the oscillations experienced on AS-507.	180 to 285 225 to 267 268 to 351 405 to 463	Decision made to "Fly-as-is" on AS-508. ECP 6683 approved to install accumulator on S-II-12 and static fire. Test will provide accumulator verification and thus assist in determining whether to fly accumulator on AS-509 and subs.	Closed. ECP 6683 Approved	AS-508 and Subs	6.3 9.2.3.1
3	S-IVB O_2/H_2 Burner	The O_2/H_2 burner LOX shutdown valve failed to close when the IU issued a closed signal at 9965.7 seconds. (Suspect intermittent "open" in an electrical harness or pin connector. Bendix P/N SO288E-22-5SS, Bus Module MDAC P/N 1057771.)	None	3	None	9965.7	All critical connectors to be inspected and unsatisfactory connectors to be repaired as required.	Closed	AS-508 and Subs	12.4, 7.6
4	TU/RF System	Command and Communications System (CCS) signal dropped out at 19,105.5 seconds while operating on the omni antenna. (Suspect high temperature in area of omni antenna coaxial cables; possibly caused by exposure to sunlight after spacecraft/LM separation.)	None	3	Extended operation of this system is required to achieve an AS-508 mission objective of lunar impact of S-IVB/IU	19,105.5	Thermal shrouds to protect all IU components being fabricated.	Closed.	AS-508 and Subs	16.4.4
5	S-IVB/IU Trajectory	S-IVB/IU did not achieve a heliocentric orbit. (Error in TLI IU state vector.)	None	3	None. Appropriate dependence on tracking data to determine S-IVB/IU state vector was established for AS-508 and subsequent lunar impact missions.		None. Experience acquired during Apollo 12 mission to be considered by MSC/MSFC Lunar Impact Working Group to assure maximum effectiveness in conducting Lunar Impact Maneuver.	Closed	AS-508 and Subs	4.3.5 10.2.1

Table 2. Summary of Deviations

ITEM	VEHICLE SYSTEM	DEVIATION	PROBABLE CAUSE	SIGNIFICANCE	PARAGRAPH REFERENCE
1	S-IC Propulsion	S-IC engine start sequence deviated from planned sequence.	Unexpected slow starting time of engine No. 4.	Under investigation. A 1-2-2 start was implemented to minimize liftoff dynamics. AS-507 liftoff dynamics were somewhat higher than on previous flights, but well within design limits.	5.2 9.2.1 9.2.2
2	S-IC Propulsion	LOX suction duct pressure decay of engine No. 5 after Center Engine Cutoff (CECO).	Leakage through the turbo-pump LOX primary seal.	This was observed on the previous four Saturn V flights. Analytical studies have now indicated the pressure drop is due to leakage through the seal and is a normal occurrence. Therefore, this pressure drop will be expected as a normal occurrence on future flights.	5.6.2
3	S-IC Hydraulics	Unexpected servoactuator hydraulic return temperature sudden increase (18°F)	Although analysis shows that loss of line insulation would not account for this much temperature rise, it should be noted that the time period does coincide with the time of maximum gas temperatures in the base region.	None. Caused no problems and temperature was well within allowable limits.	8.2
4	S-IVB Propulsion	Sudden drop in S-IVB fuel tank ullage pressure during S-IC/S-II separation.	Propellant slosh and smaller ullage volume.	None. The drop was larger than seen on previous flights, but is not considered to be a problem.	7.10.1
5	S-IVB Propulsion	S-IVB fuel tank ullage pressure lower than expected after first burn Engine Cutoff (ECO).	Unknown.	Probably none. The pressure was maintained at an average level of 19.0 psia which is slightly lower than previous flight data. This deviation is not considered to be a problem, although it may have had some influence on failure of the S-IVB/IU to slingshot.	7.5, 10.2.1
6	S-IVB Propulsion	S-IVB LOX tank ullage pressure decay during orbital coast.	Factors under investigation include heat transfer through the common bulkhead, composition of ullage gas, effects of stage maneuvers, and leakage of ullage gas.	Probably none. Since LOX tank repressurization was well within design capabilities this pressure decay was not considered a problem (even if second opportunity restart had been required). This pressure decay was larger than seen on previous flights.	7.10.2
7	IU/LVDC	Error Monitor Register indication. Error Monitor Register bit 15 was set at 17,888 seconds and cleared at 22,936 seconds. Bit 1 was set at 21,229 seconds and remained on.	Open circuit in one of the triple redundant signal paths probably caused bits 1 and 15 to be set.	Still under investigation.	10.4.1
8	IU/LVDC	Improper servo test constant in the flight program.	Requirement error.	None. A Minor Loop Error word was telemetered at 36.6 and 18,023.6 seconds indicating an unexpected zero reading in the Y (pitch) fine gimbal angle and the Z (yaw) gimbal angle, respectively.	10.3

SECTION 1

INTRODUCTION

1.1 PURPOSE

This report provides the National Aeronautics and Space Administration (NASA) Headquarters, and other interested agencies, with the launch vehicle evaluation results of the AS-507 flight. The basic objective of flight evaluation is to acquire, reduce, analyze, evaluate and report on flight data to the extent required to assure future mission success and vehicle reliability. To accomplish this objective, actual flight failures, anomalies and deviations must be identified, their causes accurately determined, and complete information made available so that corrective action can be accomplished within the established flight schedule.

1.2 SCOPE

The contents of this report are centered on the performance evaluation of the major launch vehicle systems, with special emphasis or the failures, anomalies and deviations. Summaries of launch operations and spacecraft performance are included for completeness.

The official George C. Marshall Space Flight Center (MSFC) position at this time is represented by this report. It will not be followed by a similar report unless continued analysis or new information should prove the conclusions presented herein to be significantly incorrect. Reports covering major subjects and special subjects will be published as required.

SECTION 2

EVENT TIMES

2.1 SUMMARY OF EVENTS

Range zero time, the basic time reference for this report, is 11:22:00 Eastern Standard Time (EST) (16:22:00 Universal Time [UT]). Range time is calculated as the elapsed time from range zero time and, unless otherwise noted, is the time used throughout this report. The actual and predicted range times are adjusted to ground telemetry received times. The Time-From-Base times are presented as vehicle times. Figure 2-1 shows the time delay of ground telemetry received time versus Launch Vehicle Digital Computer (LVDC) time. The difference between ground and vehicle time is a function of the LVDC clock speed and telemetry transmission distance and indicates the magnitude and sign of corrections applied to correlate range time and vehicle time in Tables 2-1, 2-2 and 2-3.

Guidance Reference Release (GRR) occurred at -16.97 seconds and start of Time Base 1 (T_1) occurred at 0.68 second. GRR was established by the Digital Events Evaluator (DEE-6) and T_1 was initiated at detection of liftoff signal provided by de-energizing the liftoff relay in the Instrument Unit (IU) at IU umbilical disconnect.

Range times for each time base used in the flight sequence program and the signal for initiating each time base are presented in Table 2-1. Start of T_2 was within nominal expectations for this event. Start of T_3 was 0.7 second early. T_4 and T_5 were initiated approximately 1.4 and 4.0 seconds later than predicted, respectively, due to variations in the stage burn times. These variations are discussed in Sections 5, 6 and 7 of this document. Start of T_6, which was initiated by the LVDC upon solving the restart equation, was 2.5 seconds later than predicted. Start of T_7 was 1.1 seconds earlier than predicted. T_8, which was initiated by the receipt of a ground command, was started 115.2 seconds later than the predicted time.

A summary of significant events for AS-507 is given in Table 2-2. Since not all events listed in Table 2-2 are IU commanded switch selector functions, deviations are not to be construed as failures to meet specified switch selector tolerances. The events in Table 2-2 associated with guidance, navigation, and control have been identified as being accurate to within a major computation cycle.

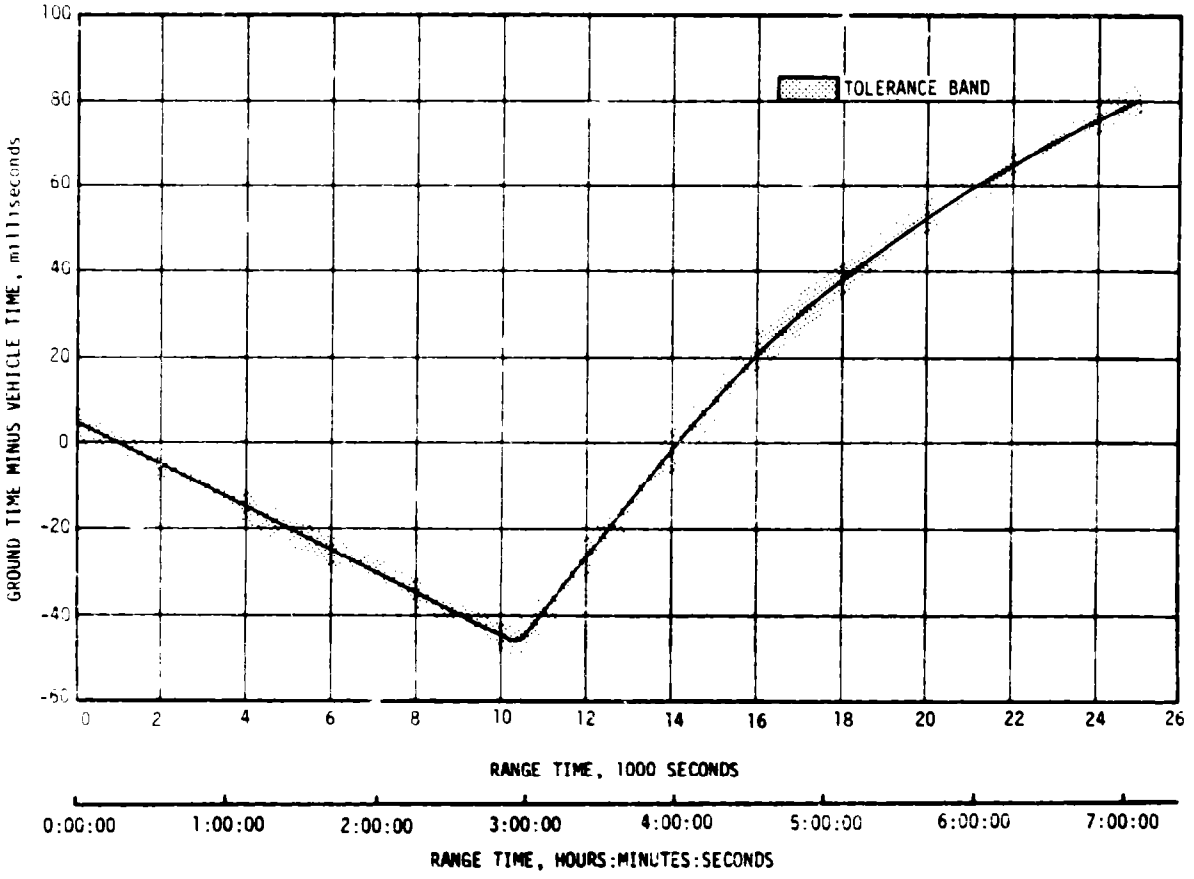

Figure 2-1. Telemetry Time Delay

The predicted times for establishing actual minus predicted times in Table 2-2 have been taken from 40M33627B, "Interface Control Document Definition of Saturn SA-507 Flight Sequence Program", and from the "AS-507 H-1 Mission Launch Vehicle Operational Flight Trajectory", dated August 12, 1969.

2.2 VARIABLE TIME AND COMMANDED SWITCH SELECTOR EVENTS

Table 2-3 lists the switch selector events which were issued during the flight but were not programed for specific times. The water coolant valve open and close switch selector commands were issued based on the condition of two thermal switches in the Environmental Control System (ECS). The outputs of these switches were sampled once every 300 seconds, beginning at 180 seconds, and a switch selector command was issued to open or close the water valve. The valve was open if the sensed temperature was too high and the valve was closed if the temperature was too low.

Table 2-1. Time Base Summary

TIME BASE	RANGE TIME SEC (HR:MIN:SEC)	SIGNAL START
T_0	-16.97	Guidance Reference Release
T_1	0.68	IU Umbilical Disconnect Sensed by LVDC
T_2	135.38	S-IC CECO Sensed by LVDC
T_3	161.79	S-IC OECO Sensed by LVDC
T_4	552.36	S-II OECO Sensed by LVDC
T_5	694.12	S-IVB ECO (Velocity) Sensed by LVDC
T_6	9464.48 (2:37:44.48)	Restart Equation Solution
T_7	10,384.12 (2:53:04.12)	S-IVB ECO (Velocity) Sensed by LVDC
T_8	16,000.25 (4:26:40.25)	Enabled by Ground Command

Table 2-3 also contains the special sequence of switch selector events which were programed to be initiated by telemetry station acquisition and included the following calibration sequence:

Function	Stage	Time (Sec)
Telemetry Calibrator In-Flight Calibrate ON	IU	Acquisition +60.0
TM Calibrate ON	S-IVB	Acquisition +60.4
TM Calibrate OFF	S-IVB	Acquisition +61.4
Telemetry Calibrator In-Flight Calibrate OFF	IU	Acquisition +65.0

Table 2-2. Significant Event Times Summary

EVENT	RANGE TIME		TIME FROM BASE	
	ACTUAL SEC	ACT-PRED SEC	ACTUAL SEC	ACT-PRED SEC
1. Guidance Reference Release (GRR)	-17.0	0.0	-17.6	0.1
2. S-IC Engine Start Sequence Command (Ground)	-8.9	0.0	-9.6	0.0
3. S-IC Engine No. 1 Start	-6.2	0.0	-6.9	0.0
4. S-IC Engine No. 2 Start	-5.9	0.0	-6.6	0.0
5. S-IC Engine No. 3 Start	-6.1	0.0	-6.7	0.0
6. S-IC Engine No. 4 Start	-6.0	0.0	-6.6	0.0
7. S-IC Engine No. 5 Start	-6.5	0.0	-7.2	0.0
8. All S-IC Engines Thrust OK	-1.4	0.1	-2.1	0.1
9. Range Zero	0.0	-	-0.7	-
10. All Holddown Arms Released (First Motion)	0.25	0.00	-0.42	-0.02
11. IU Umbilical Disconnect, Start of Time Base 1 (T_1)	0.7	0.0	0.0	0.0
12. Begin Tower Clearance Yaw Maneuver*	2.4	0.7	1.8	0.2
13. End Yaw Maneuver*	10.2	0.5	9.6	0.2
14. Begin Pitch and Roll Maneuver*	12.8	0.3	12.2	0.2
15. S-IC Outboard Engine Cant	20.6	-0.1	20.0	0.0
16. End Roll Maneuver*	32.3	1.2	31.7	0.4
17. Mach 1	66.1	-1.0	65.4	-1.1

*Time is accurate to major computation cycle dependent upon length of computation cycles.

Table 2-2. Significant Event Times Summary (Continued)

EVENT	RANGE TIME		TIME FROM BASE	
	ACTUAL SEC	ACT-PRED SEC	ACTUAL SEC	ACT-PRED SEC
18. Maximum Dynamic Pressure (Max Q)	81.1	-2.7	80.4	-2.7
19. S-IC Center Engine Cutoff (CECO)	135.24	-0.03	134.57	-0.05
20. Start of Time Base 2 (T_2)	135.4	0.1	0.0	0.0
21. End Pitch Maneuver (Tilt Arrest)*	158.1	0.2	22.7	0.0
22. S-IC Outboard Engine Cutoff (OECO)	161.74	-0.74	26.36	-0.82
23. Start of Time Base 3 (T_3)	161.8	-0.7	0.0	0.0
24. Start S-II LH_2 Tank High Pressure Vent Mode	161.9	-0.7	0.1	0.0
25. S-II LH_2 Recirculation Pumps Off	162.0	-0.7	0.2	0.0
26. S-II Ullage Motor Ignition	162.2	-0.8	0.5	0.0
27. S-IC/S-II Separation Command to Fire Separation Devices and Retro Motors	162.4	-0.8	0.7	0.0
28. S-II Engine Start Command (ESC)	163.1	-0.8	1.4	0.0
29. S-II Engine Solenoid Activation (Average of Five)	163.2	-0.7	1.4	0.0
30. S-II Ullage Motor Burn Time Termination (Thrust Reaches 75 Percent)	166.4	-0.7	4.6	0.0
31. S-II Mainstage	166.4	-0.5	4.6	0.2

*Time is accurate to major computation cycle dependent upon length of computation cycles.

Table 2-2. Significant Event Times Summary (Continued)

EVENT	RANGE TIME		TIME FROM BASE	
	ACTUAL SEC	ACT-PRED SEC	ACTUAL SEC	ACT-PRED SEC
32. S-II Chilldown Valves Close	168.1	-0.8	6.4	0.0
33. Activate S-II PU System	168.7	-0.7	6.9	0.0
34. S-II Second Plane Separation Command (Jettison S-II Aft Interstage)	192.4	-0.8	30.7	0.0
35. Launch Escape Tower (LET) Jettison	197.9	-0.8	36.1	-0.1
36. Iterative Guidance Mode (IGM) Phase 1 Initiated*	202.5	-0.8	40.7	-0.1
37. S-II LOX Step Pressurization	261.7	-0.8	100.0	0.0
38. S-II Center Engine Cutoff (CECO)	460.75	-0.74	298.96	-0.04
39. S-II LH_2 Step Pressurization	461.7	-0.8	300.0	0.0
40. Guidance Sensed Time to Begin EMR Shift (IGM Phase 2 Initiated and Start of Artificial Tau Mode)*	487.3	0.5	325.5	1.2
41. S-II Low Engine Mixture Ratio (EMR) Shift (Actual)	490.0	0.6	328.2	1.3
42. End of Artificial Tau Mode*	498.7	1.4	336.9	2.1
43. S-II Outboard Engine Cutoff (OECO)	552.34	1.36	390.54	2.04

*Time is accurate to major computation cycle dependent upon length of computation cycles.

Table 2-2. Significant Event Times Summary (Continued)

EVENT	RANGE TIME		TIME FROM BASE	
	ACTUAL SEC	ACT-PRED SEC	ACTUAL SEC	ACT-PRED SEC
44. S-II Engine Cutoff Interrupt, Start of Time Base 4 (T_4) (Start of IGM Phase 3)	552.4	1.4	0.0	0.0
45. S-IVB Ullage Motor Ignition	553.1	1.3	0.8	0.0
46. S-II/S-IVB Separation Command to Fire Separation Devices and Retro Motors	553.2	1.3	0.9	0.0
47. S-IVB Engine Start Command (First ESC)	553.3	1.3	1.0	0.0
48. Fuel Chilldown Pump Off	554.5	1.3	2.2	0.0
49. S-IVB Ignition (STDV Open)	556.6	1.6	4.3	0.2
50. S-IVB Mainstage	559.1	1.6	6.7	0.2
51. Start of Artificial Tau Mode*	559.5	1.0	7.2	-0.3
52. S-IVB Ullage Case Jettison	565.1	1.3	12.8	0.0
53. End of Artificial Tau Mode*	568.8	1.5	16.4	0.1
54. Begin Terminal Guidance*	660.4	3.9	108.0	2.5
55. End IGM Phase 3*	685.9	2.5	133.6	1.2
56. Begin Chi Freeze*	685.9	2.5	133.6	1.2
57. S-IVB Velocity Cutoff Command (First Guidance Cutoff) (First ECO)	693.91	4.05	-0.21	-0.01

*Time is accurate to major computation cycle dependent upon length of computation cycles.

Table 2-2. Significa it Event Times Summary (Continued)

EVENT	RANGE TIME		TIME FROM BASE	
	ACTUAL SEC	ACT-PRED SEC	ACTUAL SEC	ACT-PRED SEC
58. S-IVB Engine Cutoff Interrupt, Start of Time Base 5 (T_5)	694.1	4.0	0.0	0.0
59. S-IVB APS Ullage Engine No. 1 Ignition Command	694.4	4.0	0.3	0.0
60. S-IVB APS Ullage Engine No. 2 Ignition Command	694.5	4.0	0.4	0.0
61. LOX Tank Pressurization Off	695.3	4.0	1.2	0.0
62. Parking Orbit Insertion	703.9	4.0	9.8	0.0
63. Begin Maneuver to Local Horizontal Attitude*	714.2	3.7	20.1	-0.3
64. S-IVB LH_2 Continuous Vent System (CVS) On	753.1	4.0	59.0	0.0
65. S-IVB APS Ullage Engine No. 1 Cutoff Command	781.1	4.0	87.0	0.0
66. S-IVB APS Ullage Engine No. 2 Cutoff Command	781.2	4.0	87.1	0.0
67. Begin Orbital Navigation*	795.1	4.6	101.0	0.6
68. Begin S-IVB Restart Preparations, Start of Time Base 6 (T_6)	9464.5	2.5	0.0	0.0
69. S-IVB PU Mixture Ratio 4.5 On	9914.5	2.4	450.1	0.0
70. S-IVB APS Ullage Engine No. 1 Ignition Command	9960.7	2.4	496.3	0.0

*Time is accurate to major computation cycle dependent upon length of computation cycles.

Table 2-2. Significant Event Times Summary (Continued)

EVENT	RANGE TIME		TIME FROM BASE	
	ACTUAL SEC	ACT-PRED SEC	ACTUAL SEC	ACT-PRED SEC
71. S-IVB APS Ullage Engine No. 2 Ignition Command	9960.8	2.4	496.4	0.0
72. S-IVB O_2/H_2 Burner Off (Helium Heater Off)	9961.2	2.4	496.8	0.0
73. S-IVB O_2/H_2 Burner LOX Off	9965.7	2.4	501.3	0.0
74. S-IVB LH_2 Chill-down Pump Off	10,033.8	2.4	569.4	0.0
75. S-IVB LOX Chill-down Pump Off	10,034.0	2.4	569.6	0.0
76. S-IVB Engine Restart Command (Fuel Lead Initiation) (Second ESC)	10,035.1	3.1	570.6	0.0
77. S-IVB APS Ullage Engine No. 1 Cutoff Command	10,037.4	2.4	573.0	0.0
78. S-IVB APS Ullage Engine No. 2 Cutoff Command	10,037.5	2.4	573.1	0.0
79. S-IVB Second Ignition (STDV Open)	10,042.7	2.7	578.2	0.2
80. S-IVB Mainstage	10,045.2	2.7	580.7	0.2
81. Engine Mixture Ratio (EMR) Shift	10,144.9	2.4	680.5	1.3
82. S-IVB LH_2 Step Pressurization (Second Burn Relay Off)	10,314.4	2.4	850.0	0.0
83. Begin Terminal Guidance*	10,354.3	-1.7	889.8	-4.2
84. Begin Chi Freeze*	10,381.8	-1.1	917.3	-3.6

*Time is accurate to major computation cycle dependent upon length of computation cycles.

Table 2-2. Significant Event Times Summary (Continued)

EVENT	RANGE TIME		TIME FROM BASE	
	ACTUAL SEC	ACT-PRED SEC	ACTUAL SEC	ACT-PRED SEC
85. S-IVB Second Guidance Cutoff Command (Second ECO)	10,383.89	-1.12	-0.20	0.0
86. S-IVB Engine Cut-off Interrupt, Start of Time Base 7 (T_7)	10,384.1	-1.1	0.0	0.0
87. LH_2 Vent On Command	10,384.6	-1.1	0.5	0.0
88. Translunar Injection	10,393.9	-1.1	9.8	0.0
89. Begin Maneuver to Local Horizontal Attitude*	10,404.4	-1.7	20.3	-0.6
90. Begin Orbital Navigation*	10,404.4	-2.7	20.3	-1.6
91. LH_2 Vent Off Command	11,283.9	-1.1	899.8	0.0
92. Begin Maneuver to Transposition and Docking Attitude (TD&E)*	11,285.0	-2.1	900.9	-1.0
93. CSM Separation	11,884.9	-0.3	1500.8	1.1
94. CSM Dock	12,413.3	114.3	2029.1	115.4
95. SC/LV Final Separation	15,180.9	16.9	4796.7	18.0
96. Start of Time Base 8 (T_8)	16,000.2	115.2	0.0	0.0
97. S-IVB LH2 Vent On (CVS On)	16,580.4	115.2	580.2	0.0
98. Initiate Maneuver to Slingshot Attitude*	16,581.0	116.0	580.7	0.7

*Time is accurate to major computation cycle dependent upon length of computation cycles.

Table 2-2. Significant Event Times Summary (Continued)

EVENT	RANGE TIME		TIME FROM BASE	
	ACTUAL SEC	ACT-PRED SEC	ACTUAL SEC	ACT-PRED SEC
99. Begin LOX Dump	17,280.2	115.2	1280.0	0.0
100. End LOX Dump	17,338.2	115.2	1338.0	0.0
101. H_2 Nonpropulsive Vent (NPV) On	17,407.2	115.2	1407.0	0.0
102. S-IVB APS Ullage Engine No. 1 Cutoff Command	19,700.2	115.2	3700.0	0.0
103. S-IVB APS Ullage Engine No. 2 Cutoff Command	19,700.4	115.2	3700.2	0.0
104. Initiate Maneuver to Communications Attitude	20,197.0	112.0	4196.8	-3.2

Table 2-3. Variable Time and Commanded Switch Selector Events

FUNCTION	STAGE	RANGE TIME (SEC)	TIME FROM BASE (SEC)	REMARKS
High (5.5) Engine Mixture Ratio Off	S-II	487.9	T_3 +326.1	
Low (4.5) Engine Mixture Ratio On	S-II	488.1	T_3 +326.3	
Water Coolant Valve Closed	IU	781.4	T_5 +87.3	LVDC Function
Telemetry Calibrator Inflight Calibrate On	IU	1063.3	T_5 +369.1	CYI Rev 1
TM Calibrate On	S-IVB	1063.7	T_5 +369.5	CYI Rev 1
TM Calibrate Off	S-IVB	1064.7	T_5 +370.5	CYI Rev 1
Telemetry Calibrator Inflight Calibrate Off	IU	1068.3	T_5 +374.1	CYI Rev 1
Telemetry Calibrator Inflight Calibrate On	IU	5367.2	T_5 +4673.1	GYM Rev 1
TM Calibrate On	S-IVB	5367.6	T_5 +4673.5	GYM Rev 1
TM Calibrate Off	S-IVB	5368.6	T_5 +4674.5	GYM Rev 1
Telemetry Calibrator Inflight Calibrate Off	IU	5372.2	T_5 +4678.1	GYM Rev 1
Water Coolant Valve Open	IU	6479.7	T_5 +5785.6	LVDC Function
Telemetry Calibrator Inflight Calibrate On	IU	6679.2	T_5 +5985.1	CYI Rev 2
TM Calibrate On	S-IVB	6679.6	T_5 +5985.5	CYI Rev 2
TM Calibrate Off	S-IVB	6680.6	T_5 +5986.5	CYI Rev 2
Telemetry Calibrator Inflight Calibrate Off	IU	6684.2	T_5 +5990.1	CYI Rev 2
Water Coolant Valve Off	IU	6779.8	T_5 +6085.7	LVDC Function
Telemetry Calibrator Inflight Calibrate On	IU	8791.1	T_5 +8097.1	CRO Rev 2
TM Calibrate On	S-IVB	8791.6	T_5 +8097.5	CRO Rev 2
TM Calibrate Off	S-IVB	8792.6	T_5 +8098.5	CRO Rev 2
Telemetry Calibrator Inflight Calibrate Off	IU	8796.1	T_5 +8102.1	CRO Rev 2
Telemetry Calibrator Inflight Calibrate On	IU	9864.6	T_6 +400.1	ARIA Rev 2

Table 2-3. Variable Time and Commanded Switch Selector Events (Continued)

FUNCTION	STAGE	RANGE TIME (SEC)	TIME FROM BASE (SEC)	REMARKS
TM Calibrate On	S-IVB	9864.8	T_6 +400.3	ARIA Rev 2
TM Calibrate Off	S-IVB	9865.8	T_6 +401.3	ARIA Rev 2
Telemetry Calibrator Inflight Calibrate Off	IU	9869.6	T_6 +405.1	ARIA Rev 2
Telemetry Calibrator Inflight Calibrate On	IU	10,472.4	T_7 +88.3	Acquisition by Hawaii TLI
TM Calibrate On	S-IVB	10,472.8	T_7 +88.7	Acquisition by Hawaii TLI
TM Calibrate Off	S-IVB	10,473.8	T_7 +89.7	Acquisition by Hawaii TLI
Telemetry Calibrator Inflight Calibrate Off	IU	10,477.4	T_7 +93.3	Acquisition by Hawaii TLI
Burner LOX Shutdown Valve Close On	S-IVB	10,554.2	T_7 +170.1	CCS Command
Time Delay	S-IVB	10,555.5	T_7 +170.9	CCS Command
Burner LOX Shutdown Valve Close Off	S-IVB	10,555.9	T_7 +171.7	CCS Command
Water Coolant Valve Open	IU	14,580.6	T_7 +4196.4	LVDC Function
Water Coolant Valve Closed	IU	14,880.0	T_7 +4495.8	LVDC Function
Water Coolant Valve Open	IU	17,282.5	T_8 +1282.2	LVDC Function
Water Coolant Valve Closed	IU	17,580.6	T_8 +1580.3	LVDC Function
Water Coolant Valve Closed	IU	19,680.1	T_8 +3679.9	LVDC Function
S-IVB Ullage Engine No. 1 On	S-IVB	19,753.2	T_8 +3753.0	CCS Command
S-IVB Ullage Engine No. 1 Off	S-IVB	20,023.2	T_8 +4023.0	CCS Command
S-IVB Ullage Engine No. 2 Off	S-IVB	20,026.9	T_8 +4026.7	CCS Command
CCS Coax Switch Fail-Safe and High Gain Antenna	IU	21,157.0	T_8 +5156.8	CCS Command
Water Coolant Valve Open	IU	21,180.6	T_8 +5180.4	LVDC Function
Water Coolant Valve Open	IU	25,080.1	T_8 +9079.9	LVDC Function
Water Coolant Valve Closed	IU	25,380.7	T_8 +9380.4	LVDC Function
Water Coolant Valve Closed	IU	27,180.7	T_8 +11,180.4	LVDC Function
Water Coolant Valve Open	IU	29,980.7	T_8 +12,980.4	LVDC Function

SECTION 3

LAUNCH OPERATIONS

3.1 SUMMARY

The ground systems supporting the AS-507/Apollo 12 countdown and launch performed well. Several systems experienced component failures and malfunctions that required corrective actions, but all repairs were accomplished in time to maintain the launch schedule. A leak developed in a Command and Service Module (CSM) LH_2 tank during cryogenic loading, and the tank was replaced. An unscheduled hold of 6 hours was initiated at -17 hours to permit retanking cryogenics in the CSM. However, this delay time was recovered during the scheduled hold at -9 hours. Launch vehicle propellant loading was accomplished satisfactorily. Launch occurred at 11:22:00 Eastern Standard Time (EST), November 14, 1969, from Pad 39A of the Saturn Complex. Damage to the launch pad, Mobile Launcher (ML), and support equipment was minor.

3.2 PRELAUNCH MILESTONES

A chronological summary of events and preparations leading to the launch of AS-507/Apollo 12 is contained in Table 3-1.

3.3 COUNTDOWN EVENTS

The AS-507/Apollo 12 countdown started with spacecraft preparations at -98 hours on November 8, 1969, at 19:00:00 EST. The primary portion of the launch vehicle preparations was picked up at -28 hours on November 12, 1969, at 21:00:00 EST. Scheduled holds in the launch countdown sequence were 12 hours duration at -66 hours, 16 hours duration at -48 hours, 9 hours 22 minutes duration at -9 hours, and 1 hour duration at -3 hours 30 minutes. During spacecraft preparations on November 12, 1969, a leak developed in the CSM LH_2 tank No. 2 during cryogenic loading. The tank was drained and replaced using a tank from Apollo 13. An unscheduled hold was initiated at -17 hours (08:00:00 EST, November 13, 1969) for retanking cryogenics in the CSM. Loading was completed in 6 hours, and the count resumed at 14:00:00 EST. The scheduled hold at -9 hours was reduced by 6 hours, thereby averting a launch delay. Launch occurred on schedule at 11:22:00 EST, November 14, 1969, from Pad 39A of the Saturn Complex.

Table 3-1. AS-507/Apollo 12 Prelaunch Milestones

DATE	ACTIVITY OR EVENT
March 10, 1969	S-IVB-7N Stage Arrival
March 24, 1969	Lunar Module (LM)-6 Arrival
March 28, 1969	Command and Service Module (CSM)-108 Arrival
April 21, 1969	S-II-7 Stage Arrival
May 3, 1969	S-IC-7 Stage Arrival
May 5, 1969	Spacecraft/Lunar Module Adapter (SLA)-15 Arrival
May 7, 1969	S-IC Erection
May 8, 1969	Instrument Unit (IU)-7 Arrival
May 21, 1969	S-II Erection
May 22, 1969	S-IVB and IU Erections
June 7, 1969	CSM Altitude Test With Prime Crew
June 10, 1969	CSM Altitude Test With Backup Crew
June 12, 1969	Launch Vehicle (LV) Propellant Dispersion/ Malfunction Overall Test (OAT)
June 13, 1969	LM Altitude Test With Backup Crew
June 16, 1969	LM Altitude Test With Prime Crew
June 22, 1969	LM Landing Gear Installed
June 23, 1969	LM/SLA Mate
June 27, 1969	CSM/SLA Mate
July 1, 1969	Spacecraft (SC) Erection
August 17, 1969	Space Vehicle (SV) Electrical Mate
August 21, 1969	SV OAT No. 1 (Plugs In)
September 8, 1969	SV Transfer to Pad A
September 10, 1969	Mobile Service Structure (MSS) Transfer to Pad A
September 30, 1969	SV Flight Readiness Test (FRT) Completed
October 20, 1969	RP-1 Loading Completed
October 28, 1969	Countdown Demonstration Test (CDDT) Completed (Wet)
October 29, 1969	CDDT (Dry) Completed
November 8, 1969	SV Launch Countdown Started
November 14, 1969	SV Launch On Schedule

3.4 PROPELLANT LOADING

3.4.1 RP-1 Loading

The RP-1 system supported the launch countdown satisfactorily, and there were no major problems. The fill line cutoff valve in the Tail Service Mast (TSM) opened after liftoff and resulted in contamination of the RP-1 piping in the ML. Opening of the fill line cutoff valve indicates a loss of valve GN_2 control pressure. This incident has occurred on previous launches. The cause of the pressure loss is being investigated.

3.4.2 LOX Loading

The LOX system successfully supported the launch countdown. LOX loading was completed and all stage LOX replenish operations started at about -5 hours 24 minutes. During the LOX replenish operations at about -1 hour 22 minutes, the replenish pump magnetic clutch seized. Pump speed surged to motor speed (3600 RPM), and the LOX bypass control valve was driven full open. There was no evidence of system overpressure, and the relief valves did not open. The system was reverted and the backup pump chilled down. Replenish operations were restored at about -55 minutes without a hold or countdown delay.

In response to the LOX pump clutch failure, a manual clutch disengage command was issued from the firing room to remove current from the clutch field winding. The command was not received; however, the same command issued automatically as a part of the revert sequence was received. The problem was subsequently traced to a failed relay driver in the Pad A Data Transmission System (DTS).

3.4.3 LH_2 Loading

The LH_2 system supported the launch countdown satisfactorily. Vehicle LH_2 loading was completed and replenishment initiated at about -3 hours 50 minutes.

During vehicle LH_2 tank purge operations on November 7, 1969, the position switches on two LH_2 system valves (S-IVB auxiliary fill valve and storage area transfer line valve) became inoperative and were replaced. The position switch on the transfer line valve failed again and required replacement the day prior to launch.

3.4.4 Auxiliary Propulsion System Propellant Loading

Propellant loading of the S-IVB Auxiliary Propulsion System (APS) was accomplished satisfactorily. Total propellant mass in both modules at liftoff was 405 lbm of Nitrogen Tetroxide (N_2O_4) and 252 lbm of Monomethyl Hydrazine (MMH).

3.5 S-II INSULATION, PURGE AND LEAK DETECTION

The performance of the S-II stage insulation was satisfactory. All performance parameters remained within acceptable levels, and no redline limits were exceeded throughout launch preparations. No excessive hazardous gas concentrations were encountered. Operational television was used to inspect the insulation at various times during the countdown, and no significant helium leakage was detected. The total heat leak through the insulation to the LH_2 was well below specification limits.

At about -66 hours, an area of debonded insulative cork was discovered and repaired. Three relatively small bubbles in the sidewall insulation were observed on operational television prior to LOX loading. All were considered acceptable for flight. No subsequent changes in the insulation bubbles were observed.

The S-II-7 stage was the last stage to have helium purged insulation. The purge system was used in conjunction with the leak detection system for detecting hazardous gas concentrations within the insulation while diluting or removing the leaking gases.

3.6 GROUND SUPPORT EQUIPMENT (GSE)

3.6.1 Ground/Vehicle Interface

Performance of the ground service systems supporting all stages of the launch vehicle was satisfactory. Extension of the primary damper arm was interrupted at about -9 hours 30 minutes because of interference between the damping cylinder rod and the Q-ball cover retract cable. A strong southwest wind of 20 to 30 knots had blown the cable against the damper arm, and cover removal might have resulted if extension operations had been continued. A similar condition existed during damper arm retraction scheduled at -3 hours 38 minutes. In both instances, the cable sheath attached to the ML hammerhead crane had to be disassembled to obtain sufficient cable slack to allow free arm movement; however, this was accomplished with no countdown delays. The Q-ball retraction system functioned satisfactorily later.

The Holddown Arms (HDA) and inflight umbilical disconnects functioned within design limits at vehicle liftoff. The HDA's were released at 0.25 second (all released within an 8 millisecond period). The TSM retractions were normal. Service Arm (SA) total retract times to safe angles were within specifications.

Postlaunch inspection revealed that overall damage to the launch site (Pad A), ML, and support equipment from the blast and flame impingement was minor. A quench valve on SA No. 2 (Industrial Water System) failed to open after liftoff. There was no apparent damage to the arm as a result. The lack of damage was due primarily to favorable wind conditions and

spillover from quench valves above. A detailed discussion of the GSE will be contained in the Kennedy Space Center Apollo/Saturn V (AS-507) Ground Systems Evaluation Report.

3.6.2 MSFC Furnished Ground Support Equipment

Performance of the mechanical and electrical equipment supporting the launch operations was satisfactory. The Environmental Control System (ECS) was operated with the Instrument Unit (IU) temperature control system disabled (per MSFC direction); therefore, the water/methanol temperature was controlled by the Ground Support Cooling Units (GSCU). Blast damage to the equipment was normal. Minor GSE deviations encountered during countdown were as follows:

a. At approximately -16 hours 15 minutes, the S-IVB gas heat exchanger high-level sensor cycled randomly with no simulation applied (also cycled earlier in the countdown). The discrete was masked during LH_2 loading with filling of the heat exchanger controlled by manual override. At approximately -3 hours 40 minutes, the low-level sensor failed to drop out; the LH_2 fill valve was operated manually in response to gas outlet temperature changes.

b. Excessive noise was noticed in the ML power supply to the IU at about -15 hours. The system was transferred to the redundant power supply while the original power supply was replaced with a spare. Subsequent troubleshooting revealed the source of the noise to be a vibrating sheet metal side panel on the power supply mechanical assembly. The panel was repaired, and the original power supply retained on the ML through launch for use as a spare.

c. The rate gyro digital ramp generator No. 1 (ramp No. 2), which drives the Flight Control/EDS Rate Gyros, failed hardover at approximately -6 hours 51 minutes. As a result, all command gyros were driven momentarily to maximum precession. This condition suggested a malfunction of the driver amplifier in the ramp generator panel. The problem was corrected by procuring a previously calibrated driver amplifier from ML 3 for use in ML 2.

3.6.3 Camera Coverage

Upon review of the film coverage, the following conditions were observed:

a. The S-II stage forward umbilical cover did not secure upon SA withdrawal from the vehicle. This condition also occurred during the AS-506 launch.

b. The lightning discharge (2 bolts) that occurred at 36.5 seconds was observed on films from three cameras. One of these cameras was located on the ML access elevator; the other two were located about 1300 feet from the vehicle (launch pad sites No. 4 and No. 5).

SECTION 4

TRAJECTORY

4.1 SUMMARY

The trajectory parameters from launch to translunar injection were close to nominal. The vehicle was launched on an azimuth 90 degrees east of north. A roll maneuver was initiated at 12.8 seconds that placed the vehicle on a flight azimuth of 72.029 degrees east of north.

The space-fixed velocity at S-IC Outboard Engine Cutoff (OECO) was 10.4 m/s (34.1 ft/s) less than nominal. The space-fixed velocity at S-II OECO was 17.3 m/s (56.8 ft/s) less than nominal. The space-fixed velocity at S-IVB first guidance cutoff was 0.6 m/s (1.9 ft/s) less than nominal. The altitude at S-IVB first guidance cutoff was 0.5 kilometer (0.2 n mi) lower than nominal and the surface range was 18.1 kilometers (9.8 n mi) greater than nominal.

The space-fixed velocity at parking orbit insertion was 0.5 m/s (1.7 ft/s) less than nominal and the flight path angle was 0.014 degree less than nominal. The eccentricity was 0.00032 greater than nominal. The apogee was 0.2 kilometer (0.1 n mi) greater than nominal and the perigee was 4.0 kilometers (2.2 n mi) less than nominal.

The parameters at translunar injection were also close to nominal. The eccentricity was 0.00100 less than nominal, the inclination was 0.019 degree greater than nominal, the node was 0.033 degree lower than nominal, and C_3 was 60,828 m^2/s^2 (654,747 ft^2/s^2) less than nominal. The space-fixed velocity was 1.6 m/s (5.2 ft/s) less than nominal and the altitude was 1.6 kilometers (0.9 n mi) less than nominal.

Following Lunar Module (LM) ejection, the vehicle was maneuvered to an inertially fixed attitude as required for the evasive maneuver. The evasive maneuver was accomplished by an Auxiliary Propulsion System (APS) ullage burn, after which the vehicle was oriented to a slingshot attitude fixed relative to local horizontal. The slingshot maneuver velocity change was accomplished by a LOX dump, APS ullage burns, and LH_2 vent. The S-IVB/IU closest approach of 5707 kilometers (3082 n mi) above the lunar surface did not provide sufficient energy to escape the earth-moon system. The failure to achieve slingshot was due to the application of an excessively long ullage engine burn which was calculated using the telemetered state vector rather than the vector obtained from tracking. Although the slingshot maneuver was not achieved, the fundamental objectives of not impacting the spacecraft, the earth or the moon were achieved.

The actual impact locations for the spent S-IC and S-II stages were determined by a theoretical free-flight simulation. The surface range for the S-IC impact point was 1.2 kilometers (0.6 n mi) greater than nominal. The surface range for the S-II impact point was 26.7 kilometers (14.4 n mi) less than nominal.

4.2 TRACKING DATA UTILIZATION

4.2.1 Tracking During the Ascent Phase of Flight

Tracking data were used from five different C-Band tracking stations during the period from the time of first motion through parking orbit insertion.

The best estimate trajectory was established by using telemetered guidance velocities as generating parameters to fit the tracking data. Approximately 15 percent of the tracking data was eliminated due to inconsistencies. A comparison of the reconstructed ascent trajectory with the remaining tracking data yielded good agreement. The launch phase portion of the trajectory (liftoff to approximately 20 seconds) was established by constraining integrated telemetered guidance accelerometer data to the early phase of the best estimate trajectory.

4.2.2 Tracking During the Parking Orbit Phase of Flight

Orbital tracking was conducted by the NASA Manned Space Flight Network (MSFN). Three C-Band radar stations furnished five data passes for use in determining the parking orbit trajectory. There were also two passes of S-Band tracking data available which were not used due to the adequate coverage provided by the C-Band radar data.

The parking orbit trajectory was obtained by integrating corrected insertion conditions forward to the S-IVB second burn restart preparation event. The insertion conditions, as determined by the Orbital Correction Program (OCP), were obtained by a differential correction procedure which adjusted the estimated insertion conditions to fit the C-Band radar tracking data in accordance with the weights assigned to the data. The venting model utilized to fit the tracking data was derived from telemetered guidance velocity data from the ST-124M-3 guidance platform.

4.2.3 Tracking During the Injection Phase of Flight

C-Band radar data were obtained from Hawaii during the latter portion of the injection phase of flight.

The injection trajectory was established by utilizing telemetered guidance velocities as generating parameters to fit the Hawaii tracking data. These data were fit through a guidance error model, initialized from the S-IVB restart vector obtained from the orbital solution, and constrained to the Translunar Injection (TLI) vector obtained from the post TLI trajectory. Comparison of the injection trajectory with the tracking data yielded good agreement.

4.2.4 Tracking During the Post Injection Phase of Flight

Tracking data from three C-Band radar stations furnished data for use in determining the post TLI trajectory. The available S-Band tracking data were not used due to the availability of the C-Band radar data during the same time periods.

The post TLI trajectory was obtained by integrating corrected injection conditions forward to S-IVB/CSM separation. The corrected injection conditions were determined by the same method outlined in paragraph 4.2.2.

4.3 TRAJECTORY EVALUATION

4.3.1 Ascent Trajectory

Actual and nominal altitude, surface range, and cross range for the ascent phase are presented in Figure 4-1. Actual and nominal space-fixed velocity and flight path angle during ascent are shown in Figure 4-2. Comparisons of total inertial accelerations are shown in Figure 4-3. The maximum acceleration during S-IC burn was 3.91 g.

Mach number and dynamic pressure are shown in Figure 4-4. These parameters were calculated using meteorological data measured to an altitude of 54.8 kilometers (29.6 n mi). Above this altitude the measured data were merged into the U. S. Standard Reference Atmosphere.

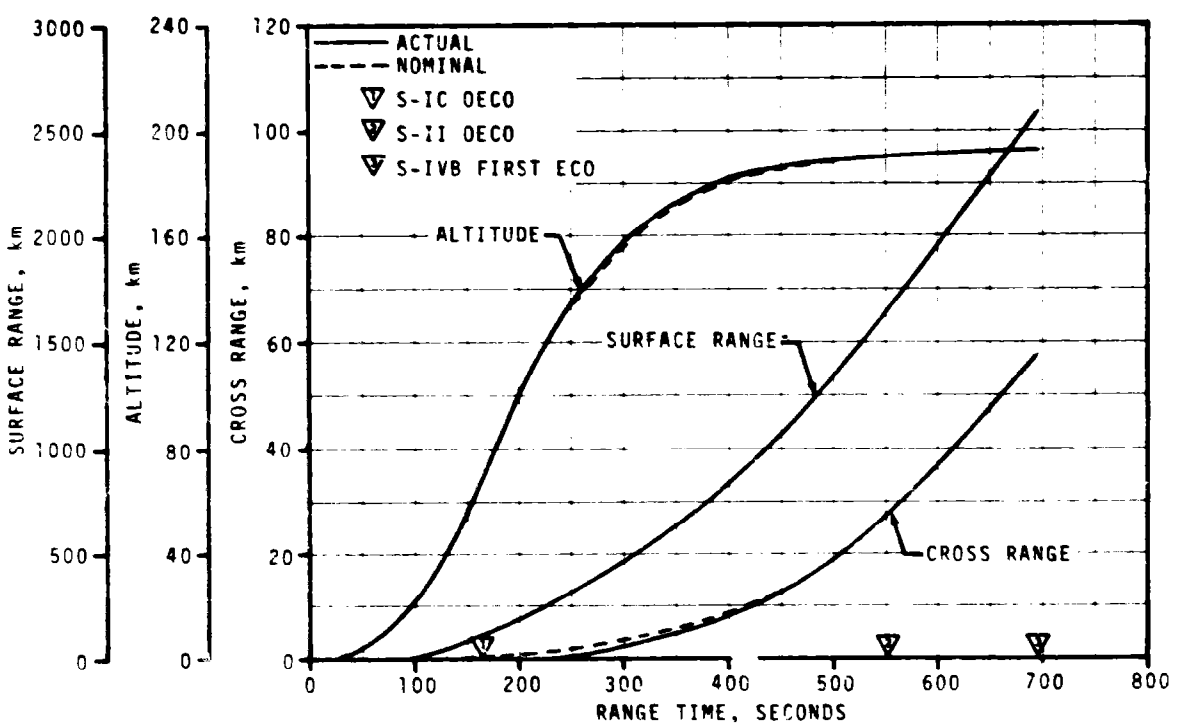

Figure 4-1. Ascent Trajectory Position Comparison

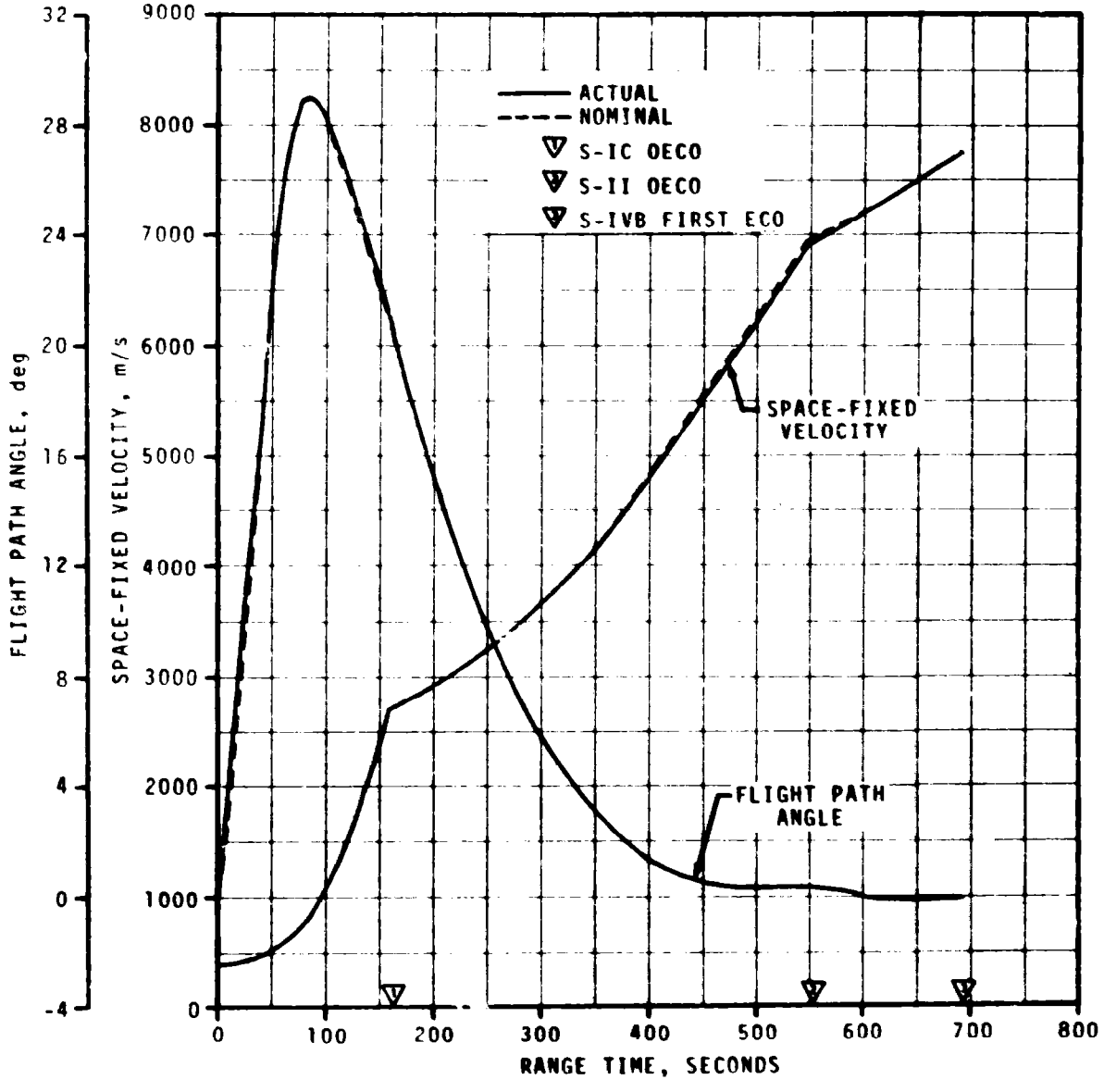

Figure 4-2. Ascent Trajectory Space-Fixed Velocity and Flight Path Angle Comparisons

Actual and nominal values of parameters at significant trajectory event times, cutoff events, and separation events are shown in Tables 4-1, 4-2, and 4-3, respectively.

The free-flight trajectories of the spent S-IC and S-II stages were simulated using initial conditions from the final postflight trajectory. The simulation was based upon the separation impulses for both stages and nominal tumbling drag coefficients. No tracking data were available for verification. Table 4-1 presents a comparison of free-flight parameters to nominal at apex for the S-IC and S-II stages. Table 4-4 presents a comparison of free-flight parameters to nominal at impact for the S-IC and S-II stages.

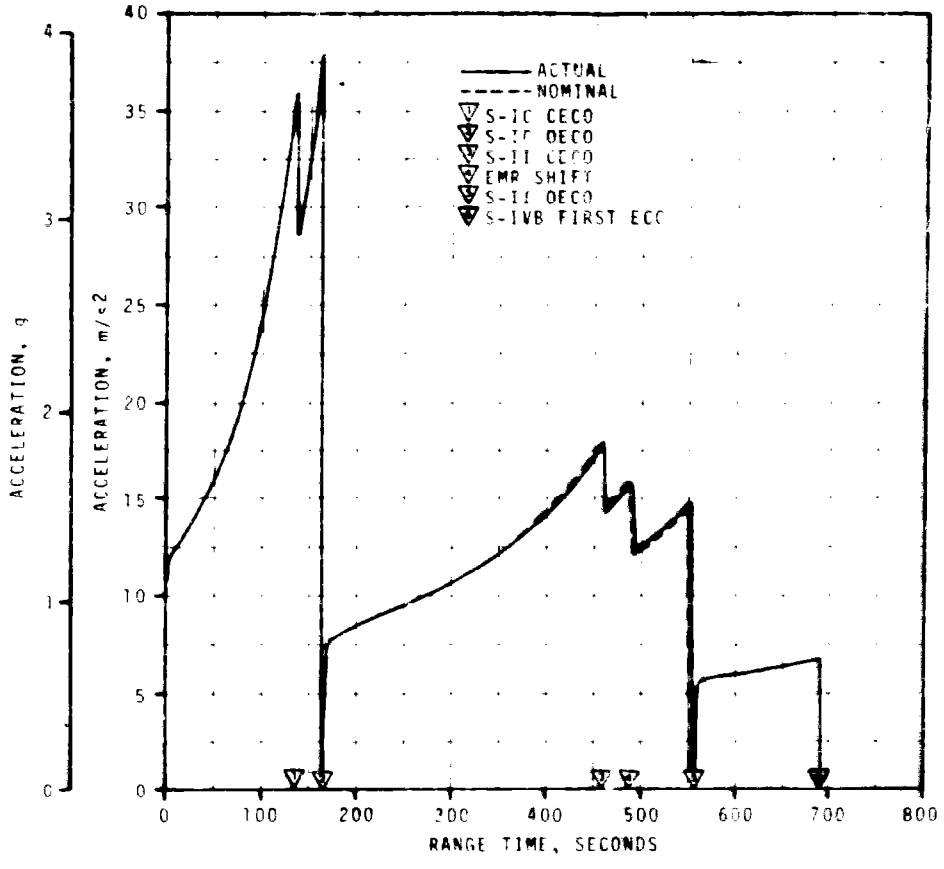

Figure 4-3. Ascent Trajectory Acceleration Comparison

4.3.2 Parking Orbit Trajectory

The actual and nominal parking orbit insertion parameters are presented in Table 4-5. The ground track from insertion to S-IVB/CSM separation is given in Figure 4-5.

4.3.3 Injection Trajectory

Comparisons between the actual and nominal space-fixed velocity and flight path angle are shown in Figure 4-6. The actual and nominal total inertial acceleration comparisons are presented in Figure 4-7. Throughout the S-IVB second burn phase of flight, the space-fixed velocity was close to nominal with deviations more noticeable towards the end of the time period. The trajectory and targeting parameters at S-IVB second guidance cutoff are presented in Table 4-2.

4.3.4 Post TLI Trajectory

The actual translunar injection conditions are compared with nominal in Table 4-6. A comparison of the actual and nominal S-IVB/CSM separation conditions is presented in Table 4-3.

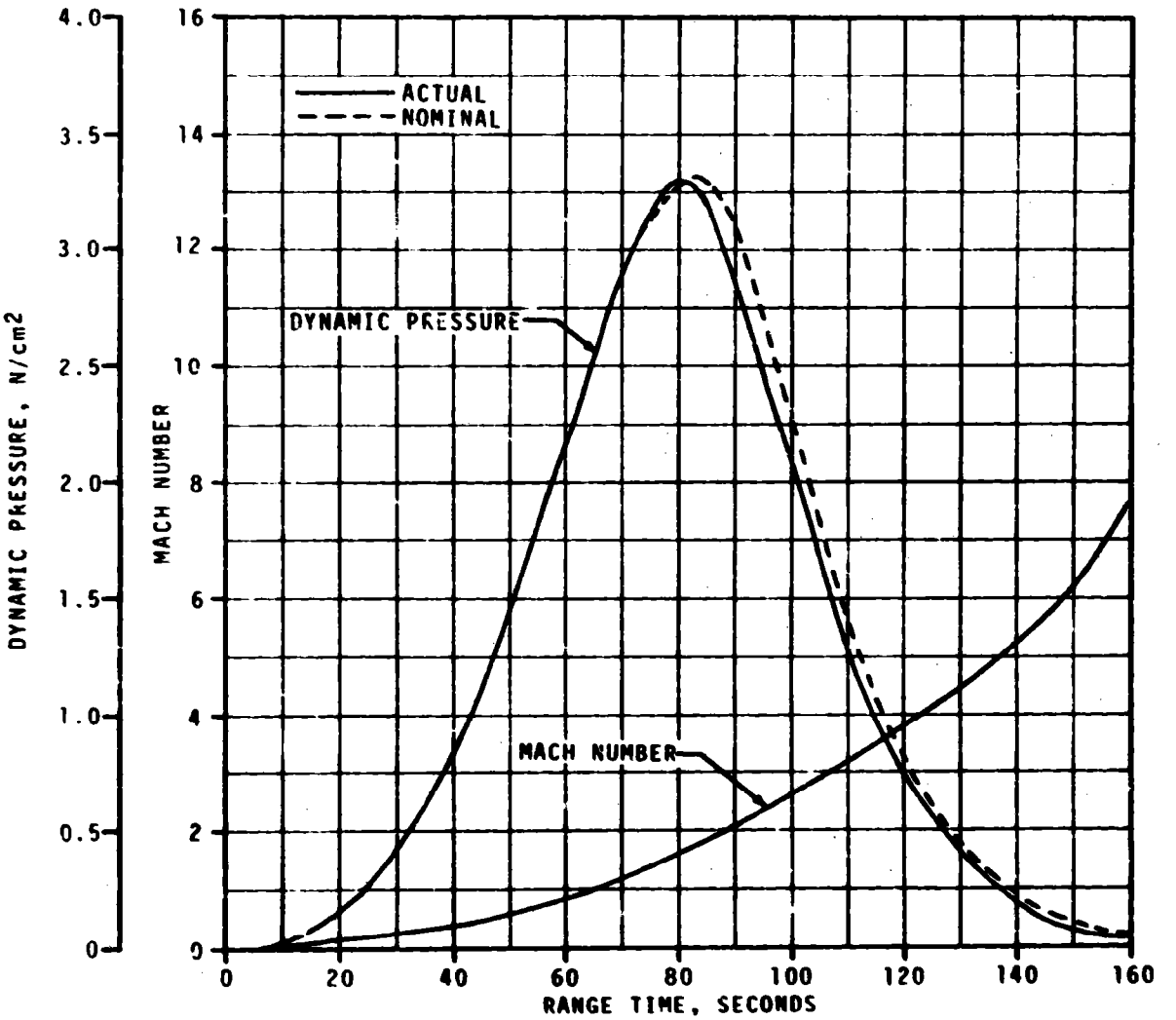

Figure 4-4. Dynamic Pressure and Mach Number Comparisons

4.3.5 S-IVB/IU Post Separation Trajectory

A time history of the actual and nominal (real-time predicted) velocity increase along the vehicle longitudinal axis for the evasive and the slingshot maneuvers is presented in Figure 4-8. Table 4-7 presents a comparison of the actual and nominal velocity increase due to the various phases of both maneuvers.

The S-IVB/IU closest approach altitude of 5707 kilometers (3082 n mi) above the lunar surface occurred 85.8 hours into the mission. The actual and nominal (real-time predicted) conditions at the closest approach to the moon are presented in Table 4-8. Actual trajectory parameters were determined by integrating a state vector computed by the Manned Spacecraft Center (MSC) from Unified S-Band (USB) tracking data obtained during the active lifetime of the S-IVB/IU. Figure 4-9 illustrates the effect of the moon as the S-IVB/IU passes through the lunar sphere of influence.

Table 4-1. Comparison of Significant Trajectory Events

EVENT	PARAMETER	ACTUAL	NOMINAL	ACT-NOM
First Motion	Range Time, sec	0.0	0.0	0.0
	Total Inertial Acceleration, m/s^2 (ft/s^2) (g)	10.74 (35.24) (1.09)	10.53 (34.55) (1.07)	0.21 (0.69) (0.02)
Mach 1	Range Time, sec	66.1	67.1	-1.0
	Altitude, km (n mi)	7.8 (4.2)	7.8 (4.2)	0.0 (0.0)
Maximum Dynamic Pressure	Range Time, sec	81.1	83.8	-2.7
	Dynamic Pressure, N/cm^2 (lbf/ft^2)	3.27 (683.0)	3.32 (693.4)	-0.05 (-10.4)
	Altitude, km (n mi)	12.8 (6.9)	13.5 (7.3)	-0.7 (-0.4)
Maximum Total Inertial Acceleration: S-IC	Range Time, sec	161.82	161.25	0.57
	Acceleration, m/s^2 (ft/s^2) (g)	38.34 (125.79) (3.91)	37.84 (124.15) (3.86)	0.50 (1.64) (0.05)
S-II	Range Time, sec	460.83	461.65	-0.82
	Acceleration, m/s^2 (ft/s^2) (g)	17.92 (58.79) (1.83)	18.17 (59.61) (1.65)	-0.25 (-0.82) (-0.02)
S-IVB 1st Burn	Range Time, sec	693.99	689.94	4.05
	Acceleration, m/s^2 (ft/s^2) (g)	6.77 (22.21) (0.69)	6.77 (22.21) (0.69)	0.00 (0.00) (0.00)
S-IVB 2nd Burn	Range Time, sec	10,384.02	10,385.09	-1.07
	Acceleration, m/s^2 (ft/s^2) (g)	14.55 (47.74) (1.48)	14.53 (47.67) (1.48)	0.02 (0.07) (0.00)
Maximum Earth-Fixed Velocity: S-IC	Range Time, sec	162.18	163.19	-1.01
	Velocity, m/s (ft/s)	2,393.3 (7,852.0)	2,402.9 (7,883.5)	-9.6 (-31.5)
S-II	Range Time, sec	553.20	551.89	1.31
	Velocity, m/s (ft/s)	6,558.6 (21,517.7)	6,575.9 (21,574.5)	-17.3 (-56.8)
S-IVB 1st Burn	Range Time, sec	703.91	699.86	4.05
	Velocity, m/s (ft/s)	7,389.1 (24,242.5)	7,389.6 (24,244.1)	-0.5 (-1.6)
S-IVB 2nd Burn	Range Time, sec	10,384.32	10,385.45	-1.13
	Velocity, m/s (ft/s)	10,382.4 (34,063.0)	10,383.3 (34,066.0)	-0.9 (-3.0)
Apex: S-IC Stage	Range Time, sec	275.6	274.9	0.7
	Altitude, km (n mi)	123.0 (66.4)	121.7 (65.7)	1.3 (0.7)
	Surface Range, km (n mi)	336.0 (181.4)	335.0 (180.9)	1.0 (0.5)
S-II Stage	Range Time, sec	583.7	578.4	5.3
	Altitude, km (n mi)	191.2 (103.2)	190.9 (103.1)	0.3 (0.1)
	Surface Range, km (n mi)	1,834.8 (990.3)	1,822.0 (983.4)	12.8 (6.9)

NOTE: Times used are vehicle times.

Table 4-2. Comparison of Cutoff Events

PARAMETER	ACTUAL	NOMINAL	ACT-NOM	ACTUAL	NOMINAL	ACT-NOM
	S-IC CECO (ENGINE SOLENOID)			S-IC OECO (ENGINE SOLENOID)		
Range Time, sec	135.24	135.27	-0.03	161.74	162.48	-0.74
Altitude, km (n mi)	44.7 (24.1)	43.9 (23.7)	0.8 (0.4)	68.1 (36.8)	67.7 (36.6)	0.4 (0.2)
Surface Range, km (n mi)	47.1 (25.4)	46.2 (24.9)	0.9 (0.5)	93.7 (50.6)	94.2 (50.9)	-0.5 (-0.3)
Space-Fixed Velocity, m/s (ft/s)	1,979.5 (6,494.4)	1,967.4 (6,454.7)	12.1 (39.7)	2,750.7 (9,024.6)	2,761.1 (9,058.7)	-10.4 (-34.1)
Flight Path Angle, deg	23.944	23.820	0.124	20.513	20.309	0.204
Heading Angle, deg	76.115	76.290	-0.175	75.231	75.354	-0.123
Cross Range, km (n mi)	-0.2 (-0.1)	0.2 (0.1)	-0.4 (-0.2)	-0.2 (-0.1)	0.3 (0.2)	-0.5 (-0.3)
Cross Range Velocity, m/s (ft/s)	-1.2 (-3.9)	3.8 (12.5)	-5.0 (-16.4)	2.6 (8.5)	8.7 (28.5)	-6.1 (-20.0)
	S-II CECO (ENGINE SOLENOID)			S-II OECO (ENGINE SOLENOID)		
Range Time, sec	460.75	461.49	-0.74	552.34	550.98	1.36
Altitude, km (n mi)	186.1 (100.5)	185.6 (100.1)	0.7 (0.4)	190.4 (102.8)	190.1 (102.6)	0.3 (0.2)
Surface Range, km (n mi)	1,109.7 (599.2)	1,117.4 (603.3)	-7.7 (-4.1)	1,638.5 (884.7)	1,637.3 (884.1)	1.2 (0.6)
Space-Fixed Velocity, m/s (ft/s)	5,722.7 (18,775.3)	5,768.8 (18,926.5)	-46.1 (-151.2)	6,959.1 (22,831.7)	6,976.4 (22,888.5)	-17.3 (-56.8)
Flight Path Angle, deg	0.502	0.542	-0.040	0.442	0.461	-0.019
Heading Angle, deg	79.632	79.621	0.011	82.501	82.461	0.040
Cross Range, km (n mi)	13.6 (7.3)	14.2 (7.7)	-0.6 (-0.4)	26.9 (14.5)	27.0 (14.6)	-0.1 (-0.1)
Cross Range Velocity, m/s (ft/s)	115.9 (380.2)	112.5 (369.1)	3.4 (11.1)	178.8 (586.6)	175.3 (575.1)	3.5 (11.5)
	S-IVB 1ST GUIDANCE CUTOFF SIGNAL			S-IVB 2ND GUIDANCE CUTOFF SIGNAL		
Range Time, sec	693.91	689.86	4.05	10,383.94	10,385.01	-1.07
Altitude, km (n mi)	190.9 (103.1)	191.4 (103.3)	-0.5 (-0.2)	352.8 (190.5)	354.4 (191.4)	-1.6 (-0.9)
Surface Range, km (n mi)	2,592.6 (1,399.9)	2,574.5 (1,390.1)	18.1 (9.8)			
Space-Fixed Velocity, m/s (ft/s)	7,790.8 (25,560.4)	7,791.4 (25,562.3)	-0.6 (-1.9)	10,795.8 (35,419.3)	10,797.9 (35,426.2)	-2.1 (-6.9)
Flight Path Angle, deg	-0.015	-0.001	-0.014	8.137	8.156	-0.019
Heading Angle, deg	88.146	88.022	0.124	63.664	63.645	0.019
Cross Range, km (n mi)	58.6 (31.6)	57.5 (31.0)	1.1 (0.6)			
Cross Range Velocity, m/s (ft/s)	272.1 (892.7)	268.8 (881.9)	3.3 (10.8)			
Eccentricity				0.96829	0.96949	-0.00120
C_3*, m^2/s^2 (ft^2/s^2)				-1,917,435 (-20,639,099)	-1,844,202 (-19,850,825)	-73,233 (-788,274)
Inclination, deg				30.360	30.340	0.020
Descending Node, deg				120.344	120.376	-0.032

NOTE: Times used are vehicle times.

* C_3 is twice the specific energy of orbit

$$C_3 = V^2 - \frac{2\mu}{R}$$

where V = Inertial Velocity
μ = Gravitational Constant
R = Radius vector from center of earth

Table 4-3. Comparison of Separation Events

PARAMETER	ACTUAL	NOMINAL	ACT-NOM
S-IC/S-II SEPARATION			
Range Time, sec	162.4	163.2	-0.8
Altitude, km (n mi)	68.7 (37.1)	68.4 (36.9)	0.3 (0.2)
Surface Range, km (n mi)	95.2 (51.4)	95.7 (51.7)	-0.5 (-0.3)
Space-Fixed Velocity, m/s (ft/s)	2,759.7 (9,054.1)	2,770.7 (9,090.2	-11.0 (-36.1)
Flight Path Angle, deg	20.430	20.213	0.217
Heading Angle, deg	75.228	75.351	-0.123
Cross Range, km (n mi)	-0.2 (-0.1)	0.3 (0.2)	-0.5 (-0.3)
Cross Range Velocity, m/s (ft/s)	2.7 (8.9)	8.9 (29.2)	-6.2 (-20.3)
Geodetic Latitude, deg N	28.871	28.869	0.002
Longitude, deg E	-79.677	-79.670	-0.007
S-II/S-IVB SEPARATION			
Range Time, sec	553.2	551.9	1.3
Altitude, km (n mi)	190.4 (102.8)	190.1 (102.6)	0.3 (0.2)
Surface Range, km (n mi)	1,644.0 (887.7)	1,643.0 (887.1)	1.0 (0.6)
Space-Fixed Velocity, m/s (ft/s)	6,961.9 (22,840.9)	6,979.1 (22,897.3)	-17.2 (-56.4)
Flight Path Angle, deg	0.432	0.451	-0.019
Heading Angle, deg	82.533	82.495	0.038
Cross Range, km (n mi)	27.0 (14.6)	27.1 (14.6)	-0.1 (0.0)
Cross Range Velocity, m/s (ft/s)	179.3 (588.3)	175.8 (576.8)	3.5 (11.5)
Geodetic Latitude, deg N	31.925	31.923	0.002
Longitude, deg E	-63.934	-63.943	0.009
S-IVB/CSM SEPARATION			
Range Time, sec	11,884.9	11,885.2	-0.3
Altitude, km (n mi)	7,073.3 (3,819.3)	7,075.1 (3,820.2)	-1.8 (-0.9)
Space-Fixed Velocity, m/s (ft/s)	7,579.0 (24,865.5)	7,580.9 (24,871.7)	-1.9 (-6.2)
Flight Path Angle, deg	45.092	45.102	-0.010
Heading Angle, deg	100.194	100.077	0.117
Geodetic Latitude, deg N	28.915	28.930	-0.015
Longitude, deg E	-79.537	-79.743	0.206

NOTE: Times used are vehicle times.

Table 4-4. Stage Impact Location

PARAMETER	ACTUAL	NOMINAL	ACT-NOM
S-IC STAGE IMPACT			
Range Time, sec	554.5	554.1	0.4
Surface Range, km (n mi)	676.4 (365.2)	675.2 (364.6)	1.2 (0.6)
Cross Range, km (n mi)	6.0 (3.2)	8.1 (4.4)	-2.1 (-1.2)
Geodetic Latitude, deg N	30.273	30.253	0.020
Longitude, deg E	-73.895	-73.903	0.008
S-II STAGE IMPACT			
Range Time, sec	1,221.6	1,224.7	-3.1
Surface Range, km (n mi)	4,452.9 (2,404.4)	4,479.6 (2,418.8)	-26.7 (-14.4)
Cross Range, km (n mi)	145.9 (78.8)	145.7 (78.7)	0.2 (0.1)
Geodetic Latitude, deg N	31.465	31.438	0.027
Longitude, deg E	-34.214	-33.937	-0.277

The actual longitudinal velocity change during the slingshot maneuver was very close to nominal; however, the LVDC state vector used to target the S-IVB/IU in real time did not reflect an existing underspeed condition at TLI. This underspeed condition coupled with the slingshot maneuver caused the S-IVB/IU lunar radius of closest approach, 7445 kilometers (4020 n mi) to be greater than the maximum allowable radius for escape from the earth-moon system, namely, 5100 kilometers (2754 n mi) for AS-507 mission.

Table 4-9 presents the contributing factors which initiated the real time calculation of the additional APS burn. These factors were available in real time at Marshall Space Flight Center (MSFC). The resulting 11.2 m/s (36.75 ft/s) velocity change corresponds to an additional 270-second APS burn. Table 4-10 presents the corresponding contributors of the velocity change used to calculate the additional APS burn based on a post TLI tracking vector. This vector was not available in real time. The resulting velocity change of -1.8 m/s (-5.91 ft/s) represents approximately 45 seconds of APS burn duration. Therefore, the programed 300-second APS burn could have been shortened to 255 seconds to target to the center of the slingshot window. MSC was aware of the disagreement between the LVDC and tracking state vectors at TLI but did not relay the information to MSFC for real time processing. MSC was not aware that the existing IU vector error would significantly affect the slingshot targeting.

Table 4-5. Parking Orbit Insertion Conditions

PARAMETER	ACTUAL	NOMINAL	ACT-NOM
Range Time, sec	703.91	699.86	4.05
Altitude, km (n mi)	190.9 (103.1)	191.4 (103.3)	-0.5 (-0.2)
Space-Fixed Velocity, m/s (ft/s)	7,792.5 (25,565.9)	7,793.0 (25,567.6)	-0.5 (-1.7)
Flight Path Angle, deg	-0.014	0.000	-0.014
Heading Angle, deg	88.580	88.456	0.124
Inclination, deg	32.540	32.545	-0.005
Descending Node, deg	123.126	123.146	-0.020
Eccentricity	0.00032	0.00000	0.00032
Apogee*, km (n mi)	185.4 (100.1)	185.2 (100.0)	0.2 (0.1)
Perigee*, km (n mi)	181.2 (97.8)	185.2 (100.0)	-4.0 (-2.2)
Period, min	88.16	88.20	-0.04
Geodetic Latitude, deg N	32.682	32.681	0.001
Longitude, deg E	-53.131	-53.323	0.192

* Based on a spherical earth of radius 6,378.165 km (3,443.934 n mi).

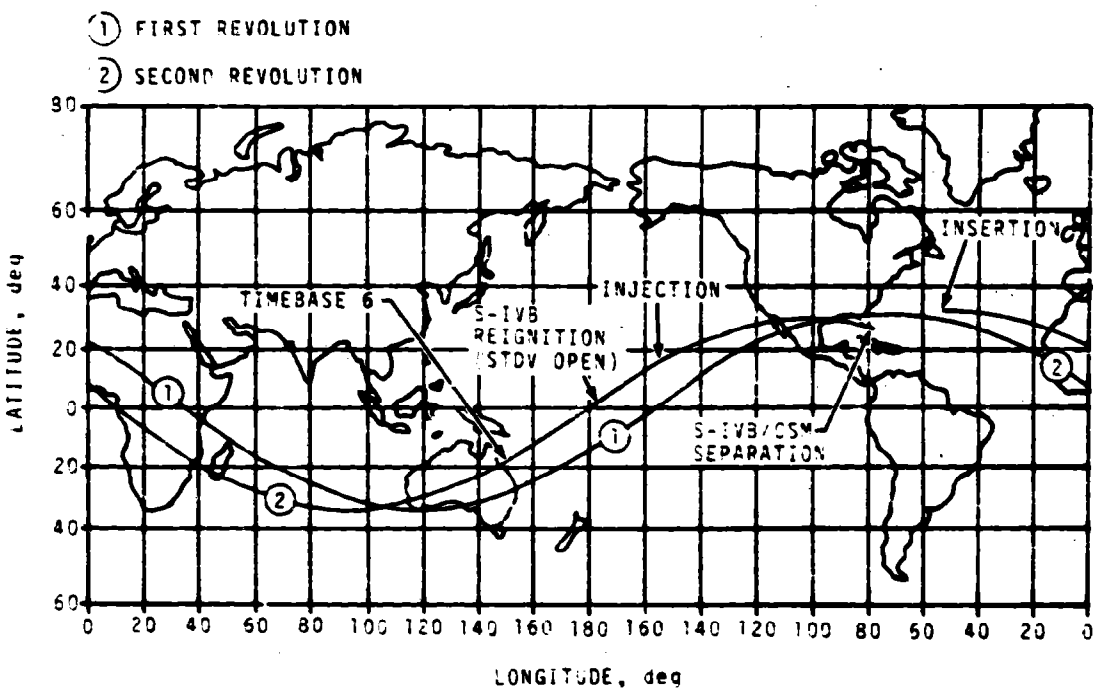

Figure 4-5. Ground Track

Table 4-6. Translunar Injection Conditions

PARAMETER	ACTUAL	NOMINAL	ACT-NOM
Range Time, sec	10,393.94	10,395.01	-1.07
Altitude, km (n mi)	368.6 (199.0)	370.2 (199.9)	-1.6 (-0.9)
Space-Fixed Velocity, m/s (ft/s)	10,786.8 (35,389.8)	10,786.4 (35,395.0)	-1.6 (-5.2)
Flight Path Angle, deg	8.584	8.603	-0.019
Heading Angle, deg	63.902	63.880	0.022
Inclination, deg	30.355	30.336	0.019
Descending Node, deg	120.338	120.371	-0.033
Eccentricity	0.96966	0.97066	-0.00100
C_3, m^2/s^2 (ft^2/s^2)	-1,834,425 (-19,745,586)	-1,773,597 (-19,090,839)	-60,828 (-654,747)

NOTE: Times used are vehicle times.

Table 4-7. Comparison of Slingshot Maneuver Velocity Increment

PARAMETER	ACTUAL	NOMINAL	ACT-NOM
Longitudinal Velocity Increase, m/s (ft/s)	38.2 (125.3)	38.1 (125.0)	0.1 (0.3)
APS Evasive Maneuver, m/s (ft/s)	2.9 (9.5)	3.0 (9.8)	-0.1 (-0.3)
Continuous Vent System*, m/s (ft/s)	2.8 (9.2)	1.5 (4.9)	1.3 (4.3)
LOX Dump, m/s (ft/s)	10.0 (32.8)	9.7 (31.8)	0.3 (1.0)
Programmed APS Burn, m/s (300 seconds) (ft/s)	11.8 (38.7)	12.7 (41.7)	-0.9 (-3.0)
Ground Commanded APS Burn, m/s (270 seconds) (ft/s)	10.7 (35.1)	11.2 (36.7)	-0.5 (-1.6)

* Latched open at T_8 + 580 seconds.

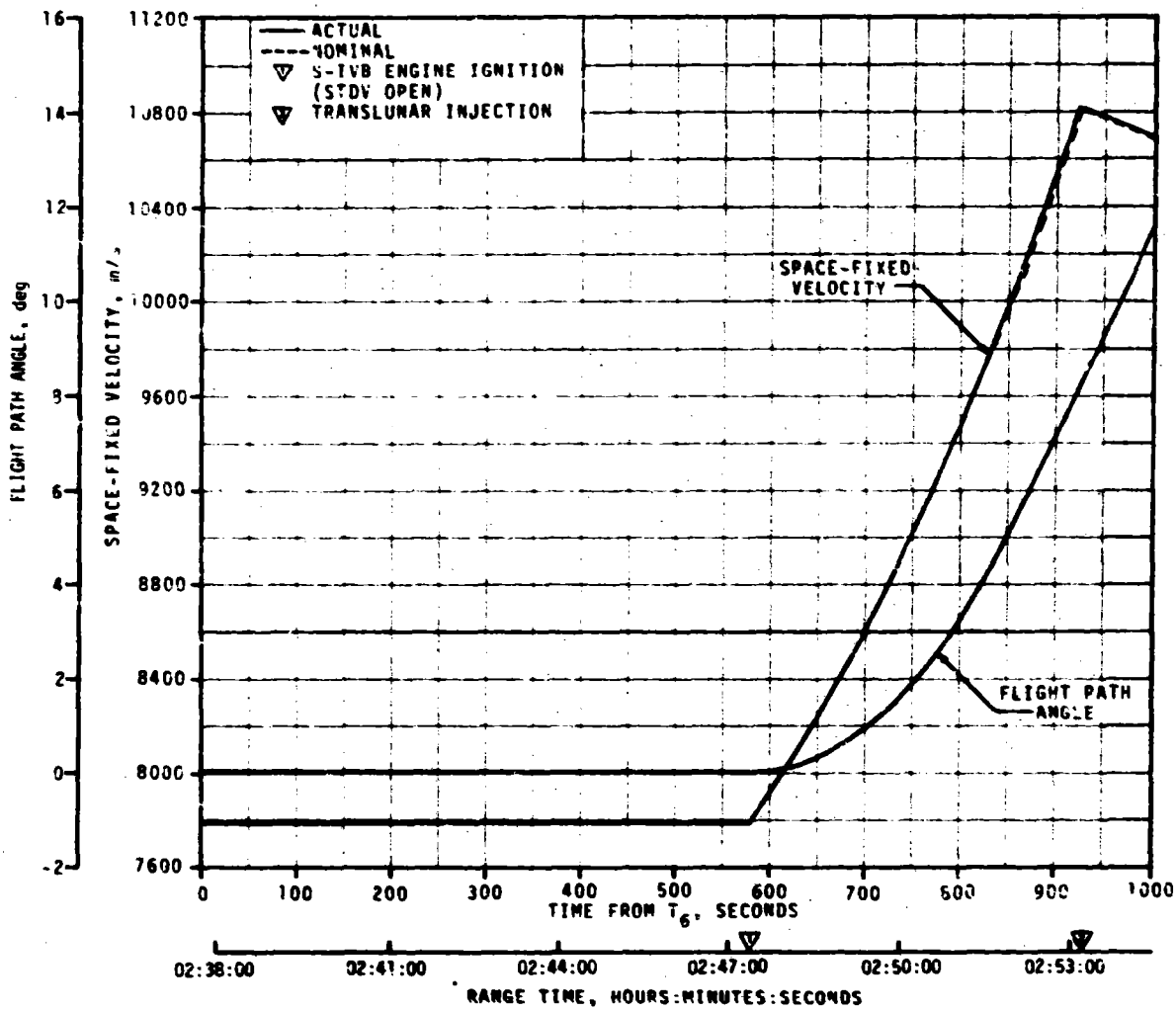

Figure 4-6. Injection Phase Space-Fixed Velocity and Flight Path Angle Comparisons

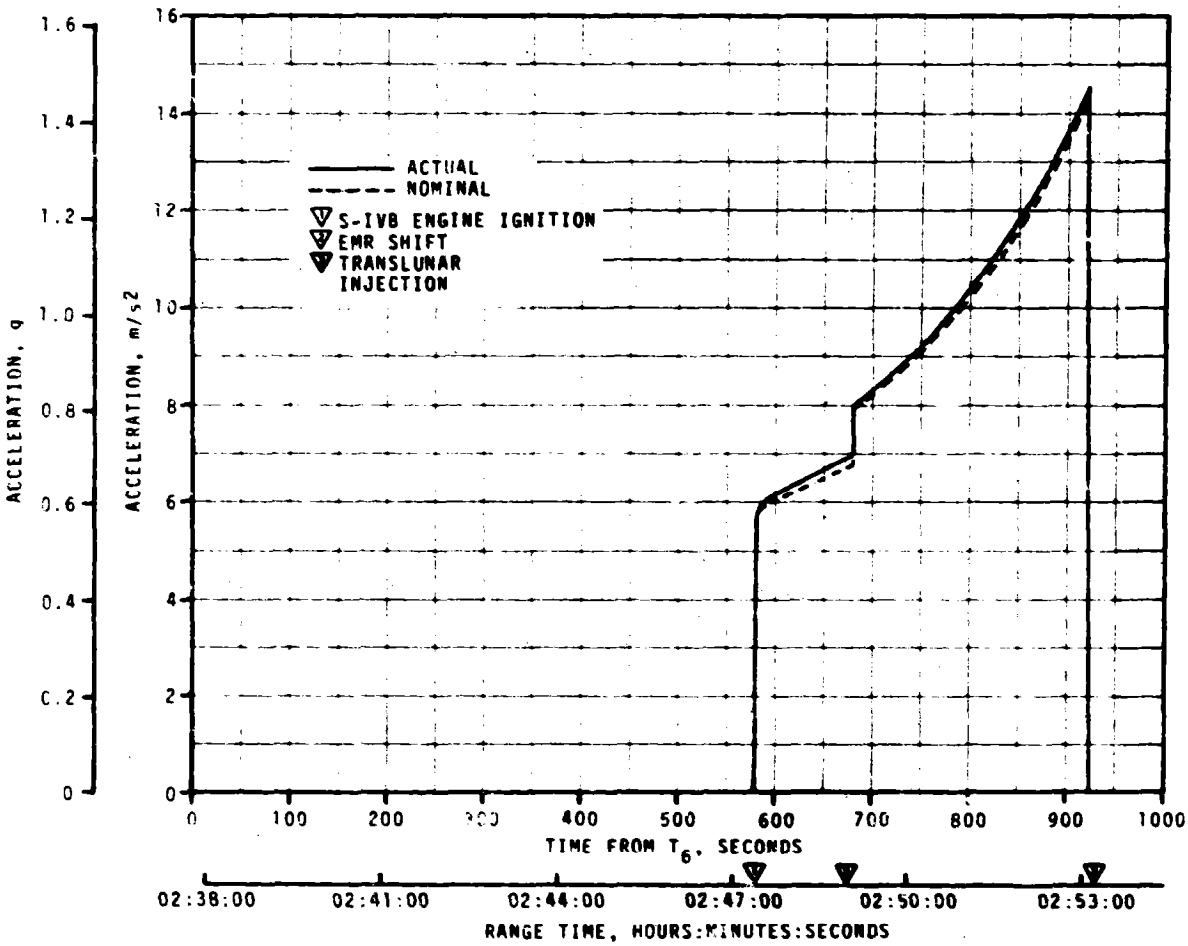

Figure 4-7. Injection Phase Acceleration Comparison

Table 4-8. Comparison of Lunar Closest Approach Parameters

PARAMETER	ACTUAL	NOMINAL	ACT-NOM
Selenocentric Distance, km (n mi)	7,445 (4,020)	3,400 (1,836)	4,045 (2,184)
Altitude Above Lunar Surface, km (n mi)	5,707 (3,082)	1,662 (897)	4,045 (2,185)
Range Time, hr.	85.8	84.1	1.7
Velocity Increase Relative to Earth from Lunar Encounter, m/s (n mi/s)	548 (0.296)	850 (0.459)	-302 (-0.163)

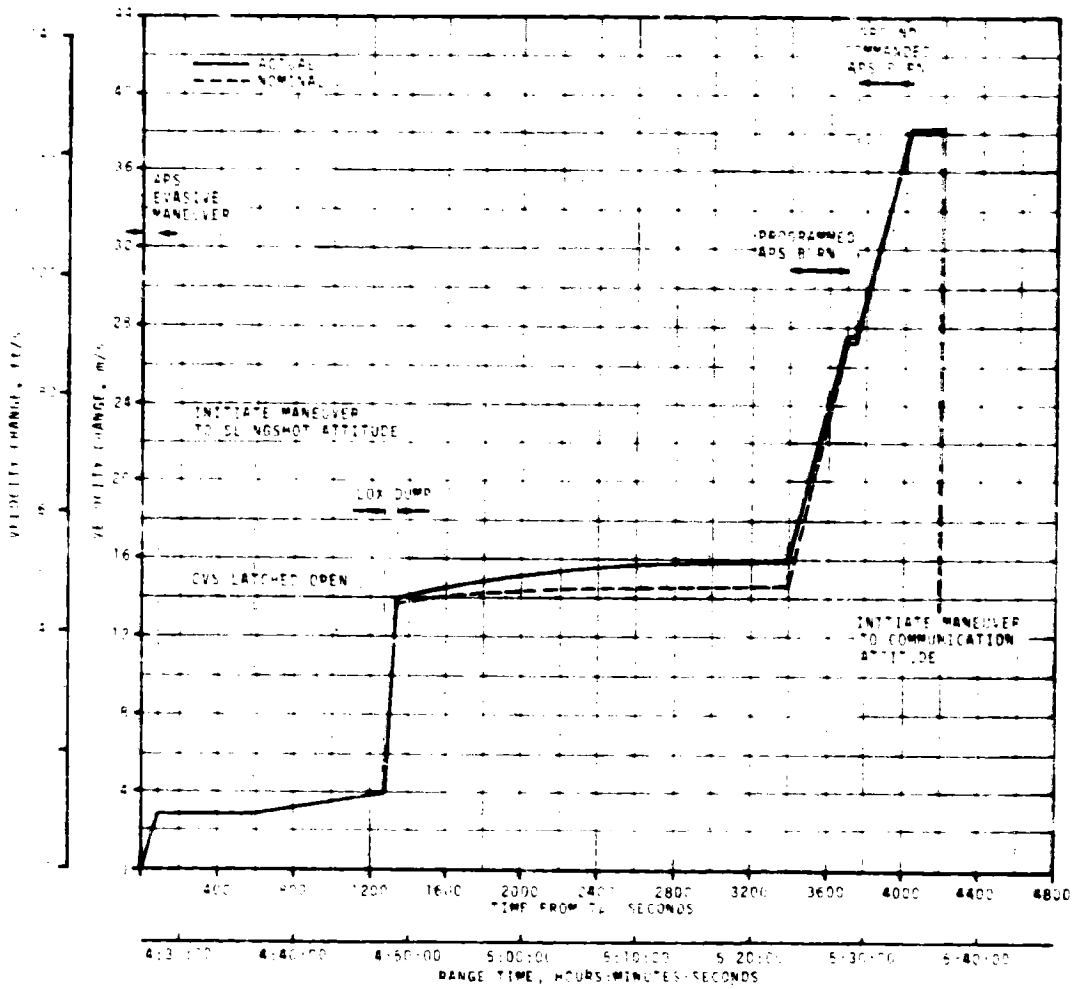

Figure 4-8. Slingshot Maneuver Longitudinal Velocity Change

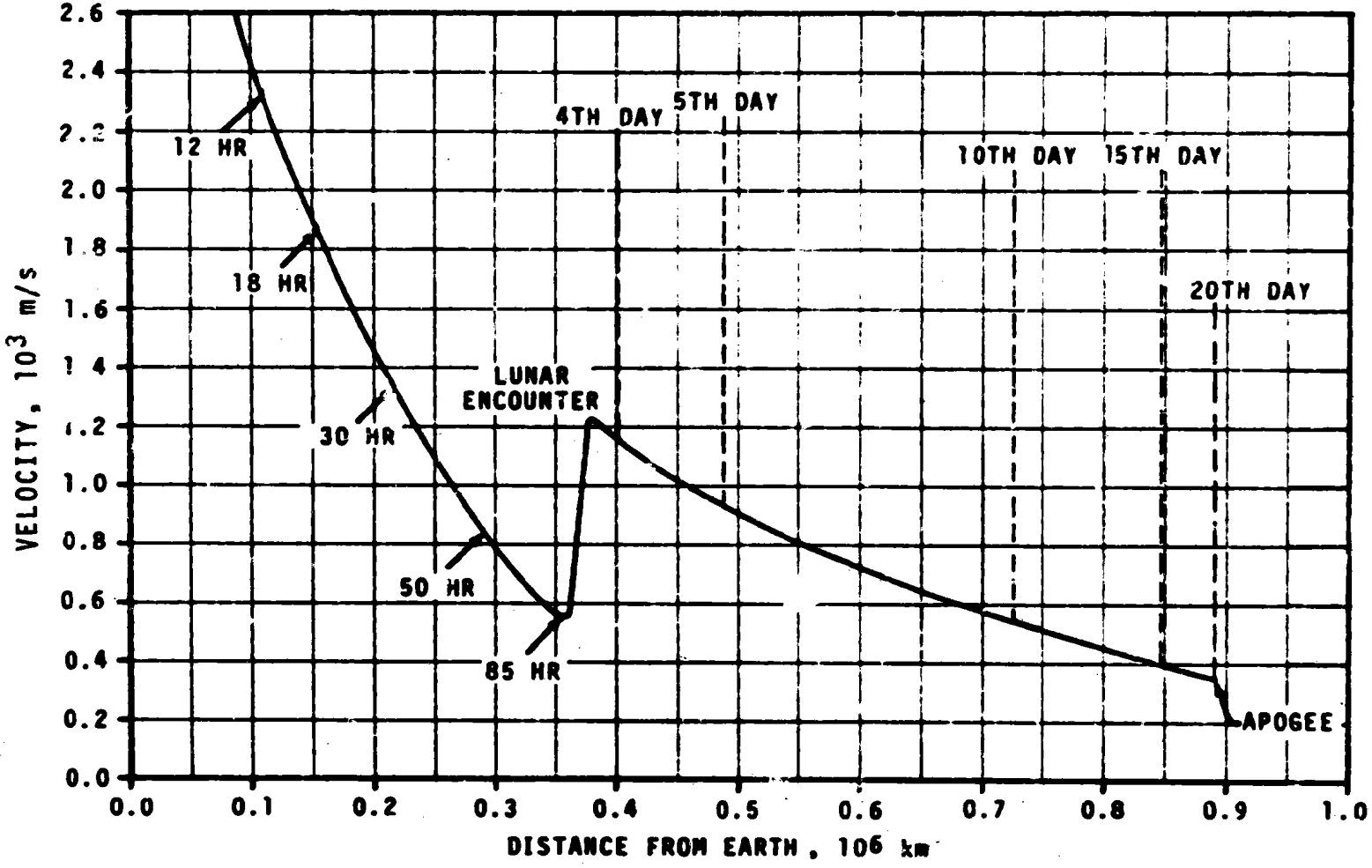

Figure 4-9. S-IVB/IU Velocity Relative to Earth Distance

Table 4-9. Velocity Change Due to APS Burn Based on TLI IU Vector Available in Real Time

	CONTRIBUTING FACTORS	APS VELOCITY CHANGE M/S (FT/S)	
1	IU Vector at TLI (indicated a slight overspeed)	1.0	(3.28)
2	Post TLI CVS (known preflight)	1.4	(4.59)
3	T_8 Initiate (slight delay from preflight estimation (115 seconds)	0.3	(0.98)
4	LOX Ullage Pressure (lower than preflight nominal approximately 4.5 psia)	2.5	(8.20)
5	Updated T_8 CVS Prediction (known preflight)	5.5	(18.04)
6	Delay in Commanded APS Burn (approximately 600 seconds)	0.5	(1.64)
	TOTAL	11.2	(36.75)

Table 4-10. Velocity Change Due to APS Burn Based on Post TLI Tracking Vector Not Available in Real Time

	CONTRIBUTING FACTORS	APS VELOCITY CHANGE M/S (FT/S)	
1	Tracking Vector Immediately After TLI (indicated significant underspeed)	-12.0	(-39.37)
2	Post TLI CVS (known preflight)	1.4	(4.59)
3	T_8 Initiate (slight delay from preflight estimation (115 seconds)	0.3	(0.98)
4	LOX Ullage Pressure (lower than preflight nominal approximately 4.5 psia)	2.5	(8.20)
5	Updated T_8 CVS Prediction (known preflight)	5.5	(18.04)
6	Delay in Commanded APS Burn (approximately 600 seconds)	0.5	(1.64)
	TOTAL	-1.8	(-5.91)

SECTION 5

S-IC PROPULSION

5.1 SUMMARY

All S-IC propulsion systems performed satisfactorily and the propulsion performance level was very close to the predicted level. Stage site thrust (averaged from liftoff to Outboard Engine Cutoff [OECO]) was 0.55 percent higher than predicted. Total propellant consumption rate was 0.26 percent higher than predicted with the total consumed Mixture Ratio (MR) 0.34 percent higher than predicted. Specific impulse was 0.20 percent higher than predicted. Total propellant consumption from Holddown Arm (HDA) release to OECO was low by 0.05 percent. The planned 1-2-2 start sequence was not attained, but caused no problems.

Center Engine Cutoff (CECO) was initiated by the Instrument Unit (IU) at 135.24 seconds as planned. Outboard engine cutoff, initiated by LOX low level sensors, occurred at 161.74 seconds which was 0.74 second earlier than predicted. This is a small difference compared to the predicted 3-sigma limits of +5.28, -3.67 seconds. The LOX residual at OECO was 42,093 lbm compared to the predicted 39,449 lbm. The fuel residual at OECO was 36,309 lbm compared to the predicted 31,965 lbm.

5.2 S-IC IGNITION TRANSIENT PERFORMANCE

The fuel pump inlet preignition pressure was 45.2 psia and within F-1 Engine Model Specification limits of 43.5 to 110 psia.

The LOX pump inlet preignition pressure and temperature were 81.9 psia and -287.7°F and were within the F-1 Engine Model Specification limits as shown in Figure 5-1.

The planned 1-2-2 start was not attained as seen in Figure 5-2. Engine position starting order was 5, 1-3, 2 and 4. Two engines are considered to start together if their combustion chamber pressures reach 100 psig in a 100-millisecond time period. Engine No. 4 reached 100 psig chamber pressure 0.207 second slower than predicted and 0.202 second later than engine No. 2, resulting in a 1-2-1-1 start. Structurally, a 1-2-2 start is desired for minimizing the start and liftoff dynamics caused by thrust buildup of the engines. The dynamic effects of other start sequences on the Saturn V structure are not fully known at this time. The 1-2-1-1 start caused no problems, although it should be noted that AS-507 liftoff

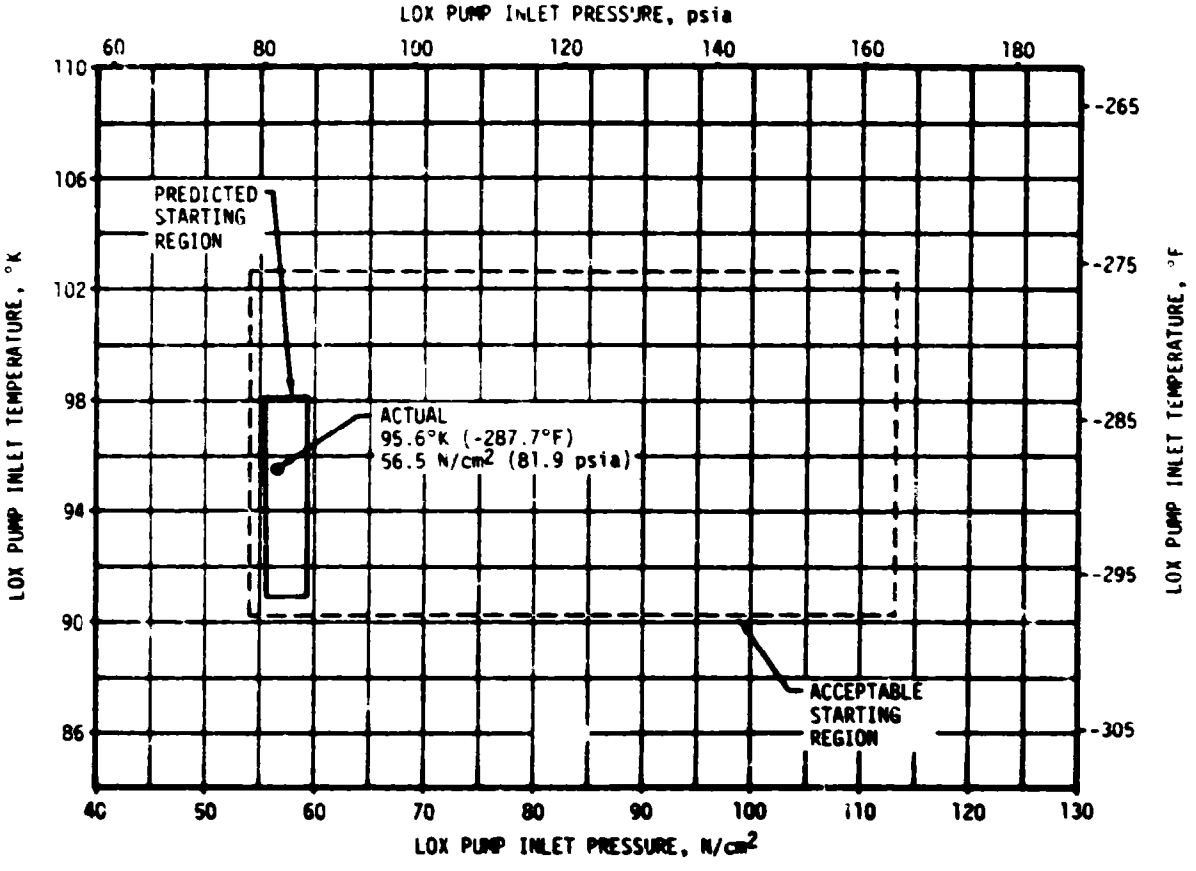

Figure 5-1. S-IC LOX Start Box Requirements

dynamics were somewhat higher than those on previous flights but were well within design limits (see paragraphs 9.2.1 and 9.2.2). By definition, a 1-2-2 start occurs where the desired engine thrust buildup sequence is as follows: The center engine is to achieve 90,000 lbf thrust (100 psig chamber pressure) a -2.960 seconds, the first pair of outboard engines at -2.660 seconds, and the second pair of outboard engines at -2.360 seconds. Each F-1 engine has distinctive starting characteristics requiring individually programed start signals in order to minimize the dispersions in achieving the 90,000 lbf thrust level at the desired time. Determination of start signal presettings is one objective of static firing the S-IC stage. With start signal presettings established by stage static firing of a particular stage there is a large probability that a 1-2-2 start will be achieved during ignition of this stage at launch. This large probability will not exist when static firing of the S-IC stages is terminated on the "follow-on" stages (S-IC-16 and subsequent stages).

The best estimate of propellants consumed between ignition and HDA release was 84,635 lbm. The predicted consumption was 85,364 lbm. Propellant loads at HDA release were 3,241,657 lbm for LOX and 1,408,194 lbm for fuel.

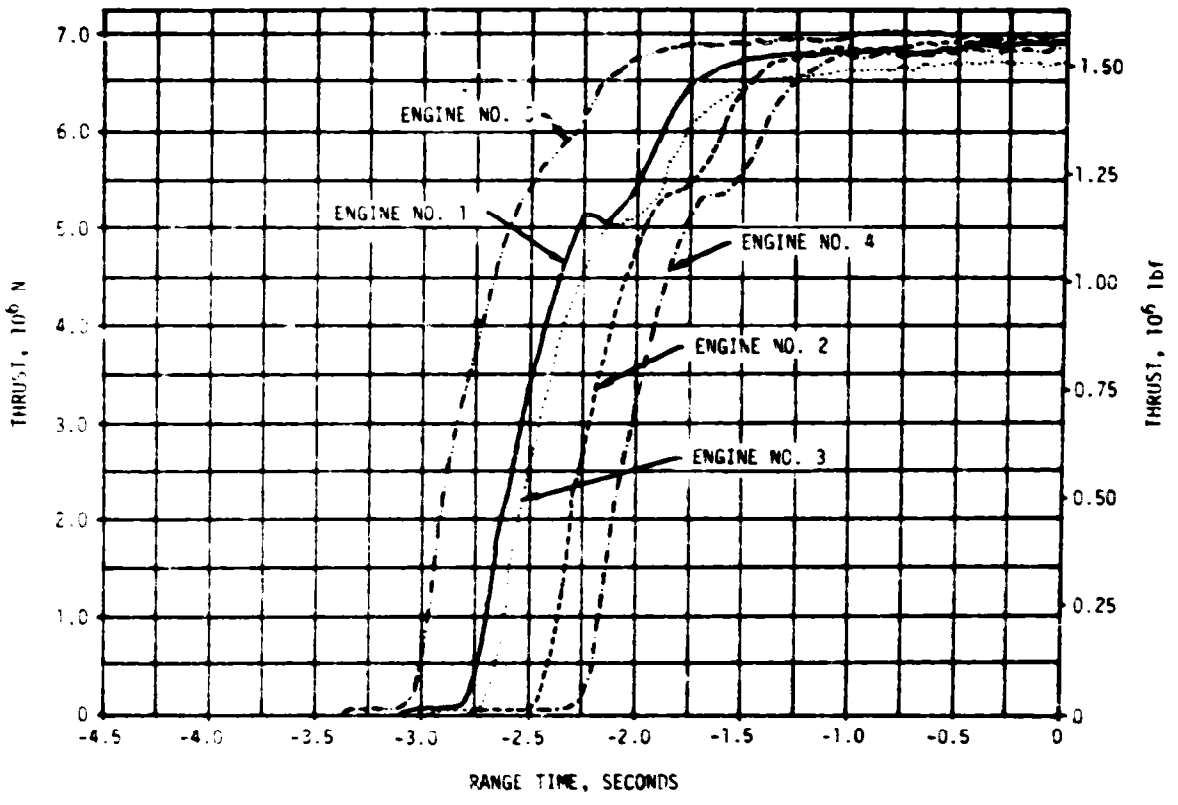

Figure 5-2. S-IC Engine Buildup Transients

5.3 S-IC MAINSTAGE PERFORMANCE

S-IC stage propulsion performance was very close to the predicted level as can be seen in Figure 5-3. The stage site thrust (averaged from range time zero to OECO) was 0.55 percent higher than predicted.

Total propellant consumption rate was 0.26 percent higher than predicted and the total consumed propellant MR was 0.34 percent higher than predicted. The specific impulse was 0.20 percent higher than predicted. Total propellant consumption from HDA release to OECO was low by 0.05 percent.

For comparing F-1 engine flight performance with predicted performance, the flight performance has been analytically reduced to standard conditions and compared to the predicted performance which is based on ground firings and also reduced to standard conditions. These values are shown in Table 5-1 at the 35 to 38-second time slice. Individual engine deviations from predicted thrust ranged from 0.066 percent lower (engine No. 4) to 0.668 percent higher (engine No. 3). Individual engine deviations from specific impulse ranged from 0.038 percent lower (engine No. 4) to 0.113 percent higher (engine No. 3).

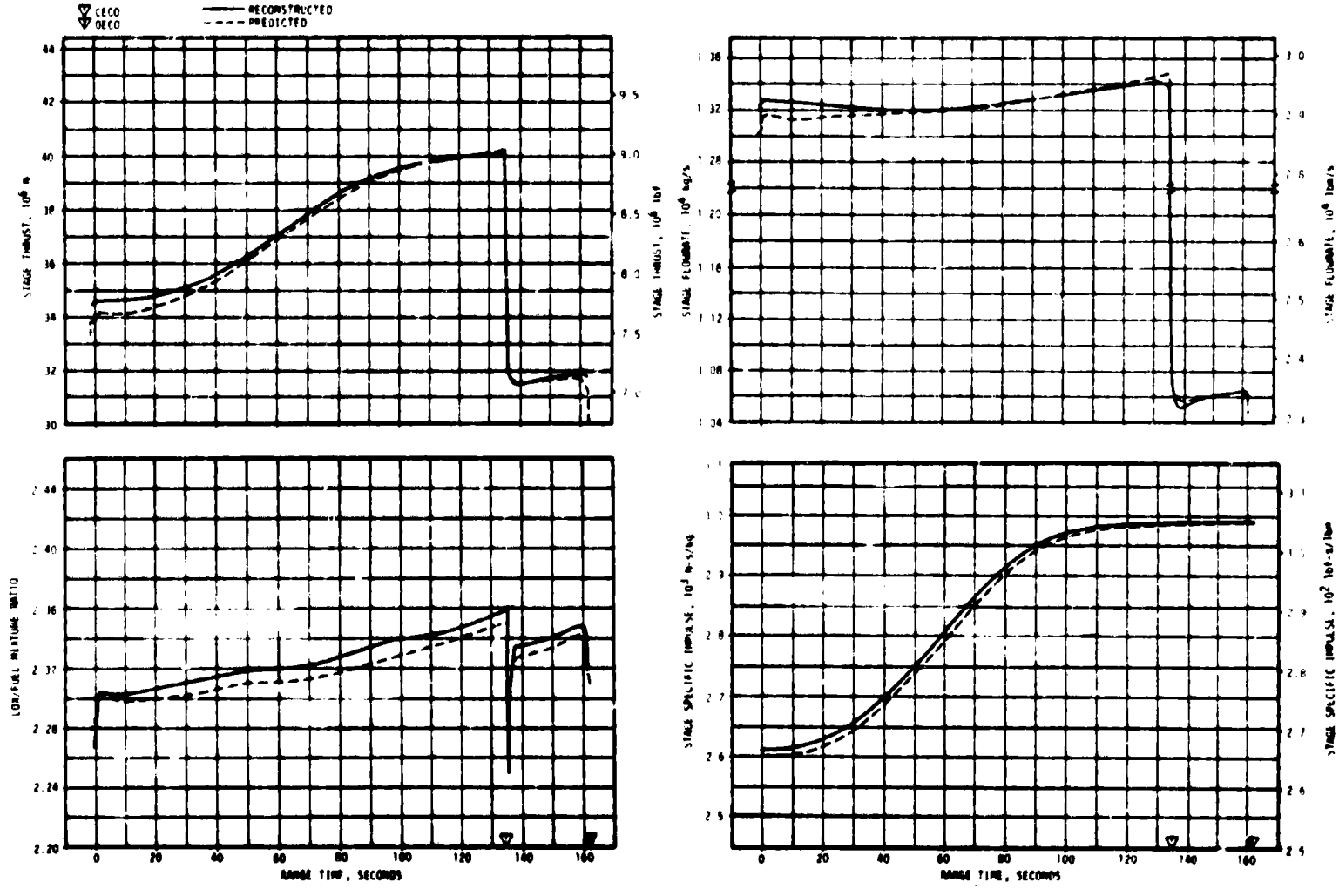

Figure 5-3. S-IC Stage Propulsion Performance

Table 5-1. S-IC Individual Engine Performance

PARAMETER	ENGINE	PREDICTED	RECONSTRUCTION ANALYSIS	DEVIATION PERCENT	AVERAGE DEVIATION PERCENT
Thrust, 10^3 lbf	1	1500	1508	0.533	0.332
	2	1525	1525	0	
	3	1498	1508	0.668	
	4	1523	1522	-0.066	
	5	1523	1531	0.525	
Specific Impulse, lbf-s/lbm	1	265.1	265.3	0.075	0.045
	2	264.4	264.4	0	
	3	264.6	264.9	0.113	
	4	265.8	265.7	-0.038	
	5	264.0	264.2	0.076	
Total Flowrate lbm/s	1	5658	5685	0.477	0.292
	2	5768	5765	-0.052	
	3	5660	5694	0.601	
	4	5729	5725	-0.07	
	5	5768	5797	0.503	
Mixture Ratio LOX/Fuel	1	2.271	2.270	-0.044	-0.079
	2	2.278	2.275	-0.132	
	3	2.268	2.266	-0.088	
	4	2.278	2.275	-0.132	
	5	2.264	2.264	0	

NOTE: Performance levels were reduced to standard sea level and pump inlet conditions. Data was taken from the 35 to 38-second time slice.

5.4 S-IC ENGINE SHUTDOWN TRANSIENT PERFORMANCE

Center engine cutoff was initiated by a signal from the IU at 135.24 seconds as planned. Outboard engine cutoff, initiated by LOX low level sensors, occurred at 161.74 seconds which was 0.74 second earlier than predicted which is a small difference compared to the predicted 3-sigma limits of +5.28, -3.67 seconds.

Thrust decay of the F-1 engines was nominal.

Engine cutoff impulse was approximately 2.8 percent higher than predicted for the outboard engines and approximately 6.7 percent lower than predicted for the center engine.

5.5 S-IC STAGE PROPELLANT MANAGEMENT

The S-IC does not have an active Propellant Utilization (PU) system. Minimum residuals are obtained by attempting to load the MR expected to be consumed by the engines plus the predicted unusable residuals. An analysis of the usable residuals experienced during a flight is a good measure of the performance of the passive PU system.

Outboard engine cutoff was initiated by the LOX low level sensors as planned, and resulted in residual propellants being very close to the predicted values. The residual LOX at OECO was 42,093 lbm compared to the predicted value of 39,449 lbm. The fuel residual at OECO was 36,309 lbm compared to the predicted value of 31,965 lbm. A summary of the propellants remaining at major event times is presented in Table 5-2.

5.6 S-IC PRESSURIZATION SYSTEMS

5.6.1 S-IC Fuel Pressurization System

The fuel tank pressurization system performed satisfactorily keeping ullage pressure within the acceptable limits during flight. Helium Flow Control Valves (HFCV's) No. 1 through 4 opened as planned and HFCV No. 5 was not required.

The low flow prepressurization system was commanded on at -97 seconds. High flow pressurization, accomplished by the onboard pressurization system, performed as expected. Helium flow control valve No. 1 was commanded on at -2.7 seconds and was supplemented by the high flow prepressurization system until umbilical disconnect.

Fuel tank ullage pressure was within the predicted limits throughout flight as shown in Figure 5-4. Helium flow control valves No. 2, 3, and 4 were commanded open during flight by the switch selector within acceptable limits. Helium bottle pressure was 3050 psia at -2.8 seconds and decayed to 490 psia at OECO. Total helium flowrate and heat exchanger performance were as expected.

Fuel pump inlet pressure was maintained above the required minimum Net Positive Suction Pressure (NPSP) during flight.

5.6.2 S-IC LOX Pressurization System

The LOX pressurization system performed satisfactorily and all performance requirements were met. The ground prepressurization system maintained ullage pressure within acceptable limits until launch commit. The onboard pressurization system subsequently maintained ullage pressure within the GOX Flow Control Valve (GFCV) band during flight.

The prepressurization system was initiated at -72 seconds. Ullage pressure increased to the pressurization switch band and flow was terminated at -57 seconds. The low-flow system was cycled on two additional times at -40 and -16 seconds. At -4.7 seconds the high-flow system was commanded on and maintained ullage pressure within acceptable limits until launch commit.

Table 5-2. S-IC Stage Propellant Mass History

EVENT	PREDICTED,LBM		LEVEL SENSOR DATA, LBM		RECONSTRUCTED,LBM	
	LOX	FUEL	LOX	FUEL	LOX	FUEL
Ignition Command	3,308,605	1,428,857	-	1,424,287	3,310,199	1,424,287
Holddown Arm Release	3,241,829	1,410,269	3,235,033	1,403,862	3,241,657	1,408,194
CECO	486,229	223,423	478,735	222,445	477,935	222,141
OECO	39,449	31,965	41,683	36,048	42,093	36,309
Separation	34,908	29,585	-	-	37,552	33,929
Zero Thrust	33,123	29,226	-	-	36,242	33,142

NOTE: Predicted and reconstructed values do not include pressurization gas so they will compare with level sensor data.

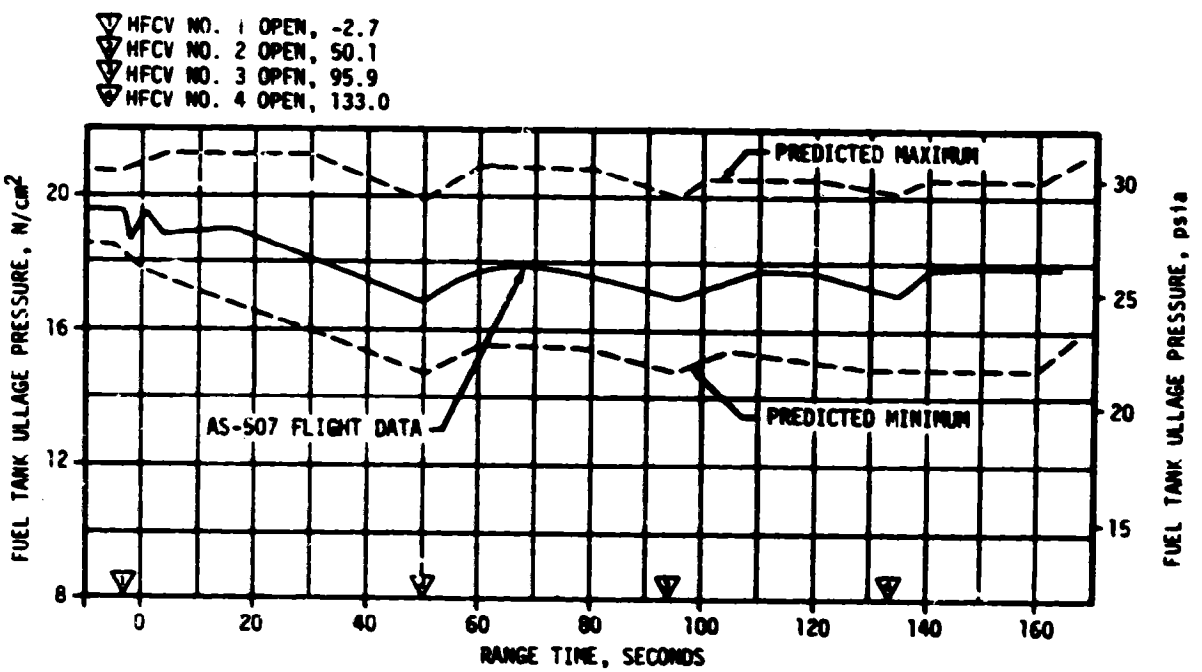

Figure 5-4. S-IC Fuel Ullage Pressure

The LOX tank ullage pressure during flight, shown in Figure 5-5, was maintained within the required limits throughout flight by the GFCV. The maximum GOX flowrate to the tank (at CECO) was 54.7 lbm/s. The heat exchangers performed as expected.

The LOX pump inlet pressure met the minimum NPSP requirement throughout flight. The engine No. 5 LOX suction duct pressure decayed after CECO similar to previous flights. Analysis has indicated that this pressure drop can be attributed to leakage through the F-1 engine LOX pump primary seal and is a normal occurrence. Therefore, the pressure drop will be expected as a normal occurrence on future flights.

5.7 S-IC PNEUMATIC CONTROL PRESSURE SYSTEM

The control pressure system functioned satisfactorily throughout the S-IC flight.

Sphere pressure was 3017 psia at liftoff and remained steady until CECO when it decreased to 2900 psia. The decrease was due to actuation of the center engine prevalves. There was a further decrease to 2544 psia after OECO. The engine prevalves were closed after engine cutoff as required.

5.8 S-IC PURGE SYSTEMS

Performance of the S-IC purge systems was satisfactory during the flight.

The turbopump LOX seal purge storage sphere pressure was within the limits of 2760 to 3300 psia until ignition and 3300 to 1000 psia from liftoff to cutoff.

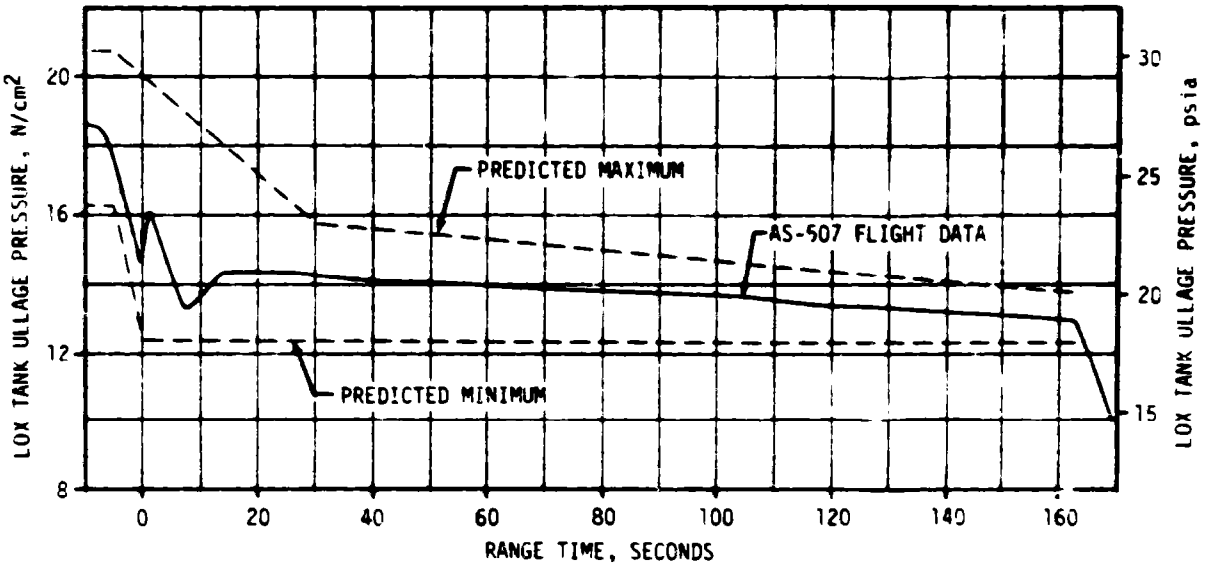

Figure 5-5. S-IC LOX Tank Ullage Pressure

5.9 S-IC POGO SUPPRESSION SYSTEM

The POGO suppression system performed satisfactorily during S-IC flight.

Outboard LOX prevalve temperature measurements indicated that the prevalve cavities were filled with helium prior to liftoff as planned. The measurements in the outboard prevalves went cold momentarily at liftoff indicating LOX sloshed on the probes. They remained warm throughout flight, indicating helium in the prevalves. At cutoff, the increased pressure forced LOX into the prevalves once more. The two measurements in the center engine prevalve indicated cold, which meant LOX was in this valve, as planned.

SECTION 6

S-II PROPULSION

6.1 SUMMARY

The S-II propulsion system performed satisfactorily throughout the flight. The S-II Engine Start Command (ESC), as sensed at the engines, occurred at 163.17 seconds. Center Engine Cutoff (CECO) occurred as planned at 460.75 seconds and Outboard Engine Cutoff (OECO) occurred at 552.34 seconds giving an outboard engine operation time of 389.17 seconds or 2.1 seconds longer than predicted. Total stage thrust, as determined by computer analysis of telemetered propulsion measurements at 61 seconds after S-II ESC, was 0.05 percent below predicted. Total propellant flowrate (including pressurization flow) was equal to the predicted, and stage specific impulse was 0.05 percent below predicted at this time slice. Stage propellant Mixture Ratio (MR) was 0.36 percent above predicted. Engine thrust buildup and cutoff transients were satisfactory.

Low frequency, low amplitude oscillations were observed on all engines during S-II boost prior to CECO. Net engine performance levels were not affected.

The propellant management system performance was satisfactory. The system used open-loop control of the engine Propellant Utilization (PU) valves similar to the AS-506 flight. The Instrument Unit (IU) command to shift Engine Mixture Ratio (EMR) from high to low was initiated upon attainment of a preprogramed stage characteristic velocity as sensed by the Launch Vehicle Digital Computer (LVDC). The IU EMR shift command occurred 2.0 seconds later than predicted and was due mainly to overloading of the S-II and the upper stages.

S-II OECO, initiated by the LOX low level cutoff sensors, was achieved following a planned 1.5-second time delay. A small engine performance decay was noted just prior to cutoff similar to AS-506. Residual propellant remaining in the tanks at OECO signal was 6138 lbm compared to the prediction of 5787 lbm.

The performance of the LOX and LH_2 tank pressurization systems was satisfactory. Ullage pressure in both tanks was more than adequate to meet engine inlet propellant requirements throughout mainstage. As commanded by the IU, step pressurization occurred at 261.7 seconds for the LOX tank and 461.7 seconds for the LH_2 tank.

The engine servicing, recirculation, helium injection and valve actuation systems all performed satisfactorily. During the launch countdown checkout, the valve actuation system receiver pressure decay rate exceeded the maximum allowable limit. This excessive pressure decay was attributed to thermal effects. The receiver pressure decay during flight was negligible.

6.2 S-II CHILLDOWN AND BUILDUP TRANSIENT PERFORMANCE

The prelaunch servicing operations required to condition the engines were satisfactorily accomplished. Thrust chamber chill requirements are -200°F maximum at prelaunch commit (-19 seconds) and -150°F maximum at engine start. Thrust chamber temperatures were within predicted limits, ranging between -294 and -263°F at prelaunch commit and between -235 and -208°F at engine start. Thrust chamber temperature warmup rates during S-IC boost agreed closely with those experienced on previous flights.

Beginning with AS-507, the Ground Support Equipment (GSE) engine start tank pressurization regulator setting was increased from 1175 ±15 psia to 1225 ±25 psia, and the minimum pressure line of the prelaunch redline box was lowered approximately 10 psi. These changes were made to reduce the possibility of low start tank pressures which were experienced on AS-506. System performance was entirely satisfactory. Both temperature and pressure conditions of the start tanks were within the required prelaunch and engine start boxes as shown in Figure 6-1.

Start tank temperature and pressure increases during S-IC boost were nominal and close to AS-506 results except for engine No. 5. Engine No. 5 start tank pressure remained constant during the final 100 seconds of boost although the temperature warmed up approximately 2°F. Other engine start tank pressures increased 10 to 25 psia. It is concluded that engine No. 5 start tank pressure relief valve was relieving during this period, however, tank pressure at S-II ESC was nominal at 1310 psia.

All engine helium tank pressures were within the prelaunch and engine start limits of 2800 to 3450 psia. The helium tank pressures ranged between 3160 and 3230 psia at prelaunch (-19 seconds) and between 3250 and 3350 psia at S-II ESC.

The LOX and LH_2 recirculation systems used to chill the feed ducts, turbopumps, and other engine components performed satisfactorily during prelaunch and S-IC boost. Engine pump inlet temperatures and pressures at engine start were well within the requirements as shown in Figure 6-2. The LOX pump discharge temperatures at S-II ESC were 13.9 to 16.4°F subcooled, which is well below the 3°F subcooling requirement.

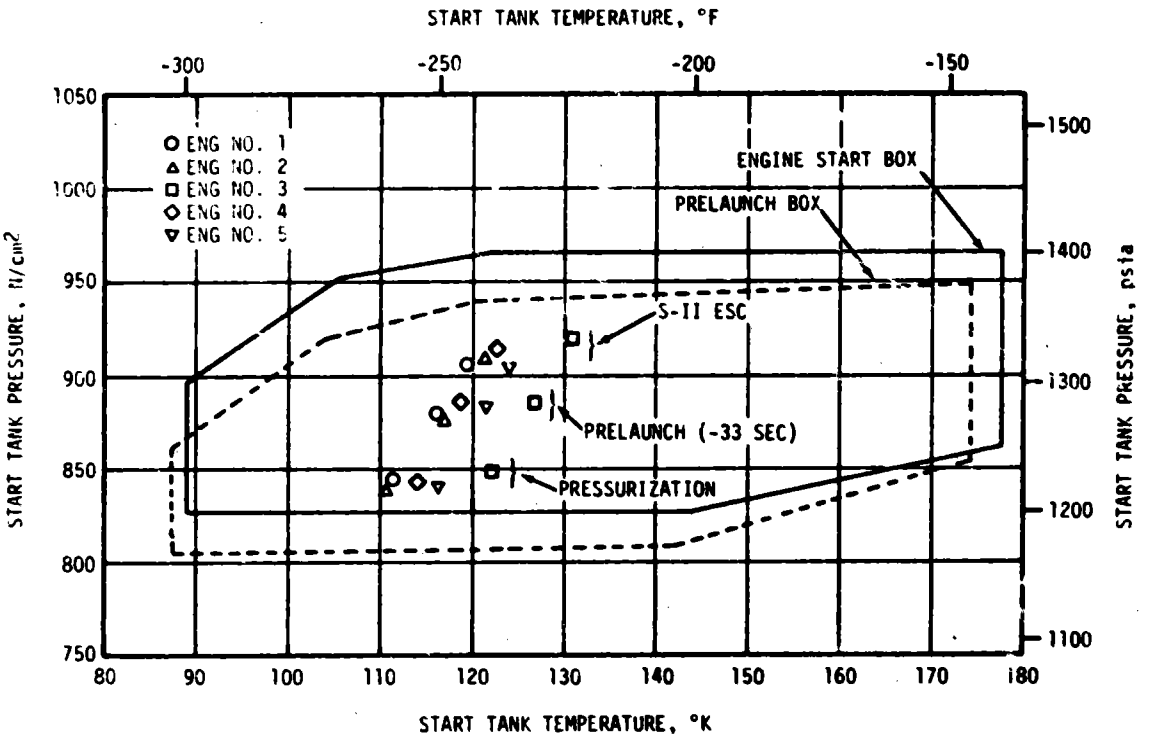

Figure 6-1. S-II Engine Start Tank Performance

Prepressurization of the propellant tanks was satisfactorily accomplished. Ullage pressures at S-II ESC were 40.2 psia for LOX and 28.5 psia for LH_2.

S-II ESC was received at 163.17 seconds and the Start Tank Discharge Valve (STDV) solenoid activation signal occurred 1.0 second later. The engine thrust buildup was satisfactory and within the required thrust buildup envelope. Two engines (No. 1 and 3) exhibited a slightly more rapid thrust buildup than the other engines, and also a small overshoot of the 100 percent thrust level at null EMR. This condition was caused by a slightly different opening action of the Main Oxidizer Valves (MOV) on these engines. The ramp rates were slower during the initial portion of the valve second stage positioning phase, however the overall valve opening times were not abnormal. Similar engine MOV operating characteristics have been infrequently observed on previous flight and stage acceptance testing. The stage thrust reached mainstage level at 166.4 seconds.

6.3 S-II MAINSTAGE PERFORMANCE

The propulsion reconstruction analysis showed that stage performance during mainstage operation was satisfactory. A comparison of predicted and reconstructed performance of thrust, specific impulse, total flowrate, and mixture ratio versus time is shown in Figure 6-3. Stage performance during the high EMR portion of the flight was very close to predicted.

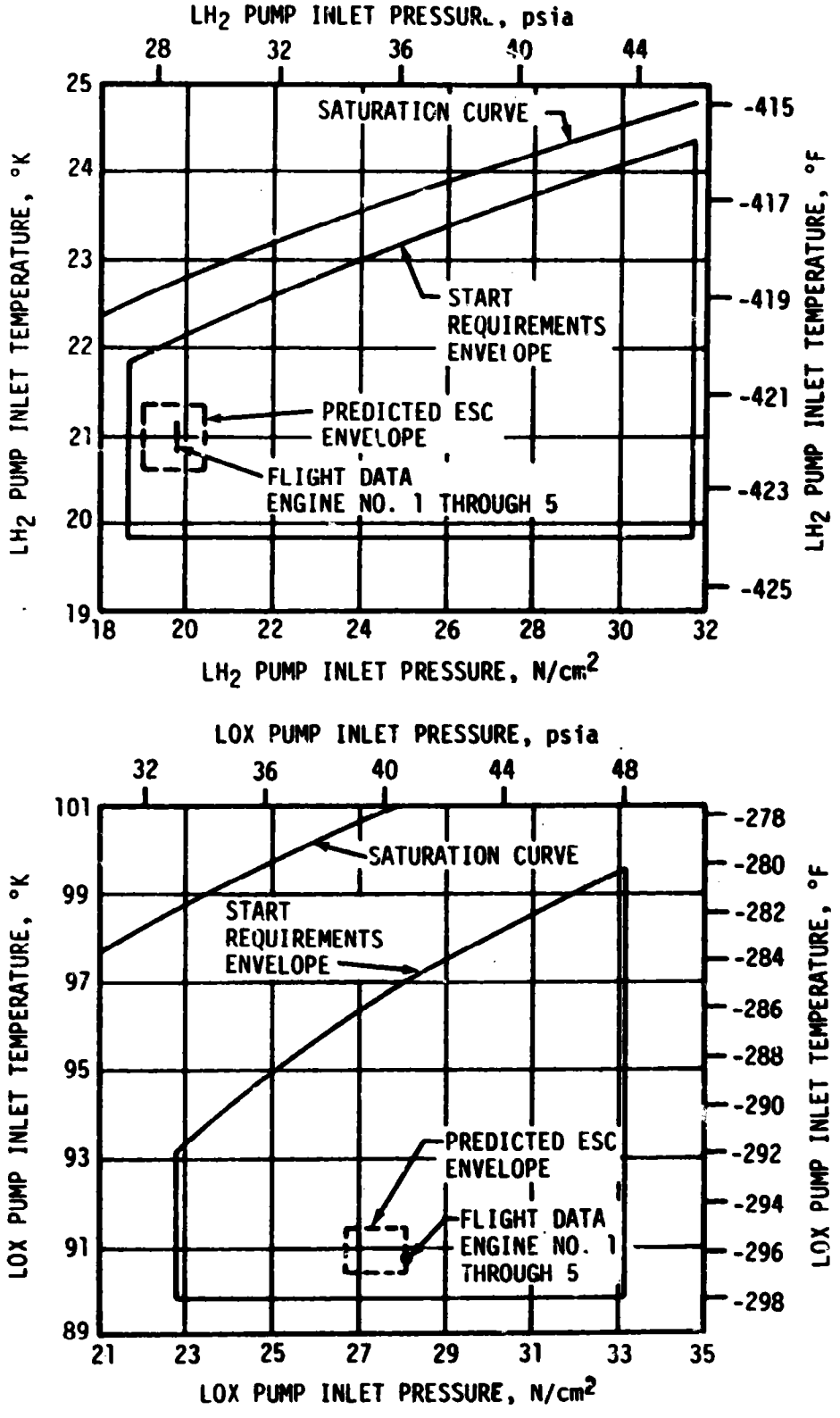

Figure 6-2. S-II Engine Pump Inlet Start Requirements

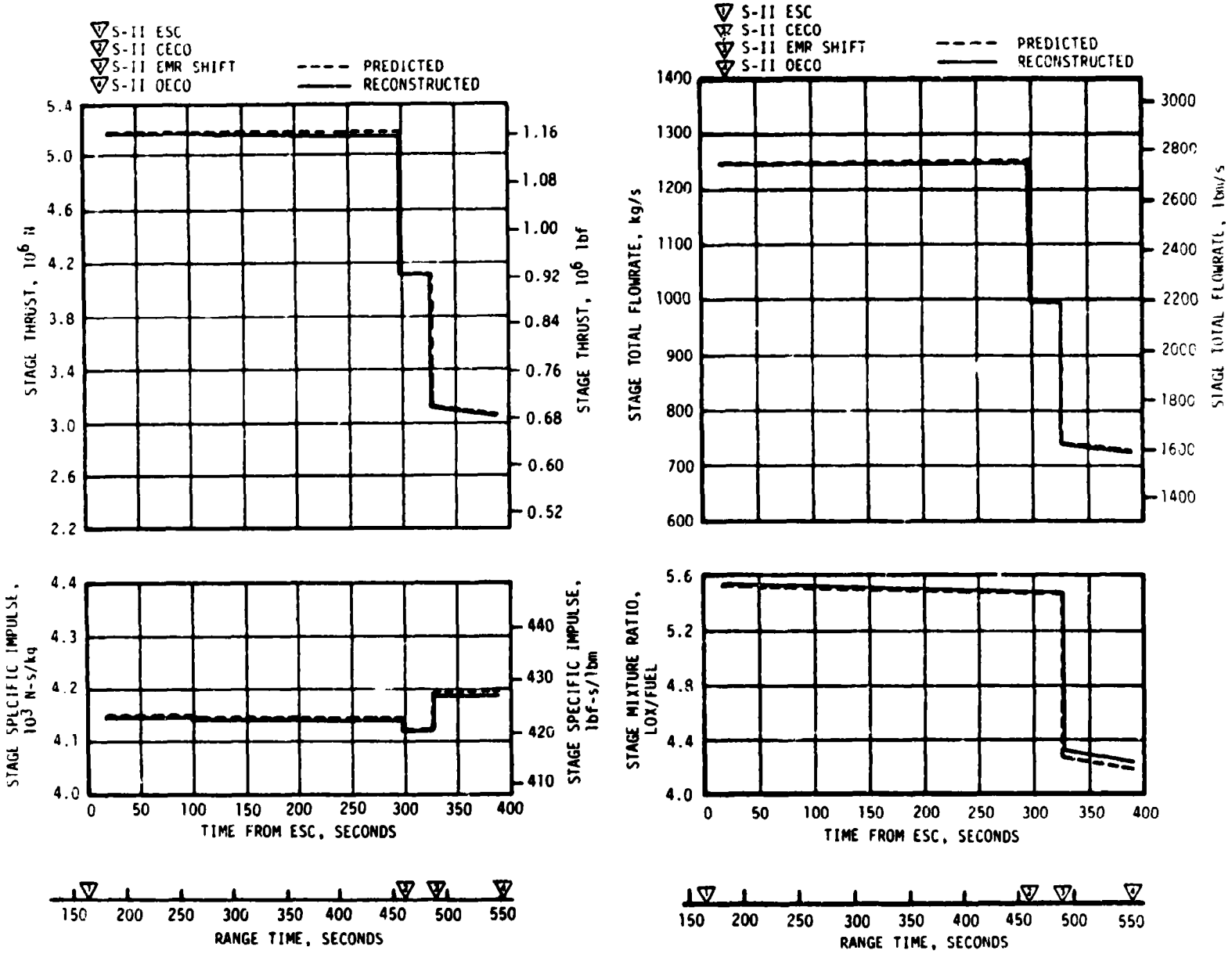

Figure 6-3. S-II Steady-State Operation

At a time slice of ESC +61 seconds, total stage thrust was 1,161,534 lbf which is only 557 lbf or 0.05 percent below the preflight prediction. Total propellant flowrate (including pressurization flow) was 2743 lbm/s which was identical to the prediction. Stage specific impulse, including the effect of pressurant gas flowrate, was 423.4 lbf-s/lbm which is 0.05 percent below the predicted level. Stage propellant MR was 0.36 percent above prediction.

At ESC +297.58 seconds (460.75 seconds), the center engine was shut down as planned. This action reduced total stage thrust by 231,089 lbf to a level of 925,145 lbf. The shift from high to low EMR operation occurred approximately 327 seconds after ESC. The change of EMR resulted in further thrust reduction, and at ESC +340 seconds the total stage thrust was 692,787 lbf; thus a decrease in thrust of 232,358 lbf is indicated between high and low EMR operation. The deviation of actual from predicted performance remained small at the lower EMR levels. S-II operation time from ESC to OECO was 389.17 seconds. The burn duration was 2.1 seconds longer than predicted.

Individual J-2 engine data, excluding the effects of pressurization flowrate, are presented in Table 6-1 for the ESC +61-second time point. Very good correlation between prediction and flight is indicated by the small deviations. Flight data reconstruction procedures were directed toward matching the engine and stage acceptance specific impulse values while maintaining the engine flow and pump speed data as a baseline.

Data presented in Table 6-1 are actual flight data and have not been adjusted to standard J-2 engine conditions. Considering data that have been adjusted to standard conditions through use of a computer program, very little difference from the results shown in Table 6-1 is observed. In comparison to the vehicle acceptance test performance, the adjusted data showed engine No. 1 to be 1.1 percent low and engine No. 2 to be 0.73 percent high in thrust, which agrees closely with performance levels achieved during engine acceptance testing.

A usual complement of minor engine performance shifts were observed during analysis of stage flight data. Available flight instrumentation does not permit a detailed investigation of the cause for each performance shift, however, the more familar ones can be recognized by their characteristic effects on basic flight parameters. A summary of identified engine performance shifts on AS-507 flight is given in Table 6-2. None of these shifts are presently considered to be unusual in either magnitude or cause. Low frequency oscillations in the 14 to 20 hertz region existed in propulsion parameters during four periods of the S-II burn. This is evident in all engine chamber pressures as seen in Figure 6-4. A detailed discussion of these oscillations is given in paragraph 9.2.3.

Table 6-1. S-II Engine Performance Deviations (ESC +61 Seconds)

PARAMETER	ENGINE	PREDICTED	RECONSTRUCTED	PERCENT INDIVIDUAL DEVIATION	PERCENT AVERAGE DEVIATION
Thrust, lbf	1	234,614	231,921	-1.15	
	2	231,399	233,298	0.82	
	3	231,642	232,413	0.33	-0.05
	4	231,559	231,113	-0.19	
	5	232,877	232,789	-0.04	
Specific Impulse, lbf-s/lbm	1	424.9	424.5	-0.09	
	2	425.8	425.4	-0.09	
	3	424.5	424.7	0.05	-0.06
	4	424.6	424.1	-0.12	
	5	426.0	425.8	-0.05	
Engine Flowrate, lbm/s	1	552.2	546.3	-1.07	
	2	543.4	548.4	0.92	
	3	545.7	547.2	0.27	0.01
	4	545.4	544.9	-0.09	
	5	546.6	546.7	0.02	
Engine Mixture Ratio, LOX/Fuel	1	5.56	5.59	0.54	
	2	5.48	5.53	0.91	
	3	5.60	5.57	-0.54	0.43
	4	5.56	5.59	0.54	
	5	5.53	5.57	0.72	

NOTE: Values exclude pressurization flow.

Table 6-2. S-II Engine Performance Shifts

ENGINE	MAGNITUDE	TYPE	TIME OF OCCURRENCE	REMARKS
1	-1800 lbf	In-run thrust shift	ESC +128 sec (291 sec)	Shift in Gas Generator (GG) oxidizer system resistance.
	-1300 lbf	Run-to-run thrust shift from engine acceptance value.	Throughout operation	Under evaluation (suspected GG system resistance shift).
3	-1800 lbf	In-run thrust shift	ESC +114 sec (277 sec)	Shift in GG oxidizer system resistance.
	+1800 lbf	In-run thrust shift	ESC +337 sec (500 sec)	Under evaluation (suspected PU system resistance shift).
5	-1200 lbf	In-run thrust decay and recovery	Between ESC +60 and ESC +105 sec (223 and 268 sec)	Under evaluation.
	-1700 lbf	In-run thrust shift	ESC +194 sec (357 sec)	Shift in GG oxidizer system resistance.
All Engines	Relatively small cyclic changes	In-run low frequency thrust oscillations	Four periods: 180 to 205 sec 225 to 267 sec 268 to 351 sec 405 to 465 sec	Refer to paragraph 9.2.3 for discussion on low frequency oscillations.

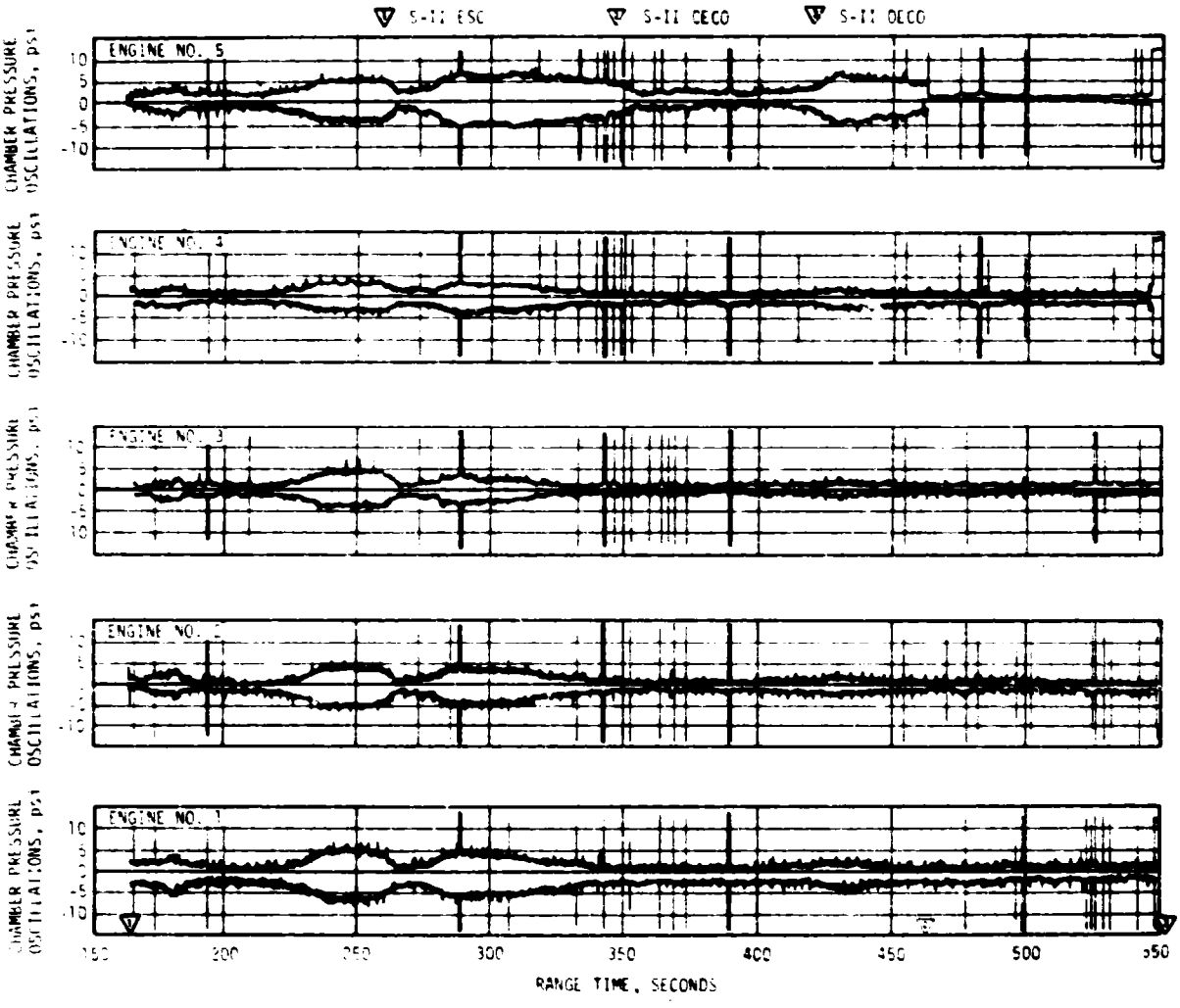

Figure 6-4. S-II Chamber Pressure Oscillations

6.4 S-II SHUTDOWN TRANSIENT PERFORMANCE

S-II CECO at the high EMR occurred on schedule at 460.75 seconds. Engine No. 5 shutdown transients were satisfactory with the decay to 5 percent thrust occurring in approximately 0.3 second.

S-II OECO sequence was initiated by the stage LOX low level sensors. The LOX depletion cutoff system again included 1.5-second delay timers. As in the three preceding flights utilizing 1.5-second delay timers (AS-504, AS-505 and AS-506), this resulted in engine thrust decay (observed as a drop in chamber pressure) prior to receipt of the cutoff signal. Due to early CECO however, the pre-cutoff decay was greatly reduced compared with AS-504 with five engines operating at shutdown. Similar to the last two flights, with four engines operating at shutdown, only engine No. 1 exhibited a significant thrust chamber pressure decay (decreased 103 psi in the final 0.33 second before cutoff). All other outboard engines thrust chamber pressure decays were approximately 27 psi.

At S-II OECO signal (552.34 seconds), total stage thrust was down to 611,266 lbf. Stage thrust dropped to 5 percent of this level within 0.75 second. The stage cutoff impulse through the 5 percent thrust level was estimated to be 113,520 lbf-s.

6.5 S-II STAGE PROPELLANT MANAGEMENT

The propellant management system performed satisfactorily during the propellant loading operation and during flight. The S-II stage employed an open-loop system utilizing fixed, open-loop commands from the IU rather than feedback signals from the tank mass sensing probes. (Open-loop operation was also used on AS-503, AS-505, and AS-506. It is also planned for use on all subsequent vehicles).

The facility Propellant Tanking Control System (PTCS) and the propellant management system successfully accomplished S-II loading and replenishment. During the prelaunch countdown, all propellant management subsystems operated properly with no problems noted.

The open-loop PU system responded as expected during flight and no instabilities were noted. Open-loop PU system operation commenced when "High EMR Select" was commanded at ESC +5.6 seconds, as planned. The PU valves then moved to the high EMR position, providing an average high EMR of 5.53 for the first phase of Programed Mixture Ratio (PMR). The IU command to shift EMR from high to low was initiated at ESC +324.2 seconds (0.5 seconds later than for the predicted trajectory) upon attainment of a preprogramed characteristic velocity as sensed by the LVDC. This deviation is attributed to time delays within the LVDC occurring after the target velocity was achieved and variations between the actual and predicted flight performance. The IU command caused the PU valves to be driven to the low EMR position, providing an average EMR of 4.40 (versus a predicted average EMR of 4.33) for the low MR portion of the flight.

The open-loop PU error at OECO was approximately 90 lbm LH_2 versus a 3-sigma tolerance of ±2500 lbm. Based on PU system data, propellant residuals (mass in tanks and LOX sump) at OECO were 1800 lbm of LOX and 4338 lbm of LH_2. The LOX residual, although differing from the official trajectory prediction, is identical to the LOX residual on the previous two flights and is considered normal for the 1.5-second time delay used in the LOX depletion engine cutoff system. Using the updated LOX residual predicted value for AS-507 would have resulted in a zero PU error. Future flight predictions (with 1.5-second timers) will reflect the new LOX residual value of 1800 lbm.

Table 6-3 presents a comparison of propellant masses as measured by the PU probes and engine flowmeters. The best estimate propellant mass is based on integration of flowmeter data utilizing the propellant residuals determined from PU system data corrected for nominal tank mismatch at OECO. Best estimates of propellant mass loaded correlates closely with the

Table 6-3. S-II Propellant Mass History

EVENT RANGE TIME	PREDICTED		PU SYSTEM ANALYSIS		ENGINE FLOWMETER INTEGRATION (BEST ESTIMATE)	
	LOX	LH_2	LOX	LH_2	LOX	LH_2
Ground Ignition, lbm	819.083	158,000	819,533*	157,613*	823,781	157,755
S-II ESC, lbm	819,083	158,000	923,149	157,445	823,781	157,755
S-II PU Valve Step (489.57 sec), lbm	83,072	23,492	88,144	23,470	86,100	24,563
S-II OECO, lbm	1452	4335	1800**	4338**	1800	4338
S-II Residual After Thrust Decay, lbm	1207	4225	Data not usable	Data not usable	1629	4284

NOTE: Table is based on mass in tanks and sump only. Propellant trapped external to tanks and LOX sump is not included.
*Based on pressurized ground loading data. Other PU system propellant quantities are based on flight data.

**Corrected data for a nominal tank mismatch.

postlaunch trajectory simulation. These mass values are 4698 lbm or 0.57 percent more than predicted for LOX and 245 lbm or 0.16 percent less than predicted for LH_2. The longer than predicted S-II burn duration (approximately 2 seconds) is attributed primarily to the LOX overload and to variations between predicted and actual performance.

6.6 S-II PRESSURIZATION SYSTEMS

6.6.1 S-II Fuel Pressurization System

LH_2 tank ullage pressure, actual and predicted, is presented in Figure 6-5 for autosequence, S-IC boost and S-II boost. The LH_2 tank vent valves were closed at -96 seconds and the ullage was pressurized to 35.7 psia in approximately 27.5 seconds. One makeup cycle was required at -44.6 seconds as a result of thermal pressure decay. Venting occurred during S-IC boost as anticipated. One venting cycle was indicated on vent valve No. 1 between 90.5 and 94.2 seconds. There was no indication that vent valve No. 2 opened. Differential pressure across the vent valve was kept below the low-mode upper limit of 29.5 psid. Ullage pressure at S-II engine start was 28.5 psia meeting the minimum engine start requirement of 27 psia. The LH_2 tank valves were switched to the high vent mode immediately prior to S-II engine start.

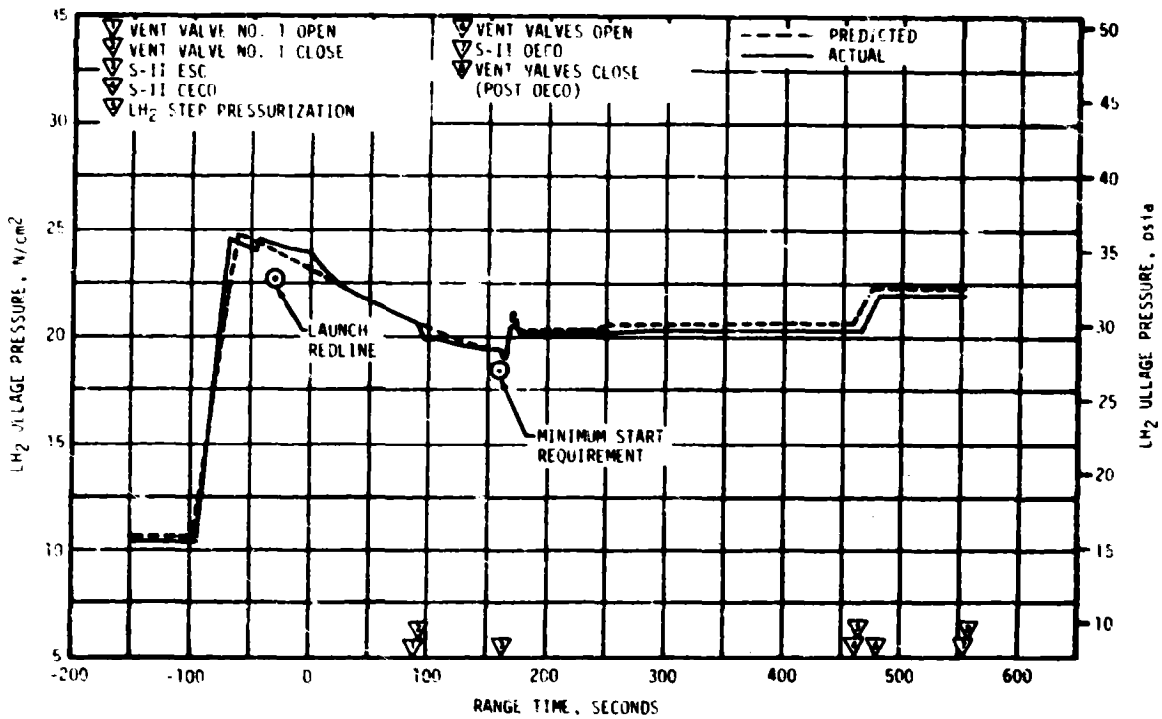

Figure 6-5. S-II Fuel Tank Ullage Pressure

LH_2 tank ullage pressure was maintained within the regulator range of 28.5 to 30 psia during burn until the LH_2 tank pressure regulator was stepped open at 461.7 seconds. Ullage pressure increased to 31.9 psia. The LH_2 vent valves started venting at 479.6 seconds and continued venting throughout the remainder of the S-II flight. Ullage pressure remained within the high-mode vent range of 30.5 to 33 psia.

Figure 6-6 shows LH_2 total inlet pressure, temperature and Net Positive Suction Pressure (NPSP). The parameters were close to predicted values. The NPSP supplied exceeded the minimum required throughout the S-II burn phase of the flight.

6.6.2 S-II LOX Pressurization System

LOX tank ullage pressure, actual and predicted, is presented in Figure 6-7 for autosequence, S-IC boost and S-II burn. After a 2-minute cold helium chilldown flow through the LOX tank, the vent valves were closed at -185.4 seconds and the LOX tank was prepressurized to the pressure switch setting of 38.9 psia in approximately 49.7 seconds. One pressure makeup cycle was required at -98 seconds as a result of pressure decay, which was followed by the slight pressure increase caused by LH_2 tank prepressurization. Ullage pressure was 40.2 psia at engine start.

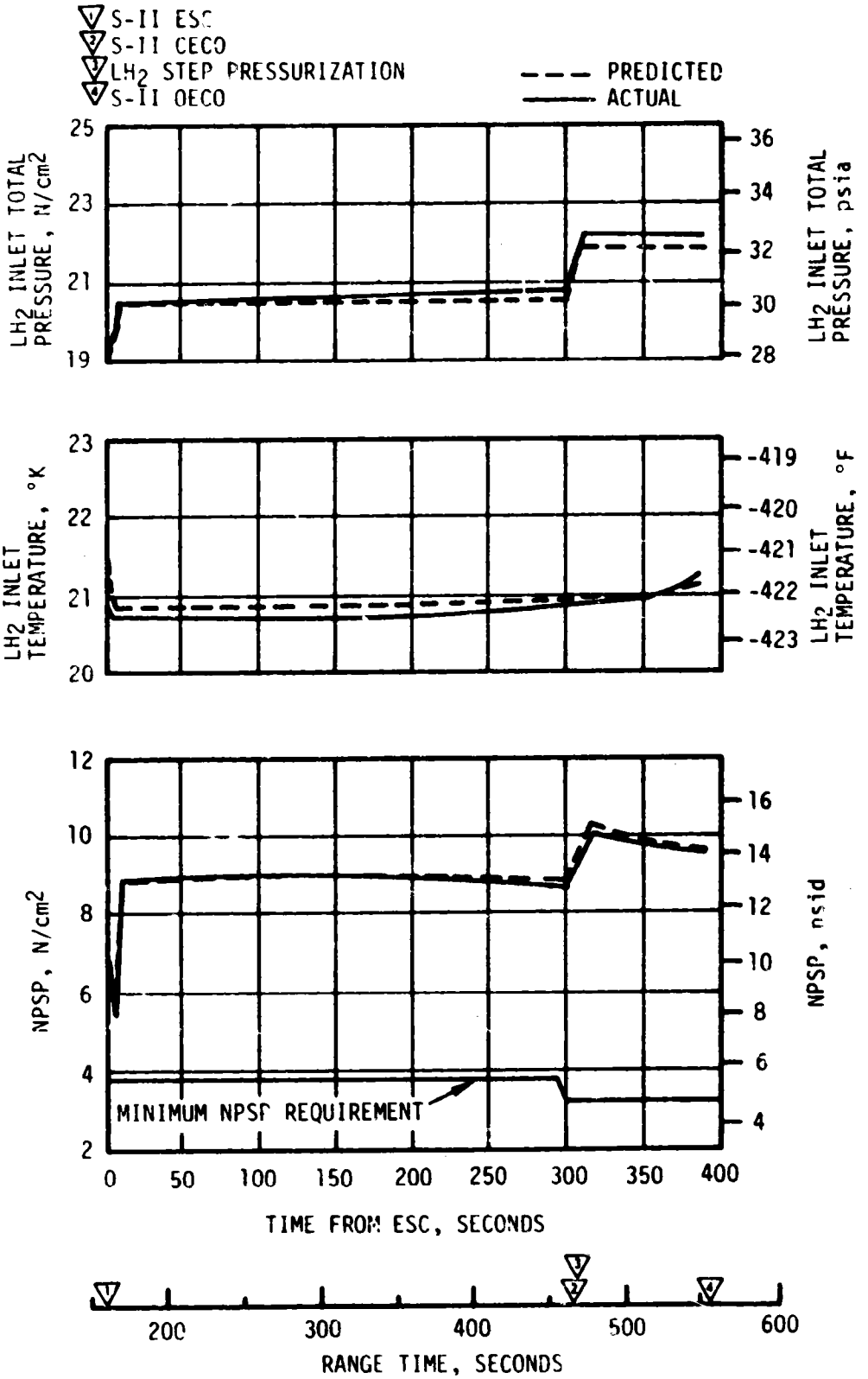

Figure 6-6. S-II Fuel Pump Inlet Conditions

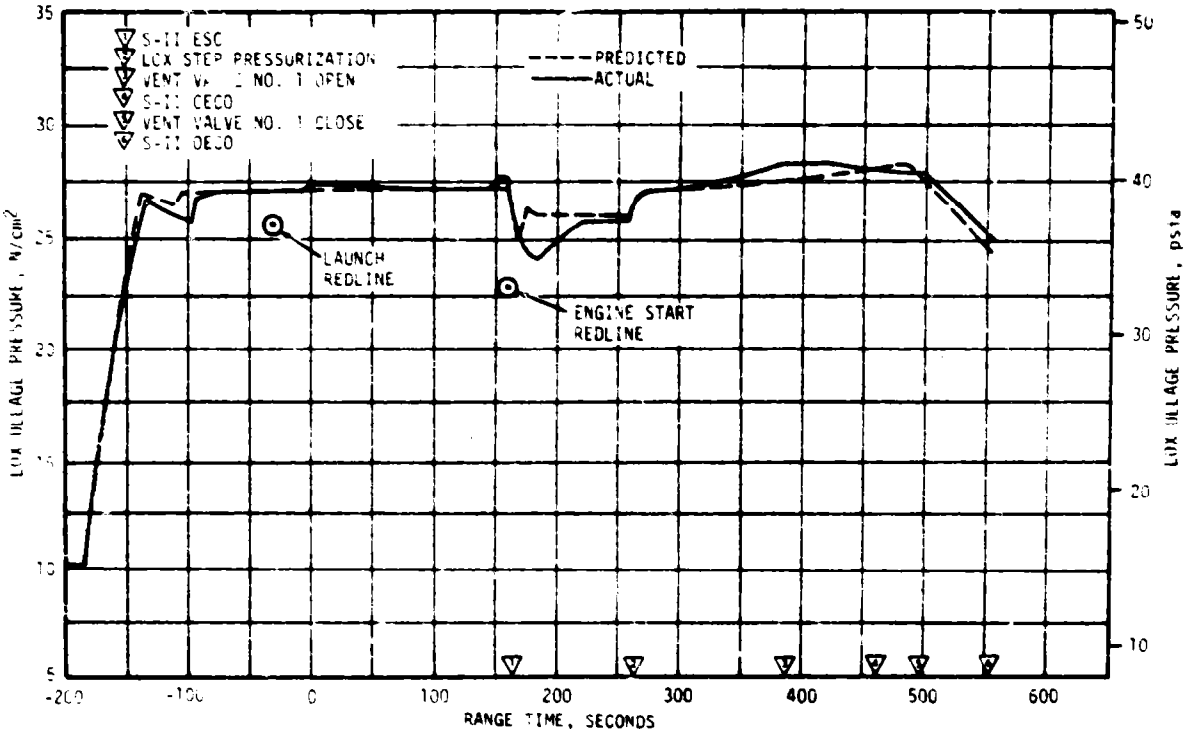

Figure 6-7. S-II LOX Tank Ullage Pressure

After the ullage pressure recovered from the initial drop at engine start, the pressure was controlled within the LOX pressurization regulator range of 36 to 38.5 psia until step pressurization. LOX step pressurization (261.7 seconds) caused the usual characteristic surge in ullage pressure followed by a slower increase until LOX tank ullage pressure reached a maximum of 40.9 psia at 386.4 seconds when the No. 1 vent valve cracked. Vent valve No. 1 reseat occurred at 40.7 psia after EMR shift. The LOX tank vent valve No. 2 did not open.

LOX pump total inlet pressure, temperature and NPSP are presented in Figure 6-8. The NPSP supplied exceeded the minimum requirement throughout the S-II boost phase. The total magnitude of LOX liquid stratification was greater than predicted. It is difficult to predict accurate temperatures at cutoff due to the 1.5-second time delay in the LOX low level cutoff circuit.

6.7 S-II PNEUMATIC CONTROL PRESSURE SYSTEM

During the initial launch countdown checkout for AS-507 flight, the valve actuation system receiver pressure decay exceeded the maximum allowable limit of 6.4 psi/min with the eleven recirculation valves closed. Five additional tests were performed to establish the receiver decay rates. The decay rates ranged from 18 psi/min for the initial test to 11.4 psi/min for the final test, with the decay rates becoming

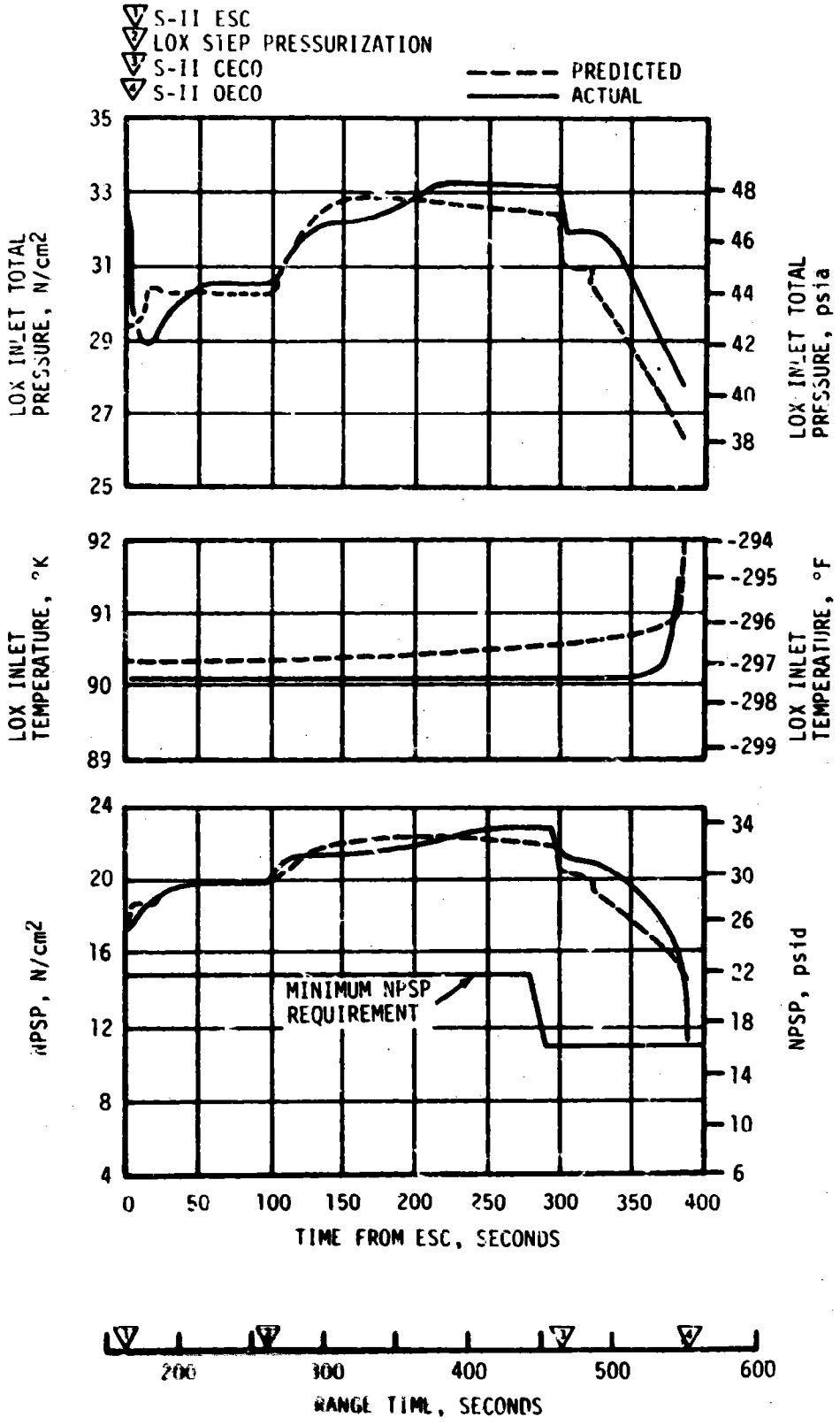

Figure S-II LOX Pump Inlet Conditions

smaller for each progressive test. It has been assessed that leakage indications during the tests were a result of thermal effects. Since there was a time interval (several minutes) between tests, gas temperatures stabilizing within the actuation system lines would cause a decay in pressure. This conclusion is further substantiated by AS-507 flight data.

At -30 seconds the receiver pressure in the valve actuation system was approximately 3050 psia. The minimum acceptable pressure for flight at -19 seconds is 2800 psia. At S-II engine start, prior to the actuation closure of the eleven recirculation valves, the receiver pressure had decayed to approximately 3040 psia. The receiver pressure dropped 160 psia when the eleven recirculation valves were actuated closed at S-II engine start; the predicted pressure drop was 150 psia. At CECO the center engine prevalves were closed which resulted in a 30 psi drop in receiver pressure; the predicted pressure drop was 50 psi. Prevalve closure at OECO resulted in a total pressure drop in the receiver of 190 psi; the predicted pressure drop was 200 psi.

An engineering change is presently being processed to revise the Test Specifications and Criteria Document which will allow a receiver pressure decay rate of 25 psi/min. In addition, a procedural change is planned to permit more time after receiver pressurization before making checks for pressure decay rates.

Regulator outlet pressure during flight remained at a constant 715 psia, except for the momentary pressure drops when the recirculation valves were actuated closed at engine start, and when the center engine and four outboard engine prevalves were actuated closed after the engines were cut off. The recovery period for the regulator outlet pressure did not exceed 20 seconds for any of the events mentioned above. The normal regulator band is 690 to 765 psia.

6.8 S-II HELIUM INJECTION SYSTEM

The performance of the helium injection system was satisfactory. Requirements were met and parameters were in good agreement with predictions. The supply bottle was pressurized to 3100 psia prior to liftoff and by ESC was 750 psia. Helium injection system average total flowrate during supply bottle blowdown (-30 to 163.03 seconds) was 72 SCFM.

SECTION 7

S-IVB PROPULSION

7.1 SUMMARY

The J-2 engine operated satisfactorily throughout the operational phase of first and second burn and had normal shutdowns. S-IVB first burntime was 137.3 seconds which was 2.5 seconds longer than predicted. The engine performance during first burn, as determined from standard altitude reconstruction analysis, deviated from the predicted Start Tank Discharge Valve (STDV) open +127-second time slice by 0.40 percent for thrust. Specific impulse was as predicted. The S-IVB stage first burn Engine Cutoff (ECO) was initiated by the Launch Vehicle Digital Computer (LVDC) at 693.91 seconds.

The Continuous Vent System (CVS) adequately regulated LH_2 tank ullage pressure at an average level of 19.0 psia during orbit, and the Oxygen/Hydrogen (O_2/H_2) burner satisfactorily achieved LH_2 and LOX tank repressurization for restart. However, the O_2/H_2 burner oxidizer valve did not shutdown at the programed time due to an intermittent electrical "open" circuit. This failure resulted in burnthrough of the LH_2 repress coil in the O_2/H_2 burner. Engine restart conditions were within specified limits. The restart at full open Propellant Utilization (PU) valve position was successful.

S-IVB second burntime was 341.2 seconds which was 3.8 seconds less than predicted. The engine performance during second burn, as determined from the standard altitude reconstruction analysis, deviated from the predicted STDV +172-second time slice by 0.76 percent for thrust and 0.05 percent for specific impulse. Second burn ECO was initiated by the LVDC at 10,383.89 seconds.

Subsequent to second burn, the stage propellant tanks were safed satisfactorily, with sufficient impulse being derived from the LOX dump to impart 32.8 ft/s to stage velocity.

7.2 S-IVB CHILLDOWN AND BUILDUP TRANSIENT PERFORMANCE FOR FIRST BURN

The propellant recirculation systems performed satisfactorily, meeting start and run box requirements for fuel and LOX as shown in Figure 7-1. The thrust chamber temperature at launch was well below the maximum allowable redline limit of -130°F. At S-IVB first burn ESC, the temperature was -136°F, which is within the requirement of -189.6 ±110°F.

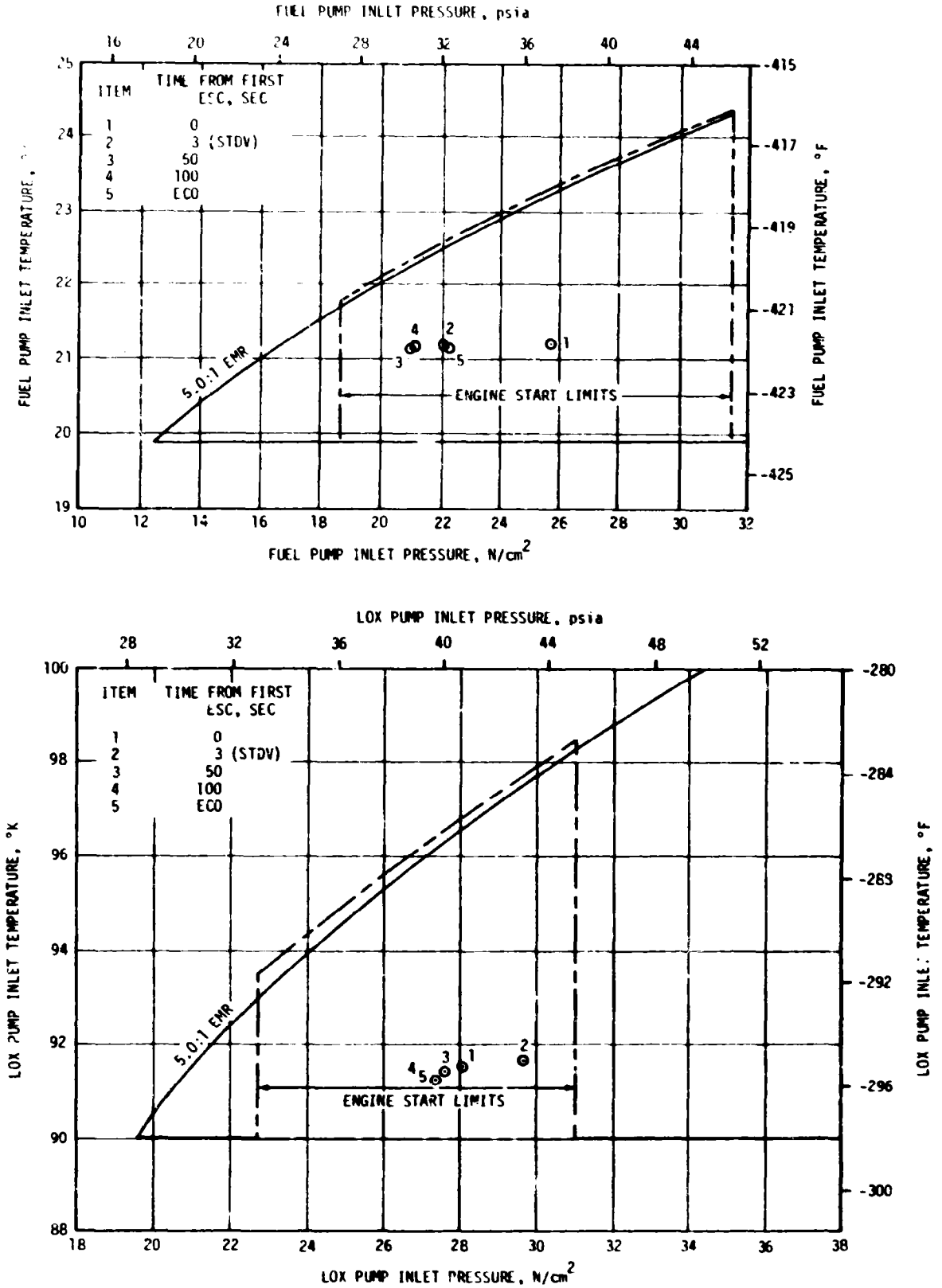

Figure 7-1. S-IVB Start Box and Run Requirements - First Burn

The chilldown and loading of the engine Gaseous Hydrogen (GH_2) start tank and pneumatic control sphere prior to liftoff was satisfactory. At first burn Engine Start Command (ESC) the start tank conditions were within the required region of 1325 ±75 psia and -170 ±30°F for start. The discharge was completed and the refill initiated at first burn ESC +3.4 seconds. The refill was satisfactory and in good agreement with the acceptance test.

The engine control bottle pressure and temperature at liftoff were 3040 psia and -170°F. LOX and LH_2 systems chilldown, which was continuous from before liftoff until just prior to first ESC, was satisfactory. At first ESC, the LOX pump inlet temperature was -295.3°F and the LH_2 pump inlet temperature was -421.9°F.

The first burn start transient was satisfactory. The thrust buildup was within the limits set by the engine manufacturer. This buildup was similar to the thrust buildups observed on AS-506 and AS-505. The PU valve was in the null position prior to first start, but shifted 0.7 degree during start as expected. The total impulse from STDV open to STDV open +2.5 seconds was 193,373 lbf-s for first start.

First burn fuel lead followed the predicted pattern and resulted in satisfactory conditions as indicated by the thrust chamber temperatures and the associated fuel injector temperatures.

7.3 S-IVB MAINSTAGE PERFORMANCE FOR FIRST BURN

The propulsion reconstruction analysis showed that the stage performance during mainstage operation was satisfactory. A comparison of predicted and actual performance of thrust, total flowrate, specific impulse, and Mixture Ratio (MR) versus time is shown in Figure 7-2. Table 7-1 shows the specific impulse, flowrates and MR deviations from the predicted at the STDV +127-second time slice.

The performance of the J-2 engine helium control system was satisfactory during mainstage operation. The engine control bottle was connected to the stage ambient repressurization bottles, therefore, there was little pressure decay. Helium usage was approximately 0.24 lbm during first burn.

The PU valve position shifted from null to 0.7 degree during first burn and shifted 0.6 degree during second burn. These shifts are approximately the same as those observed on the AS-505 and AS-506 flights and the S-IVB-508 and S-IVB-509 acceptance tests. This observed 0.6 to 0.8 degree shift in valve position during null PU operation is expected to occur on AS-508 and subsequent flights.

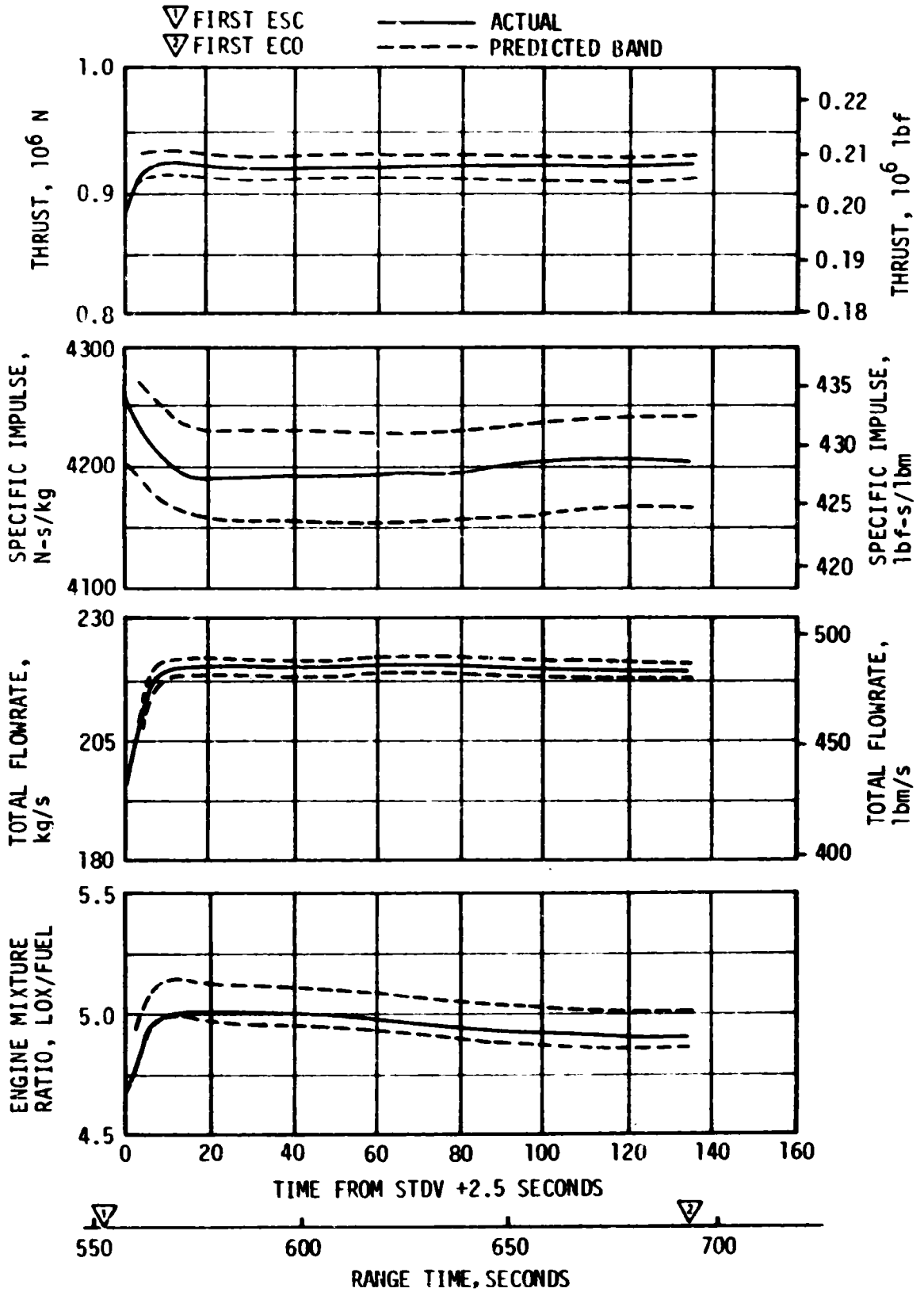

Figure 7-2. S-IVB Steady-State Performance - First Burn

Table 7-1. S-IVB Steady-State Performance - First Burn
(STDV +127-Second Time Slice at Standard Altitude Conditions)

PARAMETER	PREDICTED	RECONSTRUCTION	FLIGHT DEVIATION	PERCENT DEVIATION FROM PREDICTED
Thrust, lbf	206,125	206,956	831	0.40
Specific Impulse, lbf-s/lbm	428.91	428.90	-0.01	-0.002
LOX Flowrate, lbm/s	399.15	400.27	1.12	0.28
Fuel Flowrate, lbm/s	81.43	82.26	0.83	1.02
Engine Mixture Ratio, LOX/Fuel	4.902	4.866	-0.036	-0.82

7.4 S-IVB SHUTDOWN TRANSIENT PERFORMANCE FOR FIRST BURN

S-IVB first ECO was initiated at 693.91 seconds by a guidance velocity cutoff command which resulted in a burntime of 137.3 seconds, which was 2.5 seconds longer than predicted.

The ECO transient was satisfactory and agreed closely with the acceptance test and predictions. The total cutoff impulse to zero percent of rated thrust was 45,344 lbf-s. Cutoff occurred with the PU valve in the null position.

7.5 S-IVB PARKING ORBIT COAST PHASE CONDITIONING

The LH_2 CVS performed satisfactorily, maintaining the fuel tank ullage pressure at an average level of 19.0 psia. This was slightly below the previous flight data, but well above the level (17.0 psia) requiring corrective action by ground command. The lower than expected regulation level did not have a significant effect on orbital boiloff. The effect of this regulation level on CVS impulse is discussed in paragraph 10.2.1.

The continuous vent regulator was activated at 753.1 seconds and was terminated at 9501 seconds. The CVS performance is shown in Figure 7-3.

Calculations based on estimated temperatures indicate that the mass vented during parking orbit was 2174 lbm and that the boiloff mass was 2407 lbm.

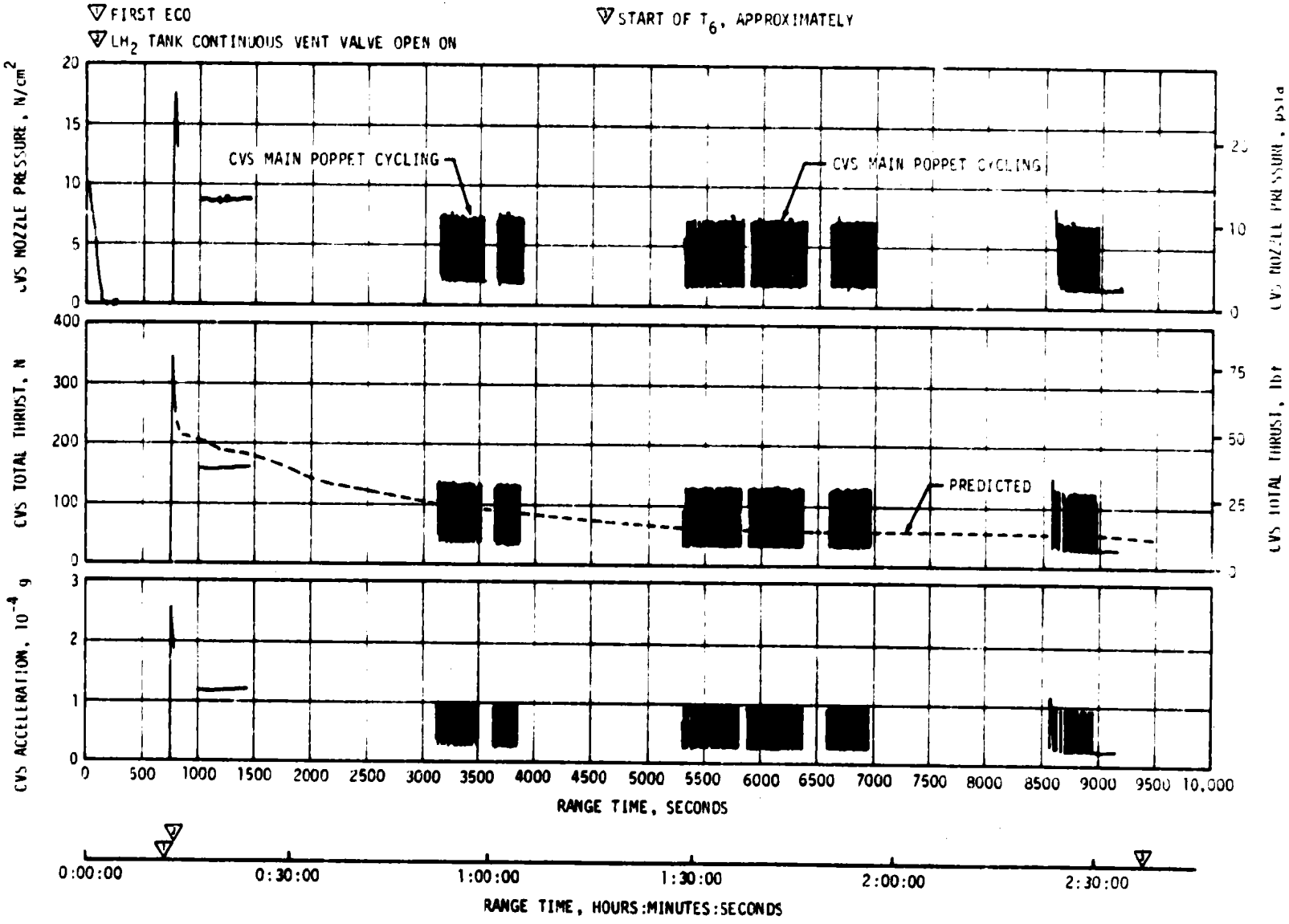

Figure 7-3. S-IVB CVS Performance - Coast Phase

7.6 S-IVB CHILLDOWN AND RESTART FOR SECOND BURN

The S-IVB LOX recirculation system satisfactorily provided properly conditioned oxidizer to the J-2 engine for restart. Fuel recirculation system performance was adequate and conditions at the pump inlet were satisfactory at second STDV. The LOX and fuel pump inlet conditions are plotted in the start and run boxes in Figure 7-4. At second ESC, the LOX and fuel pump inlet temperatures were -294.8°F and -419.0°F, respectively. Second burn fuel lead generally followed the predicted pattern and resulted in satisfactory conditions as indicated by thrust chamber temperature and the associated fuel injector temperature. The start tank performed satisfactorily during second burn blowdown and recharge sequence. The engine start tank was recharged properly and maintained sufficient pressure during coast. However, the relief valve was relieving at approximately 1280 psia. This pressure was below the expected relief setting of 1325 ±25 psia but within acceptable operating requirements. The engine control sphere first burn gas usage was as predicted; the ambient helium spheres recharged the control sphere to a nominal level for restart.

The second burn start transient was satisfactory. The thrust buildup was within the limits set by the engine manufacturer and was similar to the thrust buildup on AS-506 and AS-505. The PU valve was in the proper full open (4.5 EMR) position prior to the second start. The total impulse from STDV open to STDV open +2.5 seconds was 179,996 lbf-s.

At 9965.7 seconds the O_2/H_2 burner oxidizer shutdown valve was commanded closed as part of the burner automatic cutoff sequence. The command was not received at the actuation control module (see paragraph 12.4) and therefore the oxidizer valve did not close. The burner chamber temperature increased as the mixture ratio became LOX rich as shown in Figure 7-5 and eventually caused a burnthrough of the LH_2 tank repress primary helium coil. LH_2 tank ullage gas, and later LH_2 pressurant gas from the J-2 engine fed back through the burned out coil to sustain combustion. Combustion continued in this manner, providing a low level of thrust, until 10,350 seconds when the burner oxidizer supply line inlet, located in the oxidizer tank, was uncovered by a falling LOX level. LOX tank ullage gas continued to flow through the burner until 10,554 seconds when a ground initiated command was successful in closing the oxidizer valve. After engine cutoff, the LH_2 tank ullage gas continued to flow out through the burner except during helium dumps. Ambient and cold helium dumps were made through the LH_2 tank pressurization system and the LH_2 tank ullage gas flow was temporarily blocked. After Lunar Module (LM) ejection at 15,180.9 seconds, there is evidence, as shown in Figure 7-6, of some restriction of the burner nozzle by formation of solid hydrogen. It was during this time period (approximately 15,000 to 16,000 seconds) that the astronauts observed and photographically recorded two directional (radial and aft direction) cyclic venting emanating from the burner area.

At 15,001.2 seconds, the cold helium dump was initiated. The flow of cold helium through the burner apparently caused solid hydrogen to

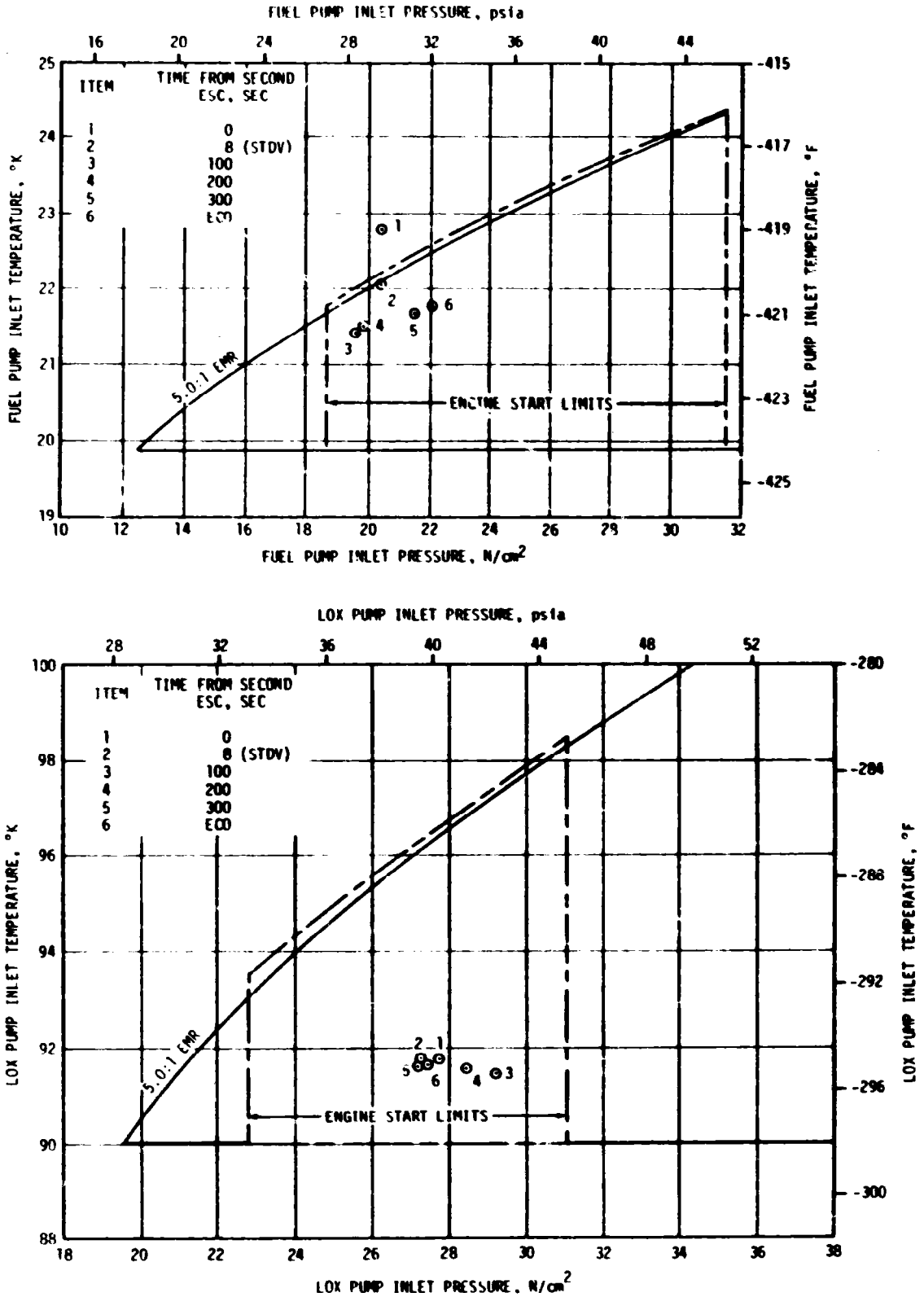

Figure 7-4. S-IVB Start Box and Run Requirements - Second Burn

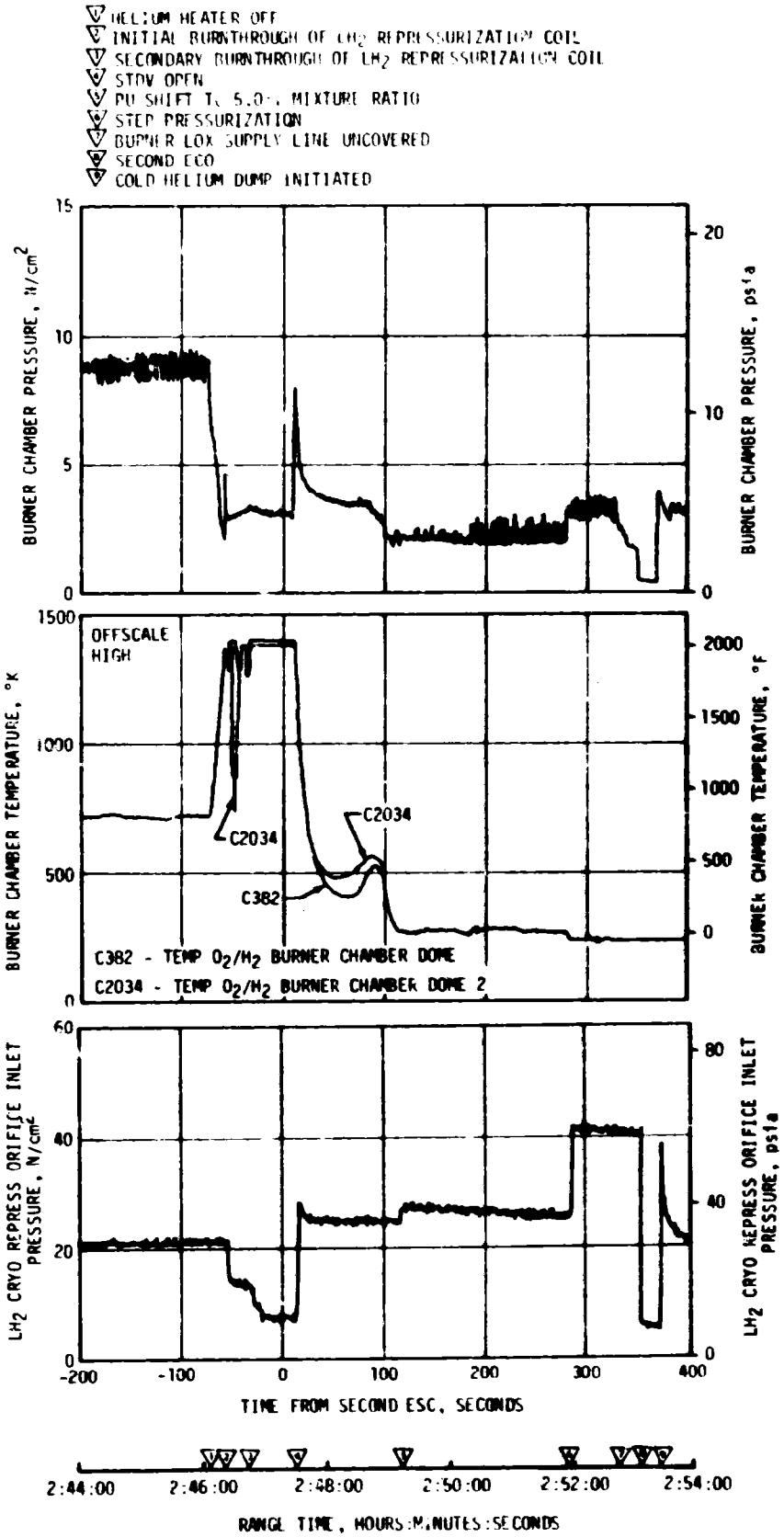

Figure 7-5. O_2/H_2 Burner Anomaly

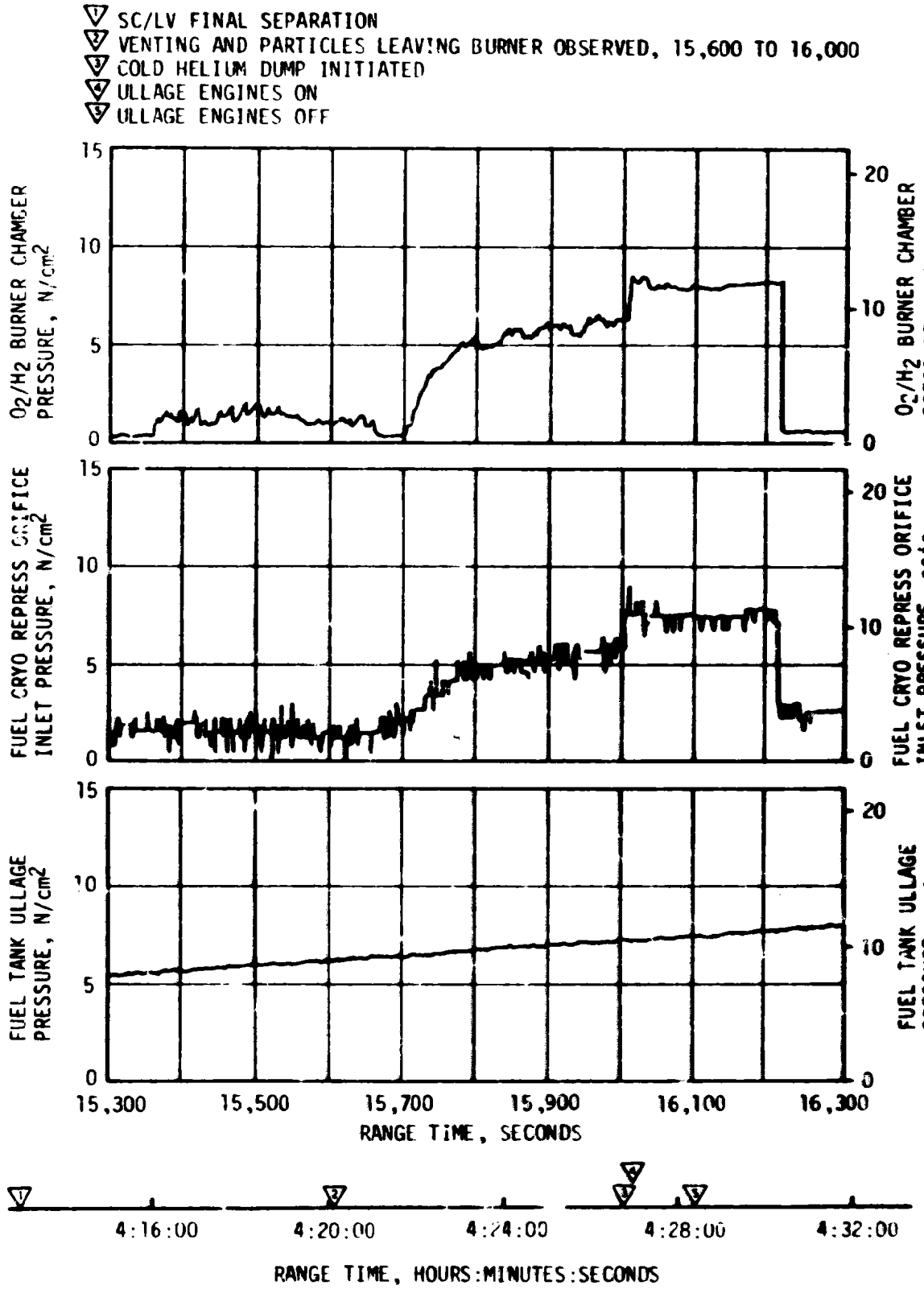

Figure 7-6. O_2/H_2 Burner Conditions During Translunar Orbit

plug the burner nozzle. The data in Figure 7-6 show an equalization of pressure between the burner chamber and the LH_2 tank ullage pressure. At 16,213 seconds, the burner chamber pressure dropped abruptly from 12 to 1 psia, apparently as a result of unplugging the burner nozzle.

The O_2/H_2 burner cutoff anomaly did not result in any problems in attainment of mission objectives.

The helium control system performed satisfactorily during second burn mainstage. There was little pressure decay during the burn due to the connection to the stage repressurization system. Approximately 0.60 lbm of helium was consumed during second burn.

7.7 S-IVB MAINSTAGE PERFORMANCE FOR SECOND BURN

The propulsion reconstruction analysis showed that the stage performance during mainstage operation was satisfactory. A comparison of predicted and actual performance of thrust, total flowrate, specific impulse, and mixture ratio versus time is shown in Figure 7-7. Table 7-2 shows the specific impulse, flowrates and MR deviations from the predicted at the STDV +172-second time slice.

7.8 S-IVB SHUTDOWN TRANSIENT PERFORMANCE FOR SECOND BURN

S-IVB second ECO was initiated at 10,383.89 seconds by a guidance velocity cutoff command for a burntime of 341.2 seconds. This burntime was 3.8 seconds shorter than predicted.

The transient was satisfactory and agreed closely with acceptance test and predictions. The total cutoff impulse to zero thrust was 45,729 lbf-s. Cutoff occurred with the PU valve in the null position.

7.9 S-IVB STAGE PROPELLANT MANAGEMENT

The PU system was operated in the open-loop mode. The PU system successfully accomplished the requirements associated with propellant loading.

A comparison of propellant mass values at critical flight events, as determined by various analyses, is presented in Table 7-3. The best estimate full load propellant masses were 0.36 percent greater for LOX and 0.37 percent greater for LH_2 than the predicted values. These deviations were well within the required loading accuracies.

Extrapolation of propellant level sensor data to depletion, using propellant flowrates, indicated that a LOX depletion cutoff would have occurred approximately 10.14 seconds after second burn velocity cutoff.

During first burn, the PU valve was positioned at null for start and remained there, as programed, for the duration of the burn. The PU valve was commanded to the 4.5 EMR position 120.6 seconds prior to second ESC,

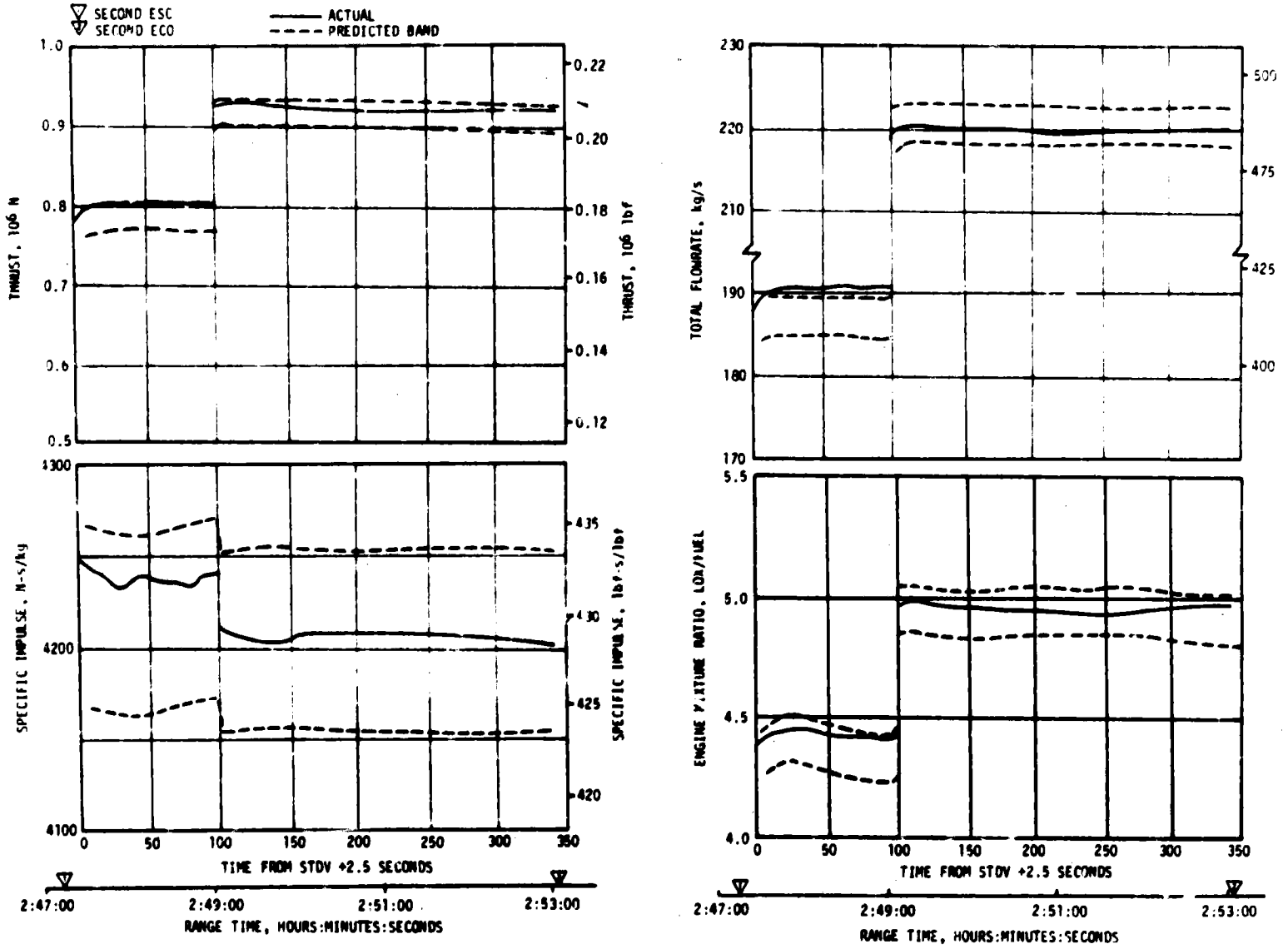

Figure 7-7. S-IVB Steady-State Performance - Second Burn

Table 7-2. S-IVB Steady-State Performance - Second Burn (STDV +172-Second Time Slice at Standard Altitude Conditions)

PARAMETER	PREDICTED	RECONSTRUCTION	FLIGHT DEVIATION	PERCENT DEVIATION FROM PREDICTED
Thrust, lbf	206,125	207,688	1563	0.76
Specific Impulse, lbf-s/lbm	428.98	429.2	0.22	0.05
LOX Flowrate, lbm/s	399.02	402.17	3.15	0.79
Fuel Flowrate, lbm/s	81.48	81.76	0.28	0.34
Engine Mixture Ratio, LOX/Fuel	4.897	4.918	0.021	0.43

and remained there for 230.4 seconds. At second ESC +109.8 seconds, the valve was commanded to the null position (approximately 5.0 EMR) and remained there throughout the remainder of the flight.

7.10 S-IVB PRESSURIZATION SYSTEMS

7.10.1 S-IVB Fuel Pressurization System

The LH_2 pressurization system operationally met all engine performance requirements. The LH_2 pressurization system indicated acceptable performance during prepressurization, boost, first burn, coast phase, and second burn.

The LH_2 tank prepressurization command was received at -96.4 seconds and the pressurized signal was received 13.0 seconds later. Following the termination of prepressurization, the ullage pressure reached relief conditions, approximately 31.7 psia, and remained at that level until liftoff as shown in Figure 7-8. A small ullage collapse occurred during the first 17 seconds of boost. The ullage pressure returned to the relief level by 85 seconds due to self pressurization. At S-IC cutoff the ullage pressure dropped 0.6 psid. This drop was larger than that seen on previous flights and resulted from propellant slosh and a smaller ullage volume. The pressure recovered to the relief level in approximately 20 seconds. This decay was not a problem.

Table 7-3. S-IVB Stage Propellant Mass History

EVENT	UNITS	PREDICTED*		PU INDICATED (CORRECTED)		PU VOLUMETRIC		FLOW INTEGRAL		BEST ESTIMATE	
		LOX	LH_2	LOX	LH_2	LOX	LH_2	LOX	LH_2	LOX	LH_2
S-IC Ignition	lbm	189,898	43,500	190,271	43,458	190,667	43,699	190,675	43,795	190,587	43,663
First S-IVB Ignition	lbm	189,898	43,500	190,271	43,458	190,667	43,699	190,675	43,795	190,587	43,607
First S-IVB Cutoff	lbm	136,760	32,593	135,837	32,211	135,142	32,314	135,874	32,535	135,909	32,346
Second S-IVB Ignition	lbm	135,924	29,804	135,666	29,653	135,971	29,710	135,628	30,127	135,617	29,753
Second S-IVB Cutoff	lbm	4870	2138	4634	2566	4600	2570	4630	2526	4659	2535

* Predicted values are adjusted to the actual burn times.

During first burn, the average pressurization flowrate was approximately 0.65 lbm/s providing a total flow of 94.4 lbm. All during the burn the ullage pressure was at the relief level, as predicted.

The LH_2 tank was satisfactorily repressurized for restart by the O_2/H_2 burner. (The burner cutoff anomaly is discussed in paragraphs 7.6 and 12.4.) The LH_2 ullage pressure was 30.5 psia at second burn ESC as shown in Figure 7-9. The average second burn pressurization flowrate was 0.65 lbm/s until step pressurization when it increased to 1.03 lbm/s. This provided a total flow of 250 lbm during second burn. Significant venting during second burn occurred at second ESC +279.3 seconds when step pressurization was initiated. This behavior was as predicted.

The LH_2 pump inlet NPSP was calculated from the pump interface temperature and total pressure. These values indicated that the NPSP at first burn ESC was 18.0 psid. At the minimum point, the NPSP was 7.8 psid above the required. Throughout the burn, the NPSP had satisfactory agreement with the predicted. The NPSP at second burn ESC was 2.2 psid which was 2.3 psid below the required value. The NPSP requirement was met by second STDV. This has occurred on previous flights and a request is being written to remove or change the second ESC requirement. Figures 7-10 and 7-11 summarize the fuel pump inlet conditions for first and second burns, respectively.

7.10.2 S-IVB LOX Pressurization System

LOX tank prepressurization was initiated at -167 seconds and increased the LOX tank ullage pressure from ambient to 41.0 psia within 12 seconds as shown in Figure 7-12. Three makeup cycles were required to maintain the LOX tank ullage pressure before the ullage temperature stabilized. At -96 seconds the LOX tank ullage pressure increased from 39.1 to 40.2 psia due to fuel tank prepressurization, LOX tank vent purge, and LOX pressure sense line purge. The pressure gradually increased to 41.5 psia at liftoff.

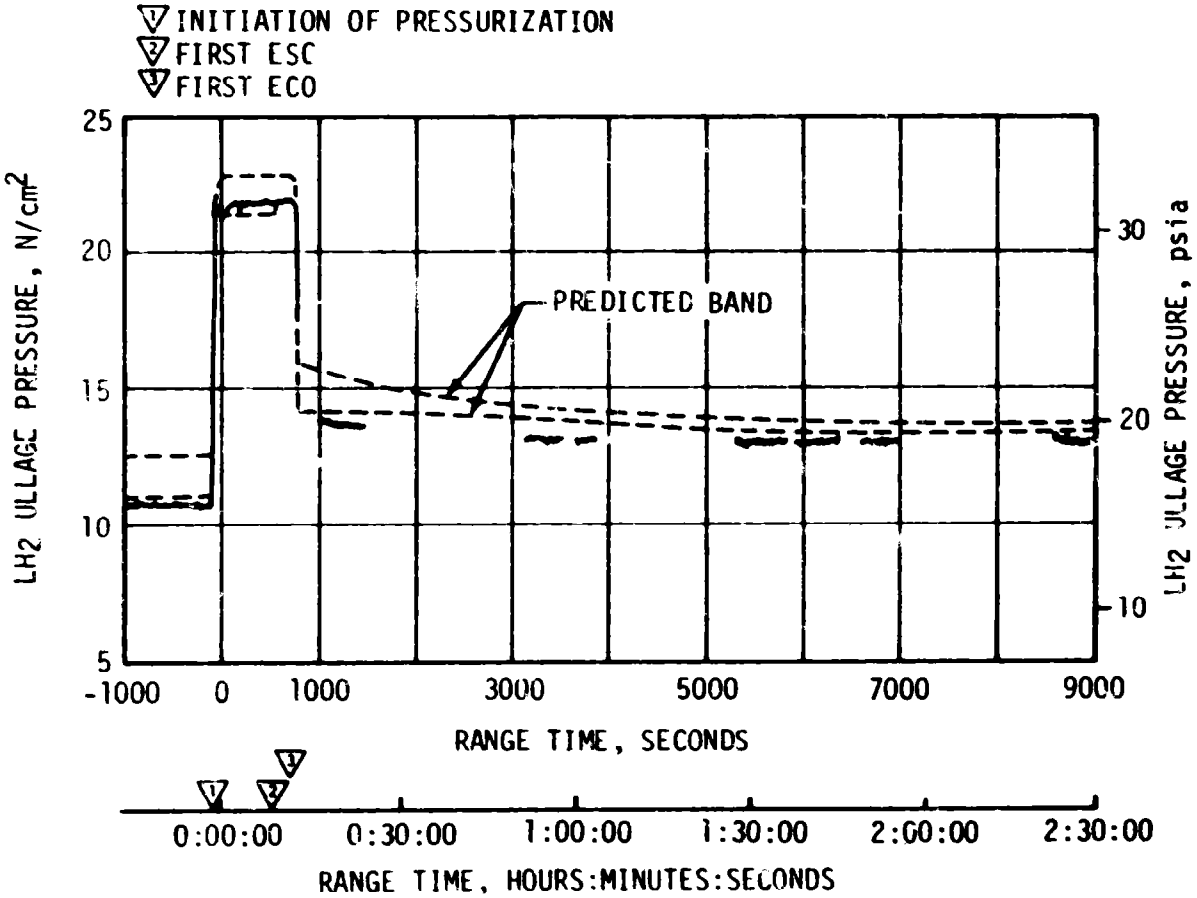

Figure 7-8. S-IVB LH_2 Ullage Pressure - First Burn and Parking Orbit

During boost there was a normal rate of ullage pressure decay caused by an acceleration effect and ullage collapse. No makeup cycles occurred because of an inhibit until after Time Base 4 (T_4). LOX tank ullage pressure was 37.0 psia just prior to ESC and was increasing at ESC due to a makeup cycle.

During first burn, two over-control cycles were initiated, as compared to the predicted one to three cycles. The LOX tank pressurization flowrate variation was 0.24 to 0.29 lbm/s during under-control system operation. This variation is normal and is caused by temperature effects. Heat exchanger performance during first burn was satisfactory.

During orbital coast the LOX tank ullage pressure experienced a decay similar to, though slightly greater than, that experienced on the AS-506 flight. This decay, although the greatest seen to date, was less than the maximum predicted decay, and was not a problem. Investigation is continuing in an attempt to determine the relative effects of factors contributing to this phenomenon. Factors under investigation include heat transfer through the common bulkhead, composition of ullage gas, effects of stage maneuvers, and leakage of ullage gases.

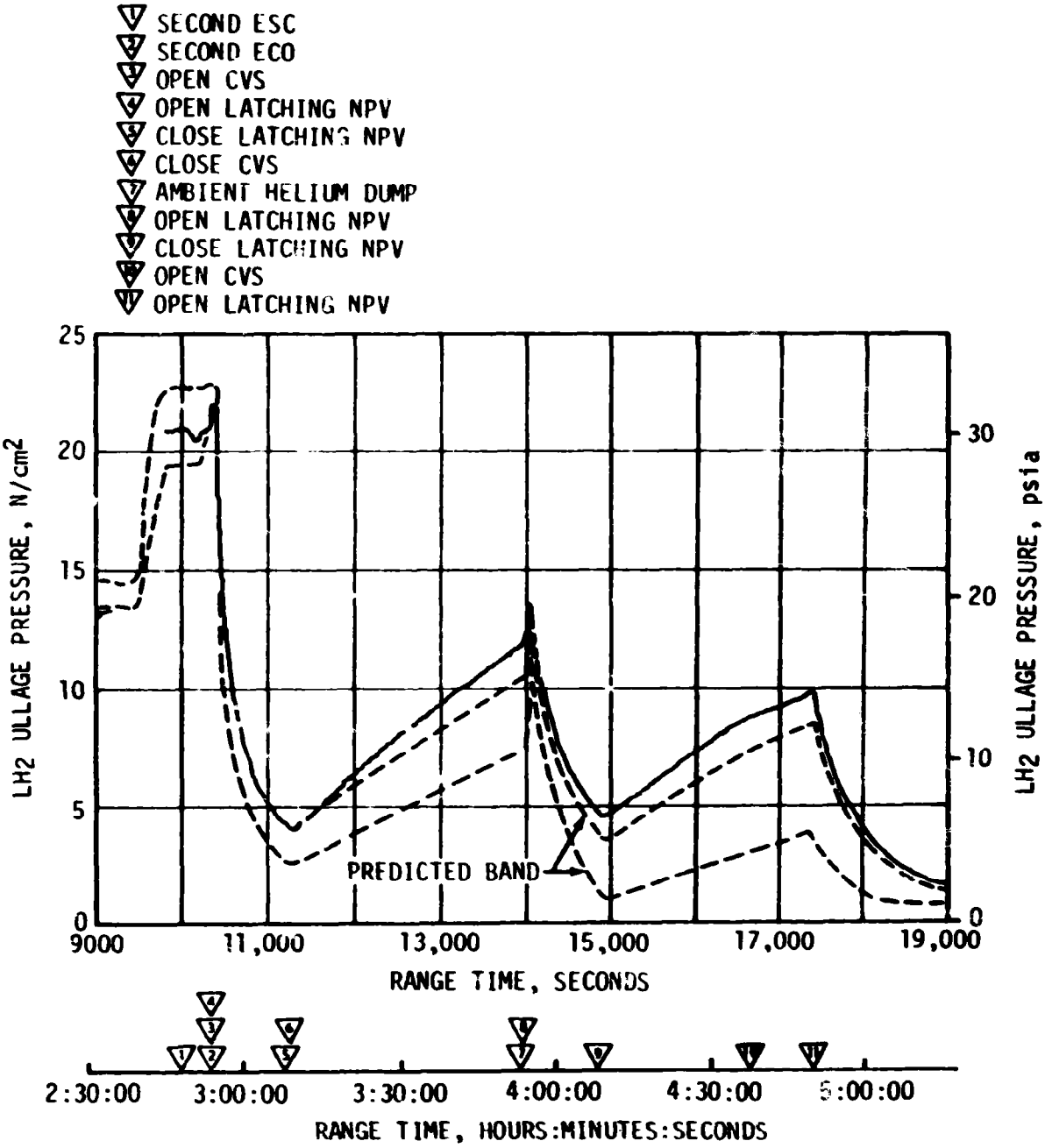

Figure 7-9. S-IVB LH_2 Ullage Pressure - Second Burn and Translunar Coast

Repressurization of the LOX tank prior to second burn was required and was satisfactorily accomplished by the burner. The tank ullage pressure was 40.0 psia at second ESC and satisfied the engine start requirements as shown in Figure 7-13.

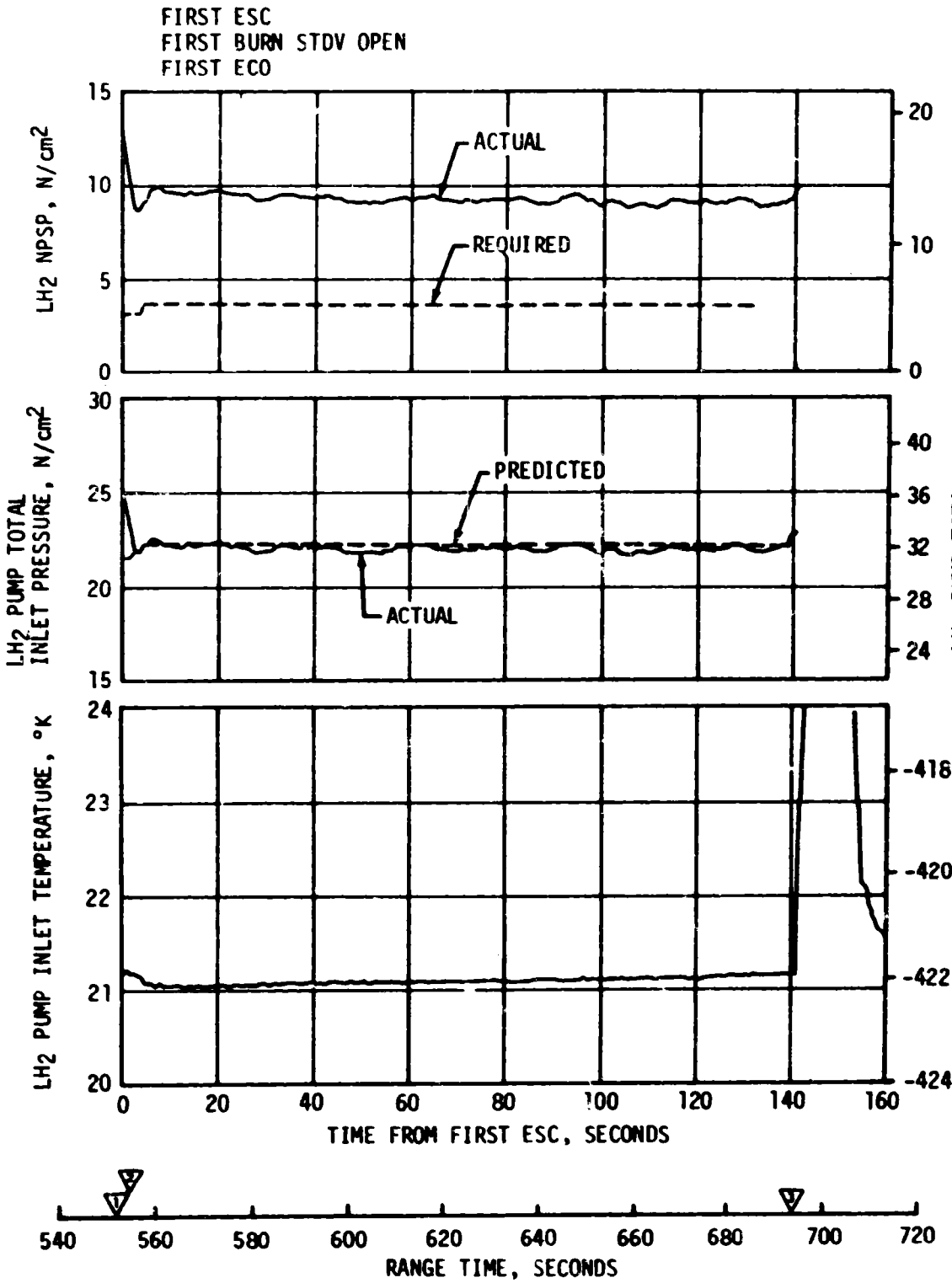

Figure 7-10. S-IVB Fuel Pump Inlet Conditions - First Burn

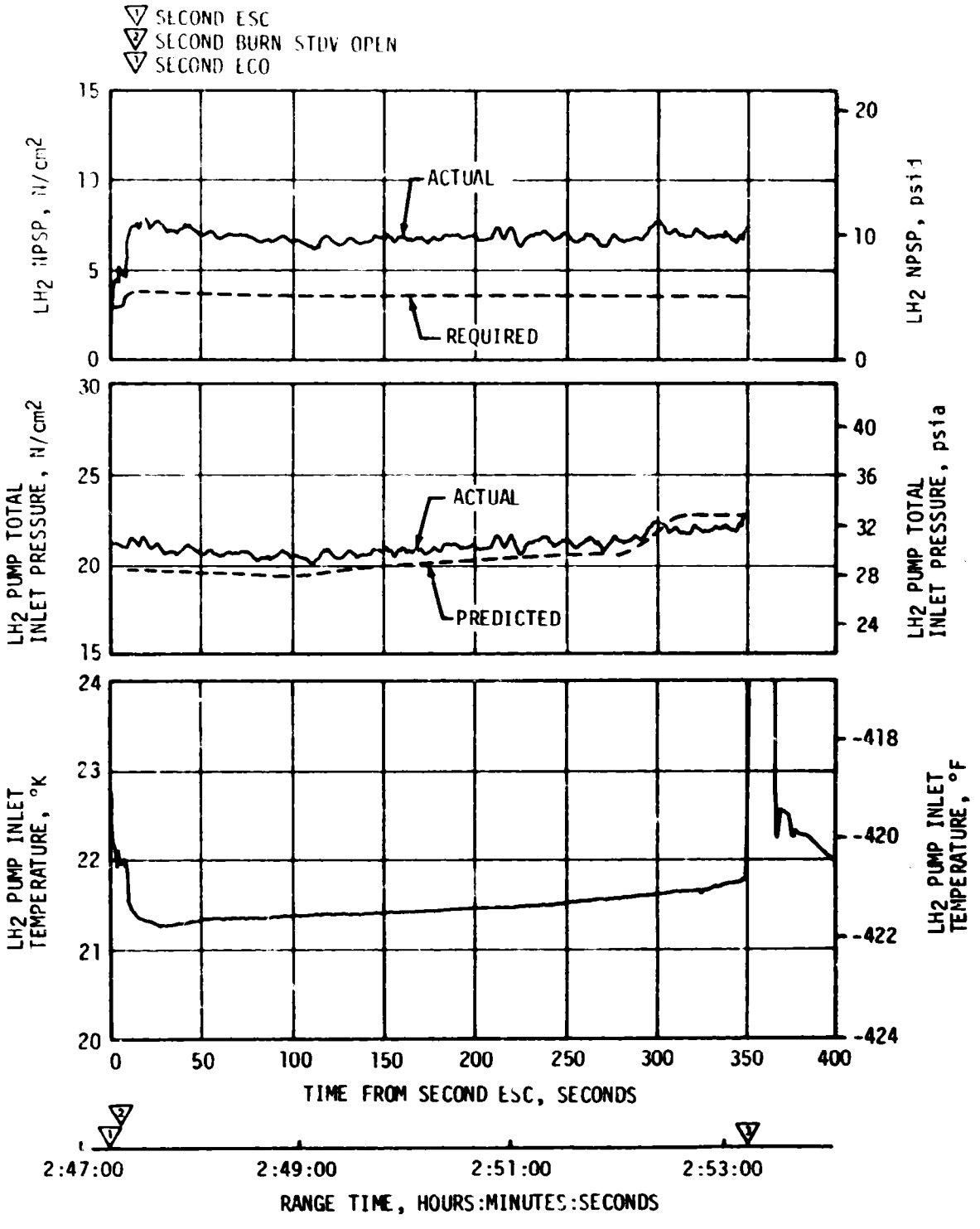

Figure 7-11. S-IVB Fuel Pump Inlet Conditions - Second Burn

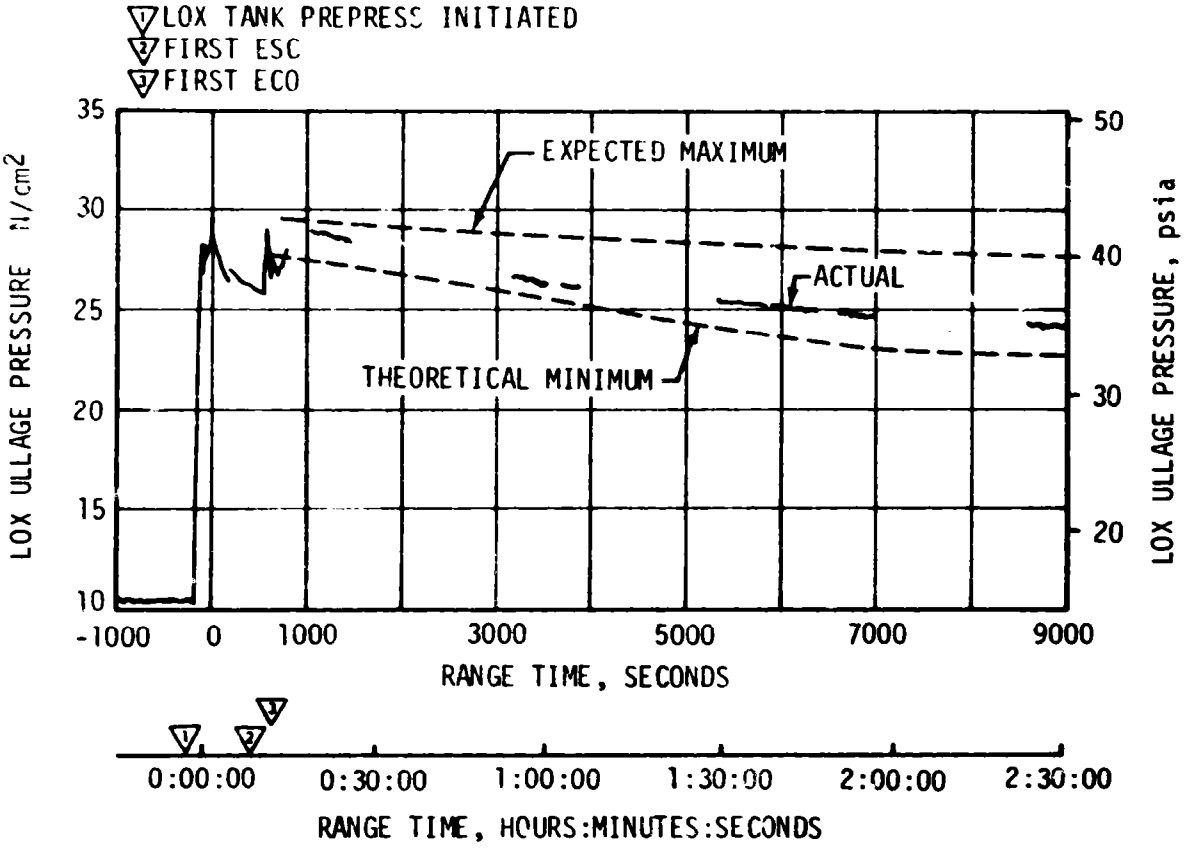

Figure 7-12. S-IVB LOX Tank Ullage Pressure - First Burn and Parking Orbit

Pressurization system performance during second burn was satisfactory and had the same characteristics noted during first burn. There was one over-control cycle as compared to zero to one predicted. Flowrate varied between 0.32 to 0.37 lbm/s. Heat exchanger performance was satisfactory.

The LOX Net Positive Suction Pressure (NPSP) calculated at the interface was 24.2 psid at first burn ESC. The NPSP decreased after start and reached a minimum value of 23.5 psid at 8 seconds after ESC. This was 10.7 psid above the required NPSP at that time.

The LOX pump static interface pressure during first burn followed the cyclic trends of the LOX tank ullage pressure. The NPSP calculated at the engine interface was 23.4 psid at second burn ESC. At all times during second burn, NPSP was above the required level. Figures 7-14 and 7-15 summarize the LOX pump conditions for the first burn and the second burn, respectively. The run requirements for first and second burn were satisfactorily met.

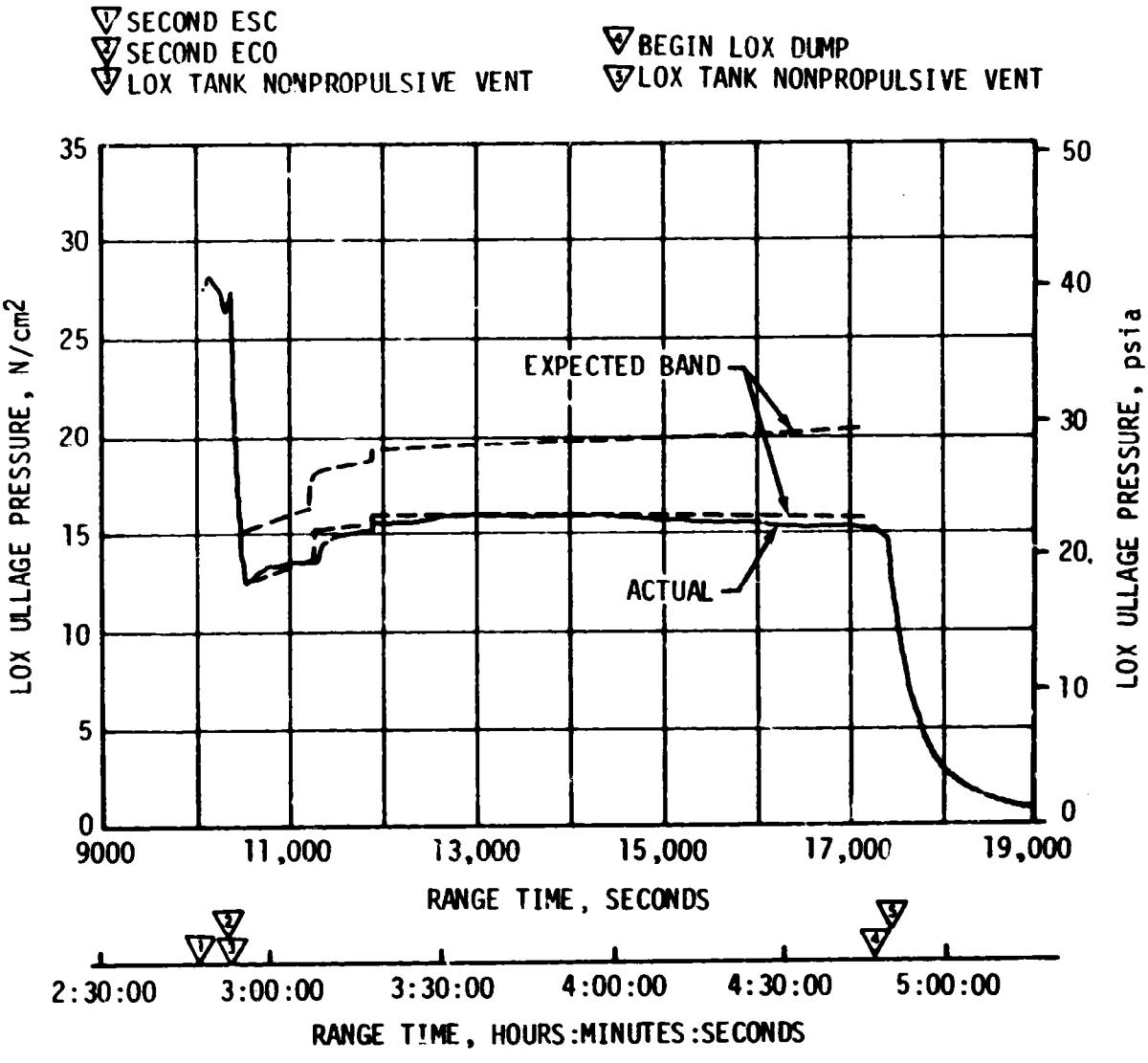

Figure 7-13. S-IVB LOX Tank Ullage Pressure - Second Burn and Translunar Coast

The cold helium supply was adequate to meet all flight requirements. At first burn ESC the cold helium spheres contained 380 lbm of helium. At the end of the second burn, the helium mass had decreased to 168 lbm. Figure 7-16 shows helium supply pressure history.

7.11 S-IVB PNEUMATIC CONTROL SYSTEM

The pneumatic control and purge system performed satisfactorily during all phases of the mission with one exception. During second burn the oxidizer tank motor container pressure experienced a greater than normal decay rate after second ESC +110 seconds, and was below LOX tank ullage pressure at second ECO but subsequently reached a normal level. The most likely cause of this decay was cracking of the motor container pressure relief valve due to vibrations. The pressure decay did not cause any problems. Pneumatic regulator operation was nominal at all times.

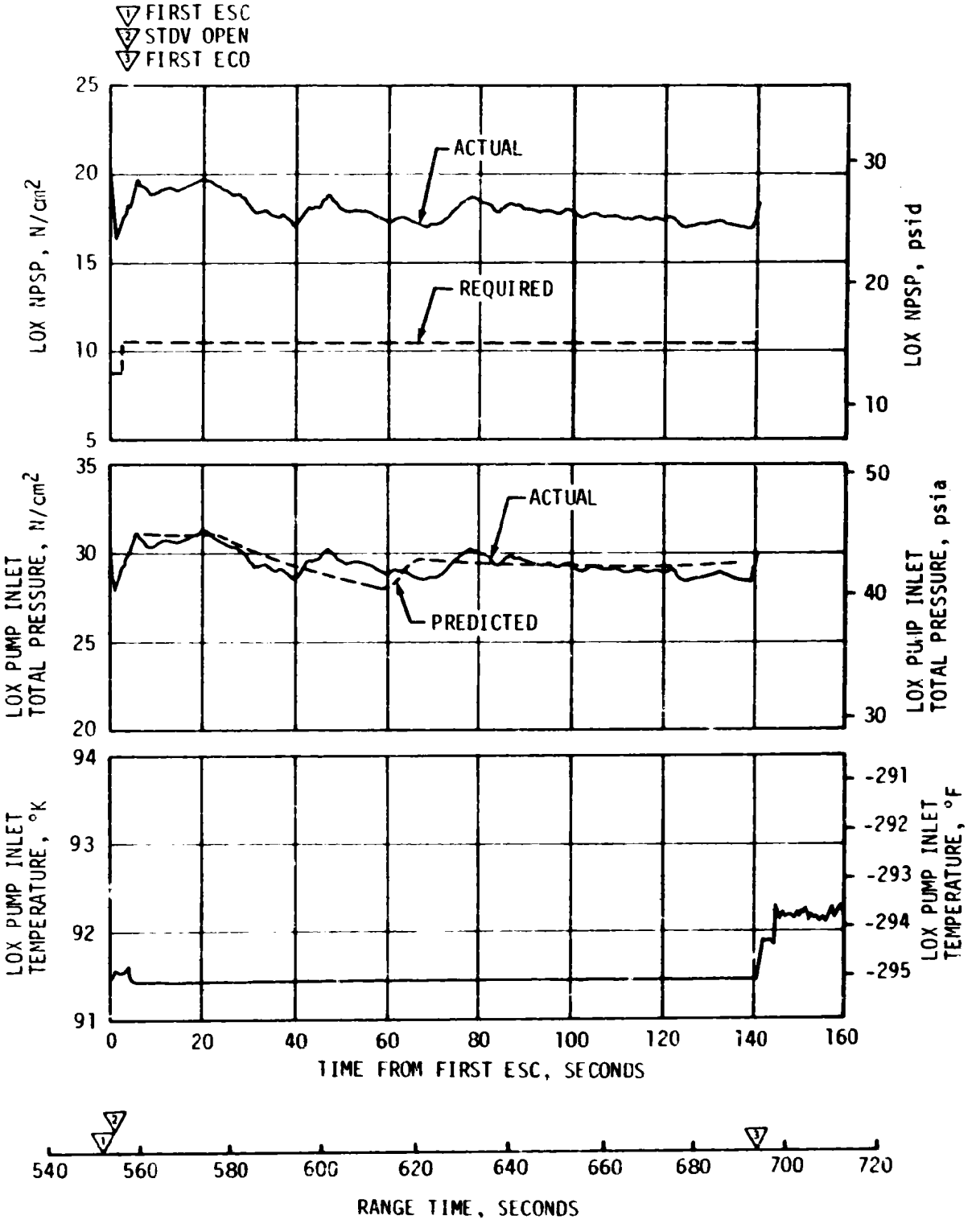

Figure 7-14. S-IVB LOX Pump Inlet Conditions - First Burn

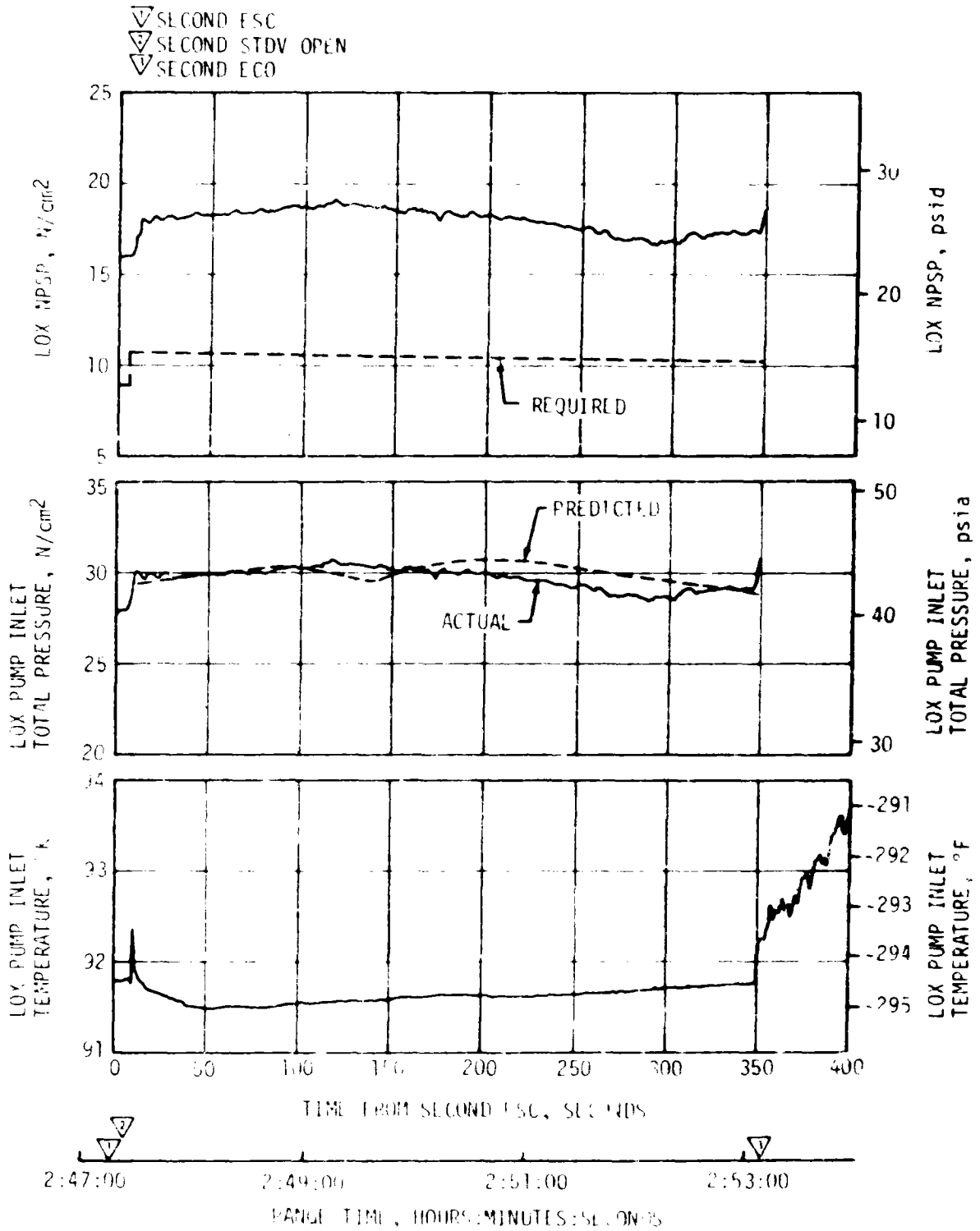

Figure 7-15. S-IVB LOX Pump Inlet Conditions - Second Burn

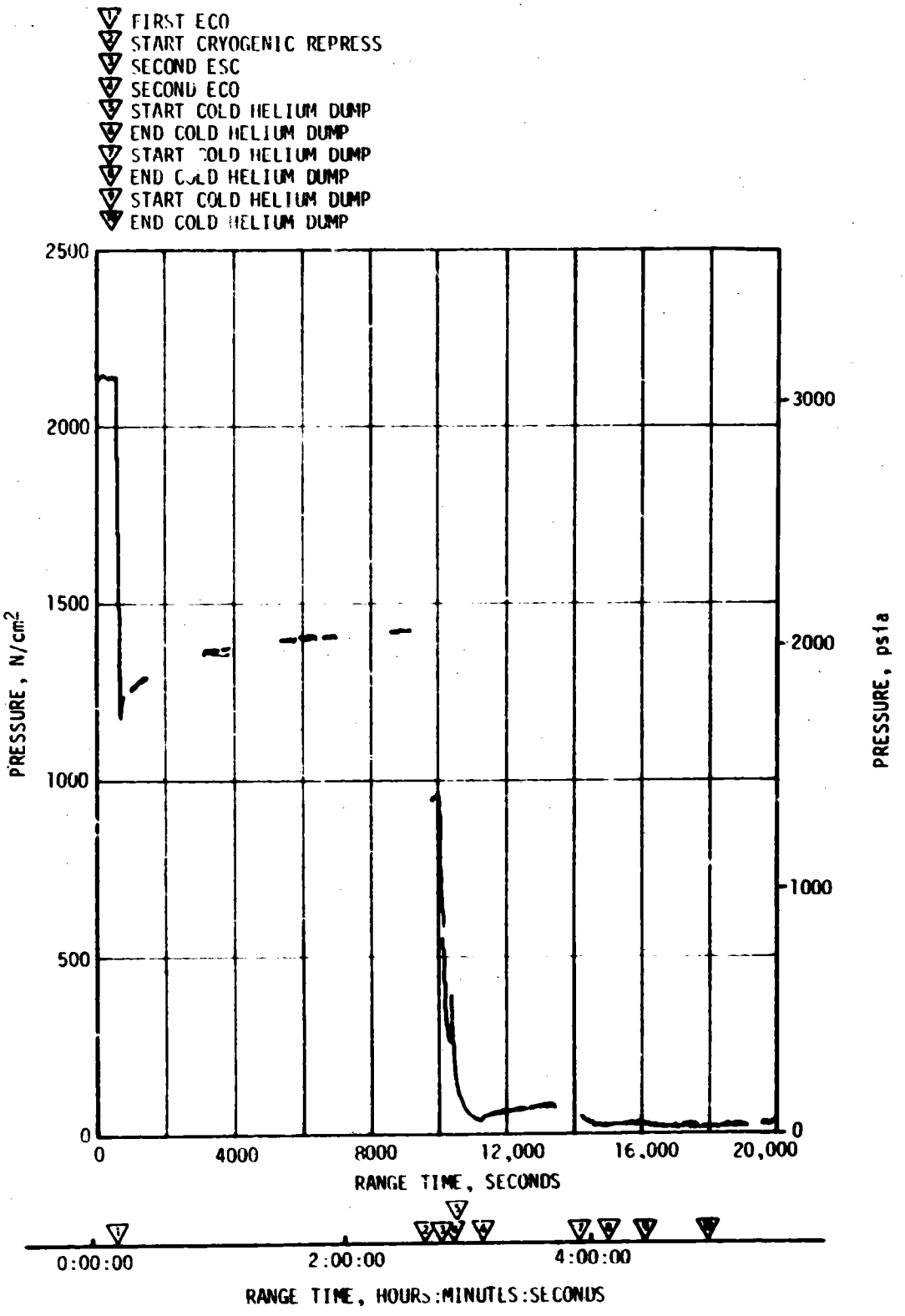

Figure 7-16. S-IVB Cold Helium Supply History

7.12 S-IVB AUXILIARY PROPULSION SYSTEM

The Auxiliary Propulsion System (APS) demonstrated nominal performance throughout the flight and met control system demands, as required, through the loss of data at 43,980 seconds. The pressurization system operation was satisfactory. The regulator outlet pressures for Module No. 1 and 2 were 193 psia. The APS ullage pressures in the propellant ullage tanks ranged from 188 to 194 psia. The helium bottle temperatures ranged from 27 to 101°F.

The oxidizer and fuel supply systems performed as expected during the flight. The propellant temperatures measured in the propellant control modules ranged from 80 to 113°F. The APS propellant usage was as expected. Table 7-4 presents the APS propellant usage during specific portions of the mission.

The performance of the attitude control thrusters and the ullage thrusters was also satisfactory throughout the mission. The thruster chamber pressures ranged from 95 to 100 psia. The ullage thrusters successfully completed the four sequenced burns of 86.7 seconds, 76.7 seconds, 80 seconds, and 300 seconds as well as the ground commanded 270-second slingshot burn.

7.13 S-IVB ORBITAL SAFING OPERATIONS

The S-IVB high pressure systems were safed following J-2 engine cutoff in order to demonstrate this capability. The thrust developed during the LOX dump was utilized to provide a velocity change for the slingshot maneuver. However, due to circumstances explained in paragraph 10.2, the slingshot was not achieved. The manner and sequence in which the safing was performed is presented in Figure 7-17.

7.13.1 Fuel Tank Safing

The LH_2 tank was satisfactorily safed by accomplishing three programed vents as indicated in Figure 7-17, utilizing both the Nonpropulsive Vent (NPV) and CVS. The LH_2 tank ullage pressure during safing is shown in Figure 7-9. At second ECO, the LH_2 tank ullage pressure was 31.8 psia and after three vents had decayed to approximately 1.0 psia. The mass of GH_2 and LH_2 vented agrees well with the 3059 lbm of liquid residual and pressurant in the tank at the end of powered flight.

7.13.2 LOX Tank Dump and Safing

Immediately following second burn cutoff, a programed 150-second vent reduced LOX tank ullage pressure from 40.0 psia to 18.0 psia as shown in Figure 7-13. Data levels were as expected with 80.0 lbm of helium and 83.8 lbm of GOX being vented overboard. As indicated in Figure 7-13, the ullage pressure then rose gradually due to self-pressurization, to 21.9 psia at the initiation of LOX dump.

Table 7-4. S-IVB /PS Propellant Consumption

TIME PERIOD	MODULE AT POSITION I		MODULE AT POSITION III	
	OXIDIZER, LBM	FUEL, LBM	OXIDIZER, LBM	FUEL, LBM
Initial Load	202.6	126.0	202.6	126.0
First Burn (Roll Control)	0.3	0.2	0.3	0.2
ECO to End of First APS Ullaging	14.3	10.8	13.3	10.3
End of First Ullage Burn to Start of Second Ullage Burn	9.5	6.2	4.1	2.7
Second Ullage Burn (76.7 sec)	12.5	9.9	11.9	9.6
Second Burn (Roll Control)	1.0	0.5	1.0	0.5
ECO to Start of Evasive Ullage Burn	17.1	10.5	12.1	7.8
Evasive Ullage Burn (80 sec)	11.9	9.4	11.9	9.4
From End of Evasive Ullage Burn to the Start of Slingshot Ullage Burn	8.2	5.3	8.0	4.7
Sequenced Slingshot Ullage Burn (300 sec)	41.8	33.2	44.0	34.8
Ground Commanded Slingshot Ullage Burn (270 sec)	40.0	32.0	41.0	33.0
From End of Ullage Burn to Loss of Data (43,980 sec)	12.4	7.8	16.0	9.4
Total Usage	169.0	125.8	163.6	122.4

Note: The APS propellant consumption presented in this table was determined from helium bottle conditions (Pressure, Volume, Temperature [PVT] method).

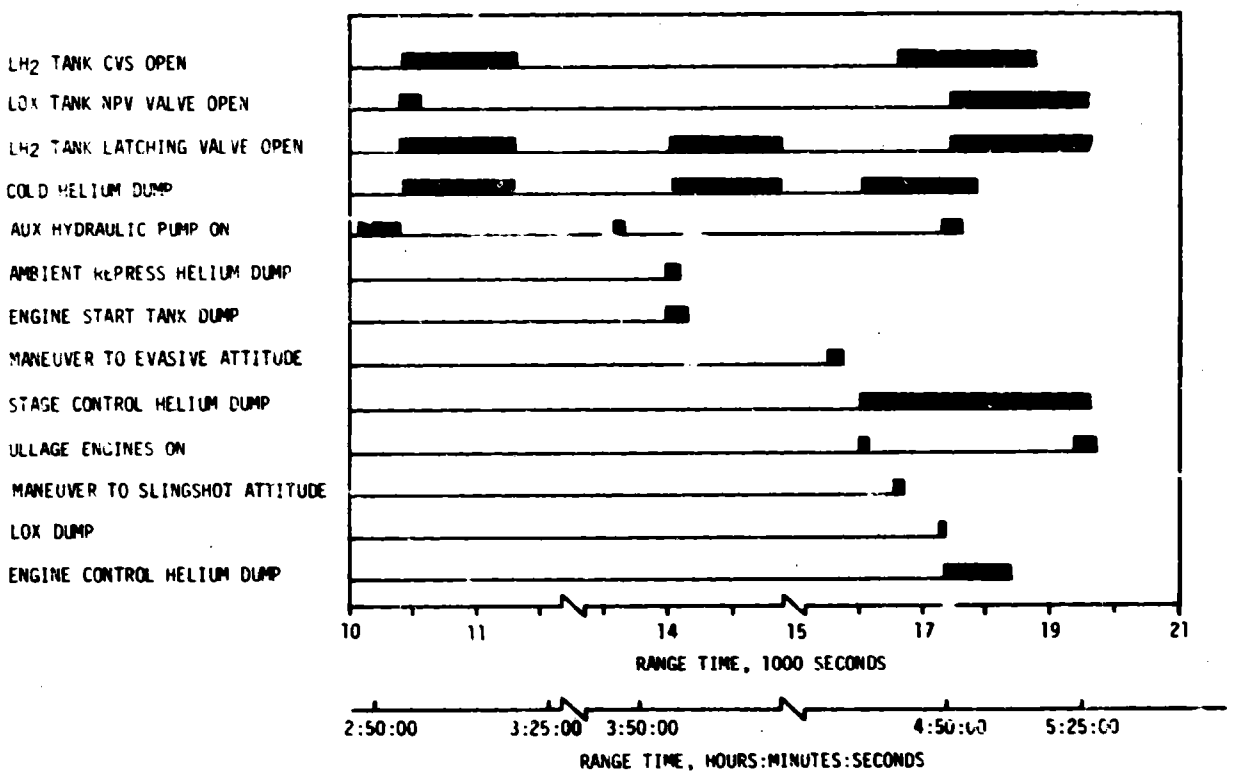

Figure 7-17. S-IVB LOX Dump and Orbital Safing Sequence

The LOX tank dump was initiated at 17,280.2 seconds and was satisfactorily accomplished. A steady-state liquid flow of 333 gpm was reached within 23 seconds.

Gas ingestion did not occur during dump. The LOX residual at the start of dump was 4401 lbm. Calculations indicate that 2649 lbm of LOX was dumped. During dump, the ullage pressure decreased from 21.9 psia to 21.5 psia.

LOX dump ended at 17,338.2 seconds as scheduled by closure of the Main Oxidizer Valve (MOV). A steady-state LOX dump thrust of 808 lbf was obtained. The total impulse before MOV closure was 40,583 lbf-s, resulting in a calculated velocity change of 32.8 ft/s. Figure 7-18 shows the LOX flowrate during dump and the mass of liquid and gas in the oxidizer tank. Figure 7-18 shows LOX ullage pressure and the LOX dump thrust produced. The predicted curves provided for the LOX flowrate and dump thrust are in agreement with the quantity of LOX dumped and the actual ullage pressure.

Two seconds following termination of LOX dump, the LOX NPV valve was opened and remained open for the duration of the mission. LOX tank ullage pressure decayed from 21.4 psia at 17,400 seconds to zero pressure at approximately 23,000 seconds.

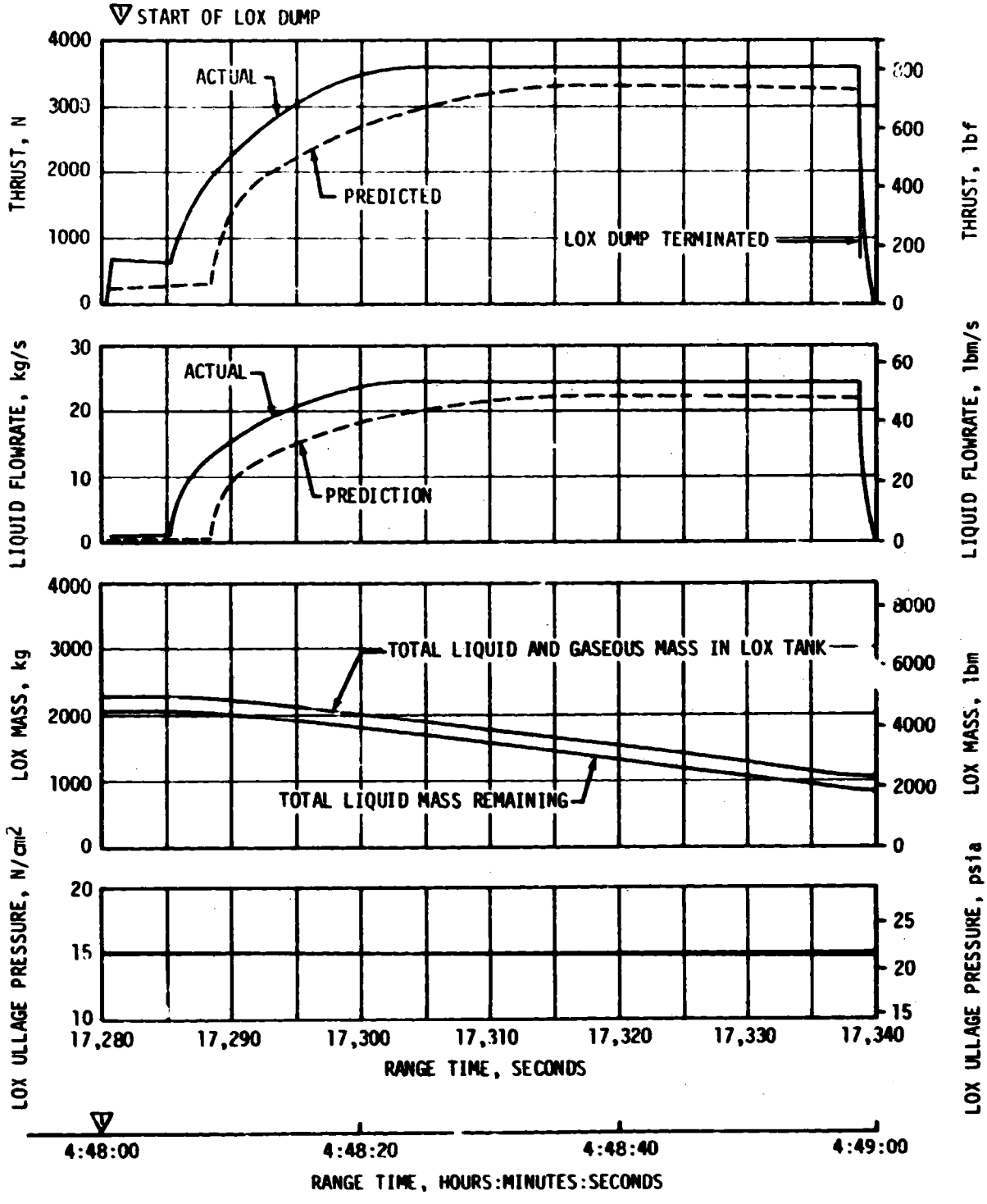

Figure 7-18. S-IVB LOX Dump Parameter Histories

7.13.3 Cold Helium Dump

Cold helium was dumped through the LH_2 cryogenic repressurization lines. Due to the coil burnthrough which occurred following the burner shutdown anomaly, most of the cold helium was dumped overboard through the burner nozzle, rather than through the fuel tank vents.

A total of approximately 160 lbm of helium was dumped during the three programed dumps, which occurred as shown in Figure 7-17.

7.13.4 Ambient Helium Dump

Approximately 41 lbm of ambient helium in the LOX and LH_2 repress spheres was dumped, via the fuel tank. The 62-second dump occurred at 13,985 seconds. The pressure decayed from 3040 psia to 520 psia.

7.13.5 Stage Pneumatic Control Sphere Safing

The stage pneumatic control sphere was safed by initiating the J-2 engine pump purge and flowing helium through the pump seal cavities to atmosphere. The safing period of 1600 seconds satisfactorily reduced the pressure in the sphere.

7.13.6 Engine Start Tank Safing

The engine start tank was safed during a period of approximately 150 seconds beginning at 13,984.9 seconds. Safing was accomplished by opening the sphere vent valve. Pressure was decreased from 1280 psia to 80 psia with 3.65 lbm of hydrogen being vented.

7.13.7 Engine Control Sphere Safing

The safing of the engine control sphere began at 17,280 seconds. The helium control solenoid was energized to vent helium through the engine purge system. The initial pressure in the sphere was 3125 psia, and it decayed to about 900 psia in 55 seconds. At this time gaseous helium from the ambient repressurization bottles began flowing to the engine control sphere. Helium from the control sphere and repressurization bottles continued to vent until 18,330 seconds. During this time, the pressure in the repressurization bottles had decayed from 900 to 250 psia. The control sphere pressure had decayed to 100 psia. Subsequent to the closing of the control solenoid, the control sphere repressurized to 175 psia without any noticeable decay in stage ambient repressurization bottle pressure. During the 1050-second safing period, a total of 21.7 lbm of helium was vented to atmosphere.

SECTION 8

HYDRAULIC SYSTEMS

8.1 SUMMARY

The S-IC, S-II, and S-IVB hydraulic systems performed satisfactorily throughout the mission. All parameters were within specification limits, although the return fluid temperature of one S-IC actuator rose unexpectedly at 100 seconds.

8.2 S-IC HYDRAULIC SYSTEM

Performance of the S-IC hydraulic system was satisfactory. All servoactuator supply pressures, return temperatures, and return pressures were within required limits, although engine No. 2 pitch servoactuator return temperature exhibited an unexpected increase from 92°F to 110°F during the period 100 to 120 seconds (see Figure 8-1). Although analysis shows that loss of line insulation would not account for this temperature rise, it should be noted that the time period does coincide with the time of maximum gas temperatures in the base region. See Figure 14-2. This temperature rise caused no problems but its cause is still under investigation.

8.3 S-II HYDRAULIC SYSTEM

S-II hydraulic system performance was normal throughout the flight. System supply and return pressures, reservoir volumes, and system fluid temperatures were within predicted ranges. Reservoir fluid temperatures were close to the predicted rate of increase. All servoactuators responded to commands with good precision, and forces acting on the actuators were well below the predicted maximum. Launch pad redlines at liftoff were met with ample margins.

8.4 S-IVB HYDRAULIC SYSTEM

The S-IVB hydraulic system performance was satisfactory during the complete mission (S-IC/S-II boost, first and second burns of S-IVB, and orbital coast).

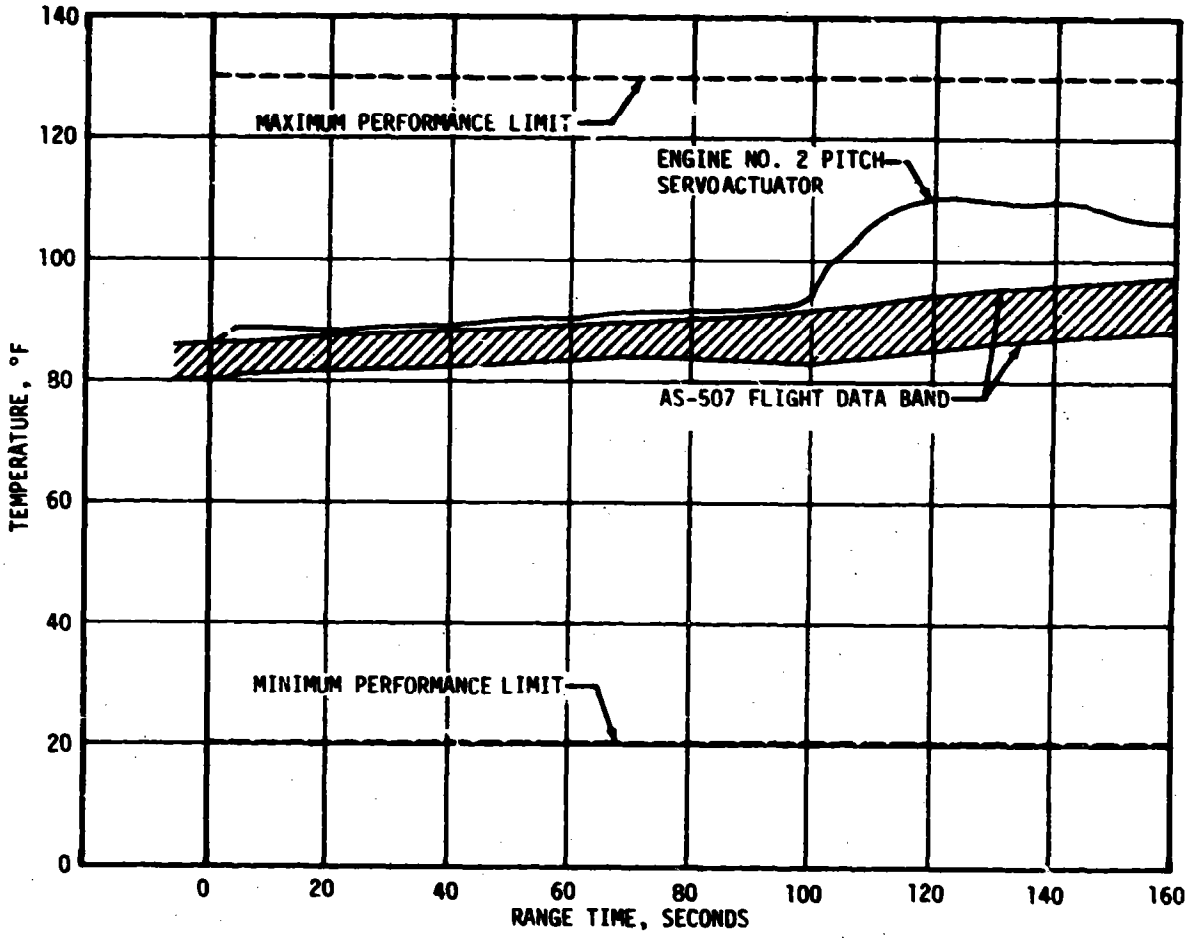

Figure 8-1. S-IC Hydraulic Systems Pitch and Yaw Actuator Return Temperature

SECTION 9

STRUCTURES

9.1 SUMMARY

The structural loads experienced during the S-IC boost phase were well below design values. The maximum Q region bending moment was 37 x 10^6 lbf-in. at the S-IC LOX tank which was less than 20 percent of design value. Thrust cutoff transients experienced by AS-507 were similar to those of previous flights. The maximum dynamics resulting from S-IC Center Engine Cutoff (CECO) were ±0.3 g at the Instrument Unit (IU) and ±0.7 g at the Command Module (CM). At Outboard Engine Cutoff (OECO) a maximum dynamic longitudinal acceleration of -0.3 g and -0.9 g was experienced at the IU and CM, respectively. The order of magnitude of the thrust cutoff responses are considered nominal.

During the S-IC stage boost phase, 4.5 to 5.2 hertz oscillations were detected beginning at 104 seconds. The maximum amplitude (±0.074 g) was measured in the IU at 122 seconds. Oscillations in the 4.0 to 5.5 hertz range have been observed on previous flights with a maximum amplitude of ±0.07 g measured on AS-506 at 107 seconds.

The most significant structural oscillations occurred during S-II burn and were higher than on any previous vehicle during the S-II flight period prior to CECO. Flight data analysis has identified four periods during which oscillation buildups occurred. The oscillations peaked at 187, 248, 313 and 431 seconds in the frequency range from 15.2 to 16.2 hertz. Oscillations in the chamber pressure, LOX sump pressure, and LOX inlet pressure occurred at the same frequency as the structural vibrations. The loading resulting from these oscillations, however, caused no structural failure or degradation.

During the S-IVB first burn, 18 hertz oscillations (measured at the S-IVB engine gimbal block) began at 603 seconds, peaked at a level of ±0.12 g at 610 seconds, and damped out by 634 seconds. These oscillations were detected at the same time period on AS-505 and AS-506. The AS-507 amplitude levels lie between those measured on the two previous flights. During S-IVB second burn, 13 hertz oscillations began at 10,335 seconds, peaked at 10,357 seconds at a level of ±0.12 g, and continued until engine cutoff at a level of approximately ±0.1 g. Previous flights have also

shown gimbal pad oscillations of approximately ±0.1 g at 13 hertz and at about the same time. The launch vehicle structural system is considered to have satisfied all mission requirements.

Three vibration measurements were made on the S-IVB aft interstage. The maximum vibration levels measured occurred at liftoff and during the Mach 1 to Max Q period.

9.2 TOTAL VEHICLE STRUCTURES EVALUATION

9.2.1 Longitudinal Loads

The structural loads experienced during S-IC boost were well below design values. The AS-507 vehicle liftoff occurred nominally at a steady-state acceleration of approximately 1.2 g. Maximum longitudinal dynamic response measured at the IU and CM was ±0.25 g and ±0.55 g, respectively, as shown in Figure 9-1. Both values are considerably larger than those on AS-506 (±0.13 g at the IU), but are within design values.

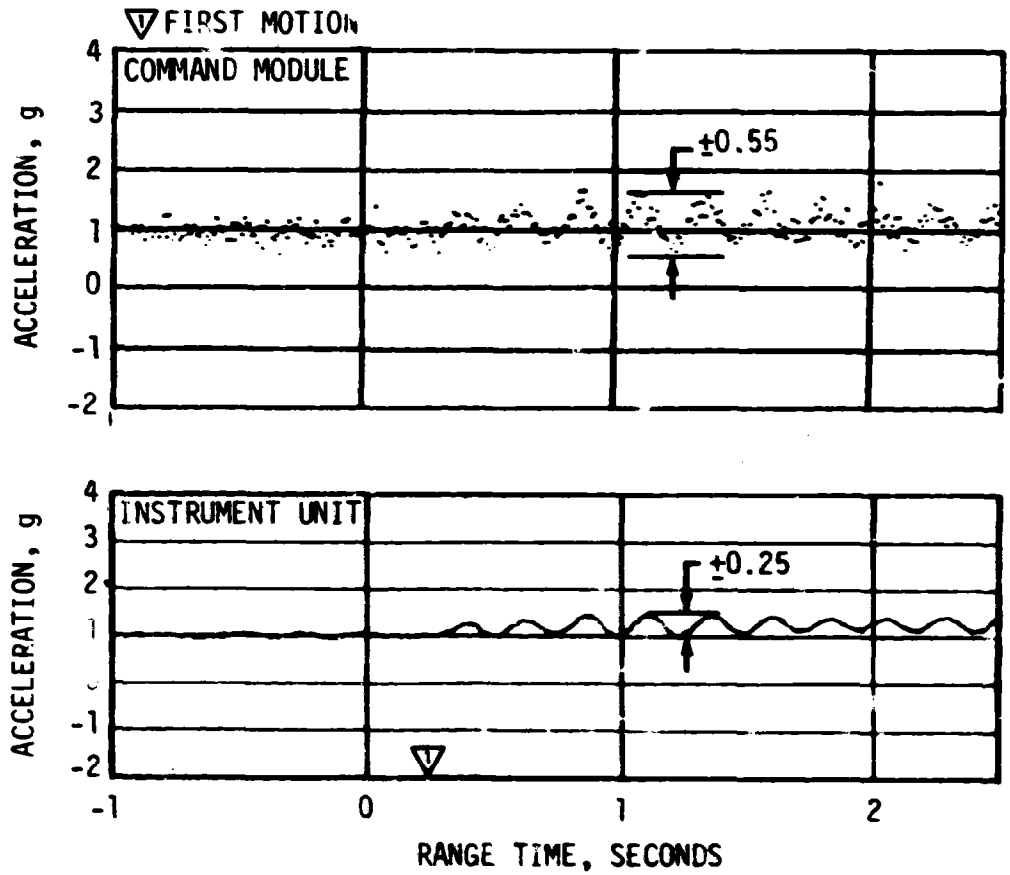

Figure 9-1. Longitudinal Acceleration at the Command Module and Instrument Unit During Thrust Buildup and Launch

The longitudinal loads experienced at the time of maximum bending moment (77.5 seconds) were nominal and are shown in Figure 9-2. There were no discernible longitudinal dynamics at this time. The steady-state longitudinal acceleration was 2.03 g.

Figure 9-2 also shows that the maximum longitudinal loads imposed on the S-IC stage thrust structure, fuel tank, and intertank occurred at 135.24 seconds (CECO) at a longitudinal acceleration of 3.71 g. The maximum longitudinal loads imposed on all vehicle structure above the S-IC intertank occurred at 161.82 seconds (subsequent to OECO) at an acceleration of 3.91 g.

9.2.2 Bending Moments

The 1-2-1-1 engine start sequence apparently introduced more lateral structural dynamic activity in the pre-release phase than had been observed on previous flights. Launch operational loads are based on a 3-sigma ignition differential of 230 milliseconds for diametrically opposed engines. (There was a 202 millisecond differential on AS-507; see Section 5). The increased twang effect from the 1-2-1-1 start sequence combined with the low-level winds (13.3 knots at the 60-foot level) experienced during launch, produced loads which were lower than the design values. The lateral accelerations measured at the IU are shown in Figure 9-3.

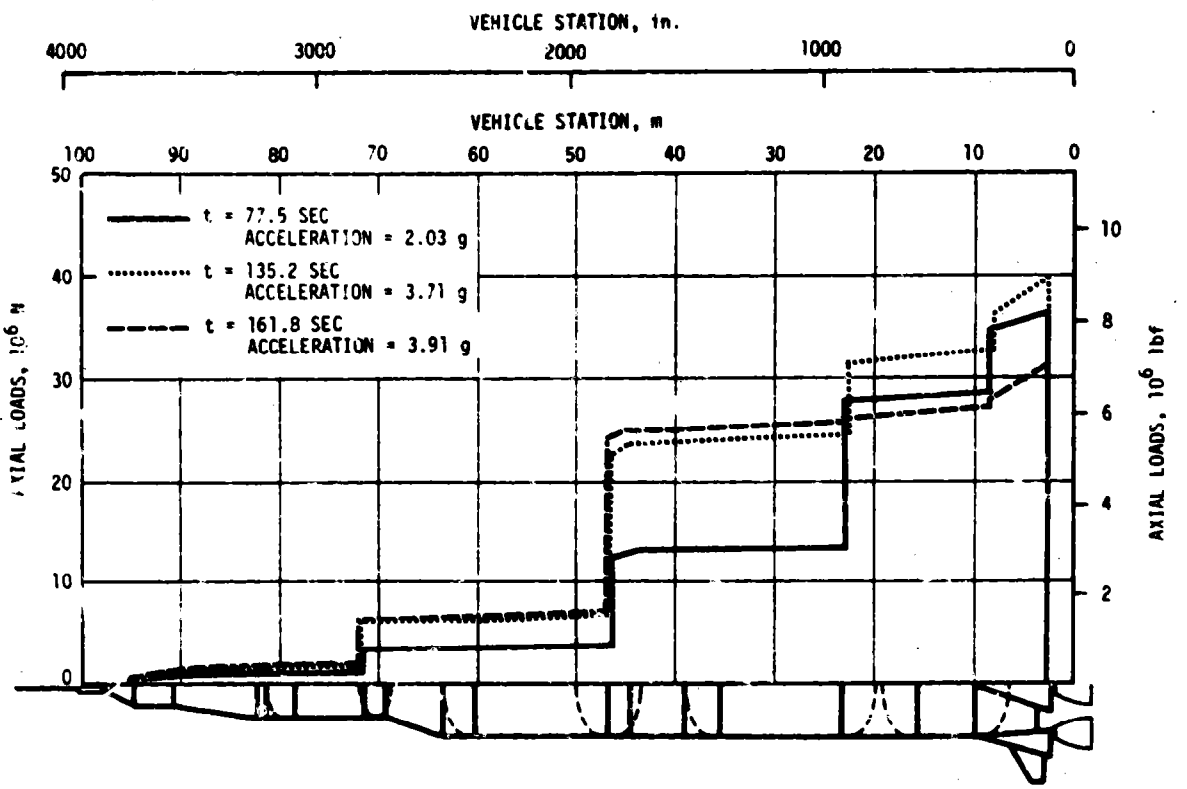

Figure 9-2. Longitudinal Loads at Time of Maximum Bending Moment, CECO and OECO

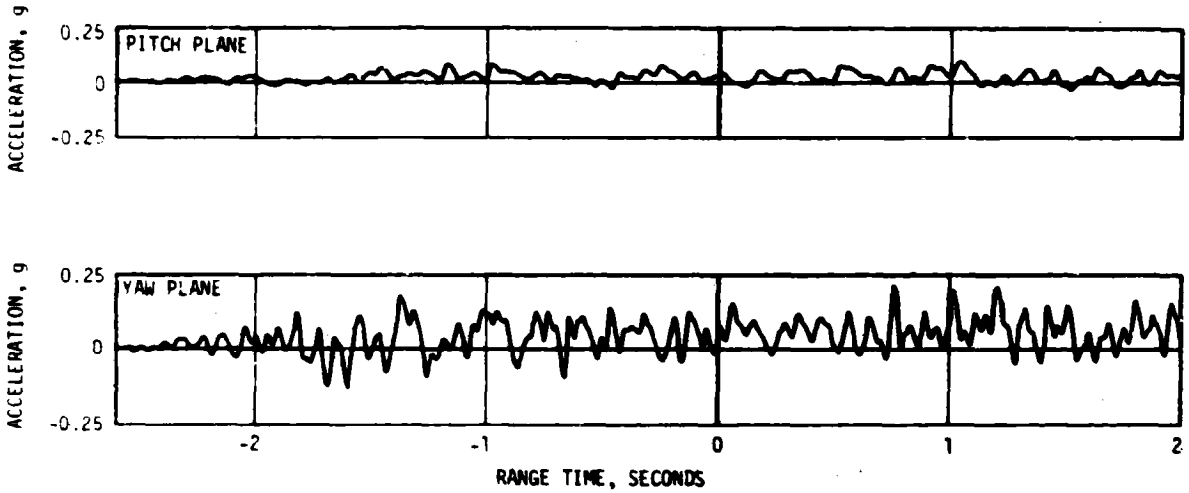

Figure 9-3. Lateral Acceleration at IU During Liftoff

The inflight winds that existed during the maximum dynamic pressure phase of the flight peaked at 92.5 knots at 46,670 feet. As shown in Figure 9-4, the maximum bending moment imposed on the vehicle at the S-IC LOX tank was 37 x 10^6 lbf-in. at approximately 77.5 seconds. This moment loading was less than 20 percent of design value. Bending moment computations were based on the measured inflight parameters, i.e., engine thrust, gimbal angle, dynamic pressure, angle-of-attack and accelerations.

9.2.3 Vehicle Dynamic Characteristics

9.2.3.1 Longitudinal Dynamic Characteristics. The most significant vehicle responses during S-IC stage boost phase were detected by the IU longitudinal accelerometer (A2-603) and the S-IC intertank longitudinal accelerometer (A1-118). As shown in Figure 9-5, low frequency (4.5 to 5.2 hertz) structural oscillations began at approximately 104 seconds and continued to CECO. The peak amplitude was ±0.074 g measured in the IU at 122 seconds. These oscillations are the normal response of the first longitudinal mode to flight environmental excitations. First mode oscillations have occurred on all previous flights. Since the AS-503 flight, the first vehicle having a POGO suppression system, the largest amplitude measured was ±0.07 g on AS-506 at 107 seconds. Spectral analysis of F-1 engine chamber pressure, Figure 9-6, show no detectible buildup of chamber pressure at the structural response frequency. POGO did not occur during S-IC boost.

The AS-507 S-IC CECO and OECO transient responses shown in Figure 9-7 were similar to those of previous flights. The maximum dynamics resulting from CECO were ±0.3 g at the IU and ±0.7 g at the CM. At OECO a maximum dynamic longitudinal acceleration of -0.3 g and -0.9 g was measured at the IU and CM, respectively.

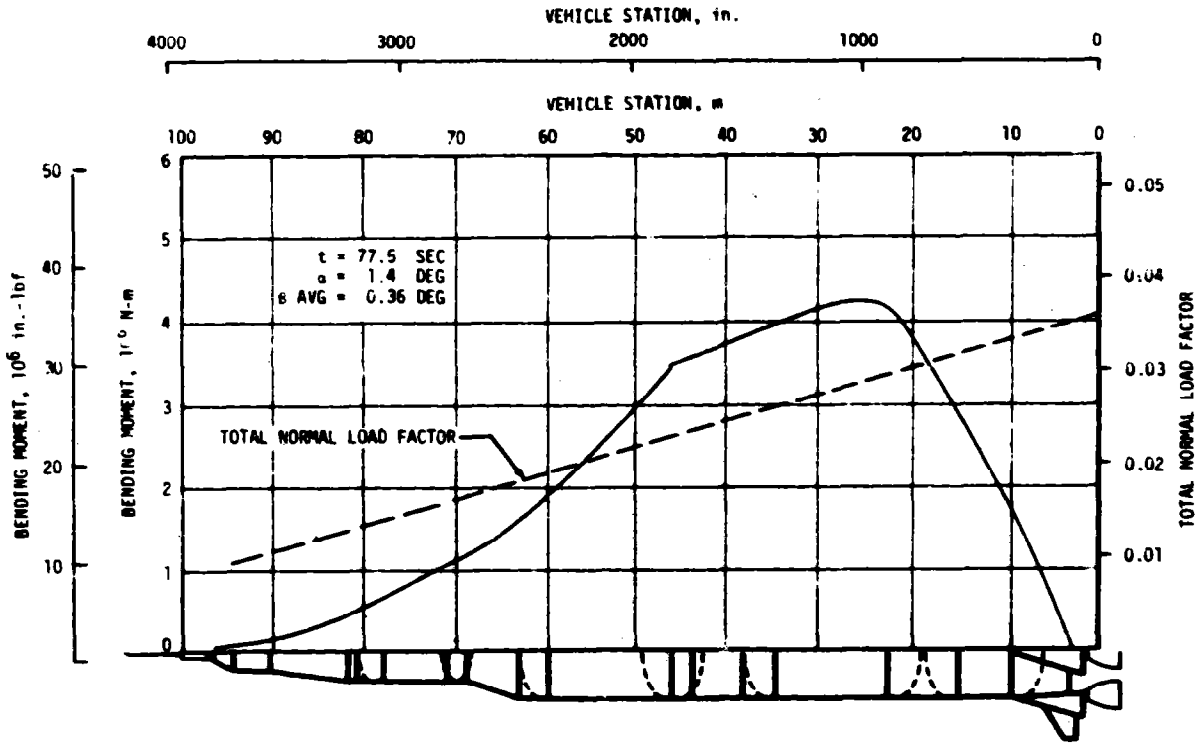

Figure 9-4. Maximum Bending Moment Near Max Q

During the S-II stage boost phase, at approximately 340 seconds, the Apollo 12 astronauts reported experiencing a buildup of structural vibrations. Flight data analysis revealed four periods during which 15.2 to 16.2 hertz oscillations occurred prior to S-II CECO, 180 to 205 seconds, 225 to 267 seconds, 268 to 351 seconds and 405 to 463 seconds. Except for the first time period the accelerations measured were higher than those observed prior to CECO during any previous flight. Acceleration amplitude-time histories of the center engine crossbeam, LOX sump and engine No. 1 thrust pad, as measured during the AS-507 flight, are compared to the AS-504 and AS-505 flight data in Figure 9-8. The principal frequency associated with each oscillation period is also included in this figure. The crossbeam oscillations peaked at 187, 248, 313, and 431 seconds. Figure 9-9 presents the center engine crossbeam, LOX sump and engine No. 1 thrust pad acceleration characteristics following S-II CECO. It is evident that CECO greatly attenuated the low frequency oscillations in the 14 to 20 hertz frequency range.

Low frequency oscillations in the 14 to 20 hertz region existed in the propulsion parameters during the same time periods observed on the structural measurements as shown in Figures 9-10, 9-11 and 6-4. Pressure amplitude-time histories for the same time periods for LOX sump, center engine LOX inlet, and engine No. 1 LOX inlet locations are shown in Figures 9-12 and 9-13. As with the acceleration data, the pressure perturbations for all engines were drastically attenuated following CECO.

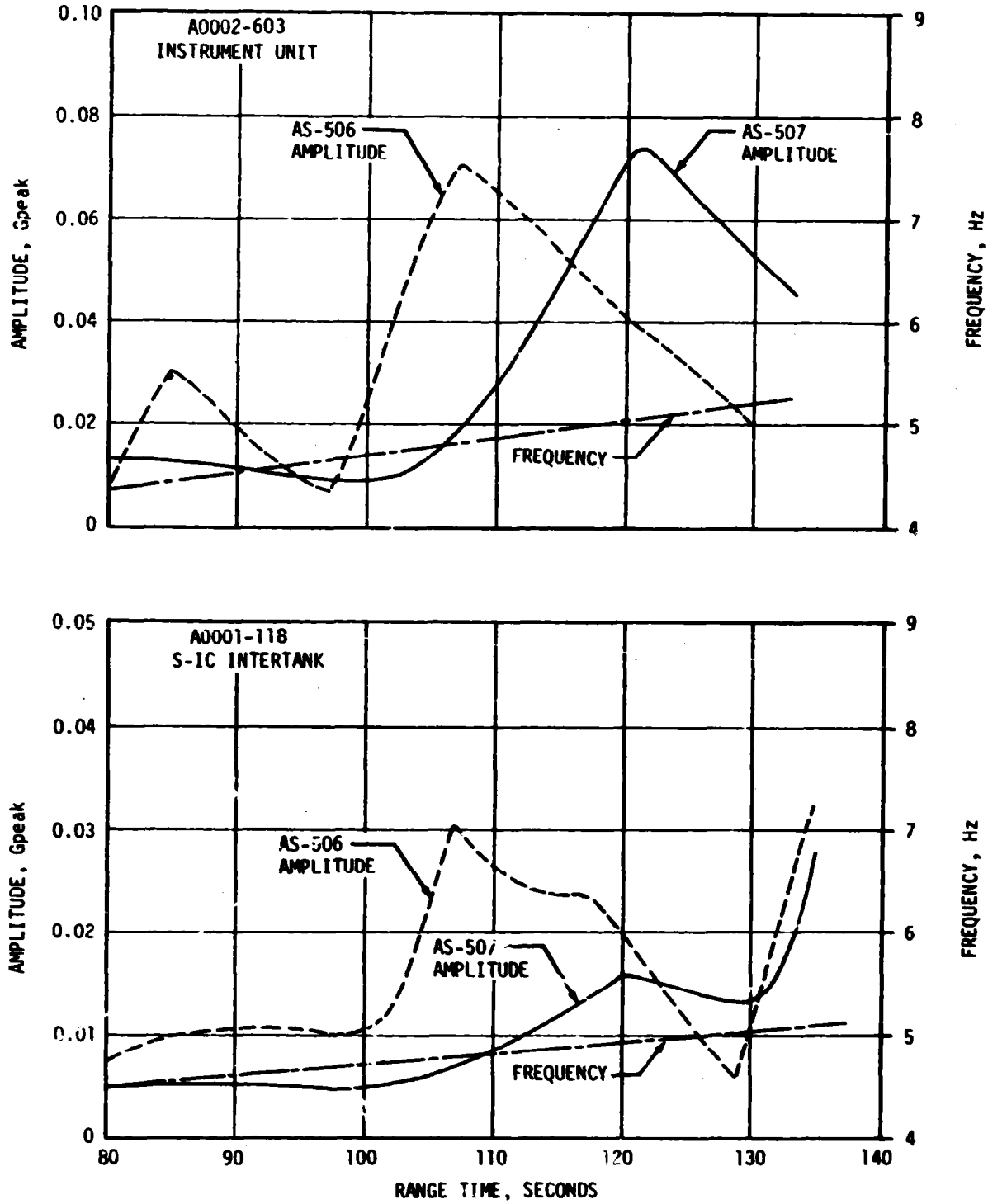

Figure 9-5. Comparison of AS-507 and AS-506 Longitudinal Responses During S-IC Boost

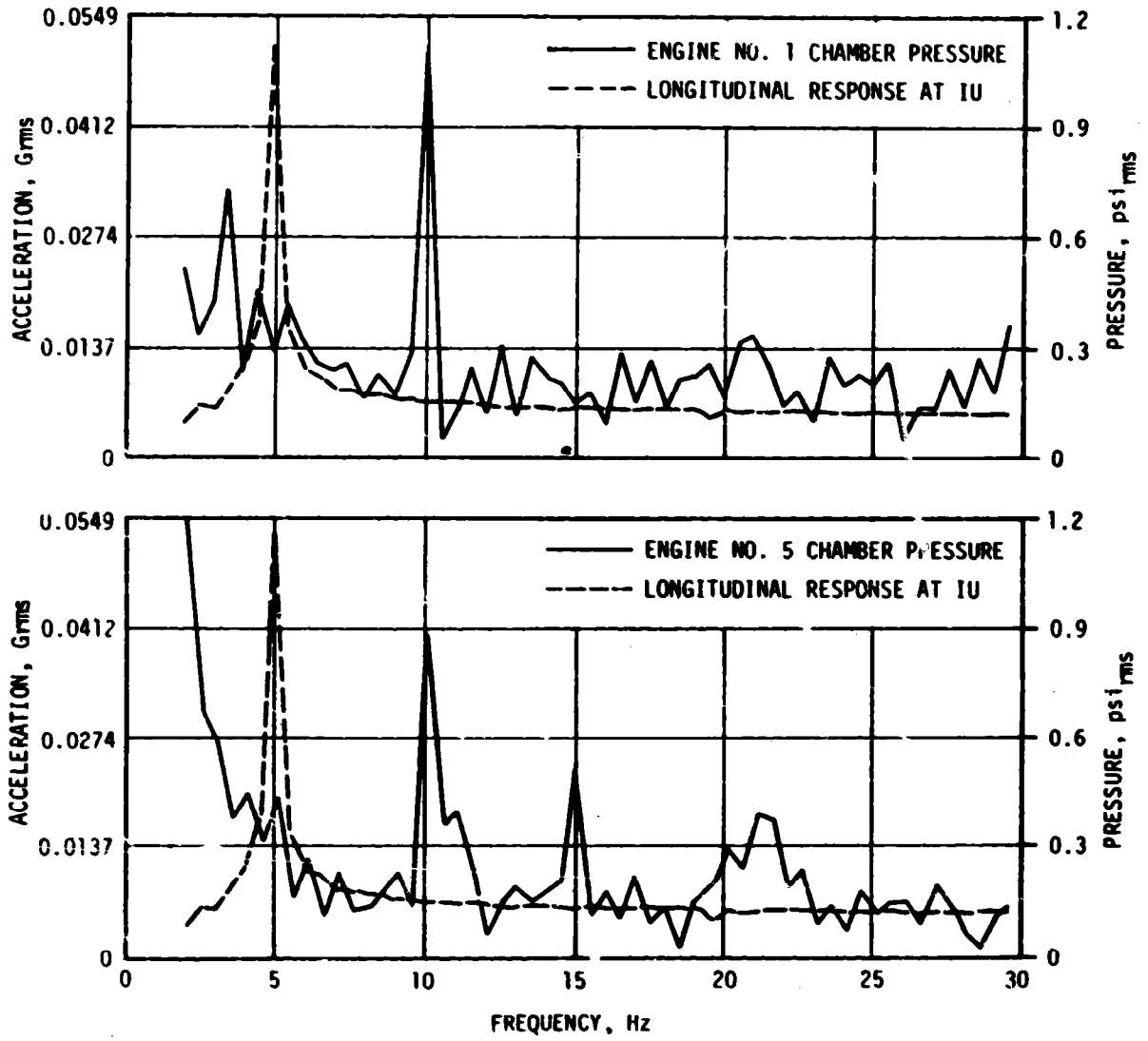

Figure 9-6. Comparison of S-IC Structural and Propulsion Responses For 120 to 122 Seconds

The maximum acceleration and pressure perturbations for each oscillation period are summarized in Table 9-1. It should be noted that the center engine related parameters are more dominant in the last two oscillation periods. It should also be noted that for the second time period the LOX sump acceleration was approximately 1.4 times higher than that observed on the crossbeam which is a departure from what has been observed on previous flights.

Figure 9-14 presents 8 to 14 hertz band-pass filtered data for the three acceleration measurements and the engine No. 1 chamber pressure measurement for the period between CECO and OECO. These data indicate a low acceleration amplitude buildup within this frequency region just prior to OECO; however, there is no apparent increase in engine No. 1 chamber pressure. Similar acceleration buildup characteristics have been observed on previous flights.

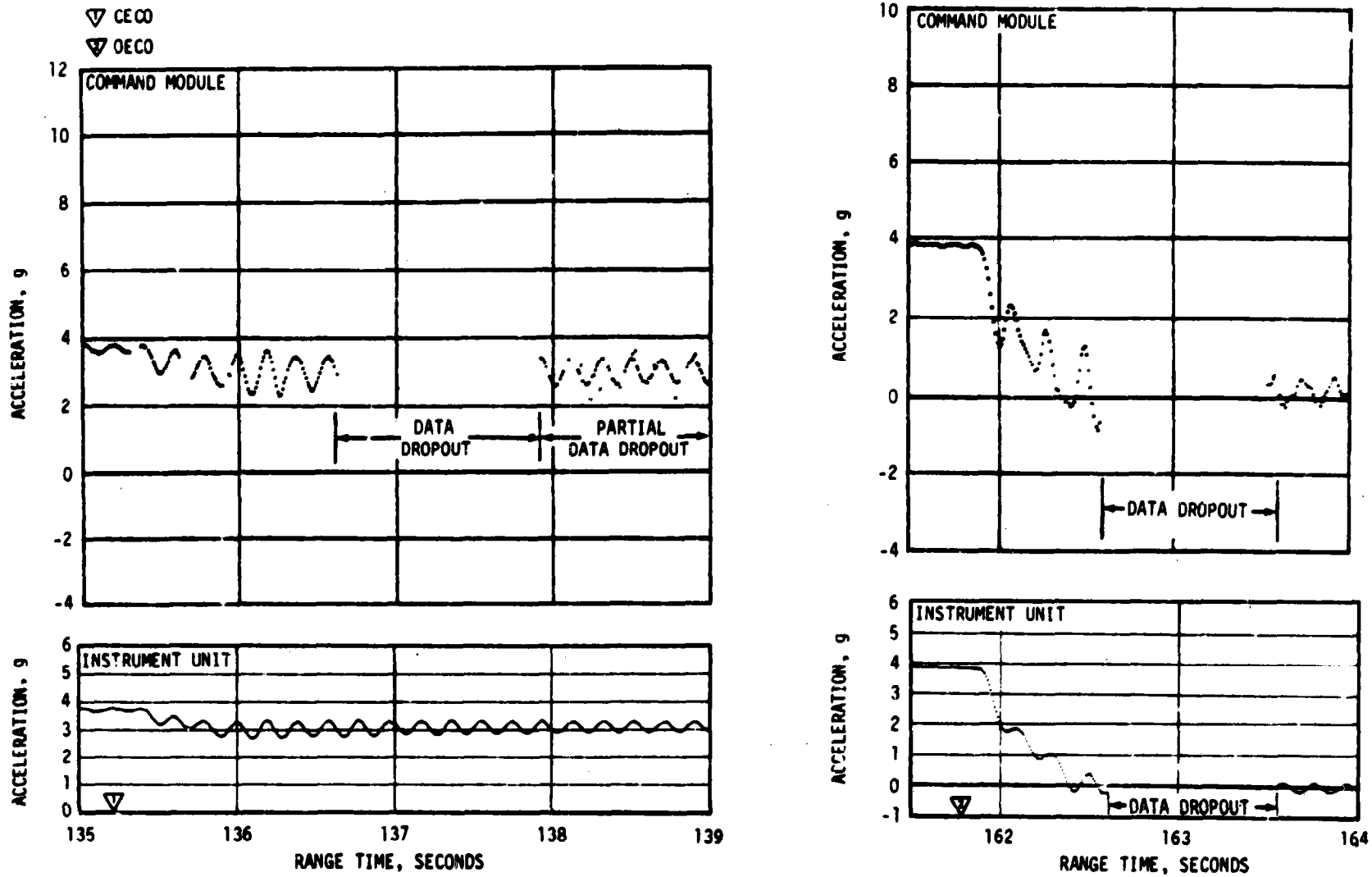

Figure 9-7. Longitudinal Acceleration at Command Module and Instrument Unit at S-IC CECO and OECO

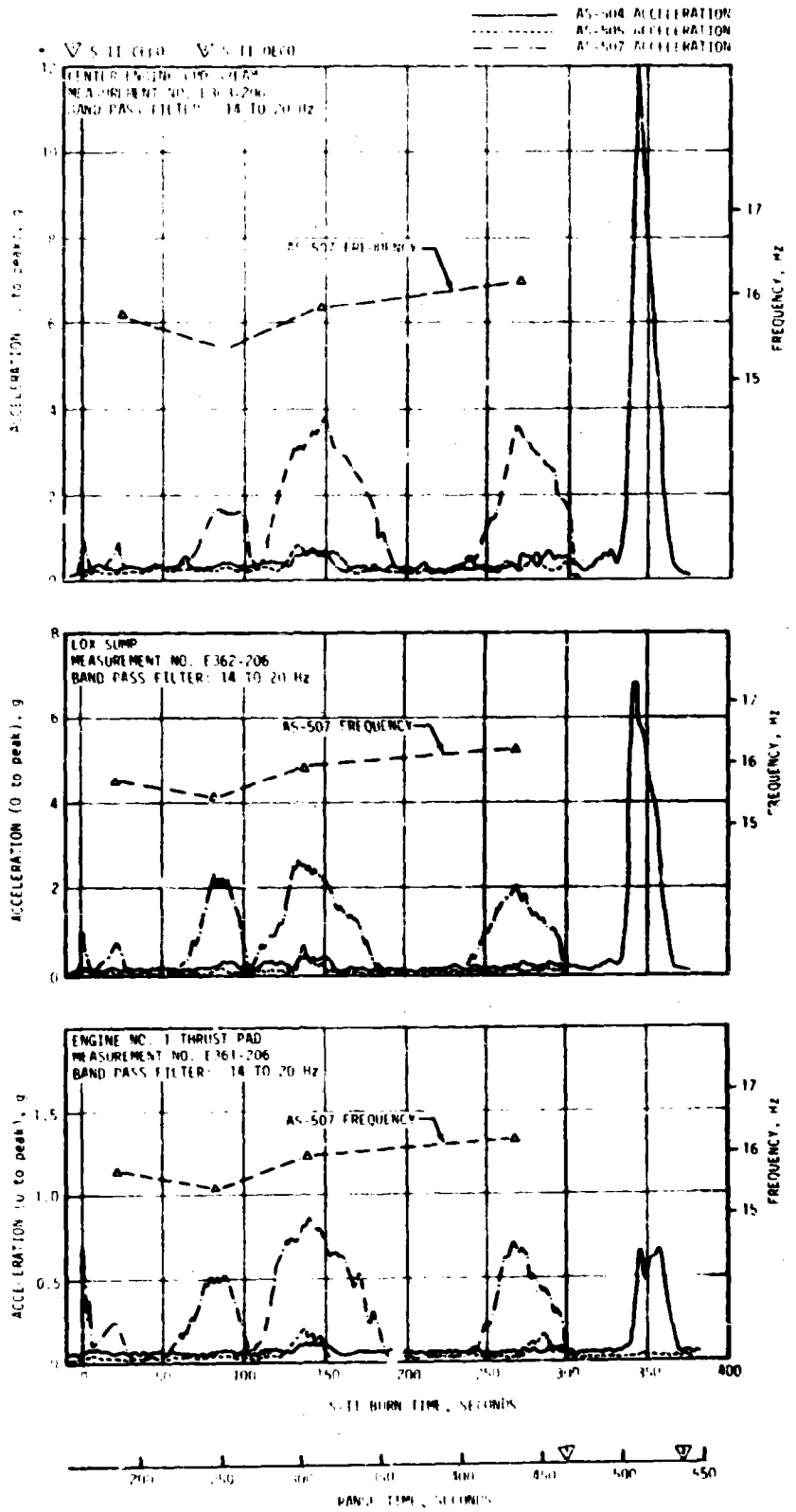

Figure 9-8. Comparison of S-II Stage Acceleration Measurements With Previous Flights

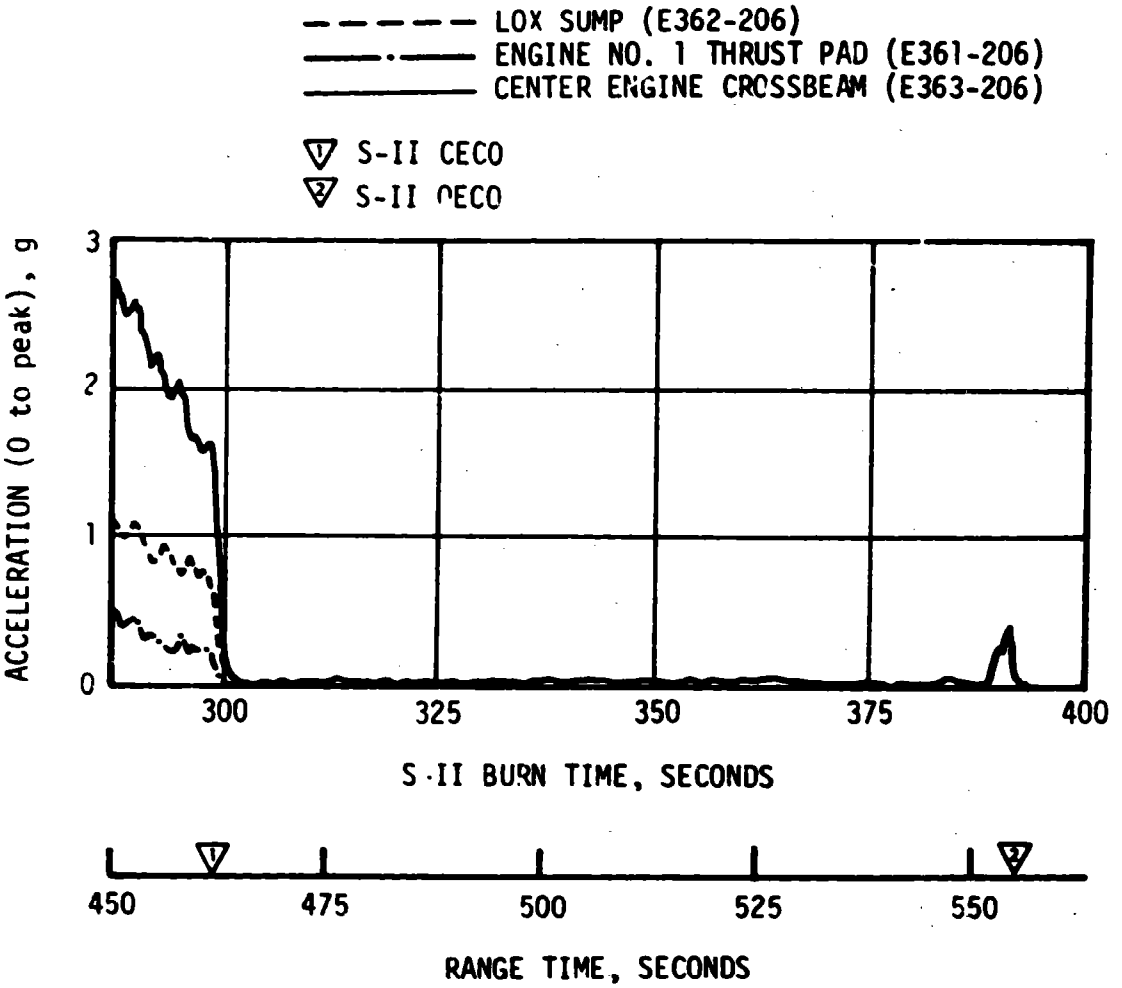

Figure 9-9. S-II Post-CECO LOX Sump, Engine No. 1 and Center Engine Crossbeam Acceleration (14 to 20 Hertz Band Pass Filter)

Although the S-II low frequency oscillations experienced prior to CECO were higher than any previous flight, mainstage performance was not impaired. The design limit load of 240,000 lbf for the crossbeam was exceeded with the computed worst-case exposure load being 243,000 lbf at 313 seconds. However, the flight dynamic loads had minor affect on the fatigue life of the beam and a factor of safety of 1.3 was maintained for the imposed loading.

The AS-507 flight data indicated that a closed loop structural/propulsion system coupling (POGO) occurred during S-II stage burn prior to CECO. The flight data also indicated that the oscillation buildups were limited; however, the limiting mechanism is not fully understood at this time. The AS-507 S-II oscillations do show that due to the coupling between the structural and propulsion system an inherent systems instability does exist and oscillations can be expected to occur during future flights. However, in view of the history of seven successful Saturn V flights and the fact that the S-II stage structure can withstand oscillation amplitude levels three times that experienced on AS-507, the decision has been made to fly AS-508 as is, i.e., without a POGO suppression system on the S-II stage.

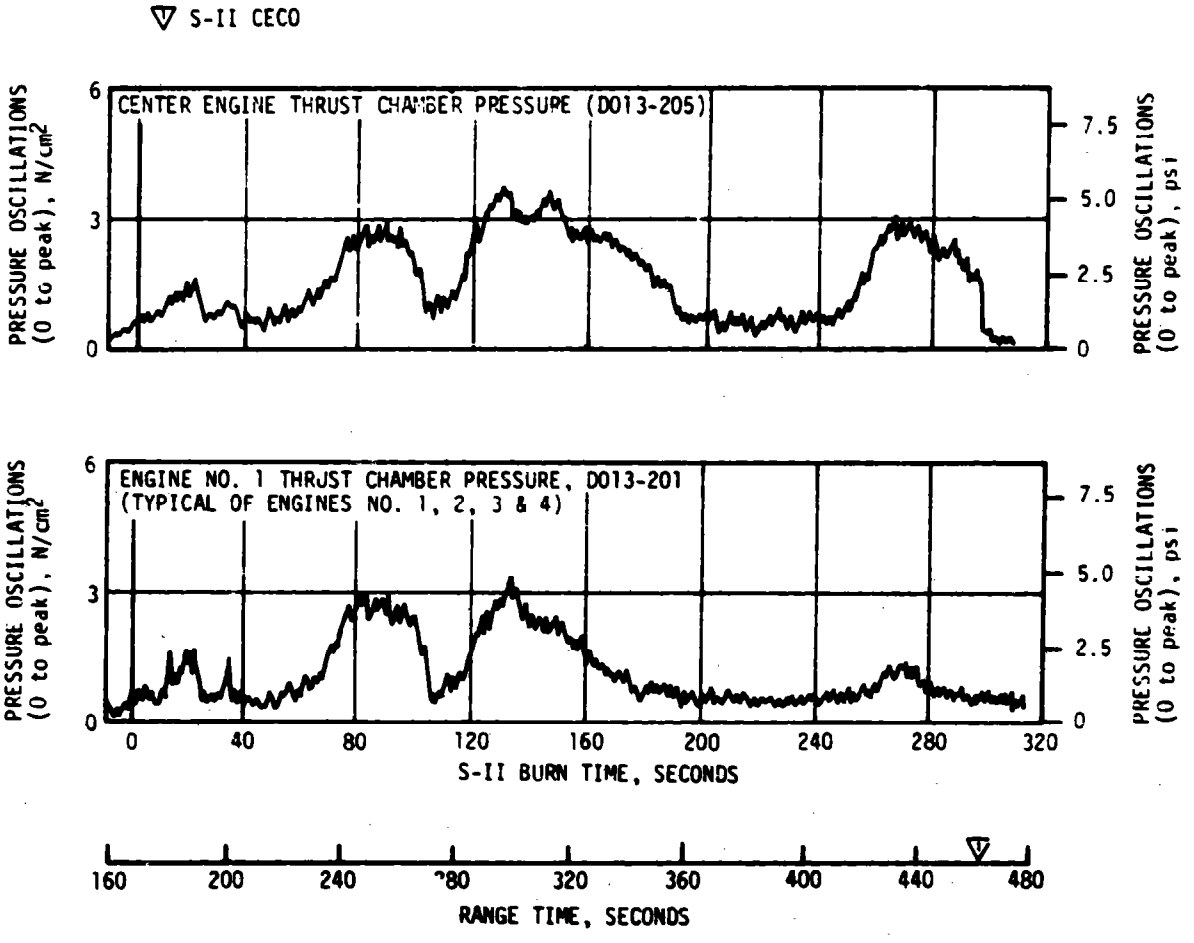

Figure 9-10. S-II Pre-CECO Thrust Chamber Pressure Characteristics (14 to 20 Hertz Band Pass Filter)

Low frequency longitudinal oscillations similar to those experienced on the AS-505 and AS-506 flights again occurred during AS-507 S-IVB first and second burns. During first burn, 19 hertz oscillations (measured at the J-2 engine gimbal block) began at 603 seconds, peaked at a level of ±0.12 g at 610 seconds, and damped out by 634 seconds as shown in Figure 9-15. These oscillations were detected at the same time period on AS-505 and AS-506. The AS-507 gimbal block amplitude levels lie between those measured on the two previous flights. The LOX suction line inlet vibration measurement reached a maximum of ±0.19 g compared to ±0.12 g on AS-506. This measurement was not available on AS-505 for comparison. A corresponding buildup occurs in chamber pressure. Figure 9-16 shows that the 19 hertz oscillations are clearly visible in both structural and propulsion measurements.

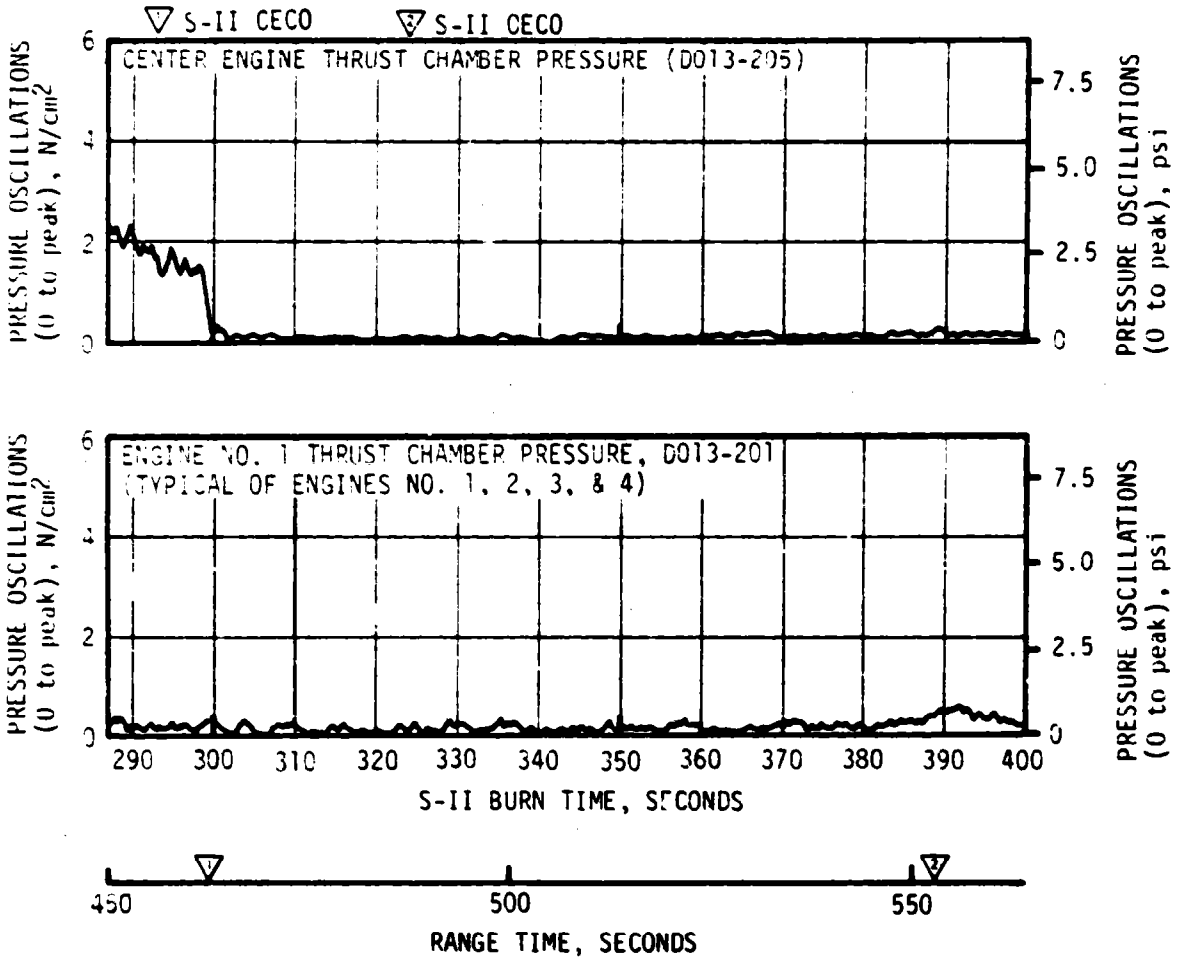

Figure 9-11. S-II Post-CECO Thrust Chamber Pressure Characteristics (14 to 20 Hertz Band Pass Filter)

During S-IVB second burn, 13 hertz oscillations began at 10,335 seconds, peaked at 10,357 seconds at a level of ±0.12 g and continued to engine cutoff, at a level of approximately ±0.1 g as shown in Figure 9-17. Previous flights have also shown gimbal pad oscillations of approximately ±0.1 g at 13 hertz and at about the same time period. As shown in Figure 9-18, the AS-507 LOX pump inlet pressures show a small 13 hertz component, but the 13 hertz chamber pressure response remains below the noise threshold. The magnitudes of the S-IVB low frequency oscillations during both first and second burns were well below design limits and did not affect the structural integrity of the stage.

9.3 VIBRATION EVALUATION

One skin and two stringer vibration measurements were made on the S-IVB aft interstage during the AS-507 flight. As shown in Figure 9-19, the skin measurement vibration levels were higher than the stringer vibration levels throughout flight, which was expected. No previous flight vibration data for the aft interstage area is available for comparison.

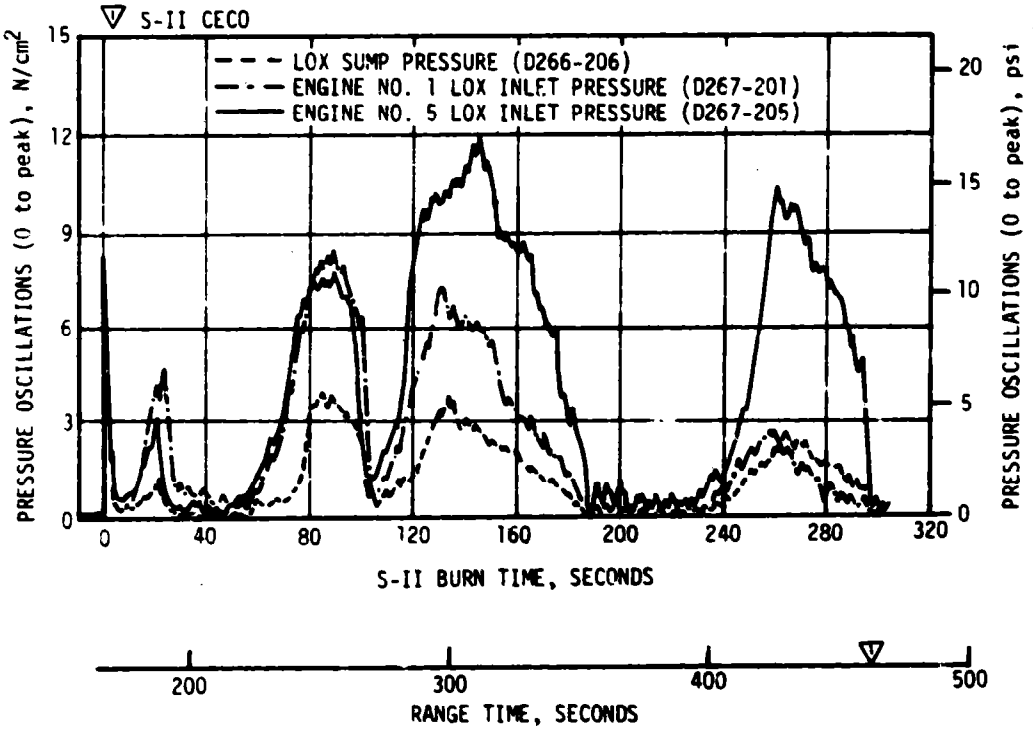

Figure 9-12. S-II Pre-CECO LOX Sump, Center Engine and Outboard Engine LOX Inlet Pressure (14 to 20 Hertz Band Pass Filter)

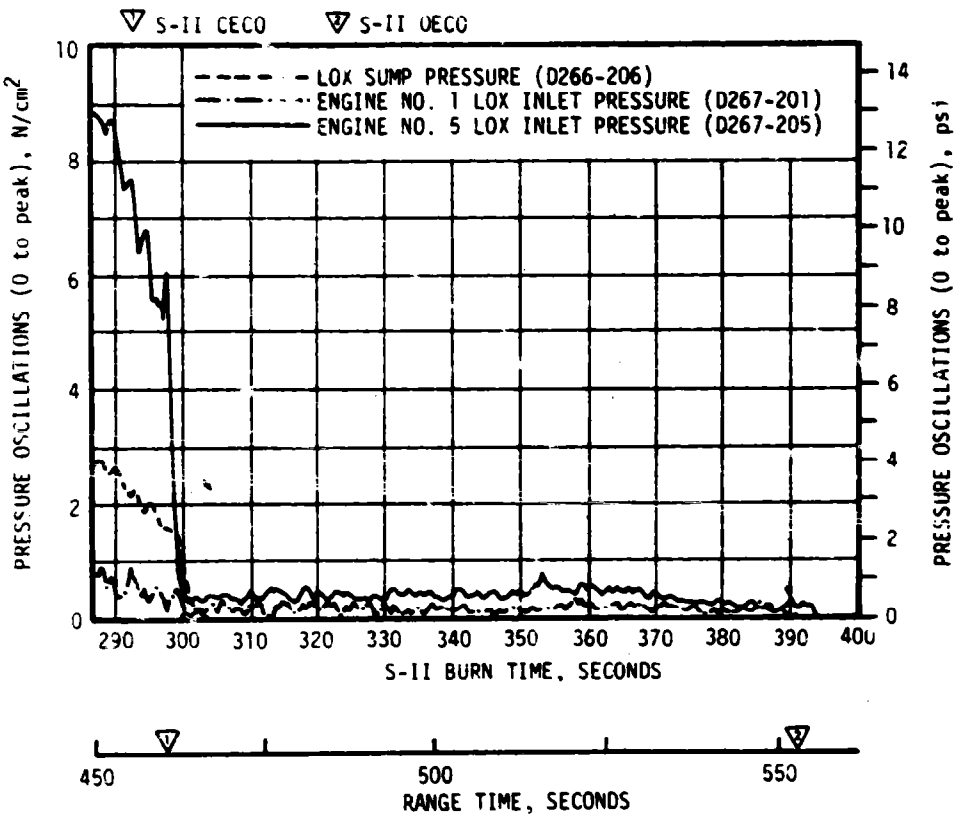

Figure 9-13. S-II Post-CECO LOX Sump, Center Engine and Outboard Engine LOX Inlet Pressure (14 to 20 Hertz Band Pass Filter)

Vibration measurements E99-411 and E100-411 (forward bending mode, pitch and yaw, respectively), installed in the S-IVB forward skirt, did not indicate any increased vibration levels following step pressurization (10,314 seconds). Both E99 and E100 indicated ±0.03 g compared to ±0.58 g for E99 and ±0.52 g for E100 on the AS-505 flight when the increase in 45 hertz vibration was observed.

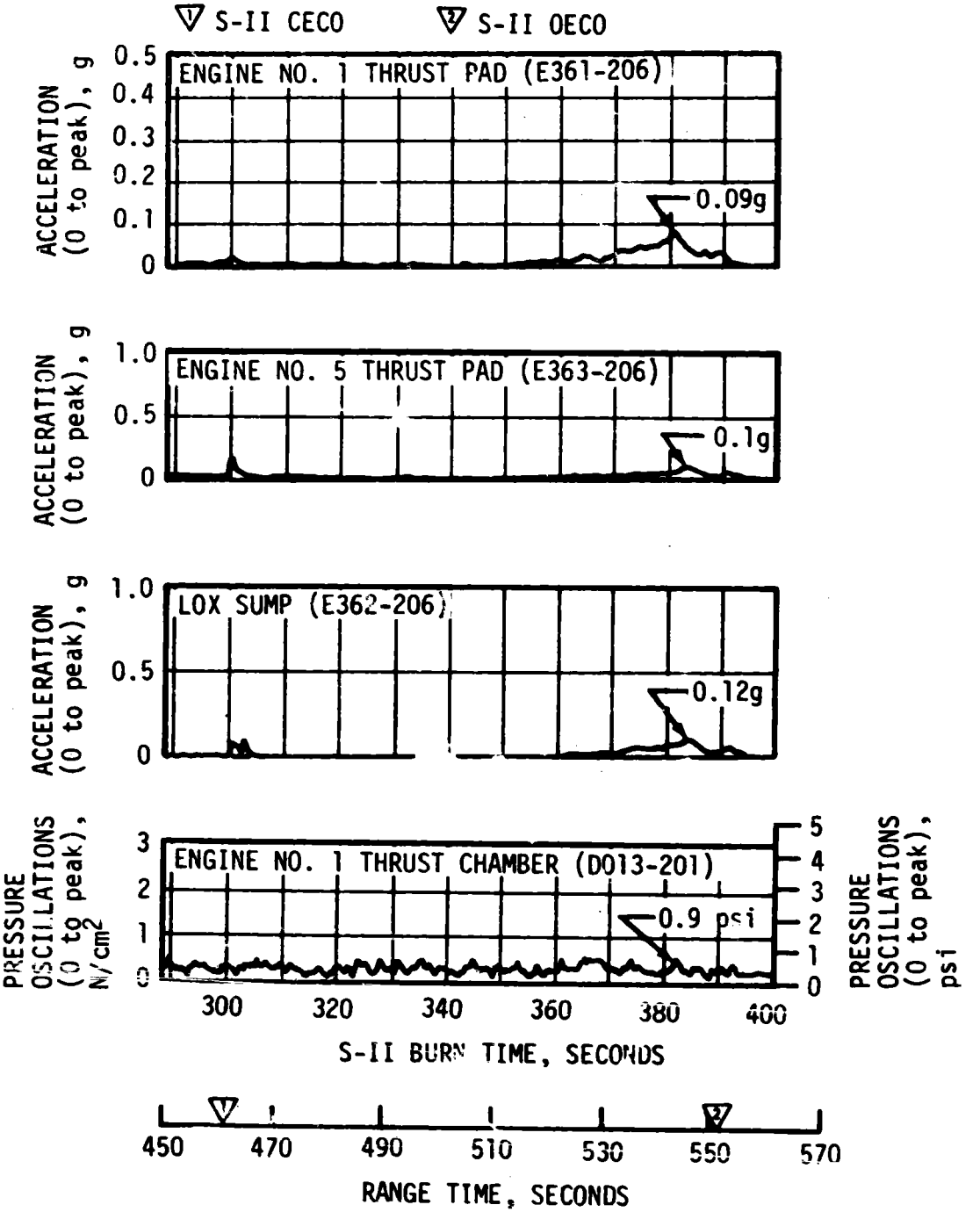

Figure 9-14. Acceleration and Pressure Characteristics from S-II CECO to OECO (8 to 14 Hertz Band Pass Filter)

Table 9-1. Summary of Peak S-II Oscillation Amplitudes

PARAMETER	TIME PERIOD (SEC)			
	180 to 205	225 to 267	268 to 351	405 to 463
Center Engine Beam, Gpeak	0.90	1.75	3.75	3.70
Engine No. 1 Thrust Pad, Gpeak	0.25	0.50	0.90	0.75
LOX Sump, Gpeak	0.75	2.40	2.60	2.10
Center Engine Chamber Pressure, psi*	2.0	4.0	5.0	4.4
Engine No. 1 Chamber Pressure, psi*	2.4	4.5	4.9	2.0
LOX Sump, psi*	1.5	5.5	5.1	3.7
Center Engine Inlet, psi*	4.0	11.0	17.5	15.0
Engine No. 1 Inlet, psi*	7.7	12.8	10.4	3.8

*0 to peak

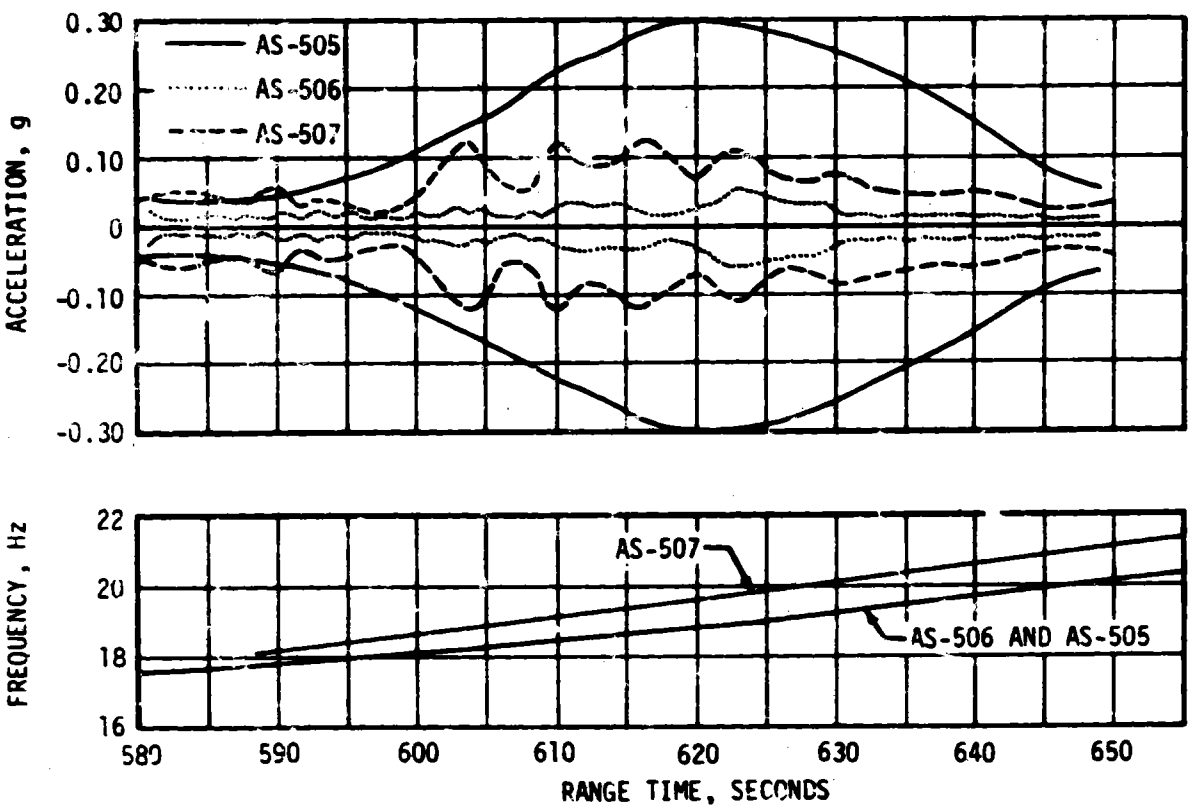

Figure 9-15. S-IVB AS-507, AS-506 and AS-505 Gimbal Pad Response Versus Flight Time - First Burn

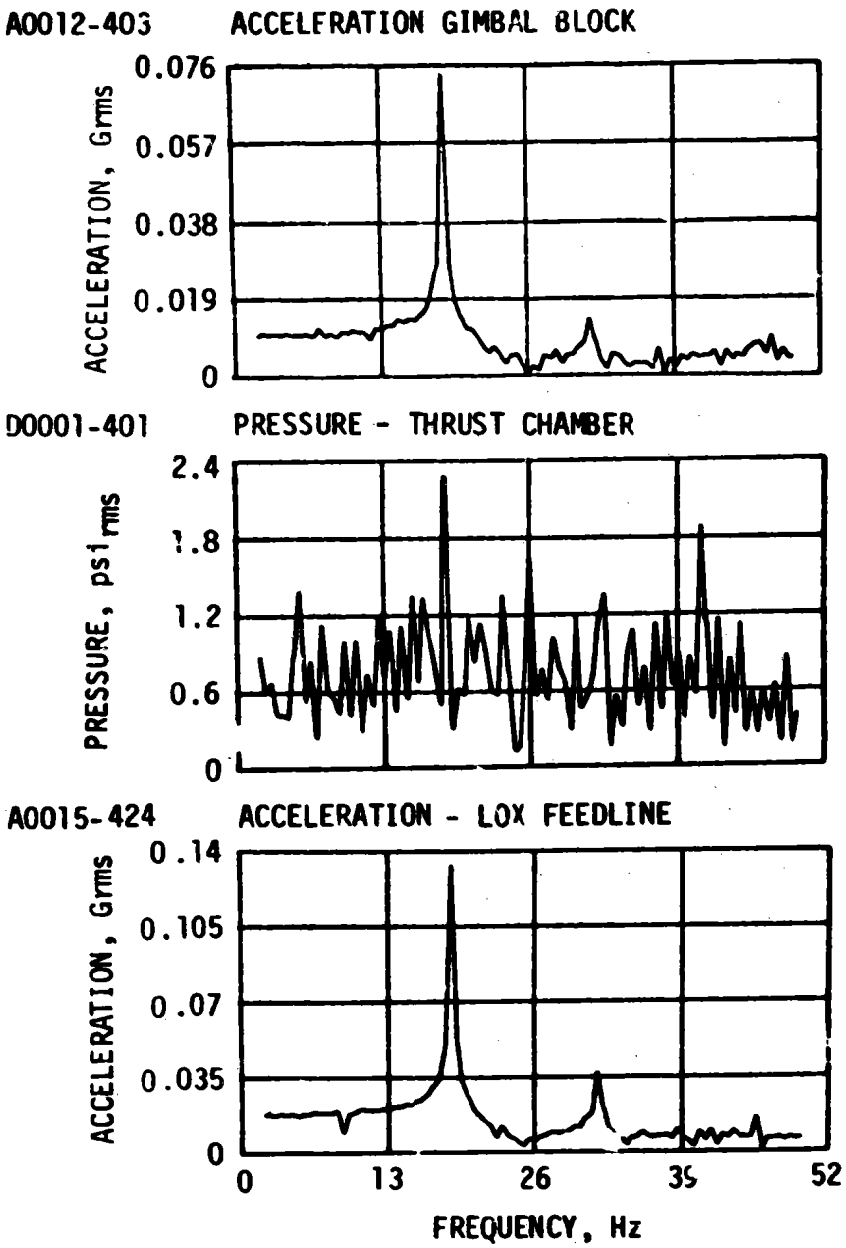

Figure 9-16. S-IVB First Burn Spectral Analysis at 610 Seconds

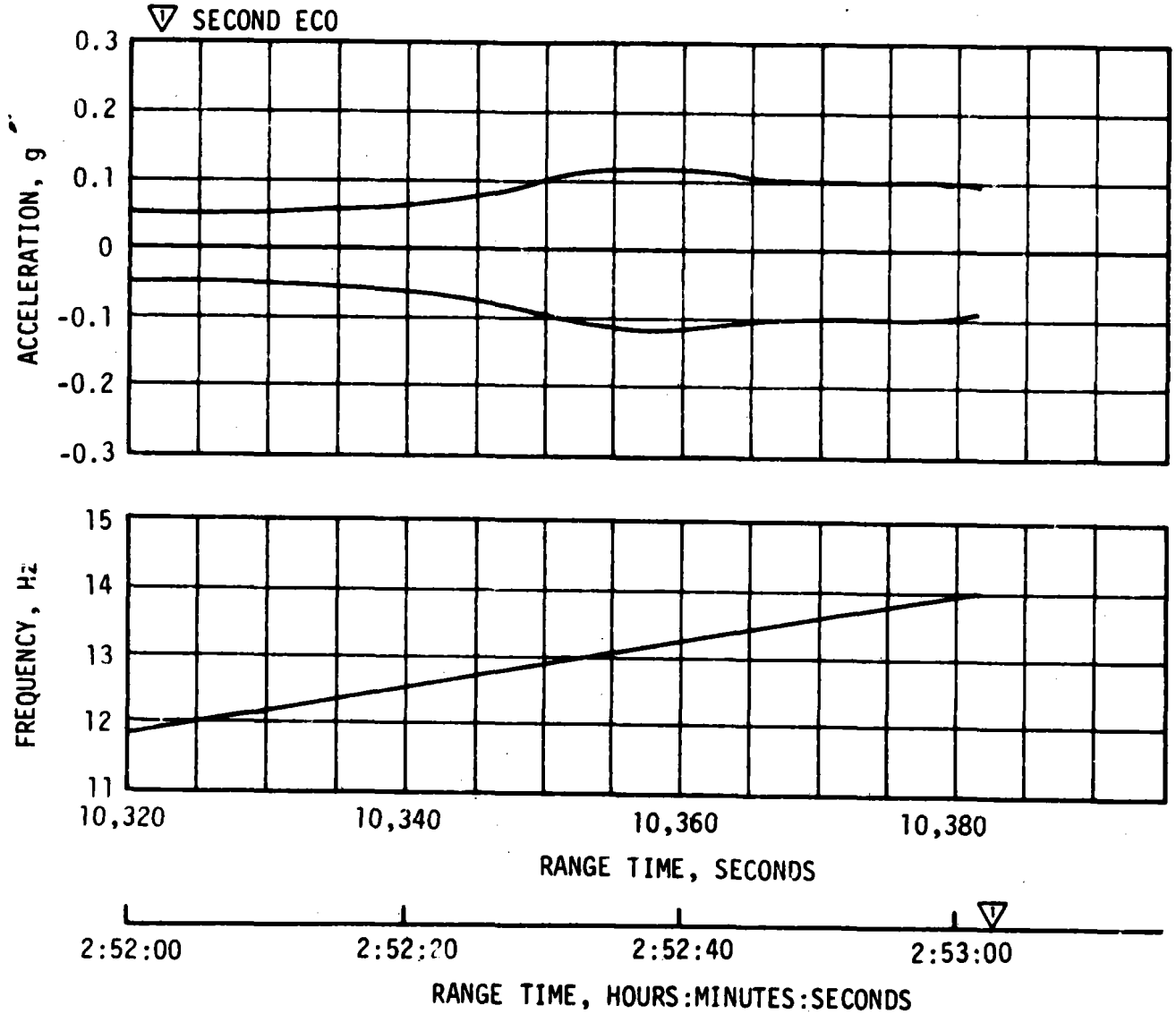

Figure 9-17. S-IVB AS-507 Gimbal Pad Response Versus Flight Time - Second Burn

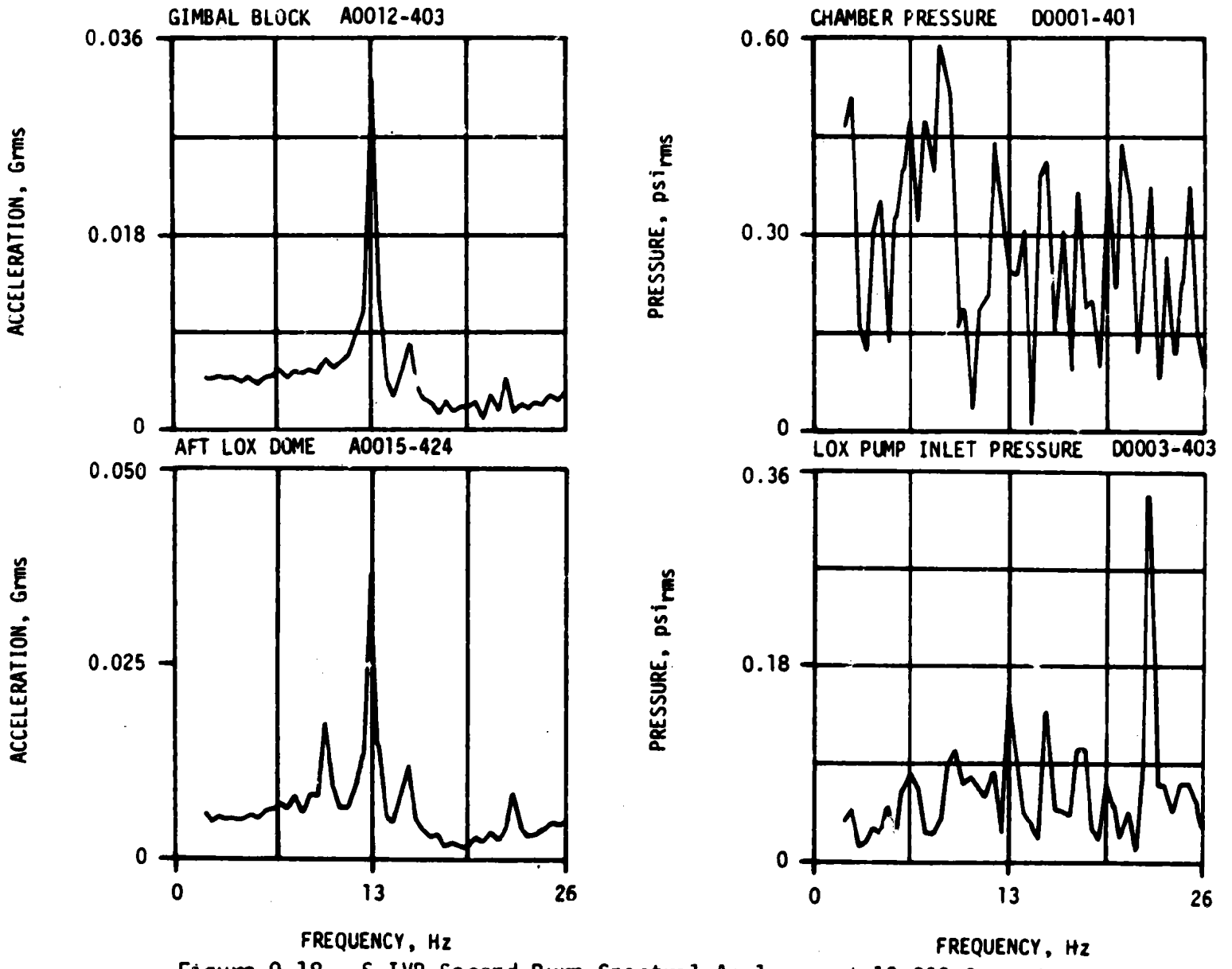

Figure 9-18. S-IVB Second Burn Spectral Analyses at 10,360 Seconds

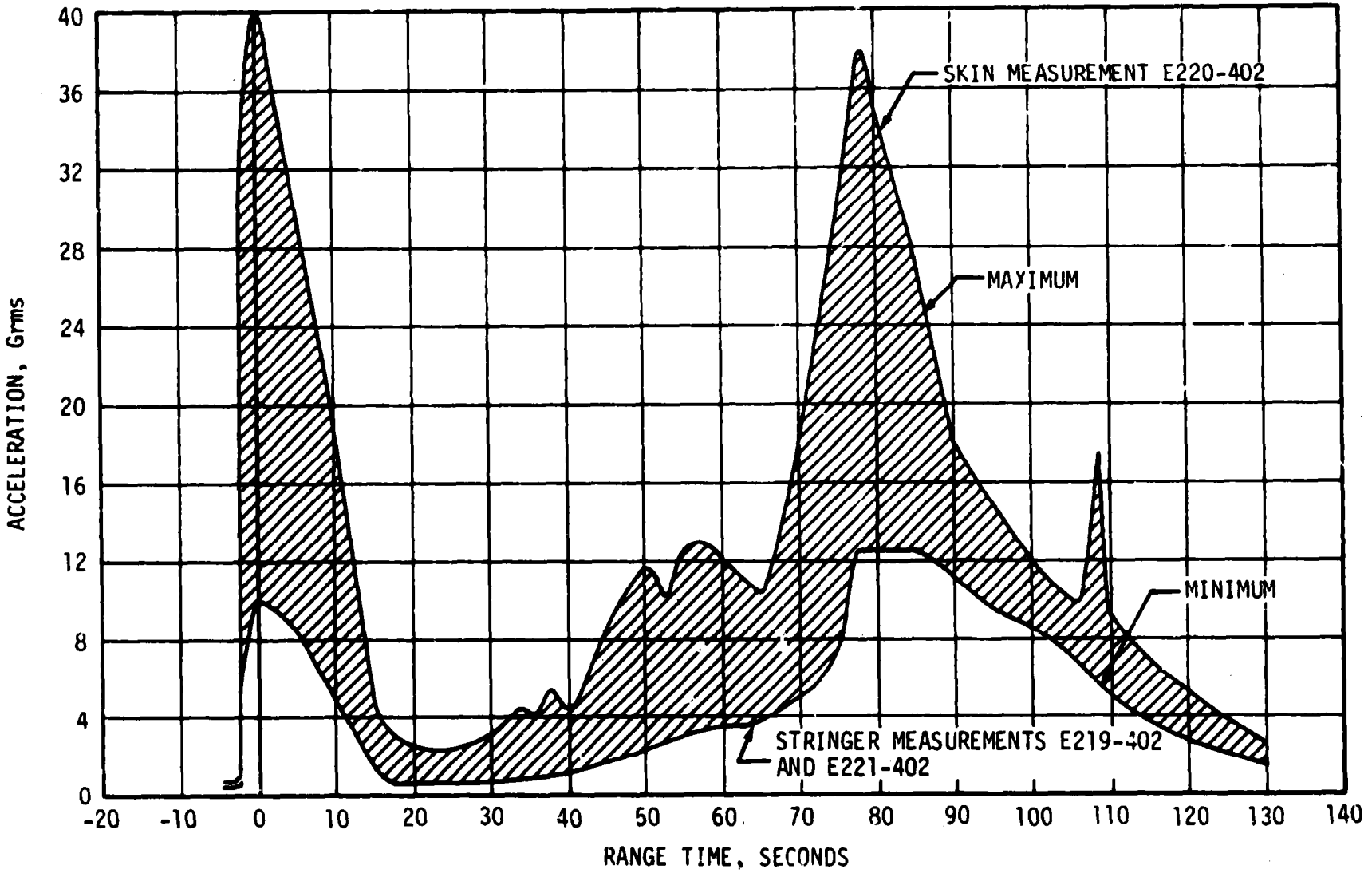

Figure 9-19. S-IVB Aft Interstage Skin and Stringer Vibration

SECTION 10

GUIDANCE AND NAVIGATION

10.1 SUMMARY

10.1.1 Flight Program

The guidance and navigation system performed satisfactorily throughout the mission. All maneuvers, switch selector event sequencing, and staging occurred very close to nominal times. The parking orbit and Translunar Injection (TLI) parameters were within the 3-sigma tolerance.

The S-IVB/IU did not achieve heliocentric orbit because it did not pass sufficiently near the moon for slingshot. The duration of the ground commanded ullage engine burn was computed using a telemetered state vector rather than a vector obtained from tracking. The difference between the two vectors at 10,417.2 seconds (23 seconds after TLI) was 5.7 m/s (18.7 ft/s). This difference was less than the allowable 3-sigma limits but exceeded the allowable limits for accomplishing slingshot. This difference was a result of rather large space-fixed component velocity differences observed prior to the S-IVB stage second burn, which was enlarged through the second active guidance period. These component velocity differences were probably caused by a combination of a scale factor gain error in the Z (downrange) accelerometer, a different from nominal LH_2 vent impulse in parking orbit and other unidentified sources.

At 36.6 seconds, the Y (pitch) gimbal counter reading changed 2.8 degrees between successive minor loop samples. The maximum acceptable change was 0.4 degree. The reading was rejected, a minor-loop error word was telemetered, and the preceding reading was used. No other excessive reading changes occurred during the mission.

10.1.2 Instrument Unit Components

The Launch Vehicle Digital Computer (LVDC), the Launch Vehicle Data Adapter (LVDA), and the -124M-3 inertial platform functioned satisfactorily. At 37.01 seconds, bit 1 (sign bit) was set in Mode Code 24 status work indicating a disagreement between the A and B counters of the Z (downrange) accelerometer. The B counter reading was used because its value was nearer to that expected by the flight program. Subsequent readings exhibited no disagreements and therefore, the A counter readings were used for the remainder of the mission.

During translunar coast, LVDC Error Monitor Register Bits 1 and 15 were set indicating two separate disagreements in two triple redundant signal paths between the LVDA and LVDC. System operation was not affected.

10.2 GUIDANCE COMPARISONS

The postflight guidance error analysis was based on comparisons of the ST-124M-3 platform measured velocities with the postflight trajectory established from external tracking data (see paragraph 4.2). The velocity differences shown in Figure 10-1 are characteristic of platform system errors. The comparisons made and reported herein are referenced to the AS-507 final (14 day) postflight trajectory. The boost-to-parking orbit portion of the trajectory was a composite fit of C-Band radar data. The parking orbit trajectory was generated from an orbit fit of Bermuda (BDA), Carnarvon (CRO) and Merritt Island Launch Area (MILA) C-Band radar. The second burn trajectory was constructed from platform measured velocities constrained to orbital solutions.

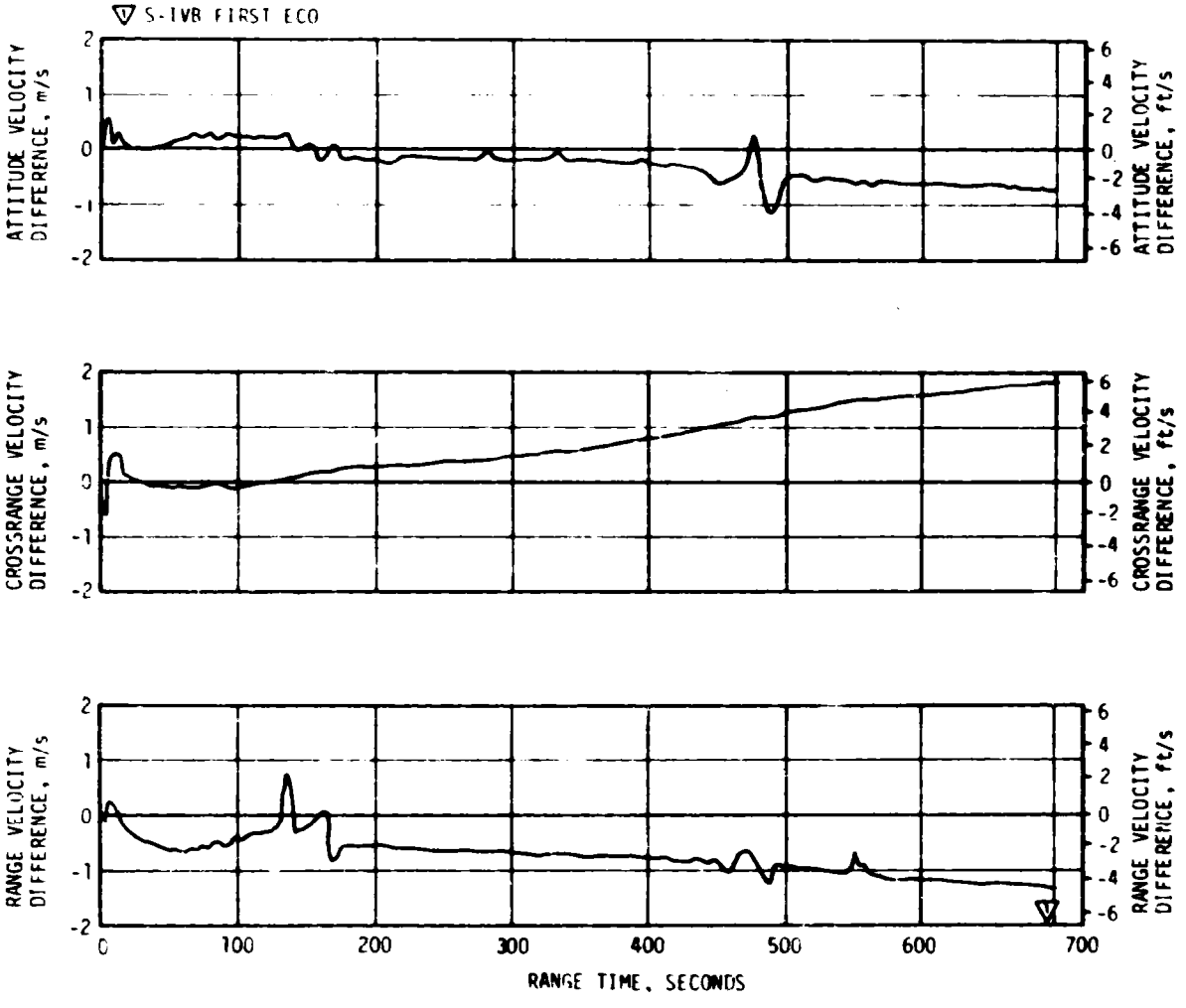

Figure 10-1. Trajectory and ST-124M-3 Platform Velocity Comparison (Trajectory Minus Guidance)

Figure 10-1 presents the comparisons of the platform measured velocities with corresponding values from the postflight trajectory. A positive difference indicates trajectory data greater than the platform measurement. The velocity differences at first S-IVB Engine Cutoff (ECO) were -0.76 m/s (-2.49 ft/s), 1.84 m/s (6.04 ft/s), and -1.34 m/s (-4.40 ft/s), for vertical, crossrange, and downrange velocities, respectively. Although these velocity differences are relatively small and within specification, the difference in the downrange component is the largest value for that component observed on a Saturn V flight. The trajectory for the remainder of the mission was relatively insensitive to crossrange velocity differences. An error analysis based on the velocity differences shown in Figure 10-1 indicates all hardware errors were very small except for the downrange accelerometer. Table 10-1 presents the velocity differences at first S-IVB cutoff for each of the Saturn V flights.

The platform velocity comparisons shown for the second S-IVB burn in Figure 10-2 reflect differences in initial state vectors for the second burn computed by the LVDC and postflight trajectory program. The LVDC state vector was in error as a result of an initial error at initialization of orbital navigation and approximately 35,585.8 N-s (8000 lbf-s) (4.4 percent) low in total impulse due to LH_2 venting. The crossrange and the downrange velocity differences shown in Figure 10-2 are not realistic,

Table 10-1. Saturn V Platform Velocity Differences at First S-IVB ECO

VEHICLE	TRAJECTORY MINUS LVDC VELOCITY DIFFERENCES M/S (FT/S)		
	$\Delta\dot{X}$	$\Delta\dot{Y}$	$\Delta\dot{Z}$
AS-501	1.9 (6.2)	-2.9 (-9.5)	-0.5 (-1.6)
AS-502	-0.7 (-2.3)	-1.85 (-6.07)	-0.3 (-0.98)
AS-503	-0.10 (-0.33)	-1.45 (-4.76)	0.10 (0.33)
AS-504	-1.42 (-4.66)	2.66 (8.73)	0.31 (1.02)
AS-505	-0.8 (-2.5)	1.0 (3.3)	-0.6 (-2.0)
AS-506	1.52 (4.99)	1.73 (5.68)	0.54 (1.77)
AS-507	-0.76 (-2.49)	1.84 (6.04)	-1.34 (-4.40)

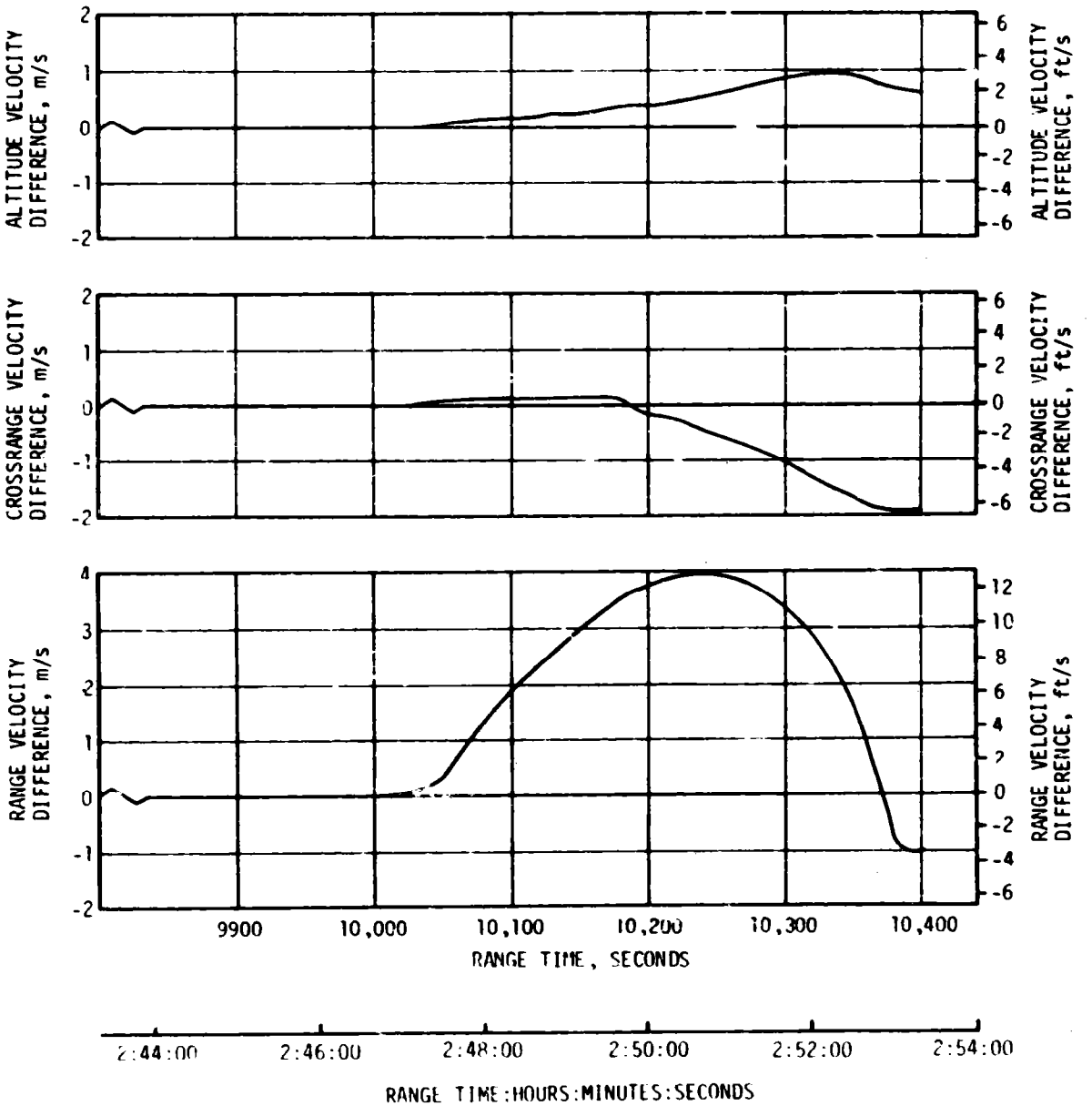

Figure 10-2. Trajectory and ST-124M-3 Platform Velocity Comparison - Second S-IVB Burn (Trajectory Minus Guidance)

because there was no ground tracking during Time Base 6 (T_6). Therefore, the trajectory state vector may not be a reliable reference. The characteristic velocity determined from the platform velocities during second burn was very near nominal. LVDC velocity was 0.46 m/s (1.51 ft/s) higher than the postflight trajectory indication and 0.5 m/s (1.64 ft/s) lower than the operational trajectory.

Velocities measured by the ST-124M-3 platform system are shown for significant event times in Table 10-2 along with corresponding values from both the postflight and operational trajectories. The differences between the telemetered velocities and the postflight trajectory values reflect some combination of small guidance hardware errors and tracking errors. The differences between the telemetered and operational trajectory values indicate differences between predicted and actual flight environment and vehicle performance.

Comparisons of navigation (PACSS 13 coordinate system) positions, velocities, and flight path angle at significant flight event times are presented in Table 10-3. The guidance (LVDC) and postflight trajectory values are in relatively good agreement for the boost-to-parking orbit burn mode. However, the downrange velocity component errors are larger than those observed on previous Saturn V flights. Although the differences are well within 3-sigma specifications and the accuracy of the data compared, component error buildup during Earth Parking Orbit (EPO) are more sensitive to downrange initial errors than to either of the other components. Figure 10-3 shows the buildup of the velocity differences during EPO. Since T_6 was not covered by either telemetry or tracking, comparisons are shown at ignition of second S-IVB burn. The difference in total position and velocity at second ignition is very small, but the component differences are rather large. The effects of these second burn initial errors on the state vector at TLI are discussed below.

10.2.1 OMPT/LVDC Navigation State Vector Differences

The differences between Observed Mass Point Trajectory (OMPT) tracking data (postflight trajectory) and LVDC telemetry as discussed in paragraph 4.3.5 were within 3-sigma tolerances. The LVDC state vector, which was used to determine the duration of second midcourse Auxiliary Propulsion System (APS) ullage engine burn revealed that the LVDC had a total velocity magnitude 5.7 m/s (18.7 ft/s) greater than the velocity obtained from tracking data (see Table 10-4). A velocity error greater than approximately 4 m/s (13 ft/s) would prevent slingshot. The velocity tolerance is not precisely 4 m/s (13 ft/s) because of slight differences between telemetered and tracking values of geocentric radius and inertial flight path angle.

Comparisons of free-trajectory simulation runs from the OMPT and LVDC state vector at parking orbit insertion to T_6 revealed component position and velocity differences which were very close to those observed between the LVDC and OMPT as shown in Tables 10-5 and 10-6. These differences are propagated through the simulated S-IVB second burn to approximately the same differences which existed between telemetered and tracking data at TLI +23 seconds as shown in Table 10-4.

Table 10-2. Inertial Platform Velocity Comparisons (PACSS 12 Coordinate System)

EVENT	DATA SOURCE	VELOCITY M/S (FT/S)		
		VERTICAL ($\dot{X}m$)	CROSSRANGE ($\dot{Y}m$)	RANGE ($\dot{Z}m$)
S-IC OECO	Guidance	2644.95 (8677.66)	-7.05 (-23.13)	2222.90 (7292.98)
	Postflight Trajectory	2644.72 (8676.90)	-6.88 (-22.57)	2222.77 (7292.55)
	Operational Trajectory	2645.05 (8677.99)	-0.87 (-2.85)	2234.39 (7330.68)
S-II OECO	Guidance	3405.80 (11,173.88)	-1.35 (-4.43)	6797.08 (22,300.13)
	Postflight Trajectory	3405.09 (11,171.56)	0.11 (0.36)	6796.28 (22,297.51)
	Operational Trajectory	3393.42 (11,133.27)	-3.04 (-9.97)	6811.54 (22,347.57)
First S-IVB ECO	Guidance	3185.10 (10,449.80)	1.00 (3.28)	7603.85 (24,947.01)
	Postflight Trajectory	3184.35 (10,447.34)	2.82 (9.25)	7602.55 (24,942.75)
	Operational Trajectory	3174.08 (10,413.65)	1.55 (5.09)	7601.07 (24,937.89)
Parking Orbit Insertion	Guidance	3184.60 (10,448.16)	1.00 (3.28)	7605.50 (24,952.43)
	Postflight Trajectory	3183.82 (10,445.60)	2.83 (9.28)	7604.20 (24,948.16)
	Operational Trajectory	3173.53 (10,411.84)	1.56 (5.12)	7602.61 (24,942.95)
Second S-IVB ECO*	Guidance	2401.85 (7880.09)	516.50 (1694.55)	2006.80 (6583.99)
	Postflight Trajectory	2402.38 (7881.82)	514.51 (1688.02)	2005.69 (6580.35)
	Operational Trajectory	2407.53 (7898.72)	518.02 (1699.54)	2001.34 (6566.08)
Translunar Injection*	Guidance	2404.25 (7887.96)	517.65 (1698.33)	2009.55 (6593.01)
	Postflight Trajectory	2404.69 (7889.40)	515.72 (1691.99)	2008.37 (6589.14)
	Operational Trajectory	2409.69 (7905.81)	519.04 (1702.89)	2003.78 (6574.08)

*Second burn velocity data represent accumulated velocities from Time Base 6.

Table 10-3. Guidance Comparisons (PACSS 13)

EVENT	DATA SOURCE	POSITIONS METERS (FT)				VELOCITIES M/S (FT/S)				FLIGHT PATH ANGLE (DEG)
		X_S	Y_S	Z_S	R	$\dot{X}_S$	$\dot{Y}_S$	$\dot{Z}_S$	V_S	γ
S-IC OECO	Guidance	6,439,261 (21,126,184)	38,875 (127,543)	159,440 (523,097)	6,441,352 (21,133,045)	899.61 (2951.48)	113.60 (372.70)	2596.47 (8518.60)	2750.25 (9023.13)	20.5247
	Postflight Trajectory	6,439,228 (21,126,076)	38,873 (127,536)	159,396 (522,953)	6,441,318 (21,132,933)	899.24 (2950.26)	113.78 (373.29)	2597.03 (8520.44)	2750.66 (9024.48)	20.5134
	Operational Trajectory	6,438,794 (21,124,652)	39,447 (129,419)	160,190 (525,558)	6,440,907 (21,131,585)	893.01 (2929.82)	119.71 (392.75)	2610.01 (8563.02)	2761.15 (9058.29)	20.3094
S-II OECO	Guidance	6,286,258 (20,624,206)	79,482 (260,768)	1,883,596 (6,179,777)	6,562,873 (21,531,736)	-1945.78 (-6383.79)	90.65 (297.41)	6681.19 (21,919.91)	6959.35 (22,832.51)	0.4518
	Postflight Trajectory	6,286,071 (20,623,593)	79,761 (261,683)	1,883,298 (6,178,799)	6,562,611 (21,530,876)	-1946.63 (-6386.58)	92.09 (302.13)	6680.67 (21,918.21)	6959.11 (22,831.73)	0.4421
	Operational Trajectory	6,286,247 (20,624,170)	79,783 (261,755)	1,881,611 (6,173,264)	6,562,296 (21,529,843)	-1947.50 (-6389.44)	88.65 (290.85)	6698.44 (21,976.51)	6976.37 (22,888.50)	0.4611
First S-IVB ECO	Guidance	5,910,612 (19,391,772)	91,436 (299,987)	2,852,011 (9,356,991)	6,563,357 (21,533,323)	-3387.02 (-11,112.27)	77.73 (255.02)	7016.28 (23,0 .29)	7791.41 (25,562.37)	-0.0019
	Postflight Trajectory	5,910,310 (19,390,781)	91,942 (301,647)	2,851,572 (9,355,551)	6,562,902 (21,531,831)	-3388.09 (-11,115.78)	79.44 (260.63)	7015.02 (23,015.16)	7790.76 (25,560.40)	-0.01515
	Operational Trajectory	5,919,482 (19,420,873)	91,318 (299,600)	2,833,602 (9,296,594)	6,563,376 (21,533,386)	-3365.04 (-11,040.16)	78.23 (256.66,	7026.83 (23,053.90)	7791.40 (25,562.34)	-0.0010
Parking Orbit Insertion	Guidance	5,876,321 (19,279,268)	92,208 (302,520)	2,921,985 (9,586,565)	6,563,356 (21,533,320)	-3470.65 (-11,386.65)	76.56 (251.18)	6977.20 (22,891.08)	7793.11 (25,567.95)	-0.00033
	Postflight Trajectory	5,876,007 (19,278,238)	92,730 (304,232)	2,921,533 (9,585,082)	6,562,881 (21,531,762)	-3471.73 (-11,390.19)	78.28 (256.82)	6975.96 (22,887.01)	7792.50 (25,565.94)	-0.01365
	Operational Trajectory	5,885,410 (19,309,088)	92,095 (302,149)	2,903,684 (9,526,522)	6,563,376 (21,533,386)	-3448.82 (-11,315.03)	77.08 (252.89)	6987.91 (22,926.21)	7793.02 (25,567.65)	0.0001
Second S-IVB Ignition	Guidance	3,436,451 (11,274,446)	-106,928 (-350,814)	-5,603,742 (-18,384,980)	6,574,388 (21,569,514)	6643.20 (21,795.28)	113.55 (372.54)	4068.49 (13,348.06)	7790.38 (25,560.63)	0.020271
	Postflight Trajectory	3,468,449 (11,379,426)	-107,758 (-353,536)	-5,584,270 (-18,321,096)	6,574,635 (21,570,325)	6619.21 (21,716.57)	115.03 (377.40)	4104.56 (13,466.40)	7789.39 (25,555.74)	0.02797
	Operational Trajectory	3,424,121 (11,233,994)	-107,289 (-351,999)	-5,611,448 (-18,410,262)	6,574,532 (21,569,986)	6651.89 (21,823.79)	113.50 (372.36)	4053.34 (13,298.36)	7790.38 (25,559.00)	0.0219

Table 10-3. Guidance Comparisons (PACSS 13) (Continued)

EVENT	DATA SOURCE	POSITIONS METERS (FT)				VELOCITIES M/S (FT/S)				FLIGHT PATH ANGLE (DEG)
		X_S	Y_S	Z_S	R	$\dot{X}_S$	$\dot{Y}_S$	$\dot{Z}_S$	V_S	γ
Second S-IVB ECO	Guidance	5,723,200 (18,776,903)	-19,682 (-64,573)	-3,534,921 (-11,597,182)	6,726,839 (22,069,682)	6895.44 (22,622.83)	668.36 (2192.78)	8286.97 (27,188.22)	10,801.28 (35,437.27)	8.036455
	Postflight Trajectory	5,744,775 (18,847,687)	-20,174 (-66,188)	-3,504,521 (-11,497,772)	6,729,376 (22,078,005)	6859.91 (22,506.27)	667.95 (2191.44)	8308.54 (27,258.99)	10,795.80 (35,419.30)	8.1370
	Operational Trajectory	5,738,800 (18,828,084)	-18,182 (-59,652)	-3,517,351 (-11,539,865)	6,730,967 (22,083,225)	6882.03 (22,578.84)	669.96 (2198.03)	8293.57 (27,209.88)	10,797.89 (35,426.1[illegible])	8.1560
Translunar Injection	Guidance	5,791,796 (19,001,955)	-12,985 (-42,602)	-3,451,698 (-11,324,469)	6,742,350 (22,120,571)	6822.62 (22,383.92)	669.69 (2197.15)	8335.29 (27,346.75)	10,792.30 (35,407.81)	8.48424
	Postflight Trajectory	5,812,038 (19,071,319)	-13,481 (-44,229)	-3,421,138 (-11,224,206)	6,744,970 (22,129,167)	6787.38 (22,268.31)	669.47 (2196.42)	8356.81 (27,417.36)	10,786.80 (35,389.80)	8.5840
	Operational Trajectory	5,807,265 (19,052,707)	-11,471 (-37,635)	-3,434,164 (-11,266,942)	6,746,699 (22,134,839)	6808.89 (22,338.83)	671.22 (2202.17)	8341.30 (27,366.47)	10,786.90 (35,395.00)	8.6031

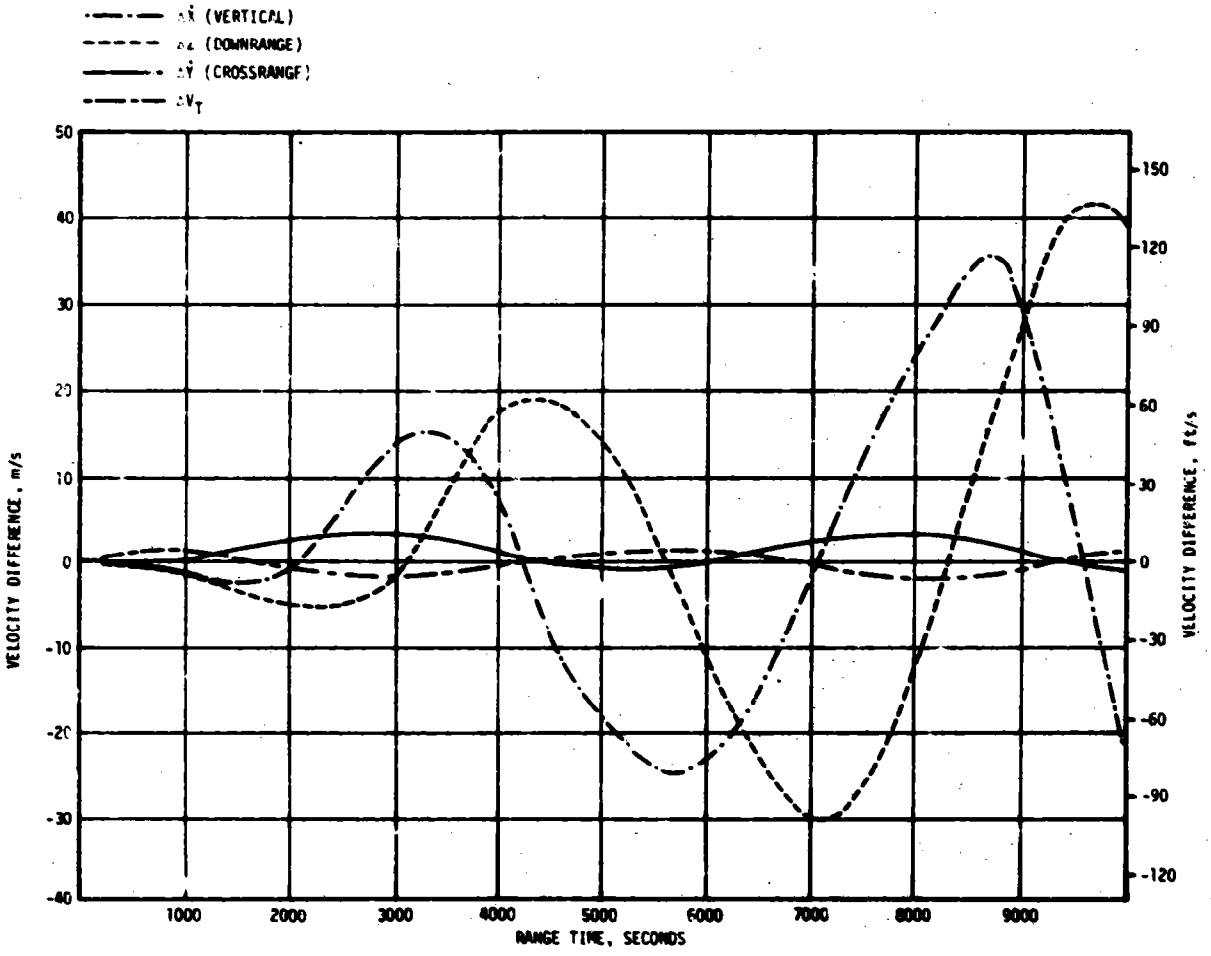

Figure 10-3. Parking Orbit Velocity Comparisons (OMPT Minus LVDC)

Table 10-4. State Vector Comparisons at TLI +23 Seconds (10,417.19 Seconds)

PARAMETER	RADAR (REAL TIME)	LVDC TELEMETRY	RADAR MINUS TELEMETRY	6D SIMULATION* MINUS LVDC
X_s, meters (ft)	5,969,800 (19,585,958)	5,948,300 (19,515,420)	21,500 (70,538)	25,400 (83,333)
Y_s, meters (ft)	1720 (5643)	2580 (8465)	-860 (-2822)	2600 (8530)
Z_s, meters (ft)	-3,225,800 (-10,583,333)	-3,256,700 (-10,684,712)	30,900 (101,379)	32,200 (105,643)
$\dot{X}_s$, m/s (ft/s)	6,613.27 (21,697.08)	6646.46 (21,805.97)	-33.19 (-108.89)	-28.53 (-93.60)
$\dot{Y}_s$, m/s (ft/s)	669.21 (2195.57)	669.98 (2198.10)	-0.77 (-2.53)	0.02 (0.07)
$\dot{Z}_s$, m/s (ft/s)	8454.77 (27,738.75)	8435.85 (27,676.67)	18.91 (62.08)	16.98 (55.71)
V_s, m/s (ft/s)	10,754.82 (35,284.84)	10,760.53 (35,303.58)	-5.71 (-18.74)	-4.76 (-15.62)

*OMPT state vector at earth parking orbit projected on through TLI.

Table 10-5. OMPT/LVDC State Vector Differences at 703 Seconds (Near Parking Orbit Insertion [POI])

PARAMETER	OMPT (14 DAY)	LVDC TELEMETRY	OMPT MINUS LVDC	CORRECTED OMPT MINUS LVDC
X_s, meters (ft)	5,889,520 (19,322,572)	5,889,800 (19,323,491)	-280 (-919)	-150 (-492)
Y_s, meters (ft)	92,420 (303,215)	91,900 (301,509)	520 (1706)	520 (1706)
Z_s, meters (ft)	2,894,230 (9,495,505)	2,894,700 (9,497,047)	-470 (-1542)	-240 (-787)
$\dot{X}_s$, m/s (ft/s)	-3439.28 (-11,283.73)	-3438.24 (-11,280.31)	-1.04 (-3.42)	-0.72 (-2.36)
$\dot{Y}_s$, m/s (ft/s)	78.75 (258.37)	77.02 (252.69)	1.73 (5.68)	1.72 (5.64)
$\dot{Z}_s$, m/s (ft/s)	6991.90 (22,939.30)	6993.21 (22,943.60)	-1.31 (-4.30)	-0.86 (-2.82)
V_s, m/s (ft/s)	7792.50 (25,565.90)	7793.10 (25,567.91)	-0.60 (-2.01)	-0.44 (-1.44)

Table 10-6. OMPT/LVDC State Vector Differences at 9812 Seconds (T_6 +348 Seconds)

PARAMETER	OMPT (14 DAY)	LVDC TELEMETRY	OMPT MINUS LVDC	6D SIMULATION* MINUS LVDC
X_s, meters (ft)	1,826,400 (5,992,126)	1,790,000 (5,872,703)	36,400 (119,423)	39,790 (130,545)
Y_s, meters (ft)	-130,100 (-426,803)	-128,900 (-422,900)	-1100 (-3609)	-1150 (-3773)
Z_s, meters (ft)	-6,313,400 (-20,713,255)	-6,323,900 (-20,747,703)	10,500 (34,448)	11,360 (37,270)
$\dot{X}_s$, m/s (ft/s)	7484.60 (24,555.77)	7497.26 (24,597.31)	-12.66 (-41.54)	-11.74 (-38.52)
$\dot{Y}_s$, m/s (ft/s)	76.38 (250.59)	75.21 (246.75)	1.17 (3.84)	1.18 (3.87)
$\dot{Z}_s$, m/s (ft/s)	2157.89 (7079.69)	2116.48 (6943.83)	41.41 (135.86)	45.25 (148.46)
V_s, m/s (ft/s)	7789.83 (25,557.19)	7790.64 (25,559.84)	-0.81 (-2.65)	-0.05 (-0.16)

*OMPT state vector at earth parking orbit projected on through TLI.

The significant state vector differences at parking orbit insertion may be correlated with a Z (downrange) accelerometer scale factor gain error. For AS-507, simulations show that the probability of achieving slingshot would be less than 50 percent with a nominal APS burn if the scale factor error approaches the 3-sigma value. This error exceeded the 3-sigma value during boost to parking orbit. During the prelaunch ST-124M-3 system test and checkout the Z accelerometer scale factor gain error was approximately 10 percent above its test specification (almost twice 3 sigma). An Unsatisfactory Condition Report (UCR) was generated and a specification waiver was approved based on primary mission requirements.

Initial impulse from venting thrust was approximately 35,585.8 N-s (8000 lbf-s) less than the programed value of 824,923 N-s (180,450 lbf-s) which was 4.4 percent less than that programed. This low impulse is indicated by the thrust curve shown in Figure 10-4. The total velocity gained from venting was very close to the predicted value but it was accumulated more slowly which caused component velocity errors.

Table 10-7 summarizes the contributing factors to the space-fixed navigation vector differences between the OMPT and the LVDC up to the second S-IVB stage burn period (T_6 +348 seconds). The table shows the error contributors to the difference of the two vectors at the end of the first boost period (700 seconds). The OMPT vector was then corrected by the identified error by inspecting the component difference curves. The resulting vector difference at T_6 +348 seconds was caused by the initial hardware errors during the boost period, the vent differences, and the small OMPT error. Table 10-8 summarizes the navigation state vector differences from parking orbit insertion to translunar coast.

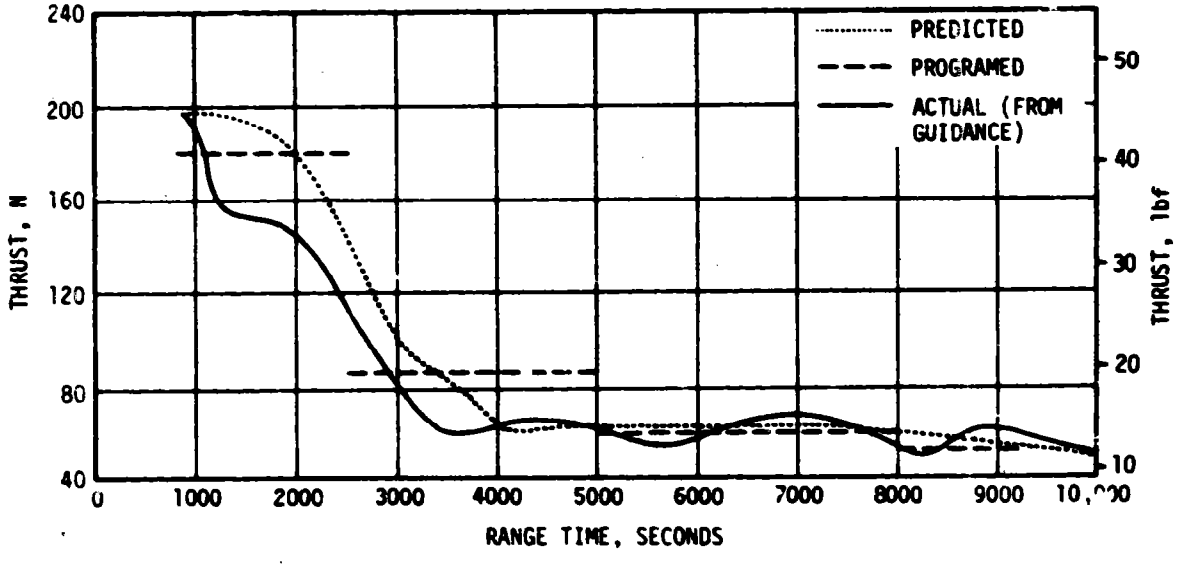

Figure 10-4. LH_2 Continuous Vent Thrust During Parking Orbit

Table 10-7. Contributing Factors to Space Fixed Navigation Vector Differences During Parking Orbit

ERROR SOURCE	ΔX_S METERS (FT)	ΔY_S METERS (FT)	ΔZ_S METERS (FT)	$\Delta \dot{X}_S$ M/S (FT/S)	$\Delta \dot{Y}_S$ M/S (FT/S)	$\Delta \dot{Z}_S$ M/S (FT/S)	ΔV_T M/S (FT/S)
PRIMARY:							
Parking Orbit Insertion Vector Error Contributors:							
ST-124M-3	-140 (-459)	523 (1716)	-234 (-768)	-0.78 (-2.56)	1.72 (5.64)	-0.87 (-2.85)	-0.34 (-1.11)
Tracking*	-140 (-459)	-3 (-10)	-236 (-774)	-0.26 (-0.85)	0.01 (0.03)	-0.44 (-1.4)	-0.36 (-1.2)
TOTAL (700 sec) (OMPT-LVDC)	-280 (-919)	520 (1706)	-470 (-1542)	-1.04 (-3.41)	1.73 ((5.67)	-1.31 (-4.30)	-0.70 (-2.3)
Result[illegible] Vector Error at T[illegible] seconds							
[illegible]-124M-3	22,800 (74,803)	-1300 (-4265)	7000 (22,966)	-7.57 (-24.84)	0.83 (2.72)	25.84 (84.78)	-0.21 (-0.69)
Venting	13,000 (42,651)	300 (984)	4900 (16,076)	-3.75 (-12.3)	0.44 (1.4)	16.09 (52.79)	0.90 (2.6)
Tracking***	600 (1969)	-100 (-328)	-1400 (-4593)	-1.38 (-4.53)	-0.10 (-0.33)	-0.52 (-1.71)	-1.40 (-4.59)
TOTAL** DELTA (OMPT-LVDC)	36,400 (119,423)	-1100 (-3609)	10 500 (34,449)	-12.7 (-41.7)	1.17 (3.84)	41.41 (135.9)	-0.81 (-2.7)

*Estimated by inspecting difference curves.
**Total difference accumulated to 9812.0 seconds using corrected OMPT at 700 seconds.
***Values based on corrected OMPT start point.

Based upon examination of the achieved end conditions, all functions of the IU/LVDC/LVDA guidance and navigation scheme were performed predictably and satisfactorily. Errors in accelerometer scale factor or bias approaching the 3-sigma values, particularly in the downrange accelerometer, are critical (when not properly accounted for) when velocity constraints similar to those for slingshot on AS-507 are necessary.

10.3 NAVIGATION AND GUIDANCE SCHEME EVALUATION

The flight program minor loop detected apparent error conditions twice during the mission at 36.6 seconds and 10,023.6 seconds. However, the natures of the conditions were different. In the first, a Y (pitch) fine gimbal angle reading exhibited a change between successive minor loops of 2.815 degrees. The maximum reasonable change for the minor loop pitch reading is 0.4 degree. The reading was, therefore, rejected and the preceding reasonable pitch gimbal value was used for attitude error calculations in the minor loop. No disagreement between the two pitch fine gimbal angle counters was detected. The subsequent readings were reasonable. The reading did not represent vehicle motion; the true nature of the change is not known. The most probable explanation is an electrical transient occurring during the sampling function. An examination of the mechanism is in progress.

At 10,023.6 seconds following entry into T_6, an unexpected zero reading was encountered in the Z (yaw) gimbal angle. This was caused by two successive zero gimbal readings while the minor-loop Chi and Theta (about that axis) differed by more than 0.06 degree. The zero readings were the result of proper hardware functions. However, the limit of 0.06 degree is a boost setting for use during active Thrust Vector Control (TVC). It replaced the orbital coast value of 1.2 degrees at T_6 -9 seconds during the conversion to boost routines in preparation for second burn. At the time of the error indication, the vehicle attitude was being controlled with the APS, and the vehicle was drifting in the system null region. Since the attitude error exceeded 0.06 degree with no change in the gimbal readings, the zero gimbal reading occurred and caused the minor loop error telemetry. System operation was unaffected. The coast limit of 1.2 degrees should be continued until the boost period is entered.

The active guidance phases start and stop times are given in Table 10-9. The rate-limited attitude commands for S-IVB first burn are given in Figure 10-5. The actual from predicted differences were attributed to variations in flight environment and performance. The corresponding attitude commands for S-IVB second burn are given in Figures 10-6 and 10-7. The differences in actual from predicted values were due to slight navigation errors and stage performance variations.

Orbital guidance events were accomplished satisfactorily. All S-IVB stage first and second burn guidance parameters indicate satisfactory operation. The orbital insertion conditions after S-IVB first burn are given in Table 10-10. The TLI parameters after S-IVB second burn are given in Table 10-11.

10.4 GUIDANCE SYSTEM COMPONENT EVALUATION

10.4.1 LVDA and LVDC Performances

At 37.01 seconds, the flight program correctly detected a disagreement of nine pulse counts in the A and B velocity accumulations from the Z (downrange) accelerometer. The maximum allowable difference was two counts. As a result, the flight program selected the accumulation nearer the computed expected value (B counter). Subsequent readings exhibited no disagreements and the A counter readings were used for the remainder of the mission. The program reaction was proper and prevented the accumulation of velocity from an unreasonable counter reading. The erroneous accumulation in the Z accelerometer A counter could have been caused by an electrical noise spike at the input to the LVDA.

Table 10-8. OMPT/LVDC Navigation State Vector Difference Summary

PARAMETER	PARKING ORBIT INSERTION (OMPT MINUS LVDC)	T_6 +348 SECONDS (OMPT) MINUS LVDC)	FREE TRAJECTORY SIMULATION* (OMPT MINUS LVDC)	VENTING ERROR	DIFFERENCE DUE TO INITIAL STATE VECTOR ERROR**	TOTAL DIFFERENCE (VENTING ERROR PLUS DIFFERENCE DUE TO INITIAL STATE VECTOR ERROR)	TRANSLUNAR INJECTION +23 SECONDS TRACKING MINUS LVDC	6D SIMULATION +23 SECONDS
Range Time, sec	700.0	9812.0	9812.0	9812.0	9812.0	9812.0	10,417.2	10,417.2
ΔX_s, meters (ft)	-280 (-918.6)	36,400 (119,422.6)	39,500 (129,593)	13,000 (42,650)	22,800 (74,803)	35,800 (117,454)	21,500 (70,538)	25,400 (83,333)
ΔY_s, meters (ft)	520 (1706)	-1100 (-3609)	-1100 (-3609)	300 (984)	-1300 (-4265)	-1000 (-3280)	-850 (-2822)	2600 (8530)
ΔZ_s, meters (ft)	-470 (-1542)	10,500 (34,448.8)	12,400 (40,682)	4900 (1607)	7000 (22,966)	11,900 (39,042)	30,900 (101,378)	32,200 (105,643)
$\Delta \dot{X}_s$, m/s (ft/s)	-1.04 (-3.41)	-12.66 (-41.54)	-12.97 (-42.55)	-3.75 (-12.3)	-7.57 (-24.84)	-11.32 (-37.14)	-33.19 (-108.9)	-28.53 (-93.60)
$\Delta \dot{Y}_s$, m/s (ft/s)	1.73 (5.68)	1.17 (3.84)	1.22 (40.0)	0.44 (1.4)	0.83 (2.72)	1.27 (4.17)	-0.77 (-2.5)	0.02 (0.07)
$\Delta \dot{Z}_s$, m/s (ft/s)	-1.31 (-4.30)	41.41 (135.86)	44.97 (147.5)	16.09 (52.79)	25.84 (84.78)	41.93 (137.57)	18.91 (62.04)	16.98 (55.71)
ΔW_s, m/s (ft/s)	-0.70 (-2.30)	-0.81 (-2.66)	-0.10 (-0.33)	0.80 (2.6)	-0.21 (-0.69)	0.59 (1.94)	-5.71 (-18.7)	-4.76 (-15.62)

*Using uncorrected OMPT at 700 seconds.
**Using corrected OMPT at 700 seconds.

Table 10-9. Start and Stop Times for IGM Guidance Commands

EVENT *	IGM PHASE (SEC)		ARTIFICIAL TAU (SEC)		STEERING MISALIGNMENT CORRECTION (SEC)		TERMINAL GUIDANCE (SEC)		CHI FREEZE (SEC)	
	Start	Stop	Start	Stop	Start	Stop	Start	Stop	Start	Stop
First Phase IGM	202.50	487.31	-	-	222.18	-	-	-	-	-
Second Phase IGM	487.31	559.53	487.31	498.68	-	550.99	-	-	-	-
Third Phase IGM	559.53	685.94	559.53	568.78	566.95	685.94	660.40	685.94	685.94	695.76**
Fourth Phase IGM	10,048.18	10,146.07	-	-	10,058.80	-	-	-	-	-
Fifth Phase IGM	10,146.07	10,381.84	10,146.07	10,148.98		10,381.84	10,354.30	10,381.84	10,381.84	10,384.12 **

* All times are for the start of the computation cycle in which the event occurred.

** Start orbital timeline.

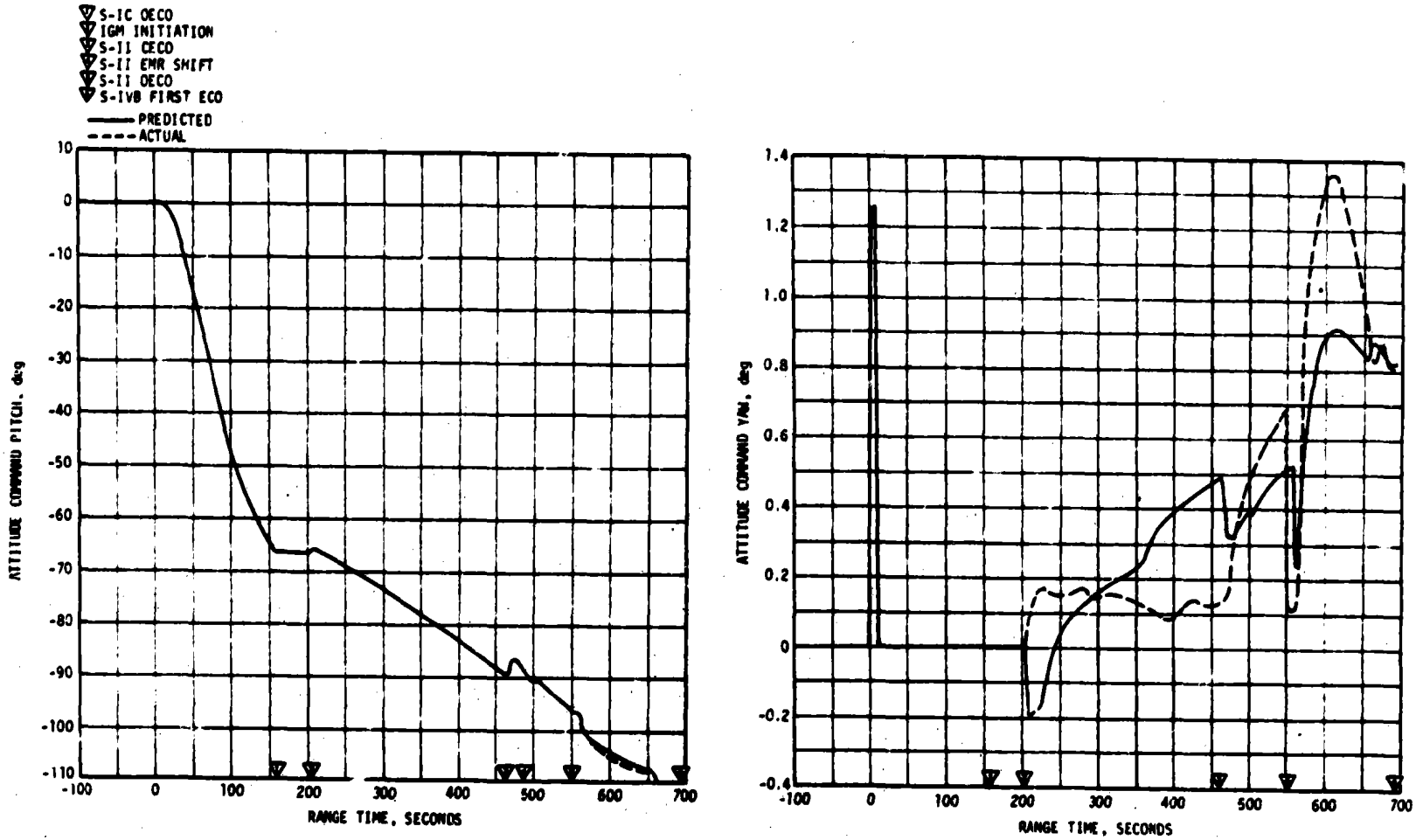

Figure 10-5. Attitude Command During Active Guidance Period

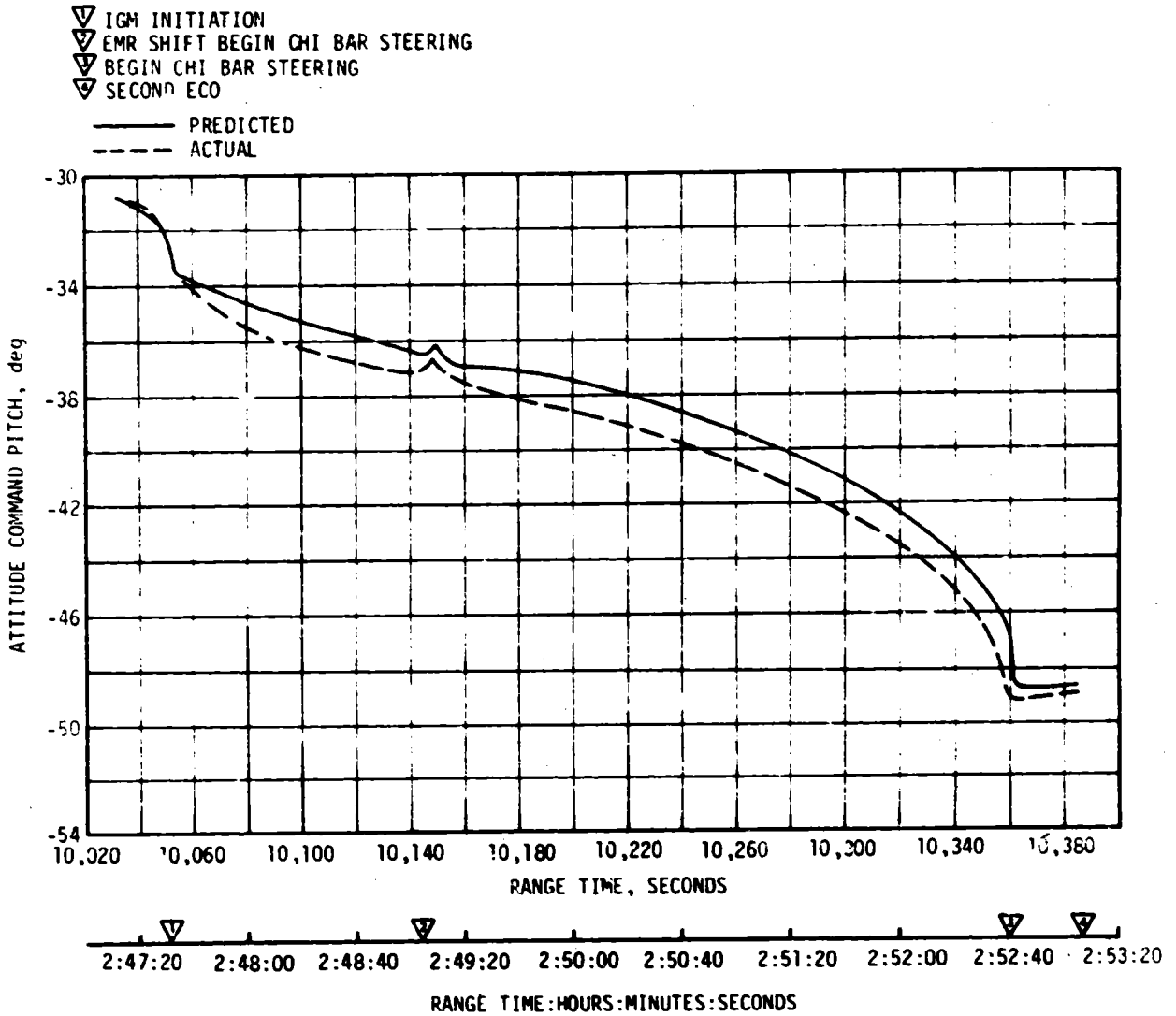

Figure 10-6. Pitch Attitude Angles During S-IVB Second Burn

Launch vehicle digital computer Error Monitor Register bits 1 and 15 were set during the mission representing disagreements between TMR logic channel signals of specific logic functions. Processed telemetry data indicates the following Error Monitor Register conditions:

CASE	ERROR MONITOR REGISTER	PERIOD (Seconds)
1	15	17,883.5 to 21,222.5
2	15 and 1	21,222.5 to 22,933.5
3	1	22,933.5 to (not defined)

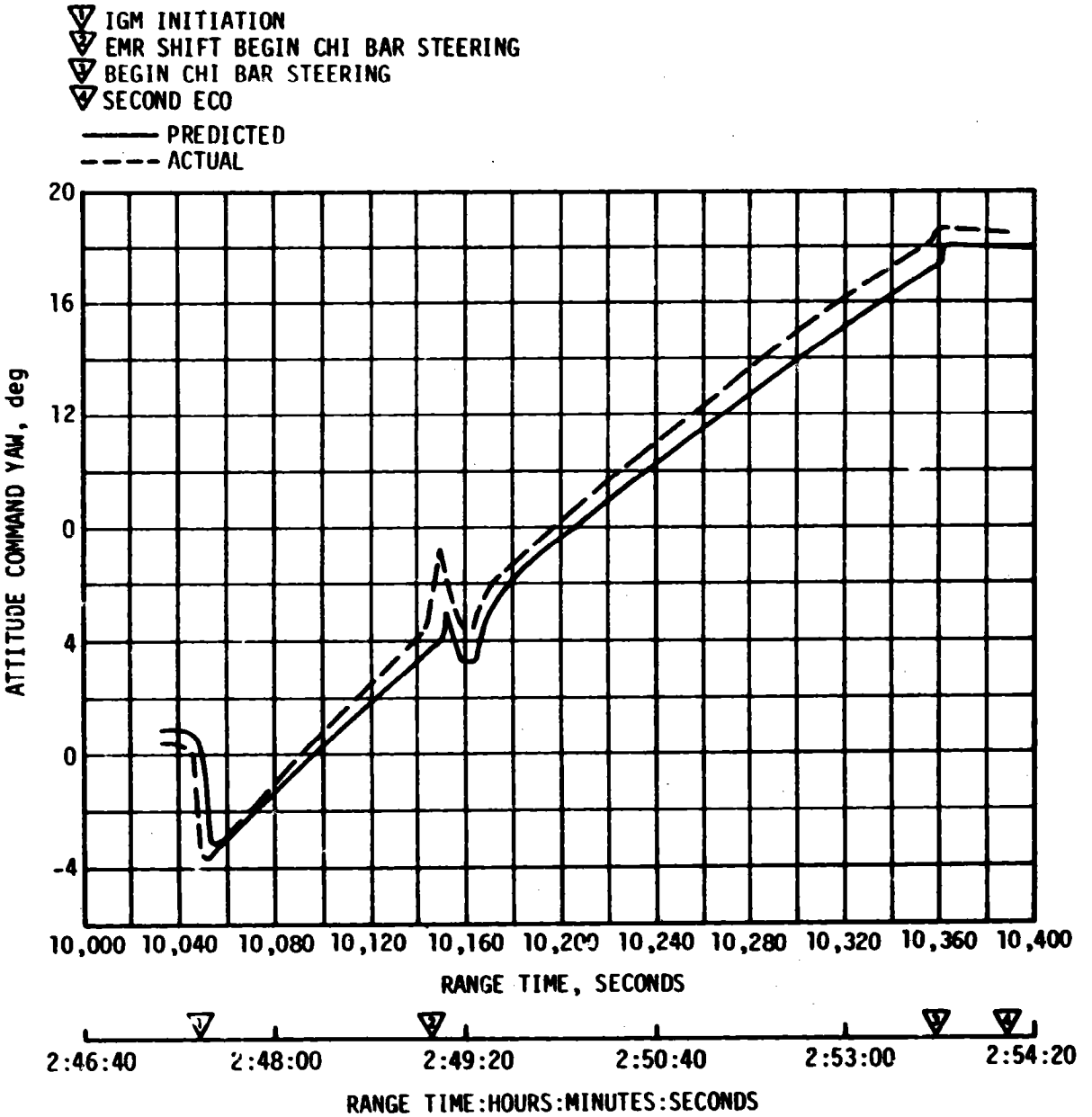

Figure 10-7. Yaw Attitude Angles During S-IVB Second Burn

Telemetered Error Monitor Register and Error Time Word (ETW) analysis indicates two failure points, one associated with data transfer from the LVDC to the LVDA, and a second associated with data address control for each logic signal. An open circuit failure mode was assumed, was effected in the laboratory by interrupting one of the TMR interface lines between the LVDC and LVDA, and was simulated by executing a digital simulation of the AS-507 mission from approximately 13,852 to 13,909 seconds.

Table 10-10. Parking Orbit Insertion Parameters

PARAMETER	OPERATIONAL TRAJECTORY (OT)	OMPT	TRAJECTORY MINUS (OT)	LVDC	LVDC MINUS OT
Space-Fixed Velocity m/s (ft/s)	7793.0 (25,567.6)	7792.5 (25,565.9)	-0.5 (-1.7)	7793.1 (25,567.9)	0.1 (0.3)
Flight Path Angle, deg	0.0001	-0.014	-0.0141	-0.0003	-0.0004
Descending Node, deg	123.146	123.126	-0.020	123.1[illegible]	0.0
Inclination, deg	32.545	32.540	-0.005	32.545	0.0
Eccentricity	0.000004	0.00032	0.000316	0.00002	0.000016

The resultant ETW and Error Monitor Register data decodes were identical to those observed in flight data. During simulation the logic signal disagreements were sensed at the same program instruction address points in the minor loop, data output, interrupt enable, and interrupt processor routines.

The signal paths between the LVDC and LVDA and the logic circuits within the LVDC/LVDA that are associated with the error conditions discussed above are triple redundant. Therefore, no degradation of the LVDC/LVDA function occurred.

10.4.2 Ladder Outputs

The ladder networks and converter amplifiers performed satisfactorily. No data have been observed that indicate an out-of-tolerance condition between Channel A and the reference channel converter-amplifiers.

10.4.3 Telemetry Outputs

Analysis of the available LVDA telemetry buffer and flight control computer attitude error plots indicated symmetry between the buffer outputs and the ladder outputs. The available LVDC power supply plots indicate satisfactory power supply performance. The H60-603 guidance computer telemetry was completely satisfactory.

10.4.4 Discrete Outputs

No valid discrete output register words (tags 043 and 052) were observed to indicate guidance or simultaneous memory failure.

10.4.5 Switch Selector Functions

Switch selector data indicate that the LVDA switch selector functions were performed satisfactorily. No error monitor words were observed that indicate disagreement in the TMR switch selector register positions or in the switch selector feedback circuits. No mode code 24 words or switch

Table 10-11. Translunar Injection Parameters

PARAMETER	OPERATIONAL TRAJECTORY (OT)	OMPT	TRAJECTORY MINUS OT	LVDC	LVDC MINUS OT
Space-Fixed Velocity m/s (ft/s)	10,788.4 (35,395.0)	10,786.8 (35,389.8)	-1.6 (-5.2)	10,792.3 35,407.8)	3.9 (12.8)
Descending Node, deg	120.371	120.338	-0.033	120.376	0.005
Inclination, deg	30.336	30.355	0.019	30.343	0.007
Eccentricity	0.97066	0.96966	-0.00100	0.97081	0.00015
C_3, m^2/s^2 (ft^2/s^2)	-1,773,597 (-19,090,839)	-1,834,425 (-19,745,586)	-60,828 (-654,747)	-1,764,879 (-18,996,999)	8718 (93,840)

selector feedback words were observed that indicated a switch selector feedback was in error. In addition, no indications were observed to suggest that the B channel input gates to the switch selector register positions were selected.

10.4.6 ST-124M-3 Inertial Platform

The inertial platform system performed as designed. The inertial gimbal temperature fell below specifications; however, there are no indications of degraded inertial performance. The temperature went below the minimum specification of 313.15°K (104.0°F) at about 8600 seconds and leveled off at 312.59°K (103.0°F) close to the value seen on previous flights.

An apparent Y (crossrange) velocity change of 1.1 m/s (3.6 ft/s) at 0.1 second was probably caused by asymmetric sampling of an oscillating accelerometer being driven by liftoff vibration. There is no evidence of accelerometer head contact with a mechanical stop.

After Command and Service Module (CSM) separation (after 15,500 seconds), the environmental control parameters exhibited abnormal behavior. This was attributed to the open IU receiving incident solar radiation.

None of the above abnormalities affected the inertial platform or its performance.

SECTION 11

CONTROL AND SEPARATION

11.1 SUMMARY

The AS-507 control system, which was essentially the same as that of AS-506, performed satisfactorily. The Flight Control Computer (FCC), Thrust Vector Control (TVC), and Auxiliary Propulsion System (APS) satisfied all requirements for vehicle attitude control during the flight. Bending and slosh dynamics were adequately stabilized. The prelaunch programed yaw, roll, and pitch maneuvers were properly executed during S-IC boost.

During the maximum dynamic pressure region of flight, the launch vehicle experienced winds that were less than 95-percentile November winds. The maximum average pitch and yaw engine deflections were the result of wind shears.

S-IC/S-II first and second plane separations were accomplished with no significant attitude deviations. Related data indicate that the S-IC retromotors performed as expected. At Iterative Guidance Mode (IGM) initiation, a pitchup transient occurred similar to that seen on previous flights. During the early portion of S-II burn, the outboard engines were required to compensate for a yaw thrust vector misalignment of the center engine. Following Center Engine Cutoff (CECO) there was a change in yaw attitude due to the change in trim conditions. S-II/S-IVB separation occurred as expected without producing any significant attitude deviations. The S-II retromotors and S-IVB ullage motors performed as expected.

Satisfactory control of the vehicle was maintained during first and second S-IVB burns and during coast in Earth Parking Orbit (EPO). During the Command and Service Module (CSM) separation from the S-IVB/IU and during the Transposition, Docking and Ejection (TD&E) maneuver, the control system maintained the vehicle in a fixed inertial attitude to provide a stable docking platform. Following TD&E, S-IVB/IU attitude control was maintained during the evasive maneuver, the maneuver to slingshot attitude, and the LOX dump and APS burns.

11.2 S-IC CONTROL SYSTEM EVALUATION

The AS-507 control system performed adequately during S-IC powered flight. The vehicle flew through winds which were less than 95 percentile for November in the maximum dynamic pressure region of flight. Less than 10

percent of the available engine deflection was used throughout flight (based on average engine gimbal angle). S-IC outboard engine cant was accomplished as planned.

All dynamics were within vehicle capability. In the region of high dynamic pressure, the maximum angles-of-attack were 2.1 degrees in pitch and 1.3 degrees in yaw. The maximum average pitch and yaw engine deflections were 0.3 degree and 0.4 degree, respectively, in the maximum dynamic pressure region. Both deflections were due to wind shears. The absence of any divergent bending or slosh frequencies in vehicle motion indicated that bending and slosh dynamics were adequately stabilized.

Vehicle attitude errors required to trim out the effects of thrust imbalance, thrust misalignment, and control system misalignments were within predicted envelopes. Vehicle dynamics prior to S-IC/S-II first-plane separation were within staging requirements.

11.2.1 Liftoff Clearances

The launch vehicle cleared the mobile launcher structure within the available clearance envelopes. Camera data showing liftoff motion were not available for the AS-507 flight, but simulations with flight data show that less than 10 percent of the available clearance was used. The ground wind was from the west with a magnitude of 6.8 m/s (13.3 knots) at the 18.3 meter (60 ft) level.

The predicted and measured misalignments, slow release forces, winds, and the thrust-to-weight ratio are shown in Table 11-1.

11.2.2 S-IC Flight Dynamics

Maximum control parameters during S-IC burn are listed in Table 11-2. Pitch, yaw and roll plane time histories during S-IC boost are shown in Figures 11-1, 11-2, and 11-3. Dynamics in the region between liftoff and 40 seconds result primarily from guidance commands. Between 40 and 110 seconds, maximum dynamics were caused by the pitch tilt program, wind magnitude, and wind shears. Dynamics from 110 seconds to S-IC/S-II separation were caused by high altitude winds, separated air flow aerodynamics, center engine shutdown, and tilt arrest. The transient at CECO indicates that the center engine cant was 0.13 degree in pitch and yaw.

At Outboard Engine Cutoff (OECO), the vehicle had attitude errors of -0.2, -0.2, and -0.1 degree in pitch, yaw, and roll, respectively. These errors are required to trim out the effects of thrust imbalance, offset Center of Gravity (CG), thrust vector misalignment, and control system misalignments. The maximum equivalent thrust vector misalignments were -0.15, 0.02 and 0.05 degree in pitch, yaw, and roll, respectively.

Table 11-1. AS-507 Misalignment Summary

PARAMETER	PREFLIGHT PREDICTED			LAUNCH		
	PITCH	YAW	ROLL	PITCH	YAW	ROLL
Thrust Misalignment, deg*	±0.34	±0.34	±0.34	-0.15	0.024	0.047
Center Engine Cant, deg	-	-	-	0.128	0.128	-
Servo Amplifier Offset, deg/eng	±0.1	±0.1	±0.1	-	-	-
Vehicle Stacking and Pad Misalignment, deg	±0.29	±0.29	0.0	-0.12	-0.06	0.0
Attitude Error at Holddown Arm Release, deg	-	-		-0.14	-0.06	-0.17
Peak Slow Release Force Per Rod, N (lbf)	415,900 (93,300)			**		
Wind	14.4 m/s (28 knots) at 18.3 meters (60 feet)			6.8 m/s (13.3 knots) at 18.3 meters (60 feet)		
Thrust to Weight Ratio	1.191			1.214		

*Thrust misalignment of 0.34 degree encompasses the center engine cant. A positive polarity was used to determine minimum fin tip/umbilical tower clearance. A negative polarity was used to determine vehicle Ground Support Equipment (GSE) clearances.
**Data not available.

Table 11-2. Maximum Control Parameters During S-IC Burn

PARAMETERS	UNITS	PITCH PLANE		YAW PLANE		ROLL PLANE	
		MAGNITUDE	RANGE TIME (SEC)	MAGNITUDE	RANGE TIME	MAGNITUDE	RANGE TIME (SEC)
Attitude Error	deg	1.09	83.0	-1.05	3.9	-1.13	14.1
Angular Rate	deg/s	-1.05	85.3	0.53	5.2	1.54	14.8
Average Gimbal Angle	deg	0.31	14.2	-0.39	3.9	-0.10	12.4
Angle-of-Attack	deg	-2.07	68.5	-1.48	57.7	-	-
Angle-of-Attack/ Dynamic Pressure Product	deg-N/cm^2	5.72	68.5	4.02	78.0	-	-
Normal Acceleration	m/s^2	-0.407	84.3	0.281	14.9	-	-

There was no significant sloshing observed. The engine response to the observed slosh frequencies showed that the slosh was well within the capabilities of the control system.

The normal accelerations observed during S-IC burn are shown in Figure 11-4. Pitch and yaw plane wind velocities and angles-of-attack are shown in Figure 11-5. The winds are shown both as determined from balloon and rocket measurements and as derived from the vehicle Q-ball.

11.3 S-II CONTROL SYSTEM EVALUATION

The S-II stage attitude control system performance was satisfactory. Analysis of the magnitude of modal components in the engine deflections revealed that vehicle structural bending and propellant sloshing had negligible effect on control system performance. The maximum values of pitch and yaw control parameters occurred in response to CECO. The maximum values of roll control parameters occurred in response to S-IC/S-II separation disturbances. The control responses were within expectations.

Between the events of S-IC OECO and initiation of IGM, the vehicle attitude commands were held constant. Significant events occurring during this interval were S-IC/S-II separation, S-II stage J-2 engine start, second plane separation, and Launch Escape Tower (LET) jettison. The attitude control dynamics throughout this interval indicated stable operation as shown in Figures 11-6 through 11-8. Steady-state attitudes were achieved within 20 seconds from S-IC/S-II separation. The maximum control parameter values for the period of S-II burn are shown in Table 11-3.

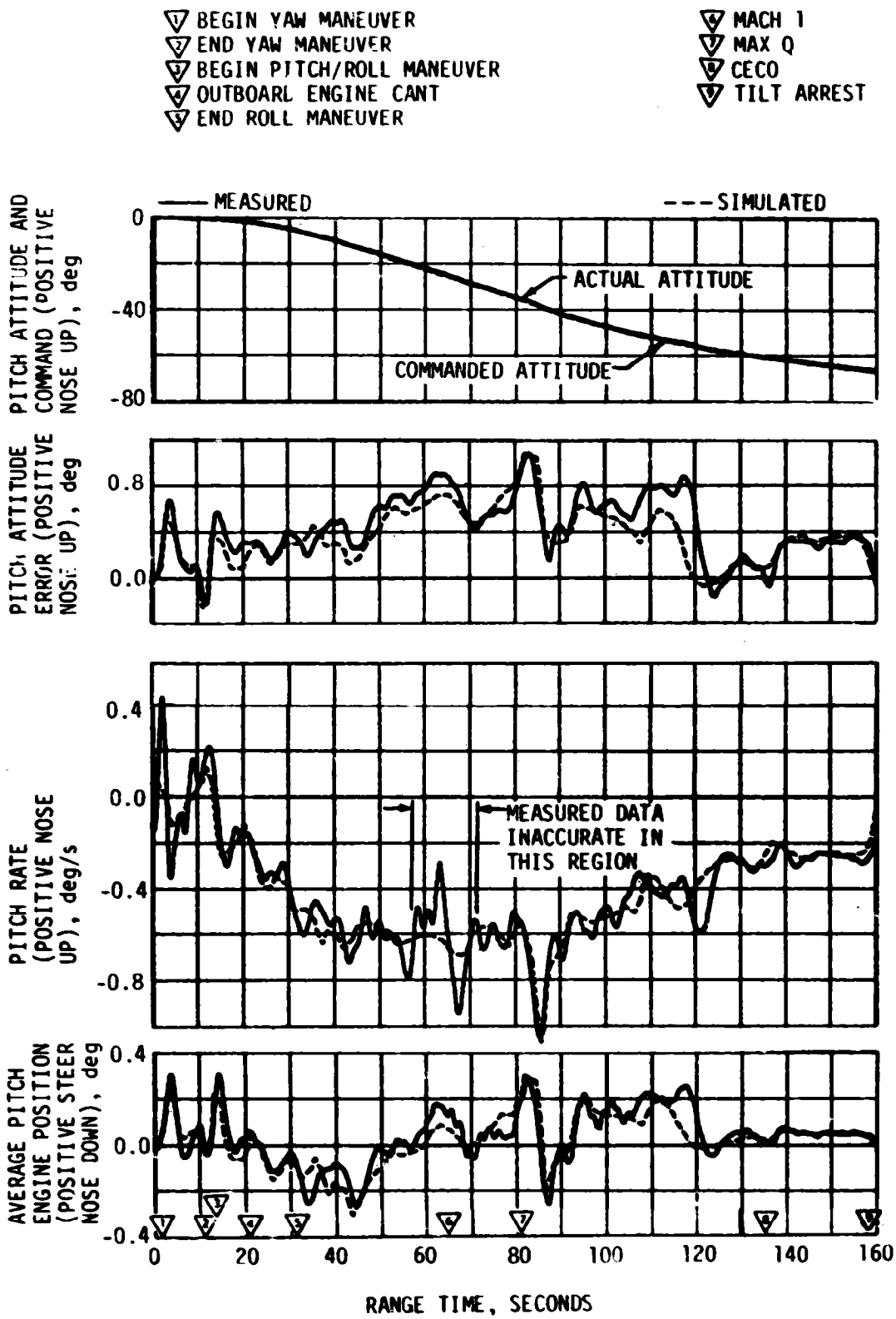

Figure 11-1. Pitch Plane Dynamics During S-IC Burn

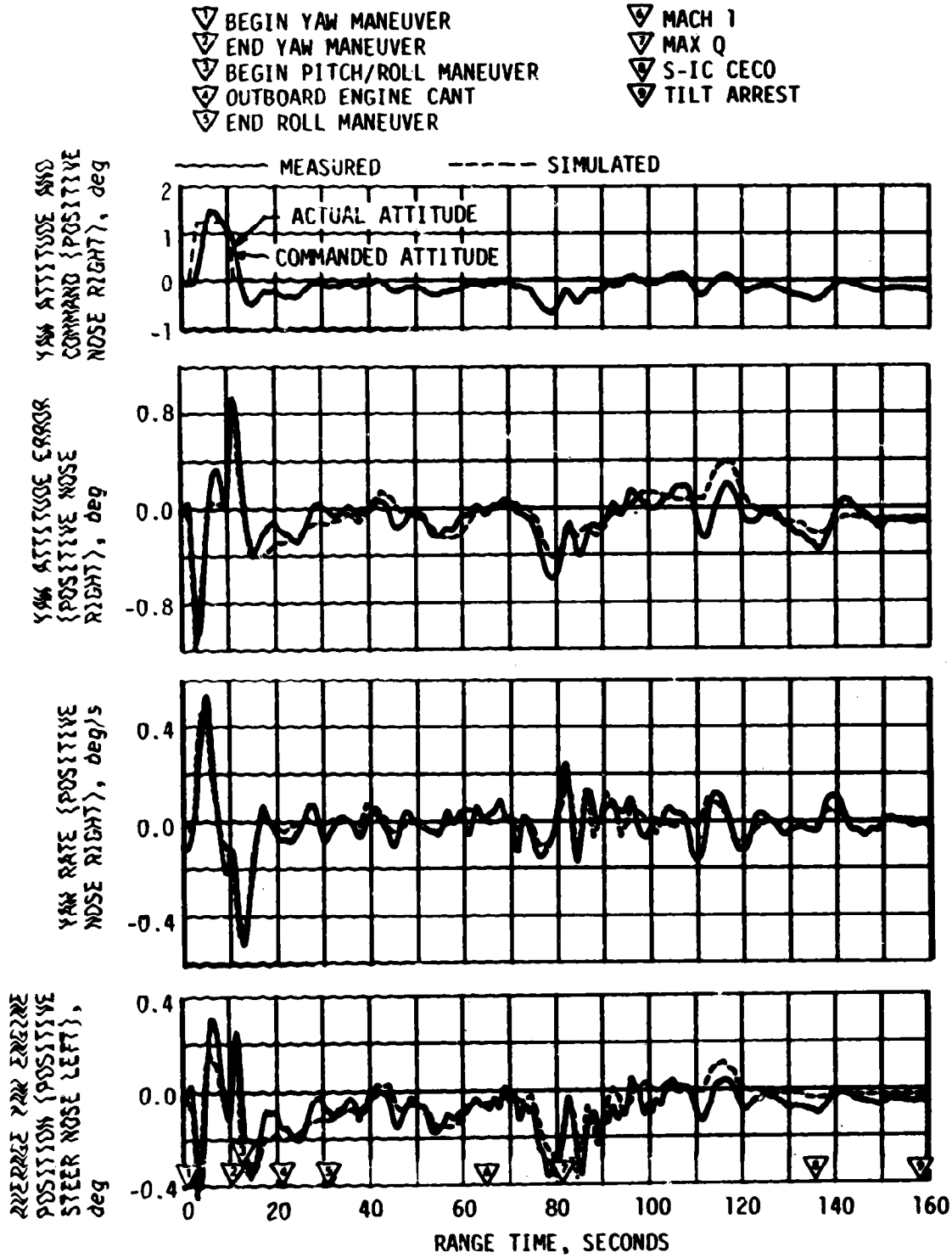

Figure 11-2. Yaw Plane Dynamics During S-IC Burn

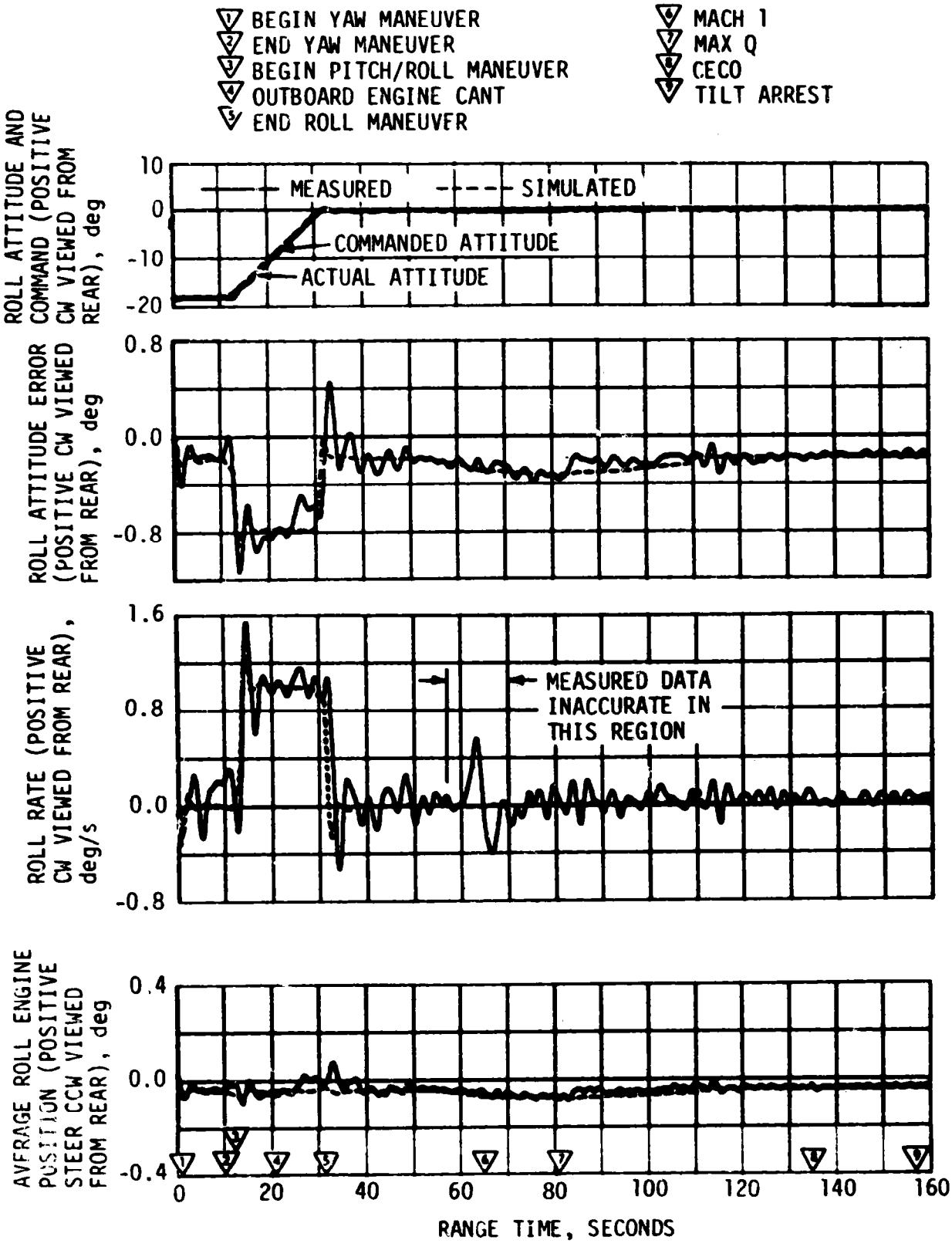

Figure 11-3. Roll Plane Dynamics During S-IC Burn

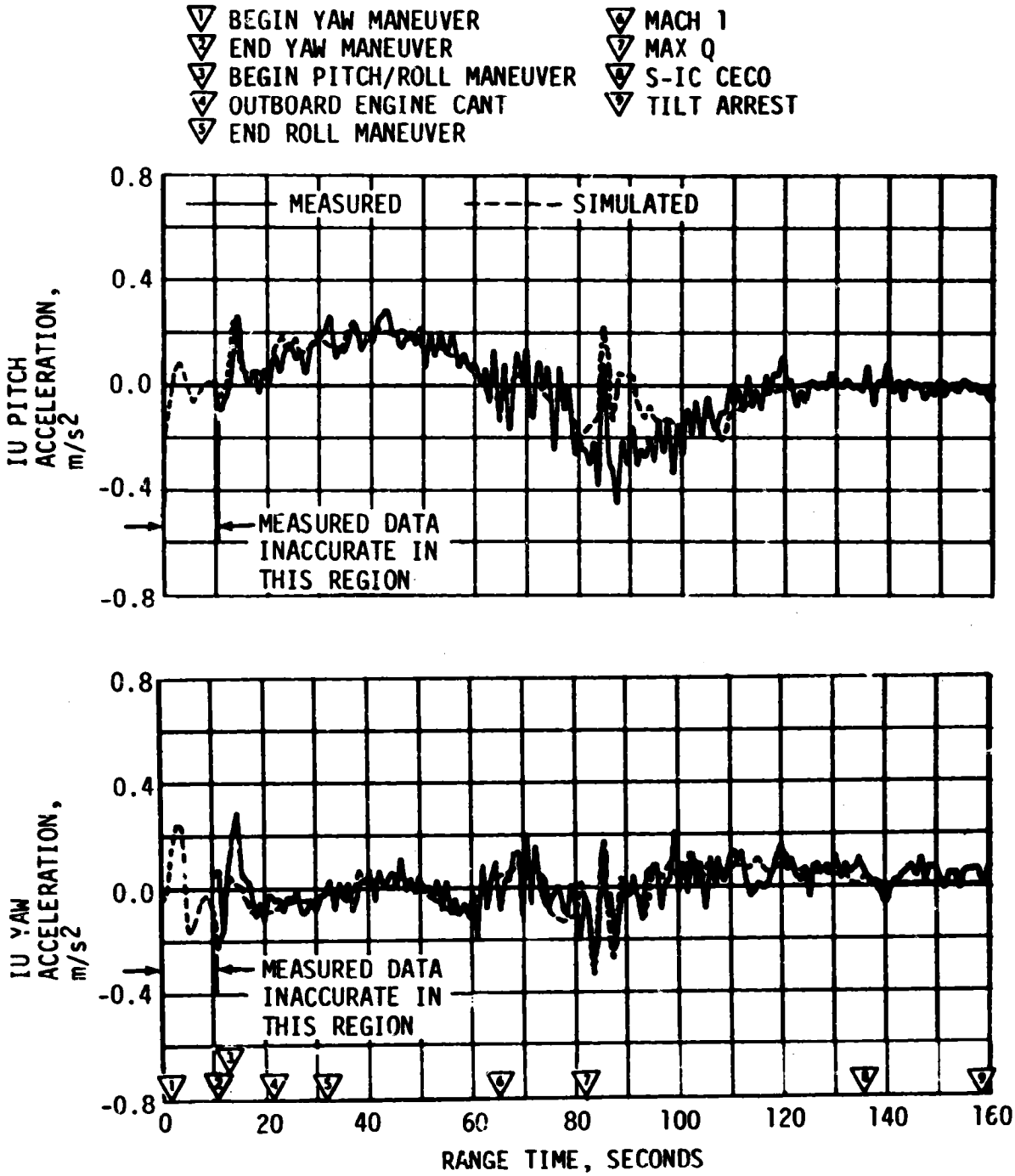

Figure 11-4. Normal Acceleration During S-IC Burn

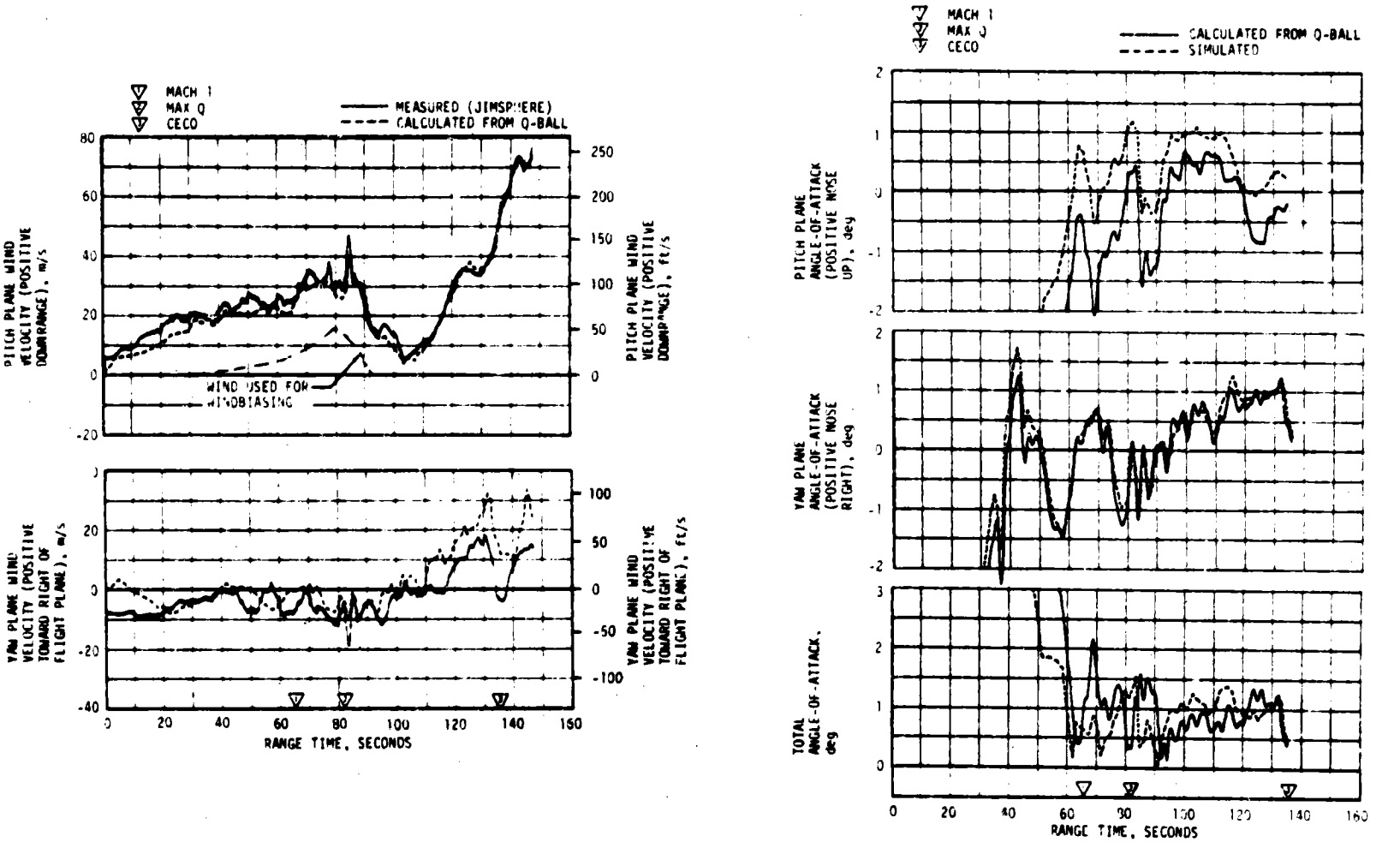

Figure 11-5. Pitch and Yaw Plane Wind Velocity and Free Stream Angles-of-Attack During S-IC Burn

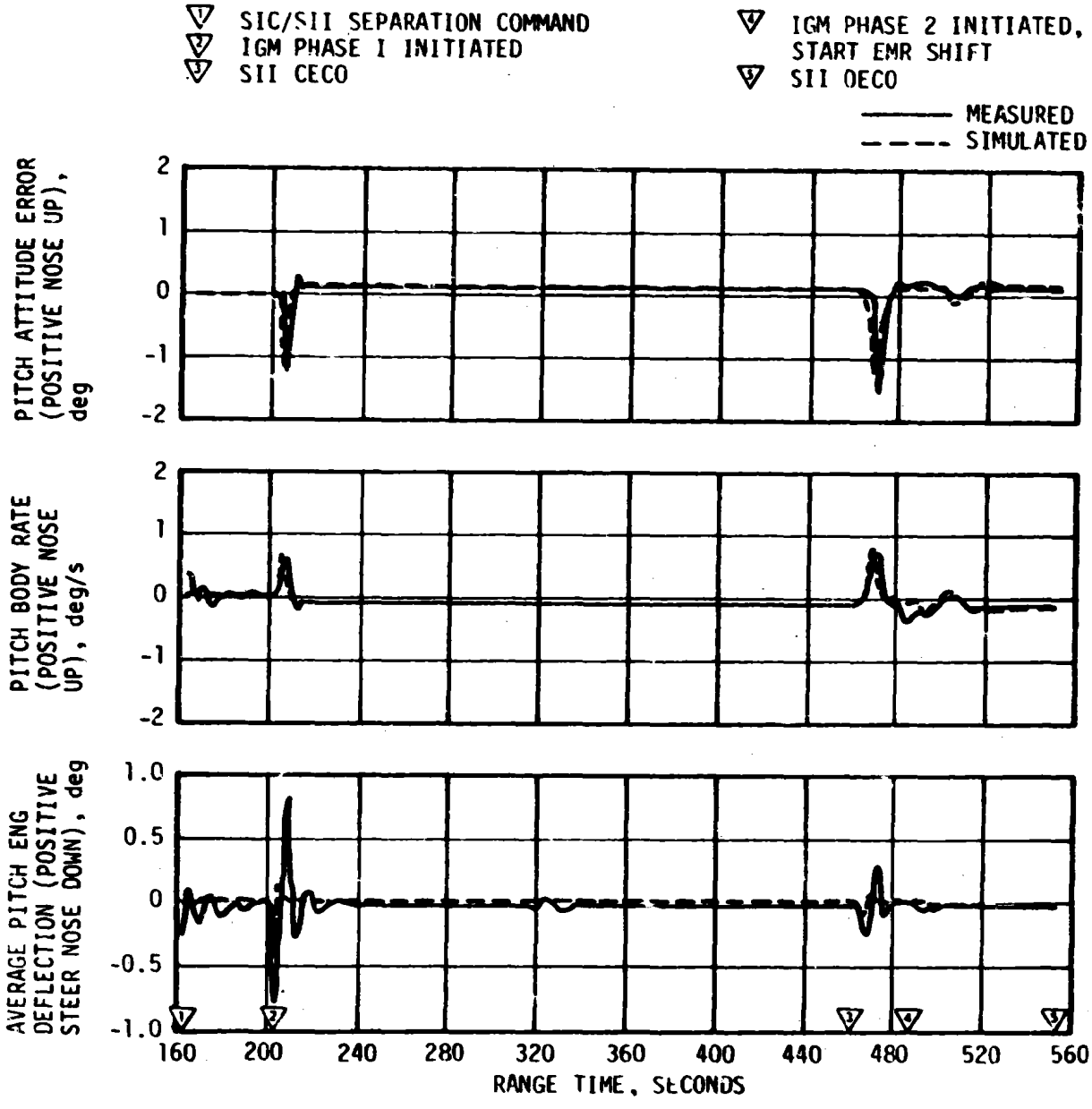

Figure 11-6. Pitch Plane Dynamics During S-II Burn

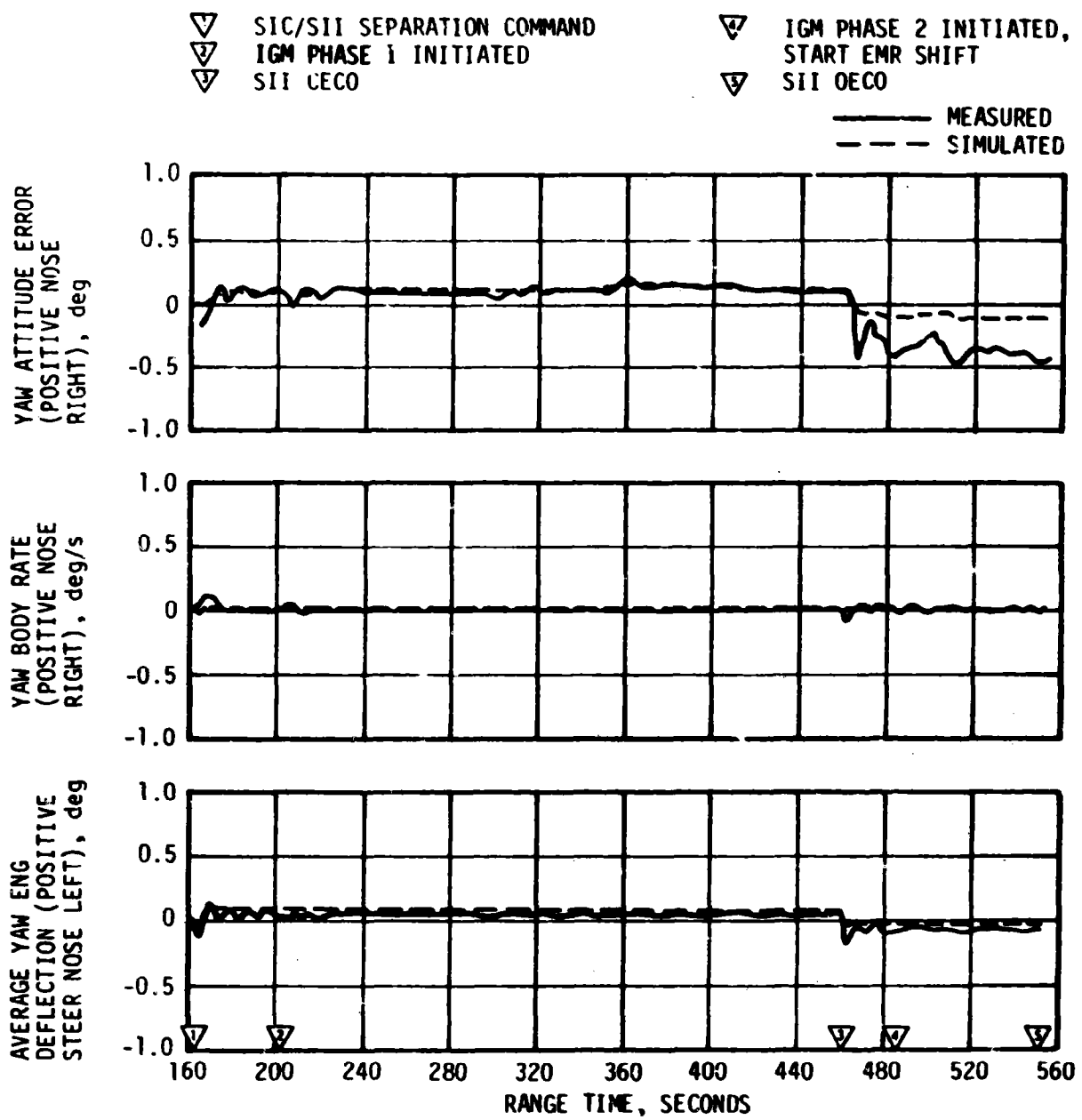

Figure 11-7. Yaw Plane Dynamics During S-II Burn

Table 11-3. Maximum Control Parameters During S-II Boost Flight

PARAMETER	UNITS	PITCH PLANE		YAW PLANE		ROLL PLANE	
		MAGNITUDE	RANGE TIME (SEC)	MAGNITUDE	RANGE TIME (SEC)	MAGNITUDE	RANGE TIME (SEC)
Attitude Error	deg	-1.5	470	-0.5	510	-1.3	165
Attitude Rate	deg/s	0.8	471	-0.1	462	1.7	166
Average Gimbal Angle	deg	-0.9	209	-0.2	464	-1.3	166

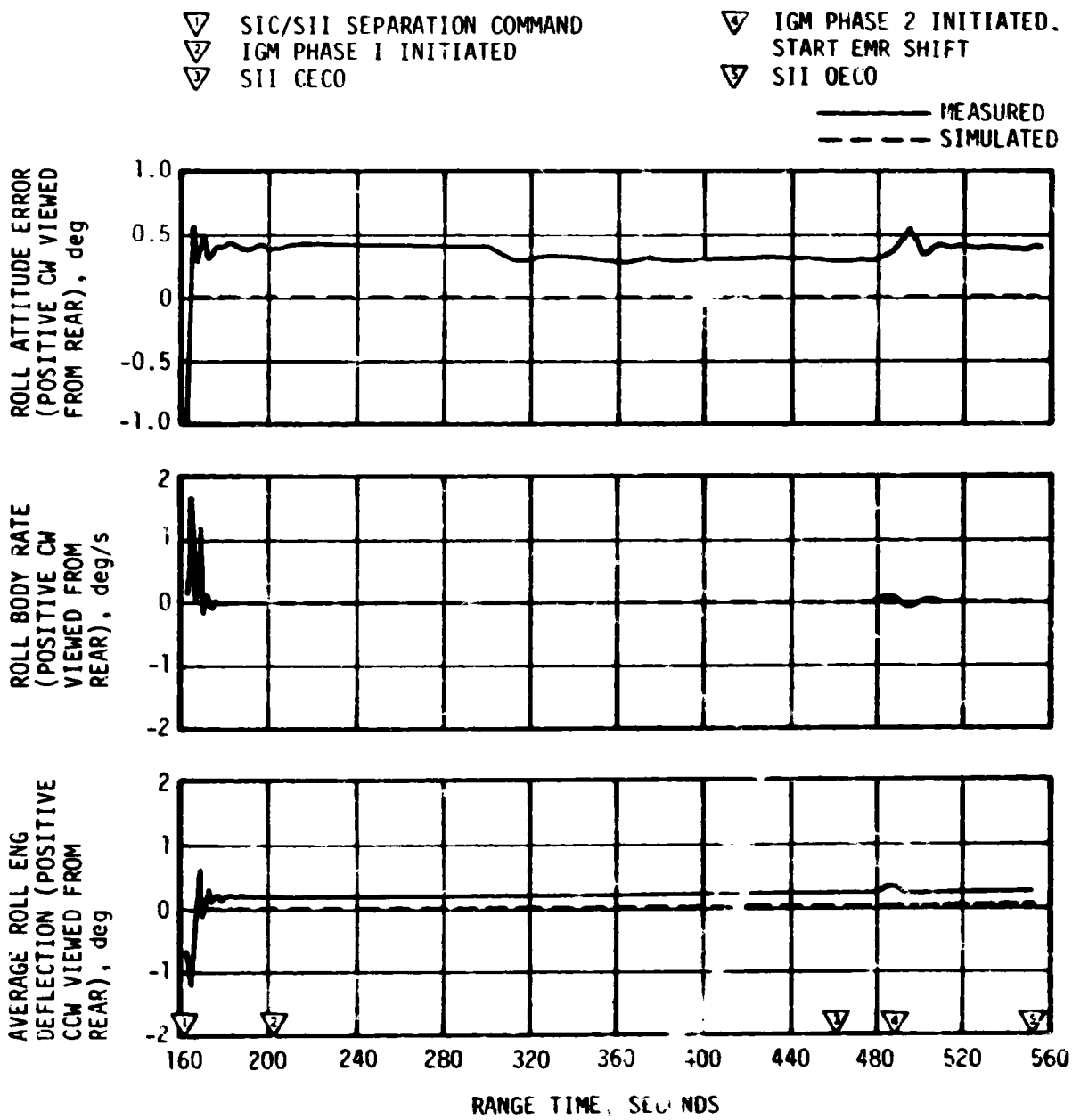

Figure 11-8. Roll Plane Dynamic During S-II Burn

At IGM initiation, the TVC received FCC commands to pitch the vehicle up. During IGM, the vehicle pitched down at a constant commanded rate of approximately -0.1 deg/s. The transient magnitudes experienced at IGM initiation were similar to those of previous flights.

During the first portion of the burn the vehicle trimmed with a yaw attitude error of 0.2 degree. This trim condition was required to balance the thrust vector misalignment of the center engine as well as other contributors. The center engine was not precanted to compensate for compliance deflection, and because of the location of the fixed links, this compliance effect occurred in the yaw plane. Following CECO, a new steady-state trim attitude error of -0.3 degree was established with a transient peak of -0.5 degree at 510 seconds. The deflections of the outboard engines in yaw at this time were the result of the change in trim conditions. The engine deflections in pitch were the result of a pitchup guidance command.

Simulated and flight data for pitch, yaw, and roll plane dynamics are compared in Figures 11-6, 11-7 and 11-8, respectively. The major differences are as follows: Steady-state yaw attitude error caused by early CECO which reflects a higher compliance than predicted for the center engine; initial transients in the roll axis which could be attributed to uncertainties in thrust buildup of the J-2 engines; and steady-state attitude errors caused by engine location misalignments and thrust vector misalignments.

11.4 S-IVB CONTROL SYSTEM EVALUATION

The S-IVB TVC system provided satisfactory pitch and yaw control during powered flight. The APS provided satisfactory roll control during first and second burns.

Control system transients at S-II/S-IVB separation and during S-IVB first and second burns at guidance initiation, Engine Mixture Ratio (EMR) shift, chi bar guidance mode, and J-2 engine cutoff were experienced as expected and were within the capabilities of the control system.

11.4.1 Control System Evaluation During First Burn

The S-IVB first burn attitude control system response to guidance commands for pitch, yaw and roll are presented in Figures 11-9, 11-10 and 11-11, respectively. The maximum attitude errors and rates occurred at IGM initiation. A summary of maximum values of the critical flight control parameters during S-IVB first burn is presented in Table 11-4.

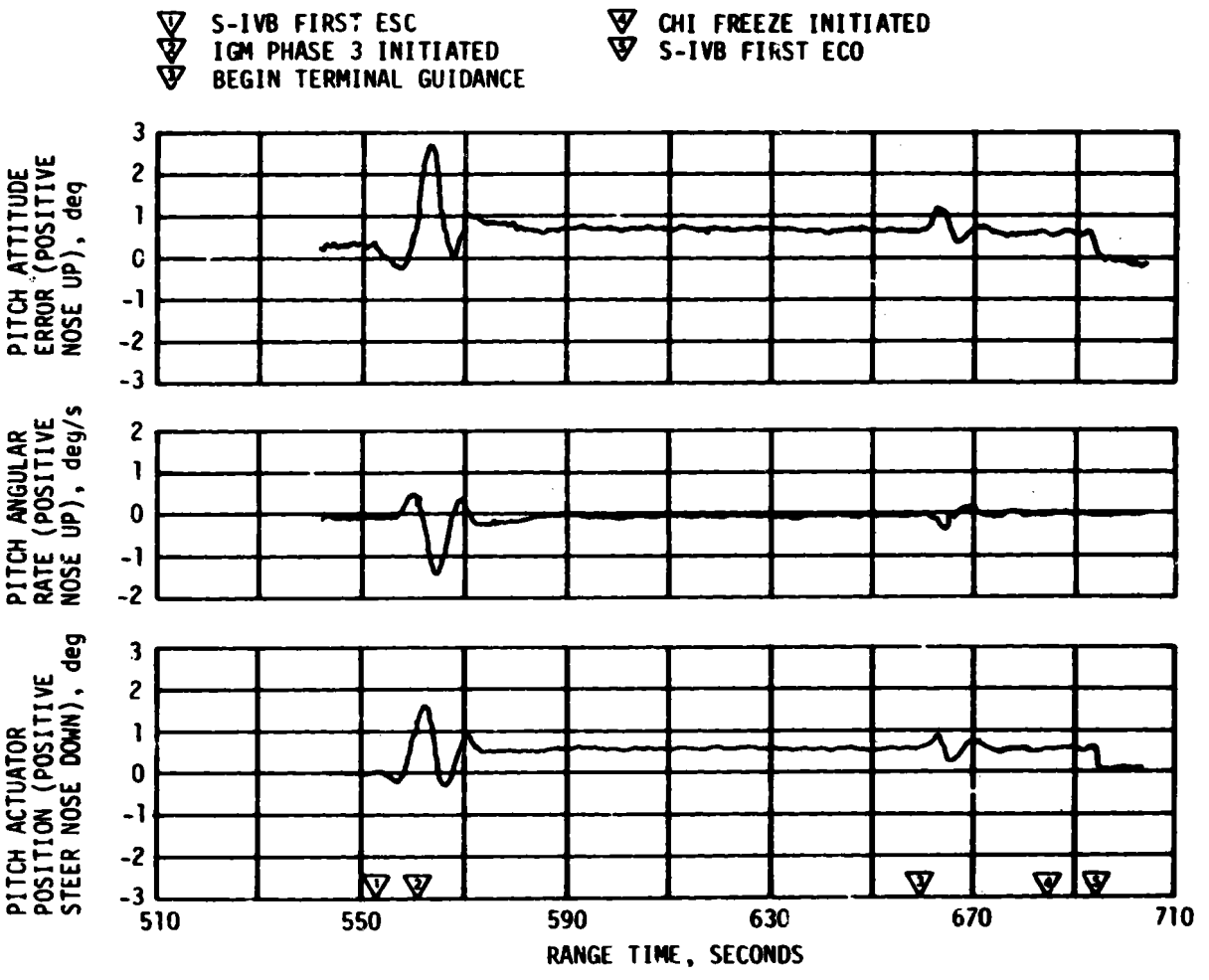

Figure 11-9. Pitch Plane Dynamics During S-IVB First Burn

The pitch and yaw effective thrust vector misalignments during first burn were 0.28 and -0.23 degree, respectively. A steady-state roll torque of 8.5 N-m (6.3 lbf-ft), clockwise looking forward, required roll APS firings during first burn. The steady-state roll torque experienced on previous flights has ranged between 61.4 N-m (45.3 lbf-ft) counterclockwise and 54.2 N-m (40.0 lbf-ft) clockwise.

11.4.2 Control System Evaluation During Parking Orbit

The coast attitude control system provided satisfactory orientation and stabilization of the vehicle in parking orbit. Pitch plane attitude control parameters during the maneuver to local horizontal following S-IVB first cutoff are shown in Figure 11-12. The maneuver to local horizontal was the only maneuver during parking orbit.

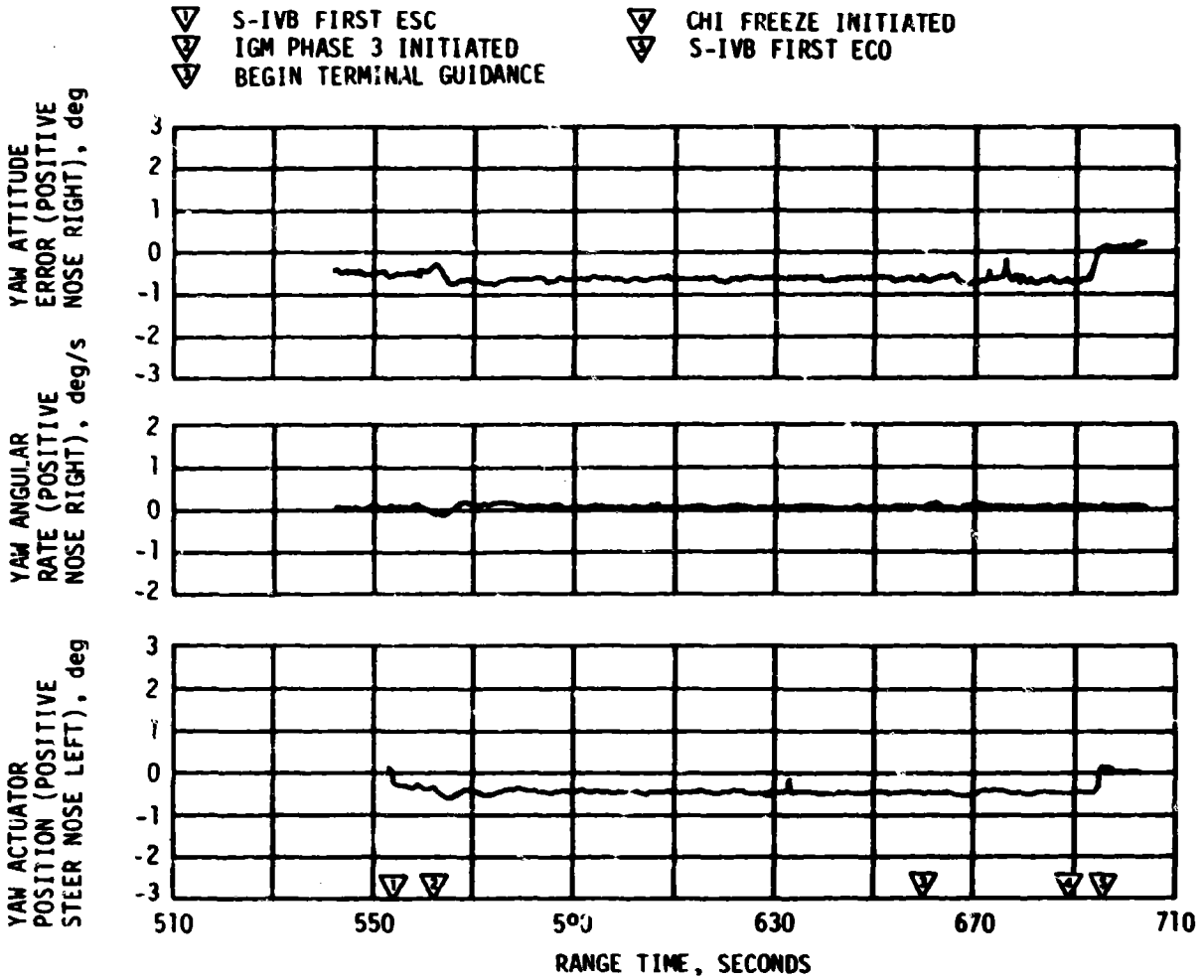

Figure 11-10. Yaw Plane Dynamics During S-IVB First Burn

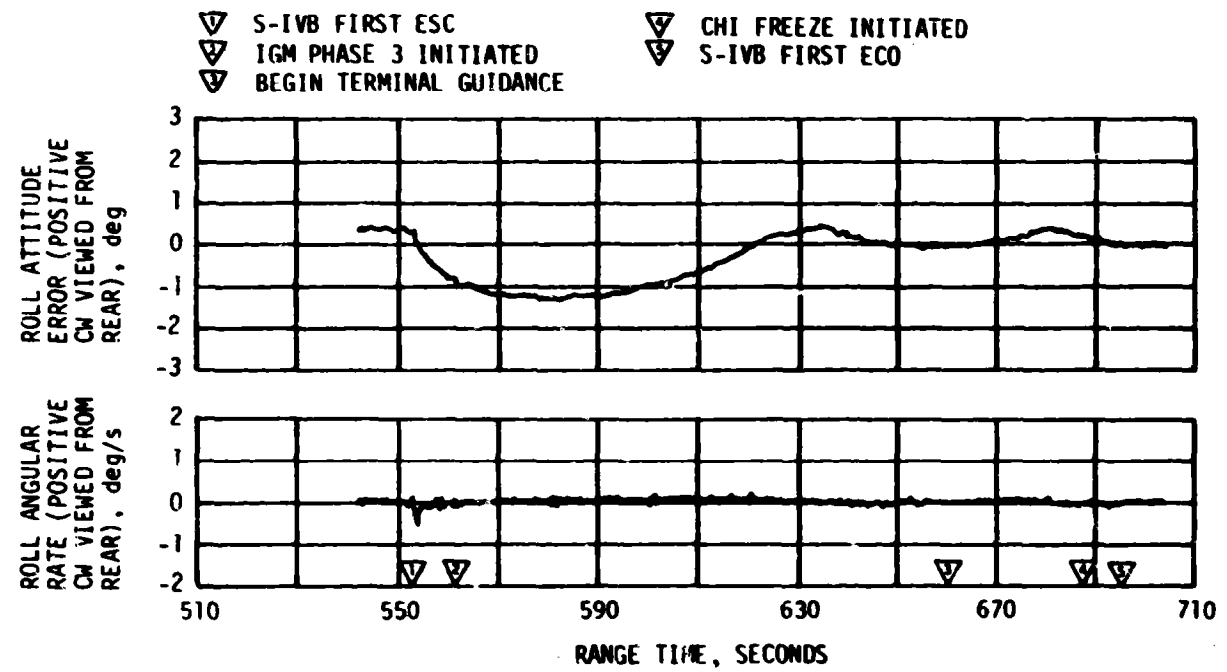

Figure 11-11. Roll Plane Dynamics During S-IVB First Burn

Table 11-4. Maximum Control Parameters During S-IVB First Burn

PARAMETER	UNITS	PITCH PLANE		YAW PLANE		ROLL PLANE	
		MAGNITUDE	RANGE TIME (SEC)	MAGNITUDE	RANGE TIME (SEC)	MAGNITUDE	RANGE TIME (SEC)
Attitude Error	deg	2.75	563.0	-0.85	566.8	-1.30	580.0
Angular Rate	deg/s	-1.50	564.6	-0.18	564.0	-0.40	558.0
Actuator Position	deg	1.50	562.4	-0.60	565.3	--	--

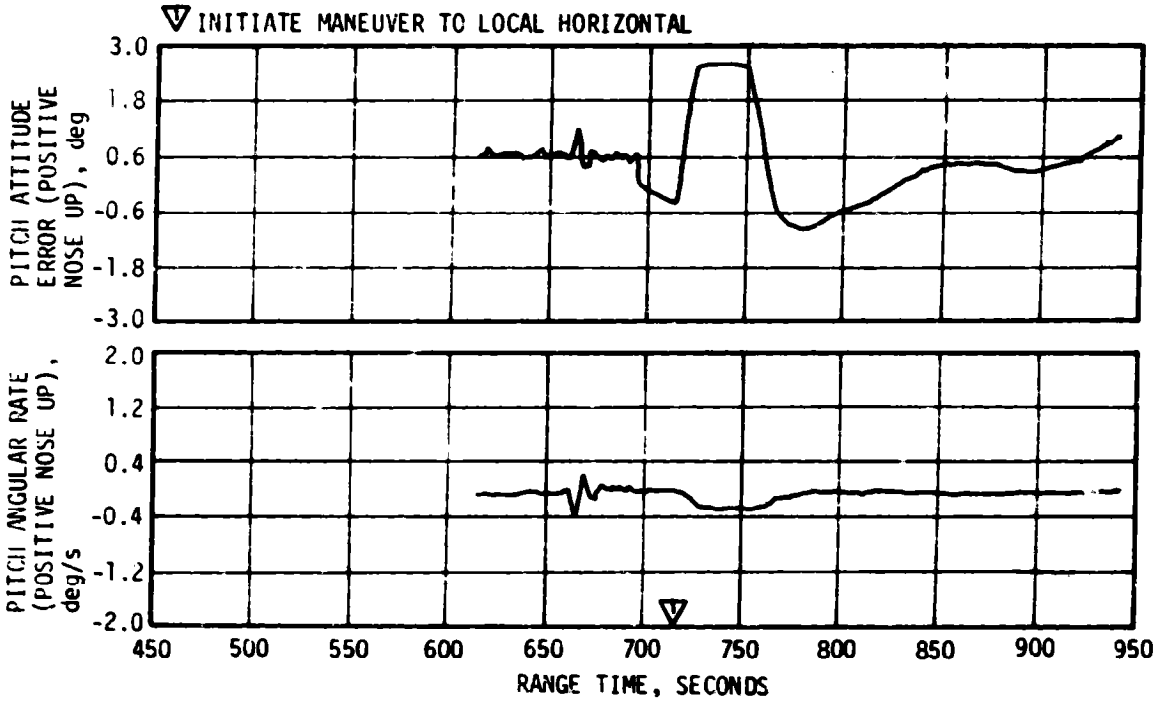

Figure 11-12. Pitch Plane Dynamics During Coast in Parking Orbit

11.4.3 Control System Evaluation During Second Burn

The S-IVB second burn attitude control system response to guidance commands for pitch, yaw and roll are presented in Figures 11-13, 11-14 and 11-15, respectively. The maximum attitude errors and rates occurred at guidance initiation and EMR shift. A summary of maximum values of the critical flight control parameters during S-IVB second burn is presented in Table 11-5.

The pitch and yaw effective thrust vector misalignments during second burn were approximately 0.38 and -0.32 degree, respectively. The steady-state roll torque during second burn ranged from 18.2 N-m (13.4 lbf-ft), clockwise looking forward, at the 4.5:1.0 EMR shift to 19.0 N-m (14.0 lbf-ft) at the 5.0:1.0 EMR shift.

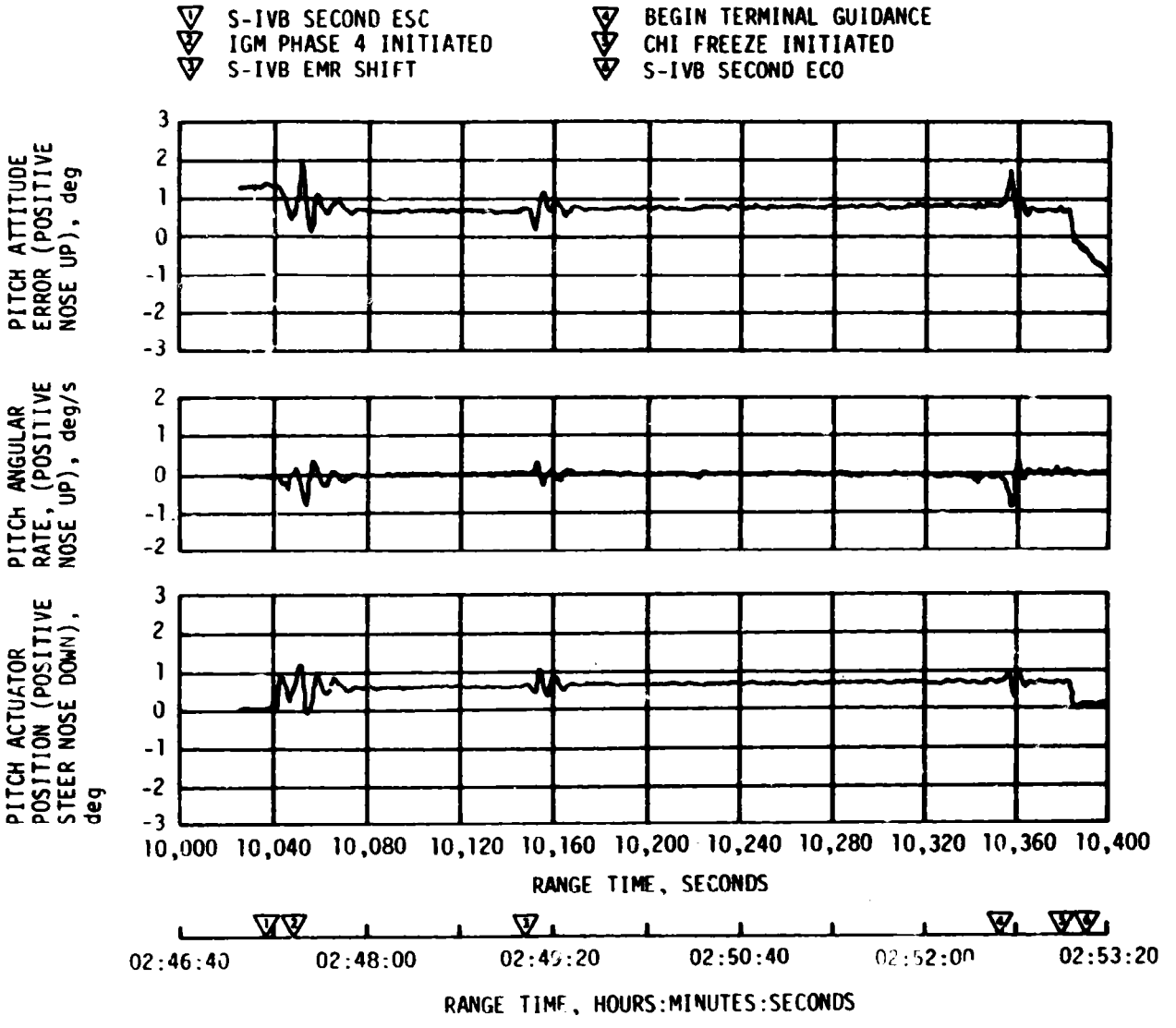

Figure 11-13. Pitch Plane Dynamics During S-IVB Second Burn

11.4.4 Control System Evaluation After S-IVB Second Burn

The coast attitude control system provided satisfactory orientation and stabilization from S-IVB second cutoff through the last data available. Pitch, yaw, and roll control for spacecraft separation are shown in Figure 11-16 and for spacecraft docking in Figure 11-17. Yaw control during the evasive maneuver is shown in Figure 11-18. Figure 11-19 shows pitch and yaw control for the maneuver to slingshot attitude. APS propellant usage for attitude control was less than the predicted nominal usage.

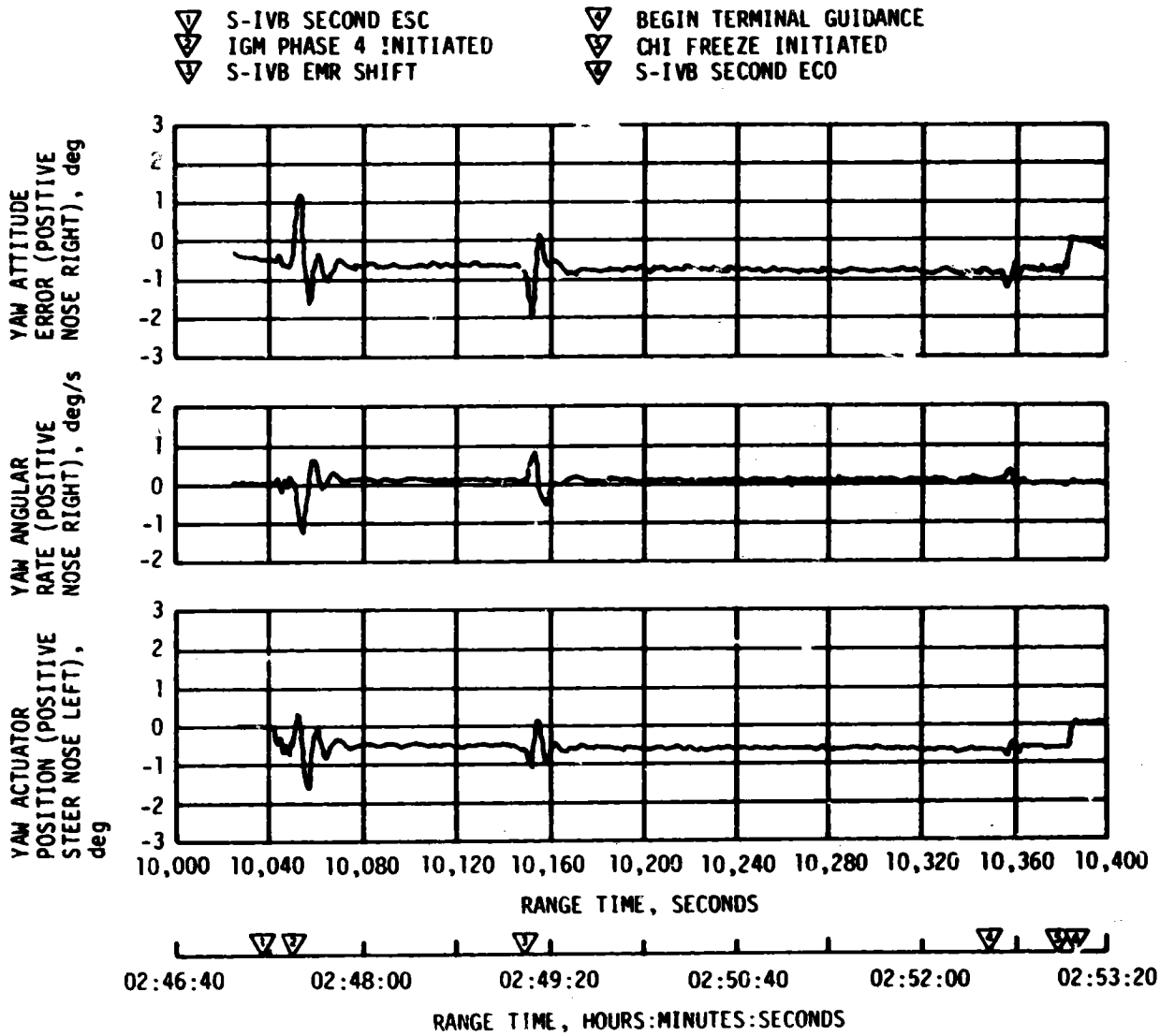

Figure 11-14. Yaw Plane Dynamics During S-IVB Second Burn

11.5 SEPARATION

S-IC/S-II separation and associated sequencing were accomplished as planned. Dynamic conditions at separation were within staging limits. Rate gyros and accelerometers located on the Instrument Unit (IU) showed no disturbances, indicating a clean severance of the stages. Data from the Exploding Bridge Wire (EBW) firing unit indicate that S-IC retromotor ignition was accomplished. The S-II ullage motors performed as predicted. Since there were no cameras on the S-II stage, calculated dynamics of the interstage and the S-II stage were used to determine if second plane separation was within the staging requirements.

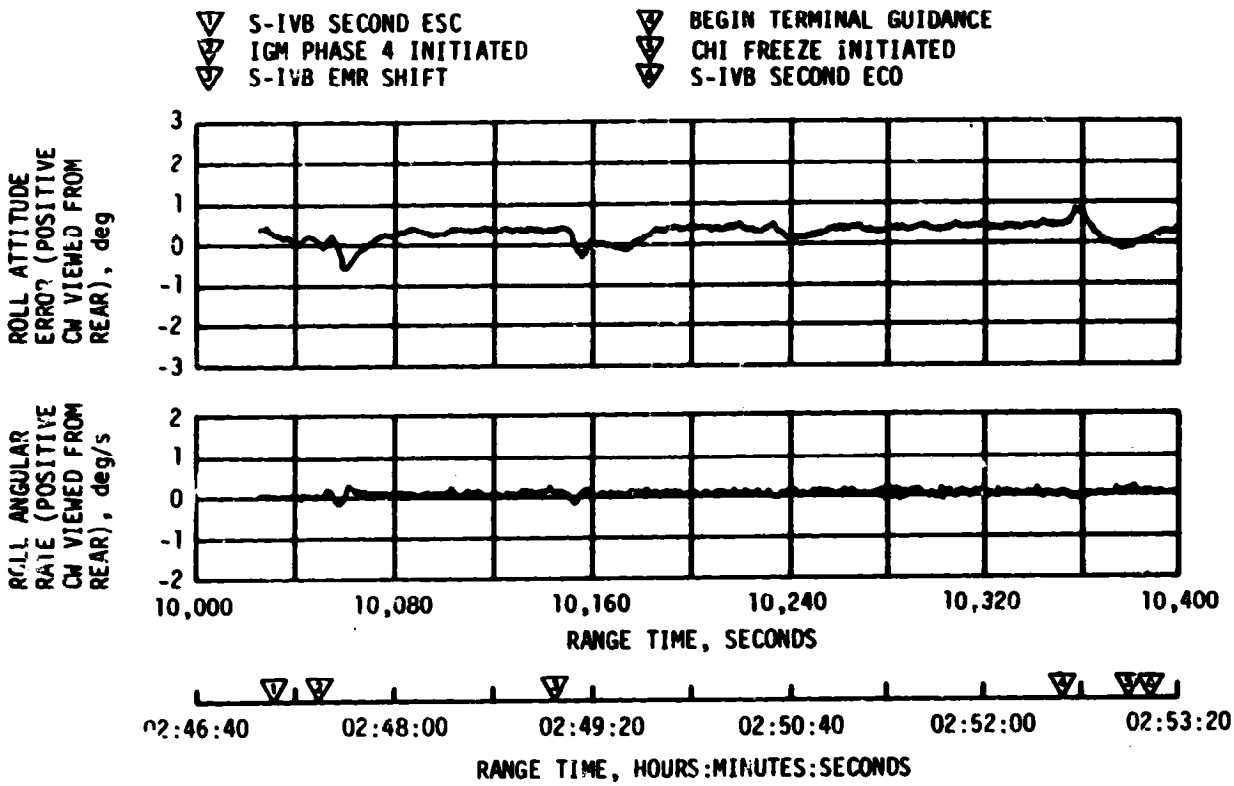

Figure 11-15. Roll Plane Dynamics During S-IVB Second Burn

Table 11-5. Maximum Control Parameters During S-IVB Second Burn

PARAMETER	UNITS	PITCH PLANE		YAW PLANE		ROLL PLANE	
		MAGNITUDE	RANGE TIME (SEC)	MAGNITUDE	RANGE TIME (SEC)	MAGNITUDE	RANGE TIME (SEC)
Attitude Error	deg	2.0	10,052.3	-2.0	10,152.2	0.8	10,357.0
Angular Rate	deg/s	-0.9	10,053.8	-1.4	10,055.1	0.3	10,153.5
Actuator Position	deg	1.10	10,052.2	-1.60	10,056.8	--	--

The S-II retromotors and the S-IVB ullage motors performed satisfactorily and provided a normal S-II/S-IVB separation. Dynamic conditions at separation were within staging limits with separation conditions similar to those observed on previous flights.

Separation of the CSM from the LV was accomplished as planned. There were no large control disturbances noted during the separation. The attitude of the LV was adequately maintained during the docking of the CSM with the Lunar Module (LM). The CSM/LM was then successfully spring ejected from the LV. There were no significant control disturbances during the ejection.

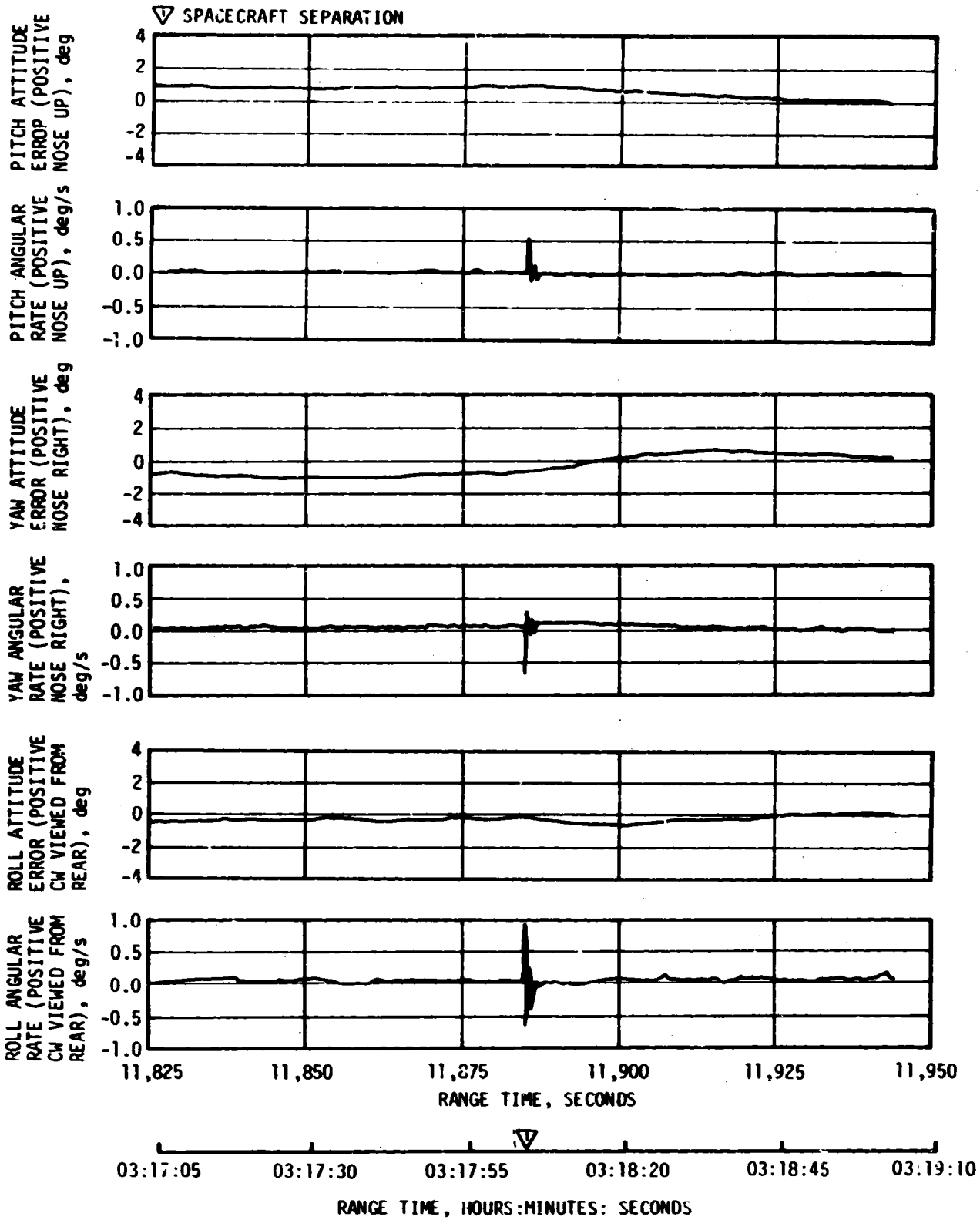

Figure 11-16. Pitch, Yaw and Roll Plane Dynamics During Spacecraft Separation

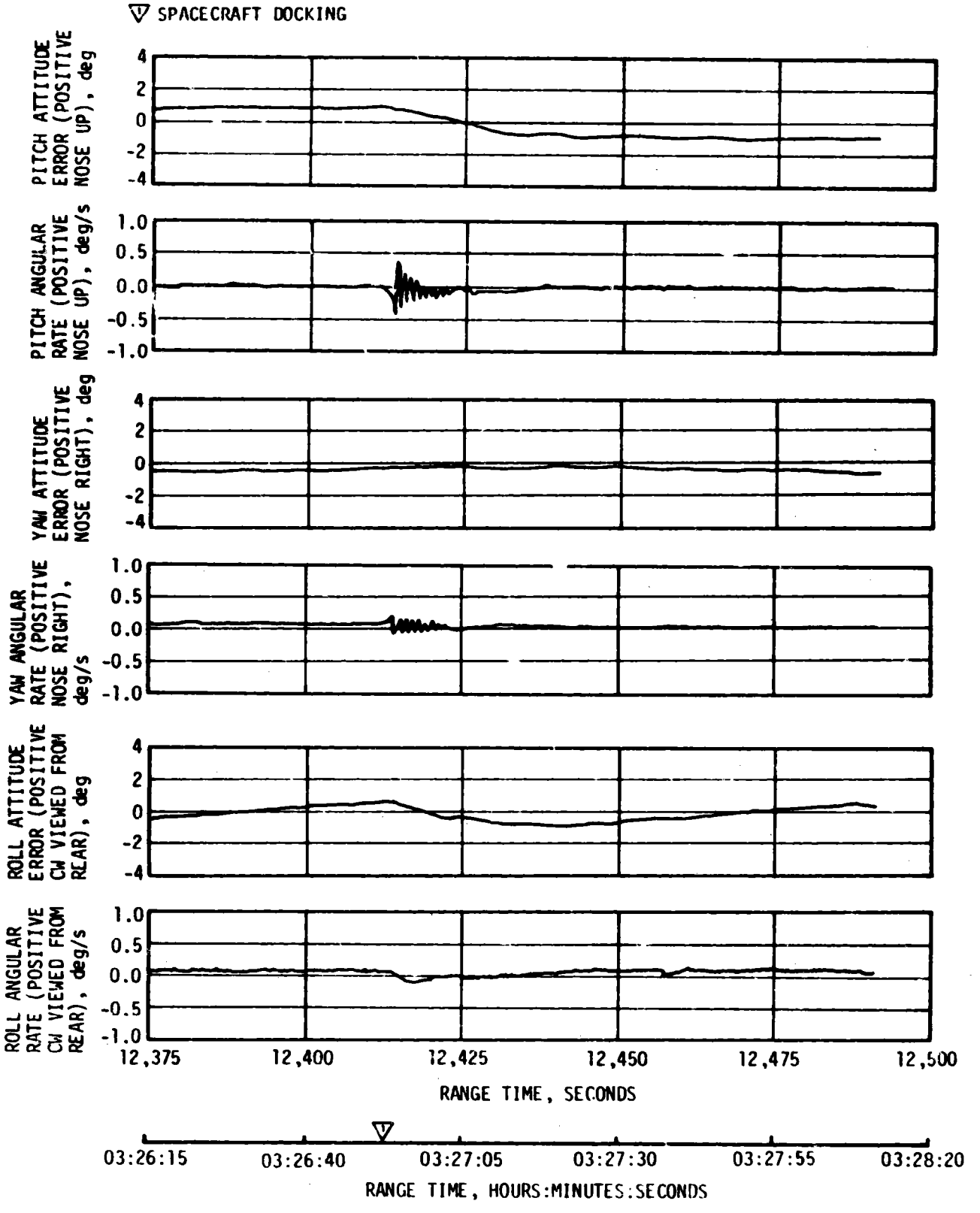

Figure 11-17. Pitch, Yaw and Roll Plane Dynamics During Spacecraft Docking

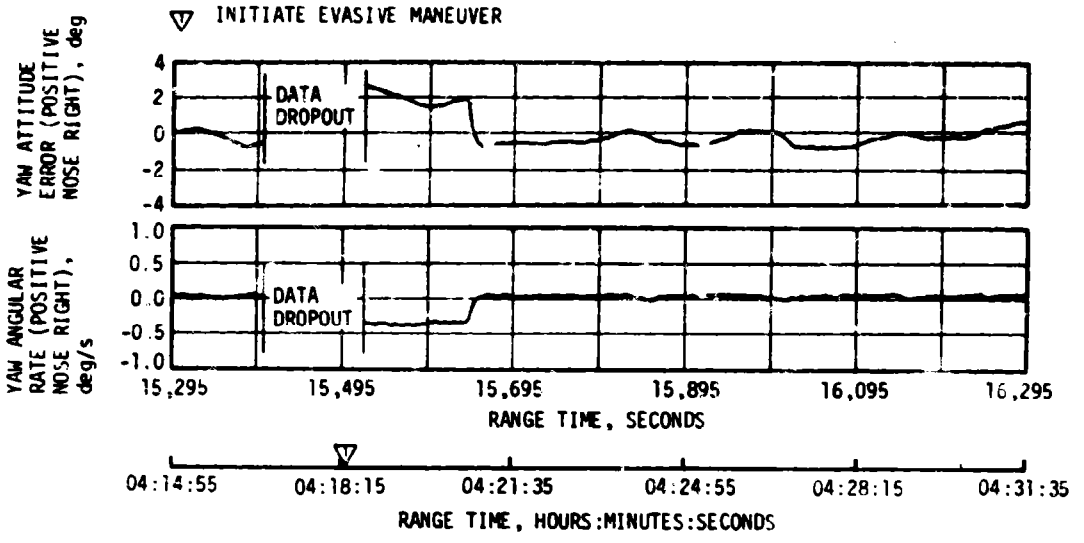

Figure 11-18. Yaw Plane Dynamics During the Evasive Maneuver

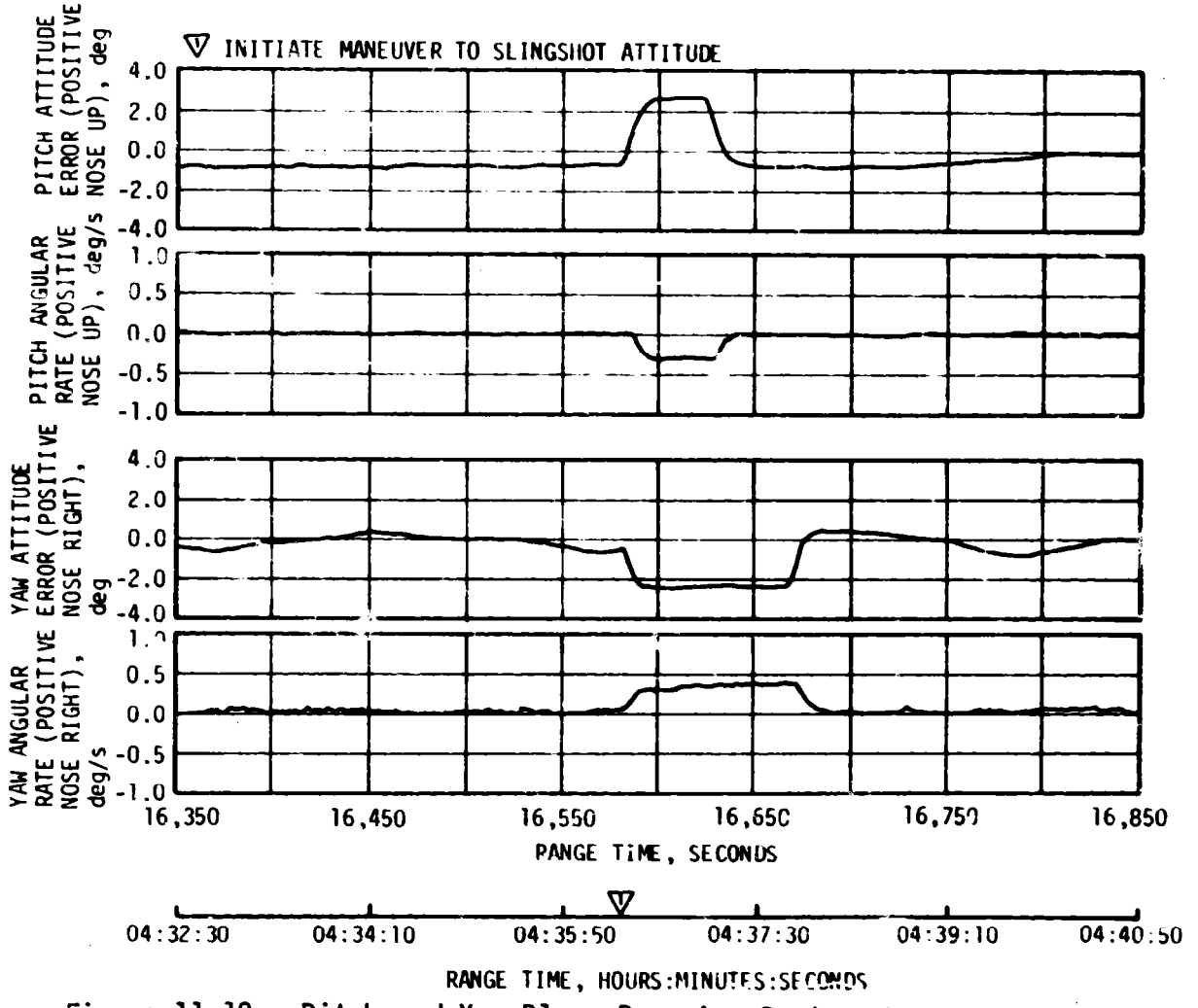

Figure 11-19. Pitch and Yaw Plane Dynamics During the Maneuver To Slingshot Attitude

SECTION 12

ELECTRICAL NETWORKS AND EMERGENCY DETECTION SYSTEM

12.1 SUMMARY

The AS-507 launch vehicle electrical systems and Emergency Detection System (EDS) performed satisfactorily throughout all phases of flight except during S-IVB restart preparations. During this time the S-IVB stage electrical systems did not respond properly to burner LOX shutdown valve "CLOSE" and telemetry calibrate "ON" commands from the S-IVB switch selector. Both of the command failures were isolated to intermittent conditions in a bus module (404A3A29) or the associated mating connector (404A3W1P29) located in the S-IVB sequencer. Operation of the batteries, power supplies, inverters, Exploding Bridge Wire (EBW) firing units and switch selectors was normal.

12.2 S-IC STAGE ELECTRICAL SYSTEM

The battery voltages remained well within performance limits of 26.5 to 32.0 vdc during powered flight. Battery currents were near predicted and below the maximum limit of 64 amperes for each battery. Battery power consumption was well within the rated capacities of the batteries as shown in Table 12-1.

Table 12-1. S-IC Stage Battery Power Consumption

BATTERY	BUS DESIGNATION	RATED CAPACITY (AMP-MIN)	POWER CONSUMPTION*	
			AMP-MIN	PERCENT OF CAPACITY
Operational	1D10	640	27.0	4.2
Instrumentation	1D20	640	85.6	13.4

*Battery power consumptions were calculated from power transfer until S-IC/S-II separation.

The two measuring power supplies remained within the 5 ±0.05 vdc design limit.

All switch selector channels functioned correctly, and all outputs were issued within their required time limits in response to commands from the Instrument Unit (IU).

The separation and retromotor EBW firing units were armed and triggered as programed. Charging times and voltages were within predicted time and voltage limits.

The command destruct EBW firing units were in the required state of readiness if vehicle destruct became necessary.

12.3 S-II STAGE ELECTRICAL SYSTEM

All battery voltages remained within specified limits throughout the prelaunch and flight periods, and bus currents remained within required and predicted limits. Main bus current averaged 36 amperes during S-IC boost and varied from 47 to 55 amperes during S-II boost. Instrumentation bus current averaged 23 amperes during S-IC and S-II boost. Recirculation bus current averaged 98 amperes during S-IC boost. Ignition bus current averaged 29 amperes during the S-II ignition sequence. Battery power consumption was well within the rated capacities of the batteries as shown in Table 12-2.

The five temperature bridge power supplies, the three 5-vdc instrumentation power supplies and the five LH_2 recirculation inverters all performed within acceptable limits.

Table 12-2. S-II Stage Battery Power Consumption

BATTERY	BUS DESIG-NATION	RATED CAPACITY (AMP-HR)	POWER CONSUMPTION*		TEMPERATURE	
			AMP-HR	PERCENT OF CAPACITY	MAX	MIN
Main	2D11	35	7.76	22.2	97.0°F	87.0°F
Instrumentation	2D21	35	3.78	10.8	88.0°F	84.0°F
Recirculation No. 1	2D51	30	5.78	19.3	88.5°F	82.0°F
Recirculation No. 2	2D51 and 2D61	30	5.82	19.4	87.0°F	81.0°F

*Power consumption calculated from -50 seconds.

All switch selector channels functioned correctly, and all outputs were issued within their required time limits in response to commands from the IU.

Performance of the EBW circuitry for the separation system was satisfactory. Firing units charge and discharge responses were within predicted time and voltage limits. The command EBW firing units were in the required state of readiness if vehicle destruct became necessary.

12.4 S-IVB STAGE ELECTRICAL SYSTEM

The voltages and currents of the three 28-vdc batteries and one 56-vdc battery stayed well within acceptable limits as shown in Figures 12-1 through 12-4. Battery temperatures remained below the 120°F limits for the powered portion of the flight. (This limit does not apply after insertion into orbit.) The highest temperature of 111°F was reached on Aft Battery No. 2, Unit 1, after S-IVB first burn cutoff. Battery power consumption is shown in Table 12-3.

The three 5-vdc excitation modules operated as expected. The seven 20-vdc excitation modules performed within acceptable limits. The LOX and LH_2 chilldown inverters performed satisfactorily and met their load requirements.

Performance of the EBW circuitry for the separation system was satisfactory. Firing units charge and discharge responses were within predicted time and voltage limits. The command EBW firing units were in the required state of readiness if vehicle destruct became necessary.

The switch selector functioned correctly and all IU commands were properly executed, except as noted in the following paragraphs.

Table 12-3. S-IVB Stage Battery Power Consumption

BATTERY	RATED CAPACITY (AMP-HRS)*	POWER CONSUMPTION**	
		AMP-HRS	PERCENT OF CAPACITY
Forward No. 1	300.0	144.4	48.1
Forward No. 2	24.75	26.6	107.3
Aft No. 1	300.0	104.2	34.7
Aft No. 2	75.0	36.9	49.1

*Rated capacities are minimum guaranteed by vendor.
**Actual usage to 43,980 seconds (12:13:00) is based on flight data.

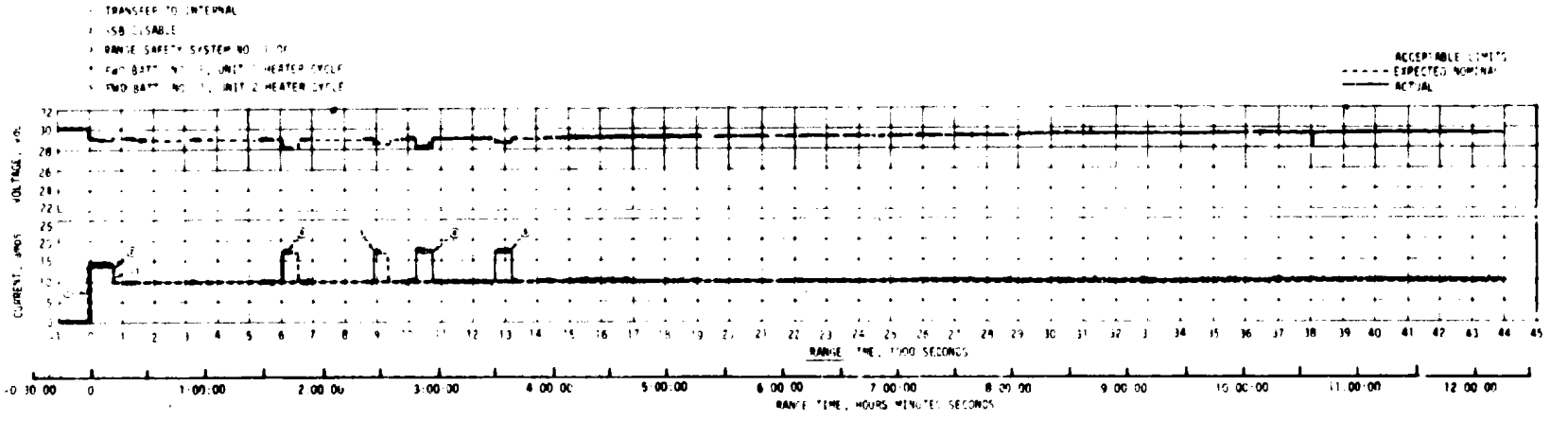

Figure 12-1. S-IVB Stage Forward Battery No. 1 Voltage and Current

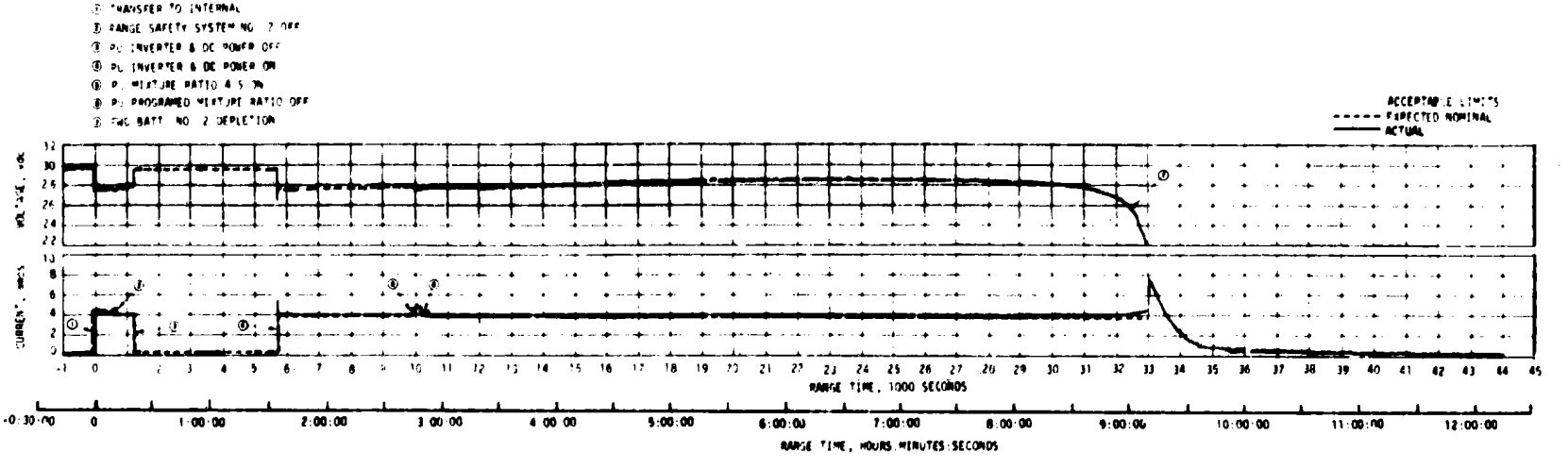

Figure 12-2. S-IVB Stage Forward Battery No. 2 Voltage and Current

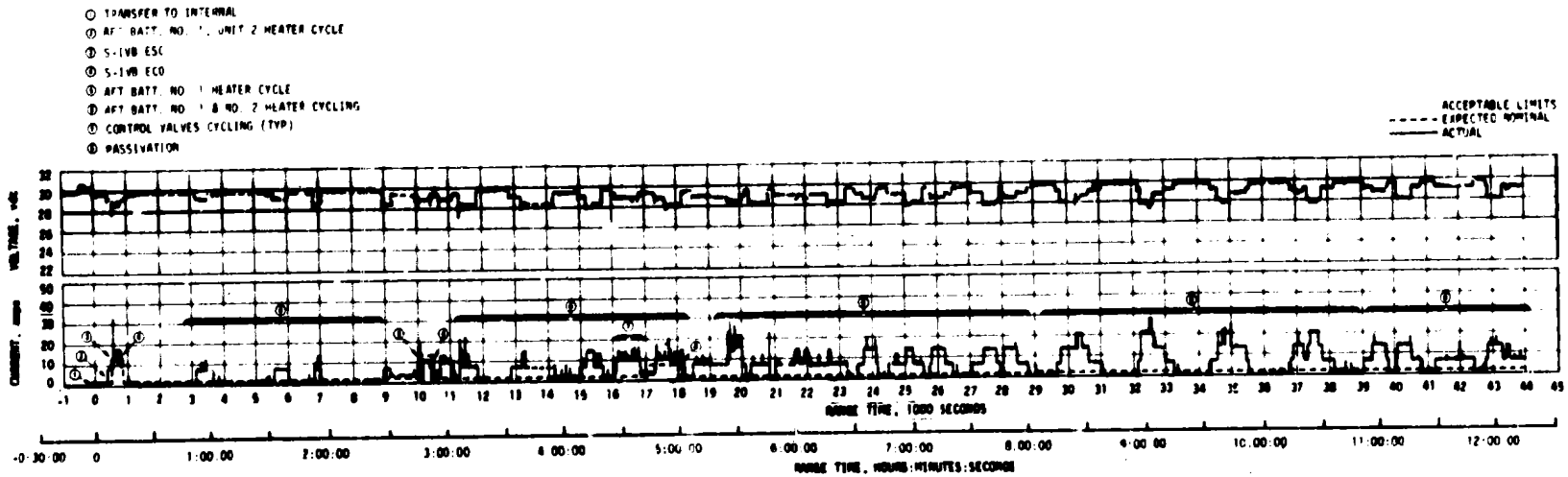

Figure 12-3. S-IVB Stage Aft Battery No. 1 Voltage and Current

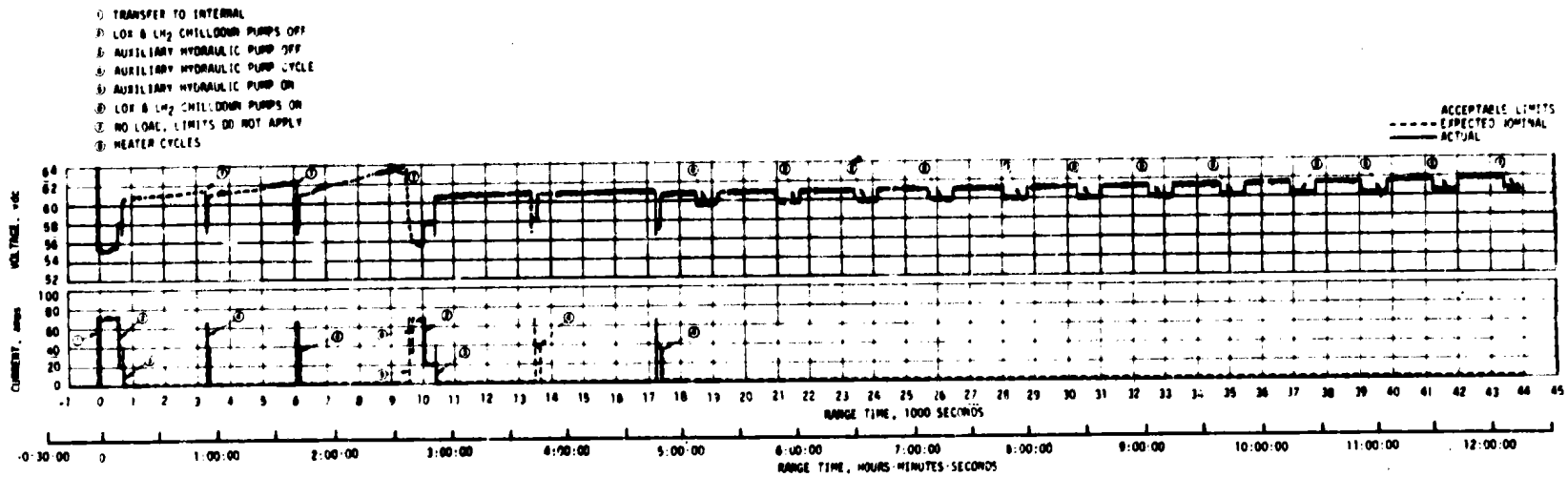

Figure 12-4. S-IVB Stage Aft Battery No. 2 Voltage and Current

At 9965.7 seconds (2:46:05.7) the burner LOX shutdown valve "CLOSE" command was sent from the S-IVB switch selector; however, the valve did not close. A subsequent ground command successfully closed the valve at 10,554.2 seconds (2:55:54.2). (See paragraph 7.6 for propulsion system effects.) Also, at 9864.8 seconds (2:44:24.8) the CP1B0 multiplexer failed to respond when a telemetry calibrate "ON" command was sent from the switch selector. The DP1B0 multiplexer did respond. Both multiplexers responded to a telemetry calibrate "ON" command at 10,472.8 seconds (2:54:32.8).

Both of the command failures were isolated to intermittent conditions in a common bus module (unit designation 404A3A29, MDAC P/N 1B57771) or the associated mating connector (unit designation 404A3W1P29, Bendix P/N S0286E-22-55S) located in the sequencer of the S-IVB aft skirt. These command circuits are shown in Figure 12-5. Further analysis indicated that the intermittent conditions were probably caused by a recessed socket or a missing socket retention spring in the 404A3W1P29 harness connector.

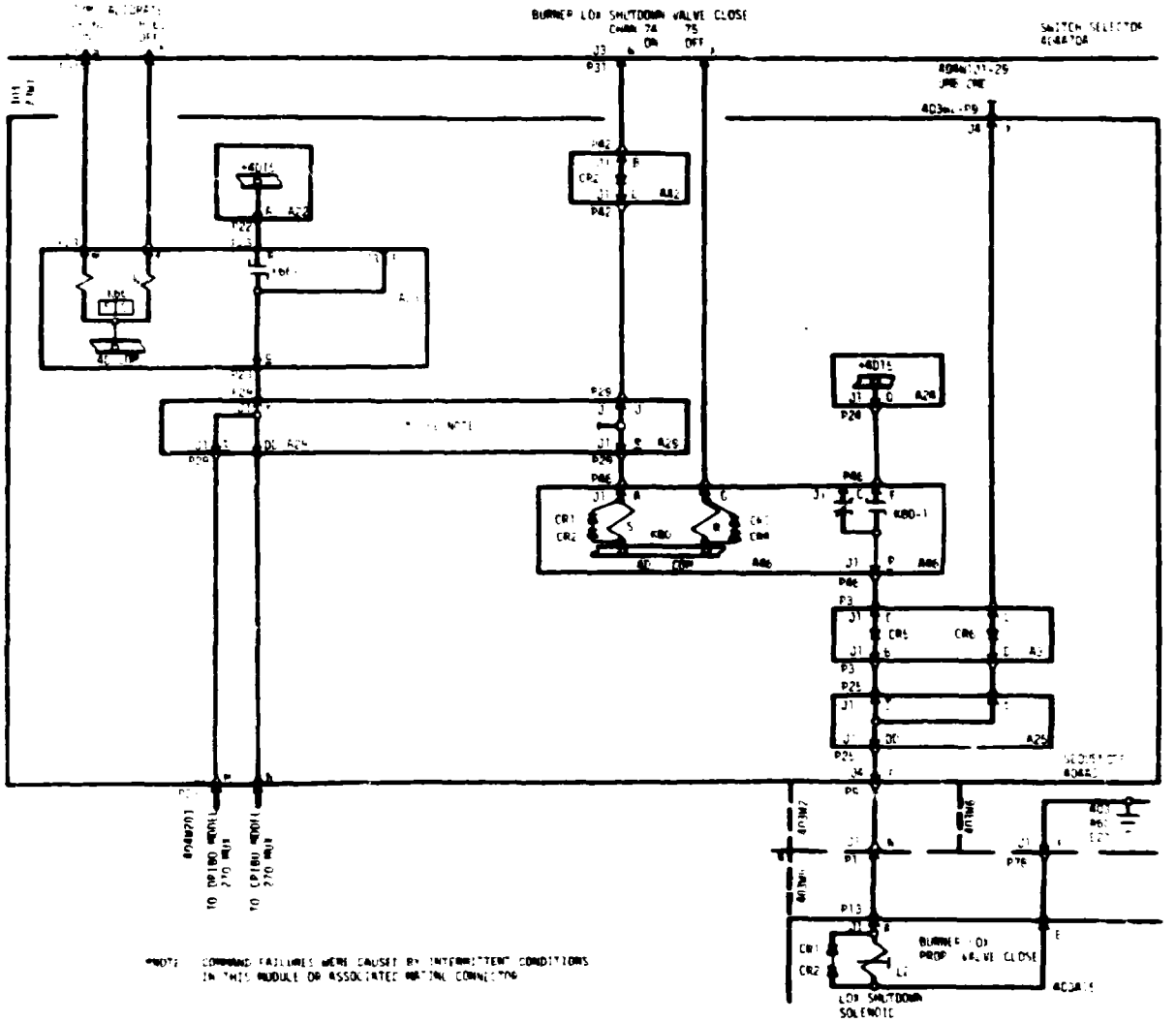

igure 12-5. Burner LOX Shutdown Valve "CLOSE" and TLM Calibrate "ON" Command Circuits

Tests are being conducted on similar bus modules and mating connectors to provide additional information as to the possible cause of the intermittent condition.

12.5 INSTRUMENT UNIT ELECTRICAL SYSTEM

All battery voltages and temperatures increased gradually from liftoff as expected. Voltages and currents remained normal on batteries 6D10 and 6D30 during launch and coast periods of flight. Battery 6D40 voltage and current remained in the normal range throughout the expected period (predicted lifetime for battery 6D40 was 38,160 seconds [10:36:00]). The 6D40 battery indicated a gradual voltage drop beginning at approximately 30,000 seconds (8:20:00) with a more rapid drop beginning at 36,000 seconds (10:00:00). The voltage level fell below the nominal range (28 ±2 vdc) at approximately 39,300 seconds (10:55:00) indicating impending failure of battery 6D40. The dropping voltage was accompanied by a rising current until 39,900 seconds (11:05:00) at which time the current also began a rapid decrease. Battery power consumption and estimated depletion times are shown in Table 12-4. Battery voltage, currents and temperatures are shown in Figures 12-6 through 12-8.

The 56-vdc power supply maintained an output voltage of 55.7 to 56.7 vdc, well within the required tolerance of 56 ±2.5 vdc.

The 5-vdc measuring power supply performed nominally, maintaining a constant voltage within specified tolerances.

The switch selector, electrical distributors, and network cabling performed nominally.

Table 12-4. IU Battery Power Consumption

BATTERY	RATED CAPACITY (AMP-HRS)	POWER CONSUMPTION*		ESTIMATED LIFETIME (HOURS)
		AMP-HRS	PERCENT OF CAPACITY	
6D10	350	261.3	74.7	16.2*
6D30	350	223.9	64.0	17.9*
6D40	350	403.5	115.3	10.9**

*Based on available flight data to 43,980 seconds (12:13:00).
**Battery 6D40 fell below the nominal range (28 ±2 volts) at this time.

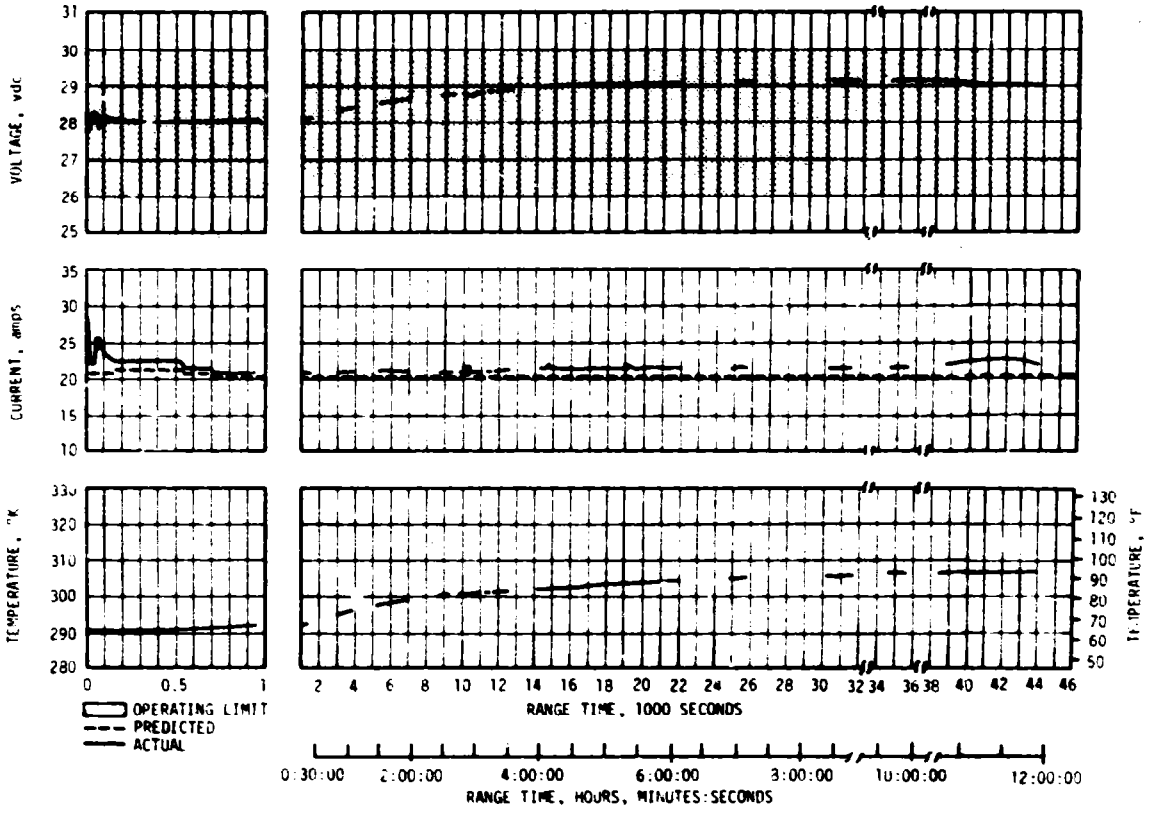

Figure 12-6. Battery 6D10 Voltage, Current and Temperature

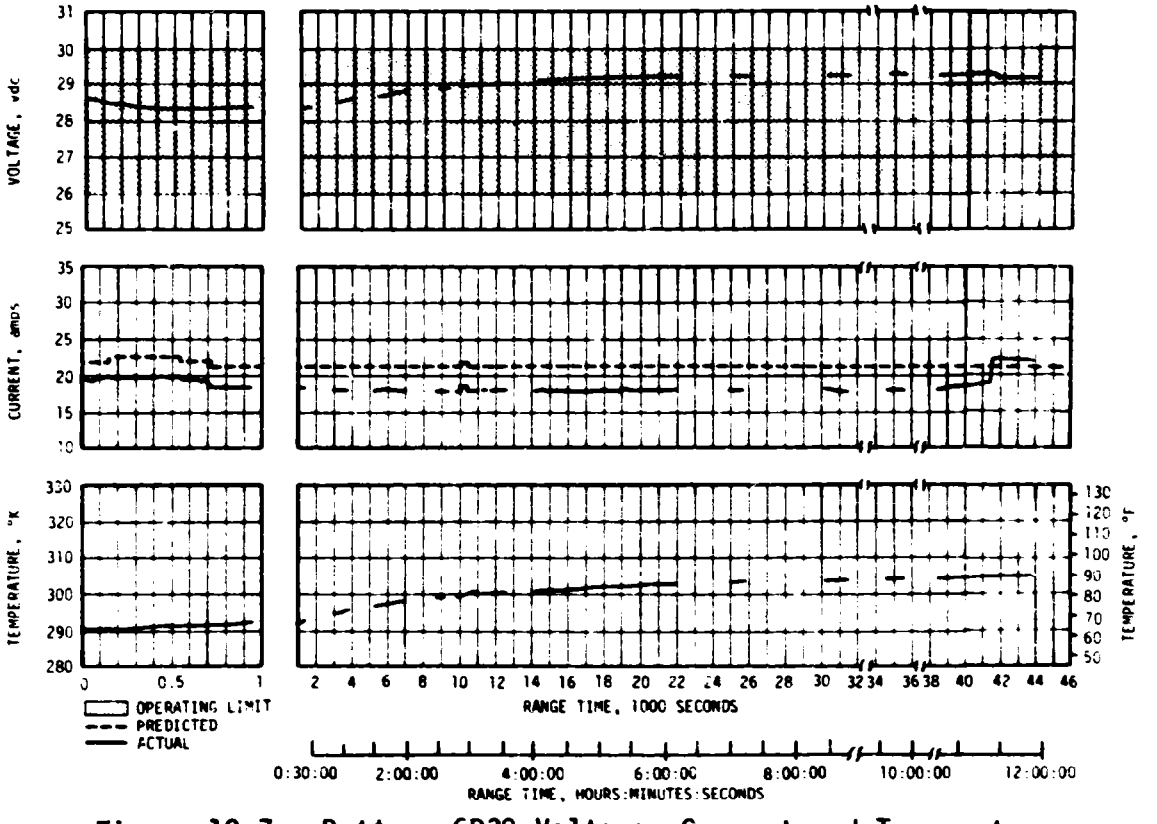

Figure 12-7. Battery 6D30 Voltage, Current and Temperature

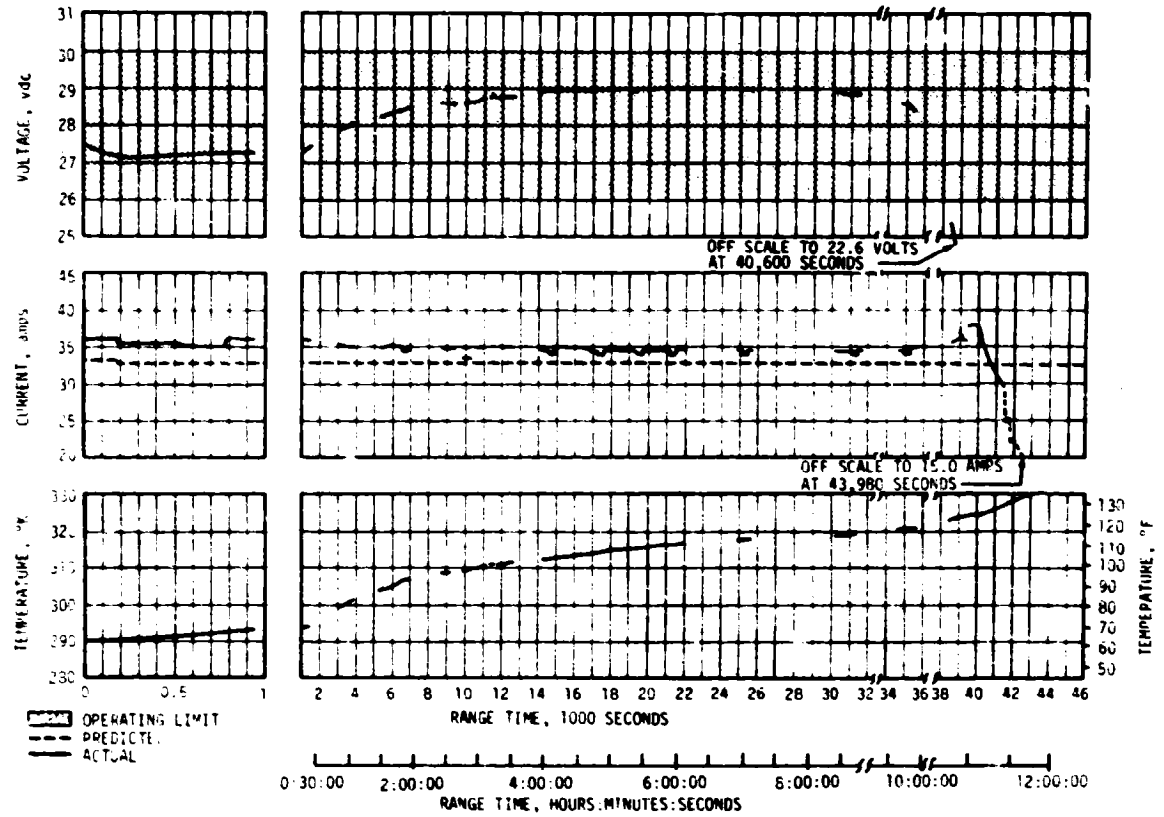

Figure 12-8. Battery 6D40 Voltage, Current and Temperature

12.6 SATURN V EDS

The performance of the AS-507 EDS was normal and no abort limits were exceeded. EDS related sequential events and discrete indications occurred as expected. The performance of all thrust OK sensors and associated voting logic, which monitor engine status, was nominal insofar as EDS operation was concerned. S-II and S-IVB tank ullage pressures remained within the abort limits and displays to the crew were normal.

The maximum angle-of-attack dynamic pressure sensed by a redundant Q-ball mounted atop the escape tower was 0.9 psid at 42 seconds. This pressure was only 28 percent of the EDS abort limit of 3.2 psid. As noted in Section 11, none of the triple redundant rate gyros gave any indication of angular overrate in the pitch, yaw or roll axes. The maximum angular rates were well below the abort limits.

SECTION 12A

TRIGGERED LIGHTNING PHENOMENON

12A.1 SUMMARY

The Apollo 12 vehicle was launched in rainy weather after consideration of Launch Mission Rule 1-404, as shown on Table 12A-1. Shortly after 36.5 seconds into the flight, there were numerous space vehicle indications of a massive electrical disturbance, followed by a second disturbance at 52 seconds. The astronauts reported that, in their opinion, the vehicle had been hit by lightning.

Data in the 36.5- and 52-second time periods were investigated regarding this problem. Camera data, telemetered data, and Launch Vehicle Data Adapter/Launch Vehicle Digital Computer (LVDA/LVDC) bit errors showed that the vehicle had been struck by lightning at 36.5 seconds. Virtually no discernable effects were noted on the launch vehicle during the 52-second disturbance. Atmospheric electrical factors and the fact that the vehicle does not have the capacitance to store sufficient energy to produce the effects noted indicate that the lightning discharge at 36.5 seconds was triggered by the vehicle. The 52-second disturbance may have been due to a lesser lightning discharge.

The launch vehicle hardware and software suffered no significant effects; therefore, the mission proceeded as scheduled. There is no evidence of vehicle pyrotechnics being endangered due to built-in protection in the

Table 12A-1. MSFC Launch Mission Rule 1-404

SEVERE WEATHER:
The vehicle will not be launched when its nominal flight path will carry it through a cumulonimbus (thunderstorm) cloud formation.
REMARKS:
The design of the Saturn V vehicle is such that it should not be subjected to launch during thunderstorm weather conditions.

circuitry. Some modification to present launch mission rules will be required to preclude launching of the vehicle when the probability of triggered lightning discharges is deemed unacceptable.

12A.2 REAL-TIME EFFECTS NOTED

Apollo 12 was the first Saturn vehicle launched in the rain. Weather conditions at launch are described in Appendix A. It was decided to launch after consideration of Launch Mission Rule 1-404 (see Table 12A-1) regarding launch in severe weather. The rationale behind the Launch Mission Rule is described in Table 12A-2.

Table 12A-2. MSFC Launch Mission Rule Background

SYSTEM BACKGROUND DATA:

SEVERE WEATHER

Thunderstorms can be critical to space vehicle ground operations because high winds are to be expected in association with thunderstorms and because associated large electrical potential gradients can create a safety hazard. These vehicle operational problems are made even more complicated because there is no known reliable method to predict (forecast) the maximum wind to be associated with a thunderstorm. Therefore, statistical methods are offered as techniques to determine the magnitude of the problem in a probabilistic sense, to establish calculated risk due to thunderstorm winds, and to form the basis for establishing launch mission rules.

Thunderstorms are critical to vehicle launch because the Saturn is not designed to fly through thunderstorms. Therefore, the present launch mission rule, relative to vehicle launch in thunderstorms, states: "The vehicle will not be launched when its flight path will carry it through a cumulonimbus (thunderstorm) cloud formation." The basis for this rule is that such a cloud formation can be observed, and the rule can be objectively applied.

Shortly after 36.5 seconds into flight, it was reported that the fuel cells in the Service Module (SM) were disconnected and that all AC power in the spacecraft was lost. Also, numerous indicator lamps were illuminated at this time. It was later reported that the inertial measurement unit on the spacecraft had lost its inertial reference at 52 seconds. It was the opinion of the astronauts that the vehicle had been hit by lightning. Investigation of this problem centered on data in the 36.5 and 52-second time periods.

12A.3 CAMERA DATA INDICATIONS

Analysis of all available ground camera data indicated that there were two lightning discharges in the vicinity of the launch pad during the 36.5-second time period. One discharge forked into two branches with both branches apparently entering the ground. These lightning effects were observed by three cameras and by the vidicon. Although camera coverage was restricted due to the low ceiling of 0.6 kilometer (2100 ft), every tracking camera showed two bright frames during this time period. The vidicon also showed brightness on several frames preceding those on which the lightning strokes were visible. Trajectory data (Section 4) show that the vehicle at this time was at 1.95 kilometers (6397.6 feet), in the clouds, and out of sight of the ground. A reconstruction of the lightning phenomenon based on camera analysis is shown in Figure 12A-1.

12A.4 LAUNCH VEHICLE DATA SYSTEM INDICATIONS

Launch vehicle telemetered data were examined in detail in the 36.5- and 52-second time periods to determine effects that could be attributed to lightning or a static discharge. Forty-five measurements in the Instrument Unit (IU) experienced a disturbance in the 36.5-second time period. S-IVB data systems experienced disturbances at this time on all 15 single sideband telemetry channels and on 45 Pulse Code Modulated (PCM) data samples. Three vibration measurements on the S-II stage were also affected at this time with one disturbance noted on the S-IC. At 52 seconds a disturbance was noted on one S-II vibration measurement. All of the disturbances noted were transients of variable amplitudes. No pattern was apparent either in geographical location or in the magnitude of the disturbance other than most measurements affected being located on the upper two stages of the vehicle (IU and S-IVB). There was no damage or subsequent data degradation noted. The nature and randomness of the transients are characteristic of effects caused by a massive external electrical disturbance such as lightning.

12A.5 IU LVDA/LVDC INDICATIONS

At approximately 36.6 seconds the LVDA pitch gimbal crossover counters indicated a change in excess of the acceptable 0.4-degree limit. At 37.01 seconds, bit 1 in mode code 24 of the LVDC was also set because redundant

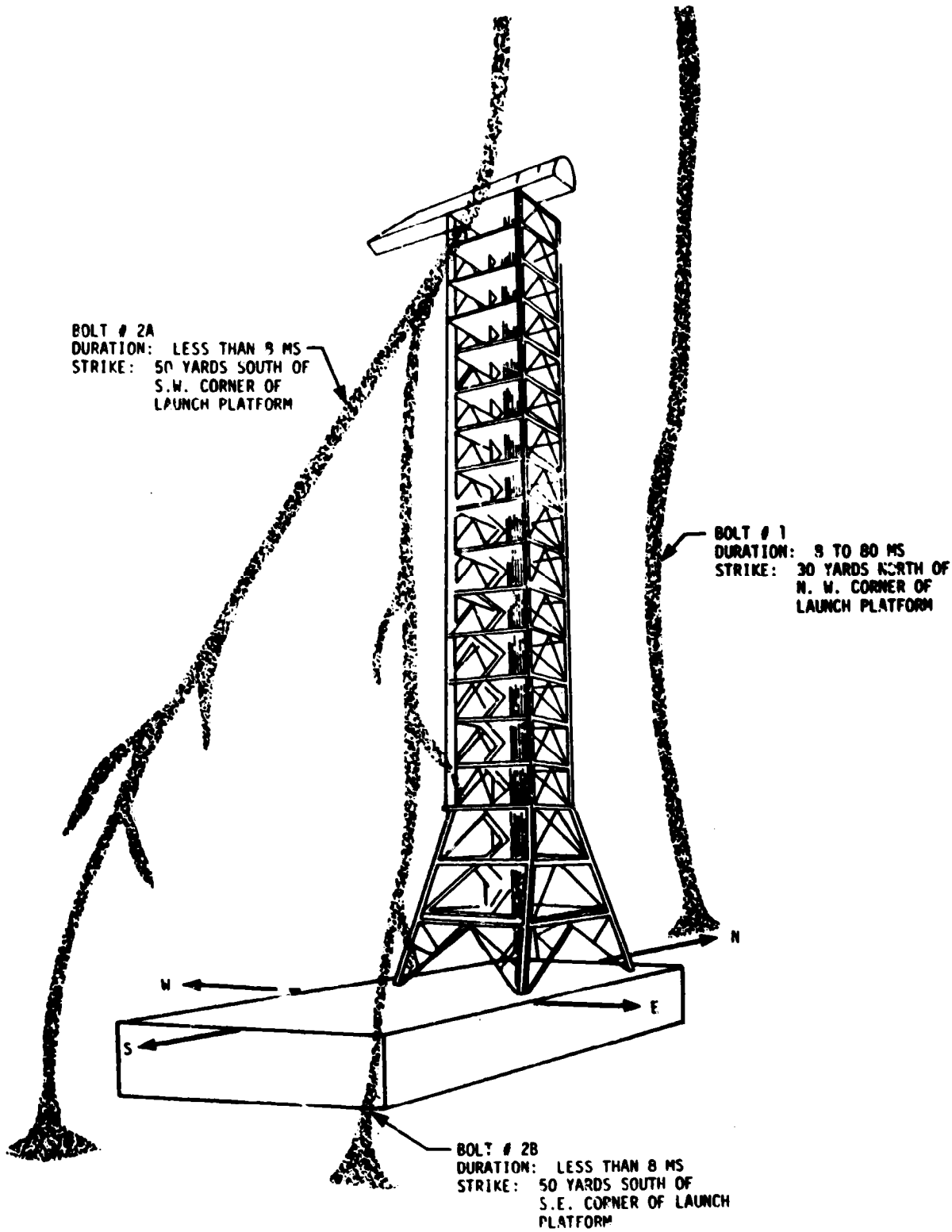

Figure 12A-1. Artist Concept of Lightning Phenomenon at 36.5 Seconds

accelerometer counters differed by 9 counts (maximum allowable difference is 2 counts). In both instances, the erroneous impulses are indicative of a strong external electrical disturbance. Subsequent operation was normal. A more complete discussion of these performance variations is contained in Section 10.

12A.6 VEHICLE PYROTECHNICS

There is no evidence that vehicle pyrotechnics were endangered by the lightning discharge. The pyrotechnics normally are fired by discharging capacitors in the Exploding Bridge Wire (EBW) networks. These capacitors are normally uncharged and require 1.0 to 1.5 seconds to be charged to operating voltages. When operating voltage is attained, the devices still will not fire until a special trigger signal is received. If the trigger signal is not received, the capacitor charge is leaked to a safe value within 15 seconds. Since duration of lightning is normally less than 0.1 second and since the system must be electrostatically shielded to provide protection against Radiofrequency Interference (RFI) to meet specification requirements, the probability of spurious ignition of the EBW's is remote.

12A.7 SUPPORTING ATMOSPHERIC ELECTRICAL EVIDENCE

Discussions with authorities knowledgeable in the field of atmospheric electricity provided the following additional information relevant to the Apollo 12 lightning problem:

a. Lightning discharges can be triggered by structures distorting a field of high potential gradient in the atmosphere. In this context, a triggered lightning discharge is one where the presence of a structure causes the discharge to occur as opposed to a natural discharge.

b. Potential gradients of sufficient strength to induce lightning discharges can exist in clouds other than cumulonimbus clouds.

c. The lightning discharge is preceded by a leader that may not be visible. These leaders occur within 0.1 second of the lightning discharge according to available evidence. However, large electrical charges are built up during the time prior to development of the leader. When branching is observed in a lightning discharge, the branches always point in the direction of propagation of the lightning.

d. A laboratory test demonstrated that a charged capacitor discharges over a much greater distance in the presence of a flame. This experiment substantiates the theory that the Apollo 12 flame plume contributed to the discharge.

e. The data do not indicate whether the discharge started at the top of the vehicle and then went down the plume or if it started at the top of the plume and traveled both ways. In either case, the electrical disturbance effect on Apollo 12 would have been the same. However, the charge at the top of the plume is near neutral, and the enhancement factor associated with radius of curvature of the "Q" ball indicates that the probability is high that the discharge occurred to the top of the vehicle.

f. To produce the effects noted on Apollo 12, the energy level due to static charge must have exceeded 10^4 joules and could have been as high as 10^8 joules. Energy levels due to static charges on the Apollo Saturn vehicle from atmospheric effects and from flame effects must be below 10^3 joules because of the relatively small capacitance of the vehicle and leaking of of charge down the plume.

g. Potential gradient measuring systems at KSC showed the existence of a high potential gradient on the ground, thereby indicating high electrical activity in the clouds. No evidence of natural lightning discharges in the local area was recorded on other instrumentation.

12A.8 CONCLUSIONS

Virtually no effects were noted on the launch vehicle during the 52-second time period. The following conclusions regarding this anomaly are therefore pertinent only to the 36.5-second time period:

a. No weather-related launch mission rule was violated on the Apollo 12 mission. This conclusion is based on the following:

   1. The vehicle did not fly through cumulonimbus (thunderstorm) clouds.

   2. The reference to cumulonimbus clouds is primarily concerned with winds aloft.

   3. The reference to electrostatic potential is primarily concerned with ground safety.

b. The vehicle was struck by a lightning discharge triggered by the vehicle itself. This conclusion is based on the following:

   1. The ionized gases in the flame plume contributed to the discharge.

   2. A fairly high current flow on or near the vehicle surface is evident.

3. Static charges on the vehicle would not have been sufficient to produce the effects noted.

4. No lightning occurred in the 6-hour period prior to launch or in the 6-hour period subsequent to S-IC cutoff.

c. The tendency of a space vehicle to encourage lightning where natural lightning discharge would not exist and the potential danger to the mission that results from this tendency indicate the necessity for some modifications to the present launch mission rules. The reasons for requiring modifications are as follows:

1. The launch vehicle is designed and tested to provide immunity from lightning phenomena in standby and storage. It is not designed to operate in the presence of a lightning discharge, however, because of computer sensitivity to induced fields greater than 1.5 gauss; it relies primarily on good design practices to minimize the effects of such an environment. Because of geometry, the spacecraft is more vulnerable to lightning than is the launch vehicle.

2. The launch vehicle is more likely to trigger lightning (and therefore be struck by it) than is an airplane, because it flies at right angles to lines of equal potential instead of parallel to them. While the lines of equal potential may be vertically oriented, such an occurrence is normally accompanied by natural lightning discharges and high turbulence of a thunderstorm that would readily indicate the excessive hazards associated with a flight path through such a cloud cell for both an aircraft and the launch vehicle.

3. Natural lightning is not requisite to the existence of a lightning hazard during vehicle boost or reentry.

d. Consideration must be given to several factors to keep launch constraints reasonable. These factors are as follows:

1. No one factor such as rain, cloud thickness, or the electrostatic potential measured on the ground necessarily indicates the presence or absence of a condition hazardous to the vehicle. For example, the presence of rain does not in itself indicate the existence of a potential gradient sufficient for triggered lightning, and conversely, the absence of rain does not preclude the possible existence of such a gradient. All of the indicators, therefore, need to be analyzed to determine the probability of a potentially hazardous condition.

2. Because the potential gradient measuring system at KSC may not reliably show the existence of hazardous potential gradients aloft, additional ground and aircraft instrumentation may be required to provide better correlation between observed ground conditions and conditions aloft. These needs, however, require better definition and a critical evaluation.

3. There is no way to assure a 100 percent guarantee that future vehicle launches will not encounter static discharges. However, the triggered lightning occurrence and significant static discharge risks may be reduced if deemed unacceptable.

4. Ground rules need to be established for interpreting data to assess the possibility of triggering lightning. At the same time, the rules must not be so arbitrary that they lead to an unnecessary launch hold.

e. Permanent detrimental effects due to lightning discharge would not be expected on the hardware or pyrotechnics. The software, however, could be influenced because of computer sensitivity to induced fields greater than 1.5 gauss.

f. A review of this anomaly with numerous authorities in the field of atmospheric electricity resulted in unanimous agreement that the evidence from vehicle measurements, atmospheric conditions, and experimental studies supports the conclusion that the vehicle was struck by a lightning discharge triggered by the vehicle itself.

SECTION 13

VEHICLE PRESSURE AND ACOUSTIC ENVIRONMENT

13.1 SUMMARY

The S-IC base heat shield was instrumented with two differential pressure measurements, one of which failed. The data from the valid measurement show good agreement with data from AS-506.

In general, the S-II heat shield forward face and the thrust cone static pressures fall within the data band of the previous flights.

Acoustical measurements were made at 12 locations on the S-IVB interstage and aft skirt. Data for liftoff appear to be valid for all 12 measurements. Flight data after 15 seconds appear to contain questionable areas for some of the measurements because the measured environment at these locations was below the range of the instrumentation.

13.2 BASE PRESSURES

13.2.1 S-IC Base Pressures

The S-IC base heat shield was instrumented with two differential (internal minus external) pressure measurements. Measurement number D0046-106 failed on the AS-507 flight and is not shown here. The AS-507 data, Figure 13-1, show good agreement with AS-506 data. The peak differential of approximately 0.15 psid occurred at the same altitudes, and the magnitudes and trends were consistent with the AS-506 flight.

13.2.2 S-II Base Pressures

The AS-507 forward face static pressure fell within the data band of the previous flights, as shown in Figure 13-2. The AS-507 static pressure, prior to interstage separation, was approximately 15 percent lower than the corresponding AS-506 value. Good agreement was obtained between flight and postflight predicted values.

The AS-507 thrust cone static pressures, Figure 13-3, fell close to the lower limit data band of the previous flights and were approximately 20 percent below the corresponding AS-506 value prior to interstage separation.

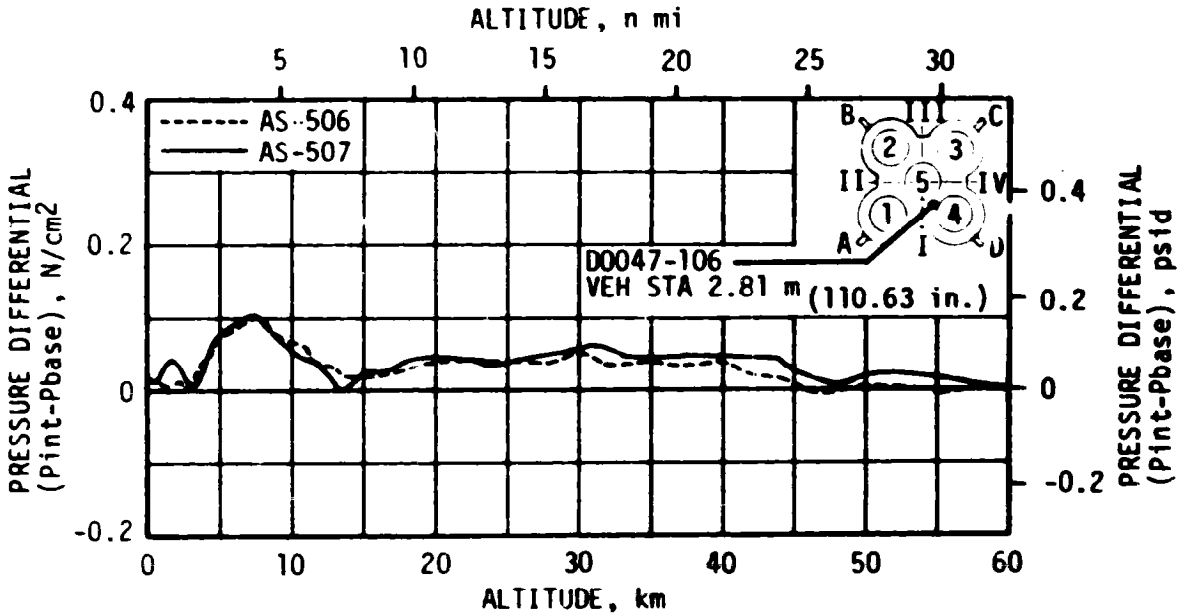

Figure 13-1. S-IC Base Heat Shield Differential Pressure

Both thrust cone and heat shield forward face static pressures were extremely low after interstage separation. Therefore, the pressure changes occurring during CECO, EMR shift, and engine cutoff are not apparent in the flight data.

The postflight prediction and the AS-507 flight data for the heat shield aft face static pressure are shown in Figure 13-4. Also shown in this figure is the data band for the previous flights. The AS-507 flight pressure falls below this data band. This trend was not expected since the engines were angled closer together during the AS-507 flight than on any previous flight; therefore, higher pressures were anticipated. However, since the transducer indicated a negative pressure prior to J-2 engine ignition and after engine cutoff, a bias was suspected. Prior to ignition, the normal pressure in the base region is approximately 0.02 psia as indicated in Figures 13-2 and 13-3. Therefore, the actual AS-507 pressure in this region could be 0.02 psi higher than the transducer indicated value.

13.3 ACOUSTIC ENVIRONMENT

13.3.1 External Acoustics

AS-507 external fluctuating pressures were measured at 12 vehicle stations located on the S-IVB interstage and S-IVB aft skirt. The locations of the 12 measurements are shown in Figure 13-5. All measurements returned data from liftoff through S-IC boost. Liftoff data appear to be valid for all 12 instruments. All flight data, telemetered after approximately 15 seconds, dropped below 140.7 decibels and remained under the measurement range for 2 of the 12 instruments. The remaining flight instruments contained varying amounts of underrange data.

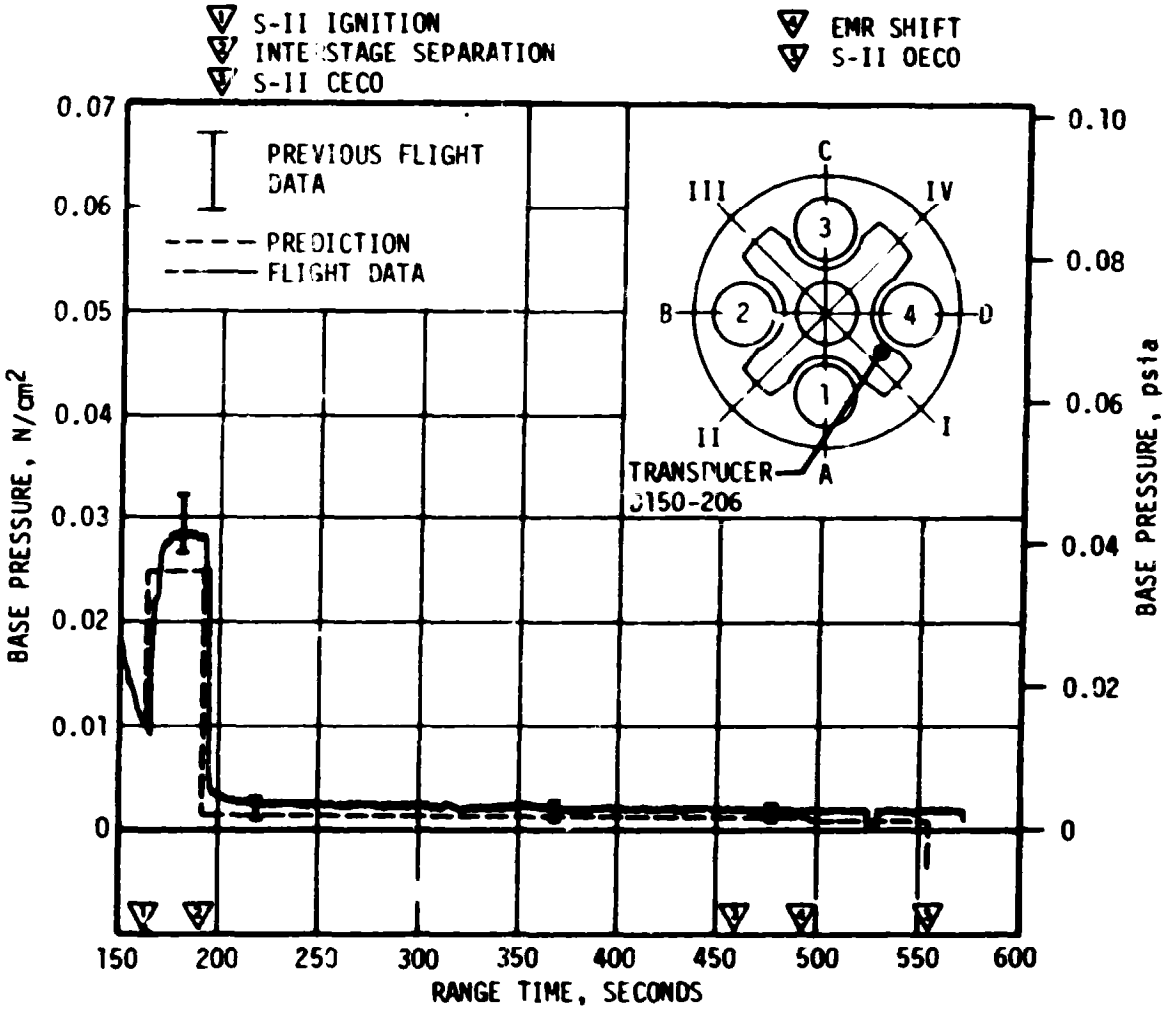

Figure 13-2. S-II Heat Shield Forward Face Pressure

The vehicle external overall sound pressure levels at liftoff are shown in Figure 13-6. Predicted values and previous flight data are included for comparison. Sound pressure spectral densities at liftoff are shown in Figure 13-7. Measurements B33-402 through B38-404, located near Position IV, show 3 to 4 decibels higher overall levels than the instruments located at or near Position III. This condition is apparently due to the location of the flame trench at Position IV. Spectral shapes are generally consistent for all instruments.

Overall fluctuating pressure time histories for S-IC boost are presented in Figure 13-8. Flight data were below the range of the instrumentation for measurements B28-402 and B32-402 and contained varying amounts of underrange data for measurements B31-402, B33-402, and B34-402. Preliminary inflight pressure spectral densities at or near maximum aerodynamic noise level are shown for 8 of the 12 measurements in Figure 13-9. Pressure spectrums are not included for those instruments where data are underrange or questionable at the time slice indicated.

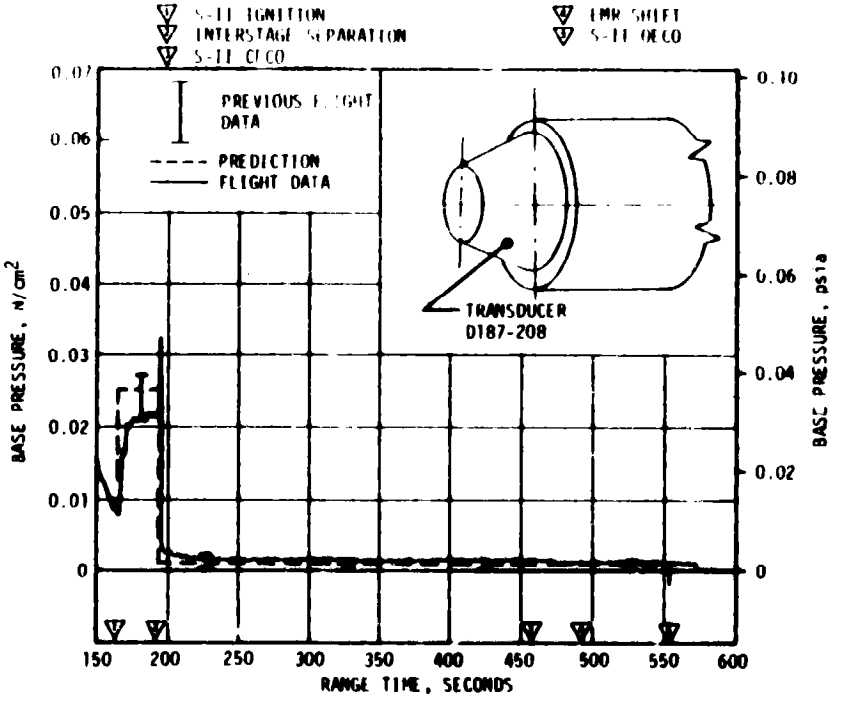

Figure 13-3. S-II Thrust Cone Pressure

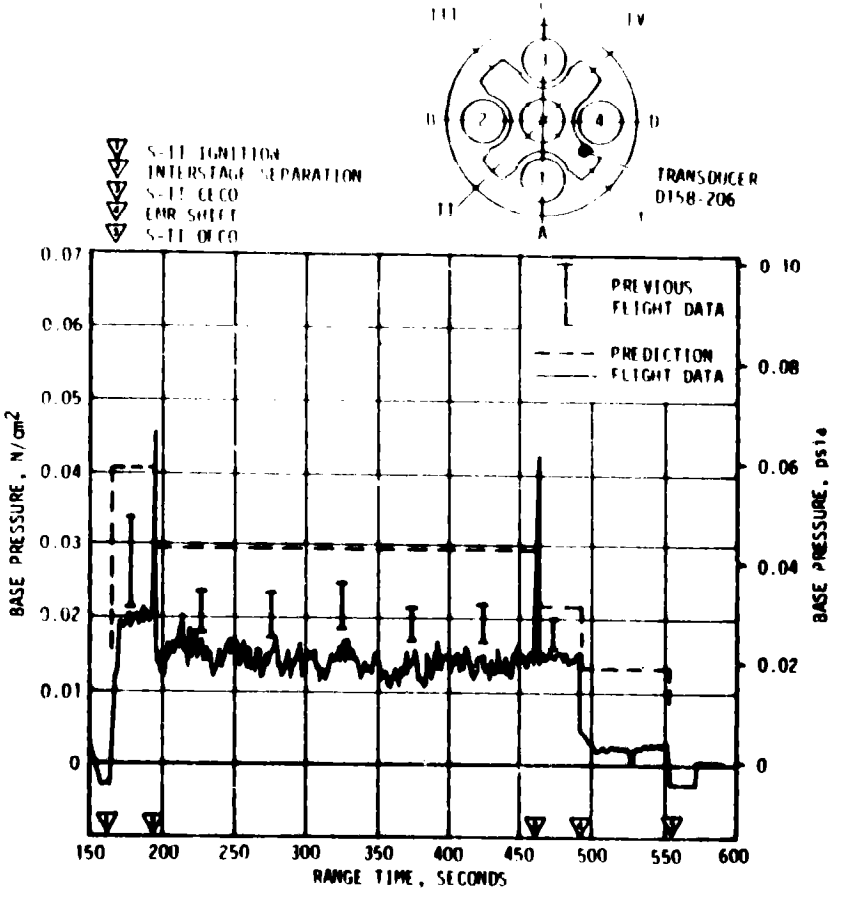

Figure 13-4. S-II Heat Shield Aft Face Pressure

INSTRUMENT NUMBER	VEHICLE STA METERS (IN.)	INSTRUMENT NUMBER	VEHICLE STA METERS (IN.)
B0028-402	64.72 (2548)	B0034-402	64.87 (2554)
B0029-402	65.38 (2574)	B0035-402	65.76 (2589)
B0030-402	65.76 (2589)	B0036-402	69.24 (2726)
B0031-402	68.86 (2711)	B0037-404	70.36 (2771)
B0032-402	69.42 (2733)	B0038-404	70.71 (2784)
B0033-402	64.24 (2529)	B0039-404	70.71 (2784)

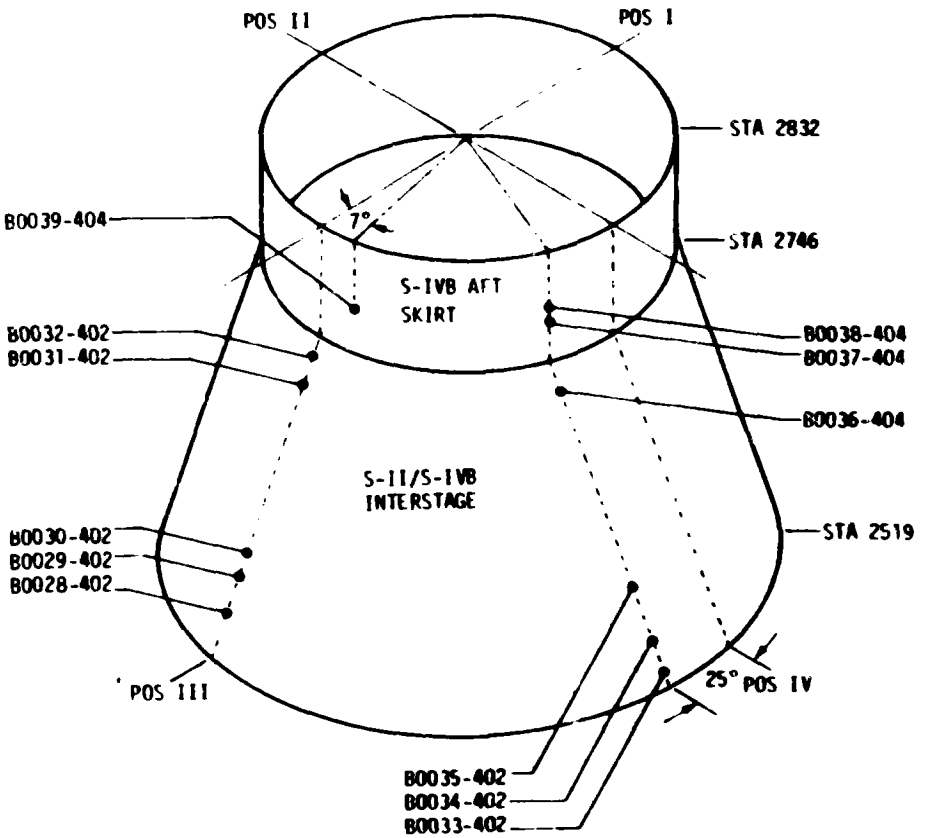

Figure 13-5. AS-507 Acoustic Instrumentation

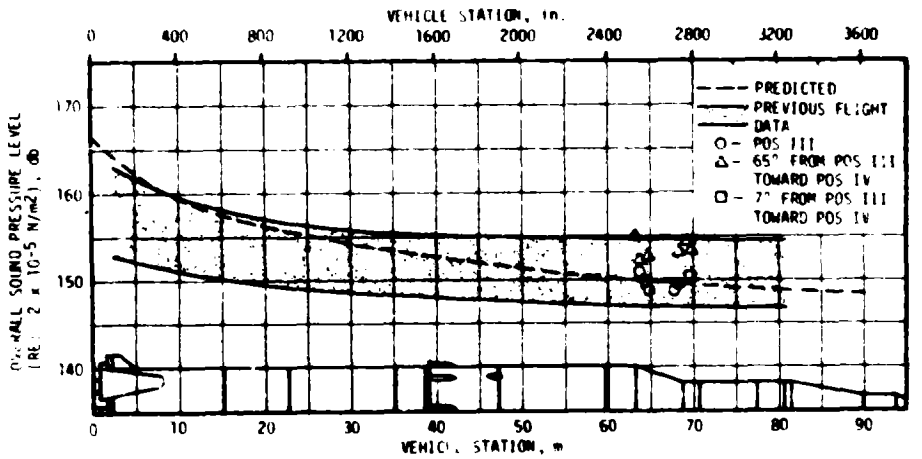

Figure 13-6. Vehicle External Overall Sound Pressure Level at Liftoff

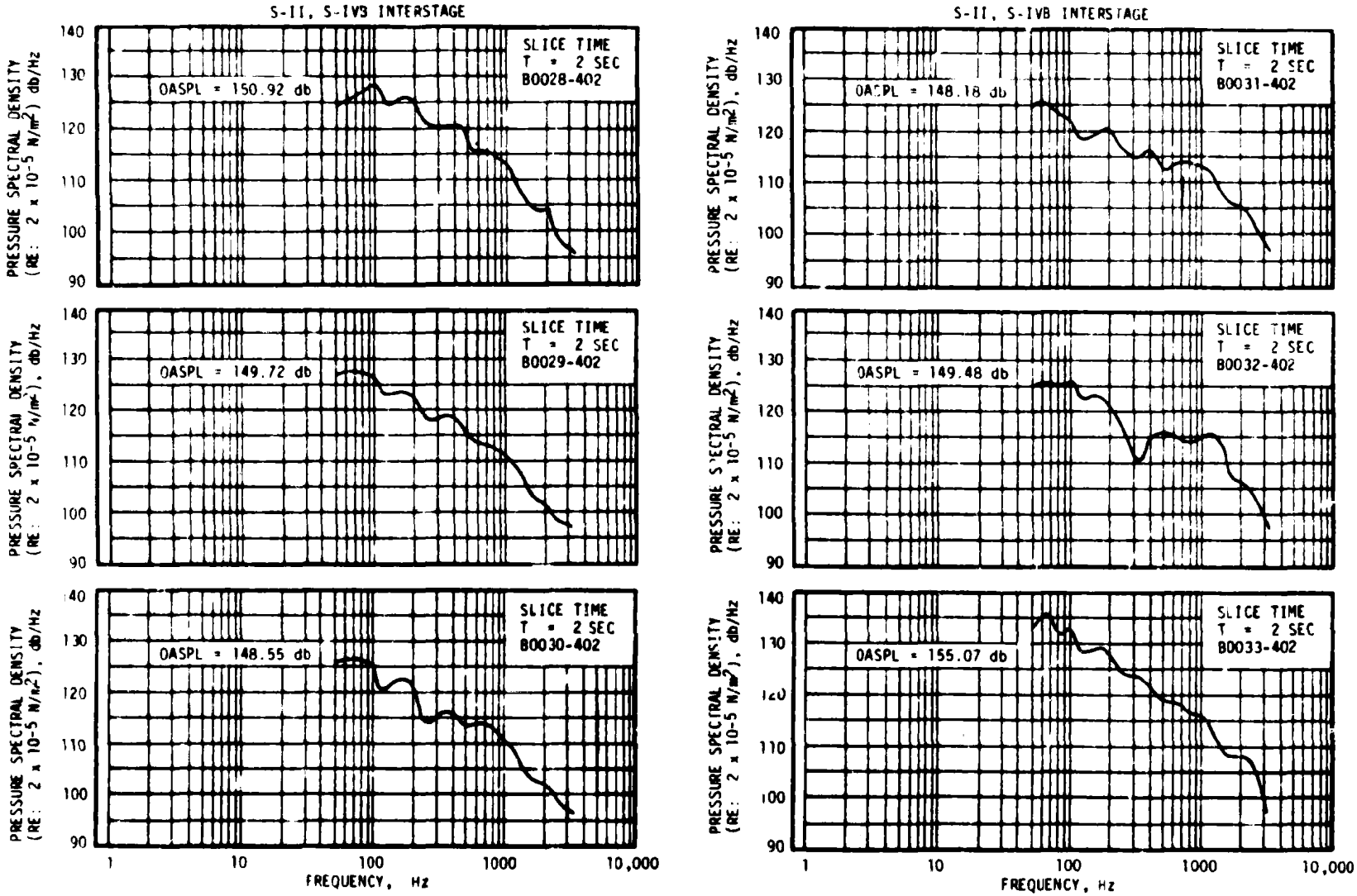

Figure 13-7. Vehicle External Sound Pressure Spectral Densities at Liftoff (Sheet 1 of 2)

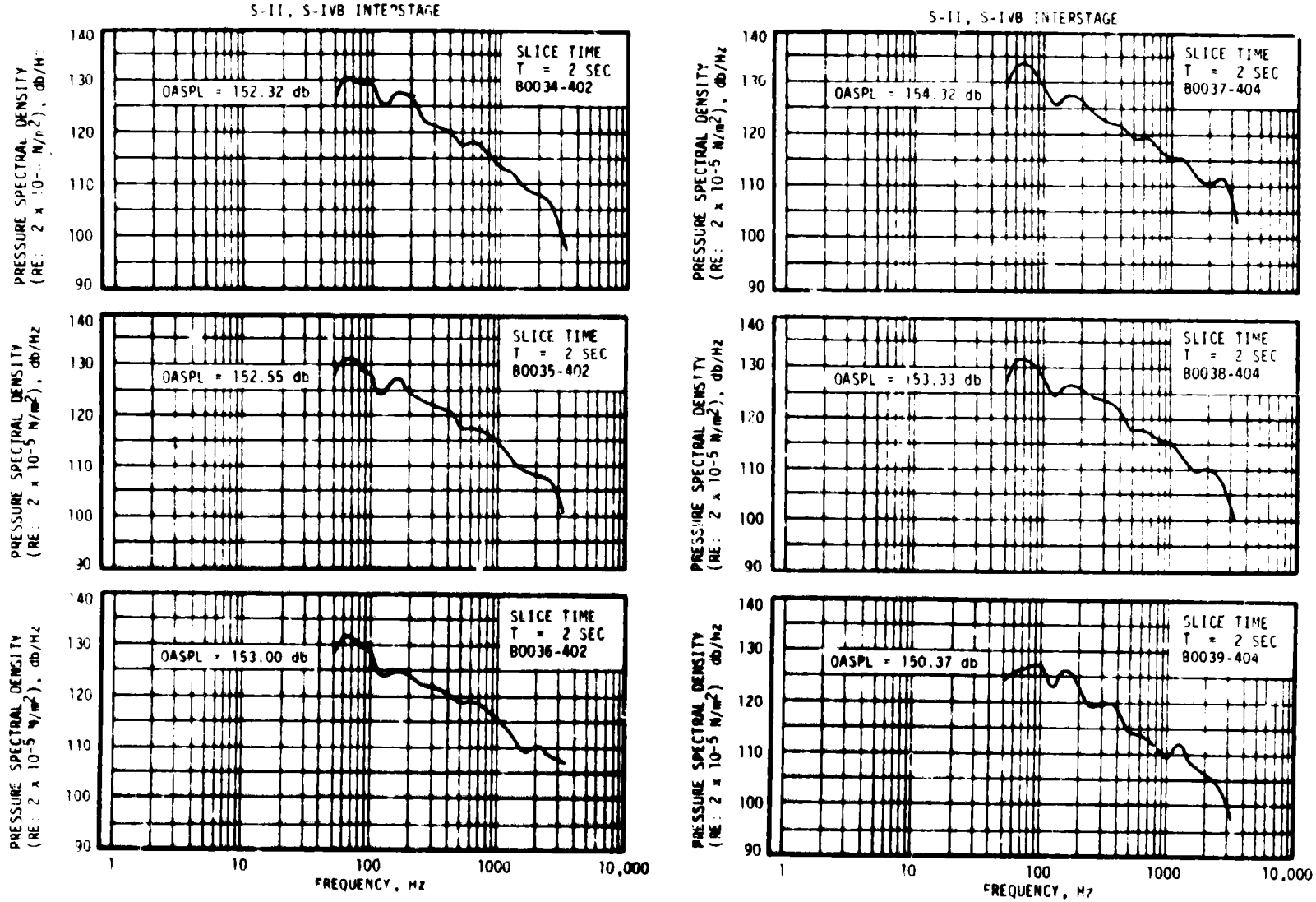

Figure 13-7. Vehicle External Sound Pressure Spectral Densities at Liftoff (Sheet 2 of 2)

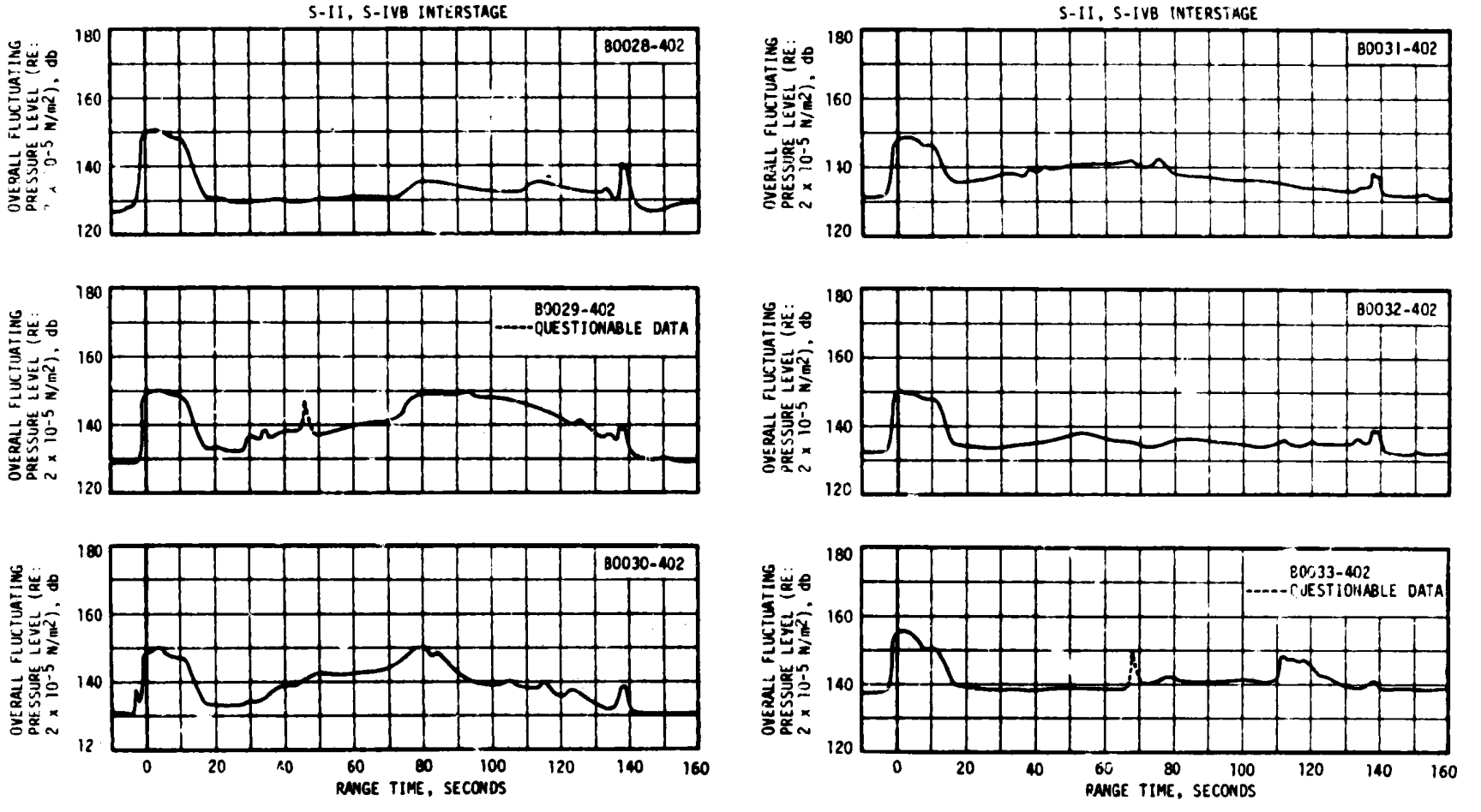

Figure 13-8. Vehicle External Overall Fluctuating Pressure Level (Sheet 1 of 2)

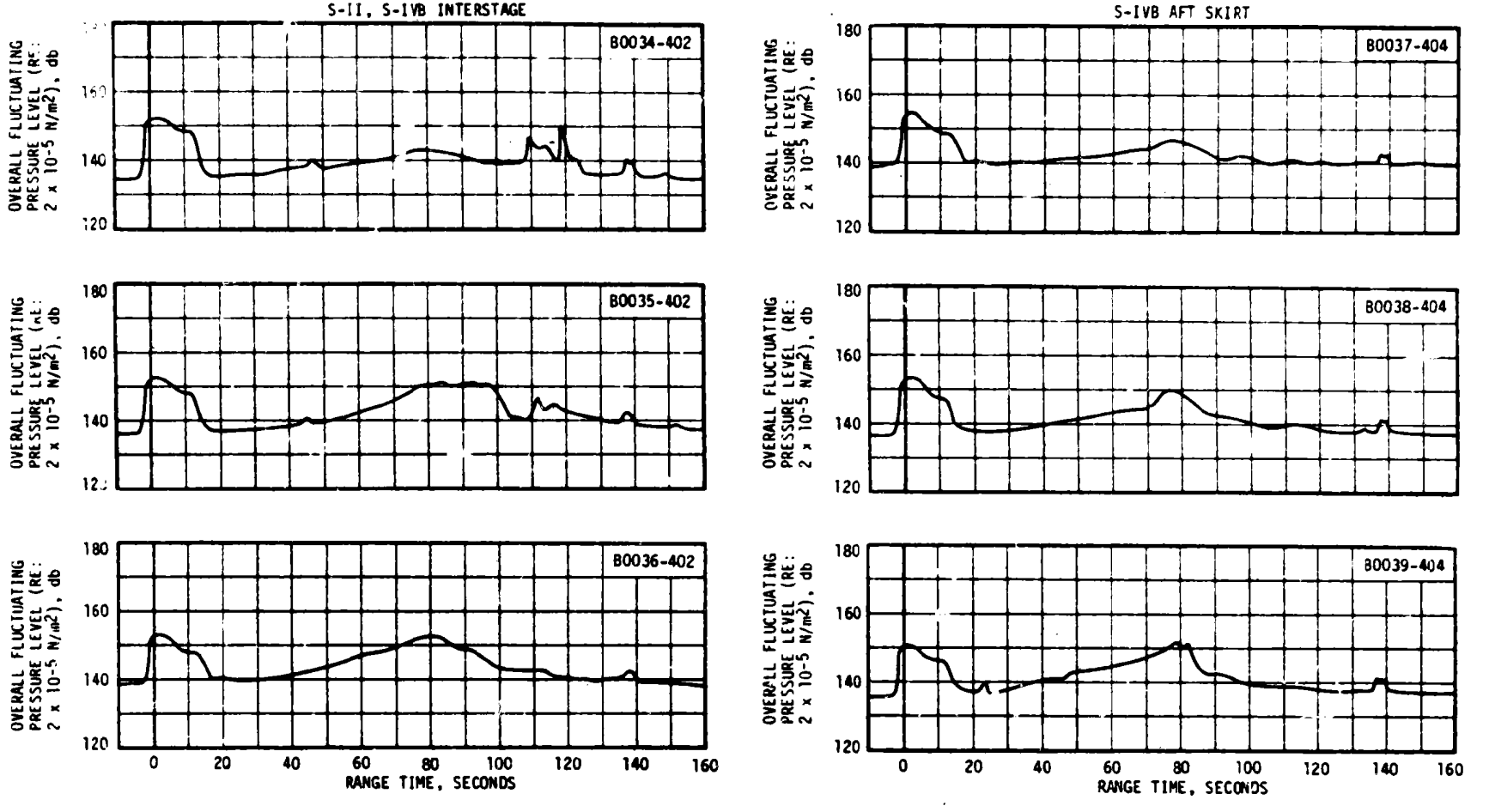

Figure 13-8. Vehicle External Overall Fluctuating Pressure Level (Sheet 2 of 2)

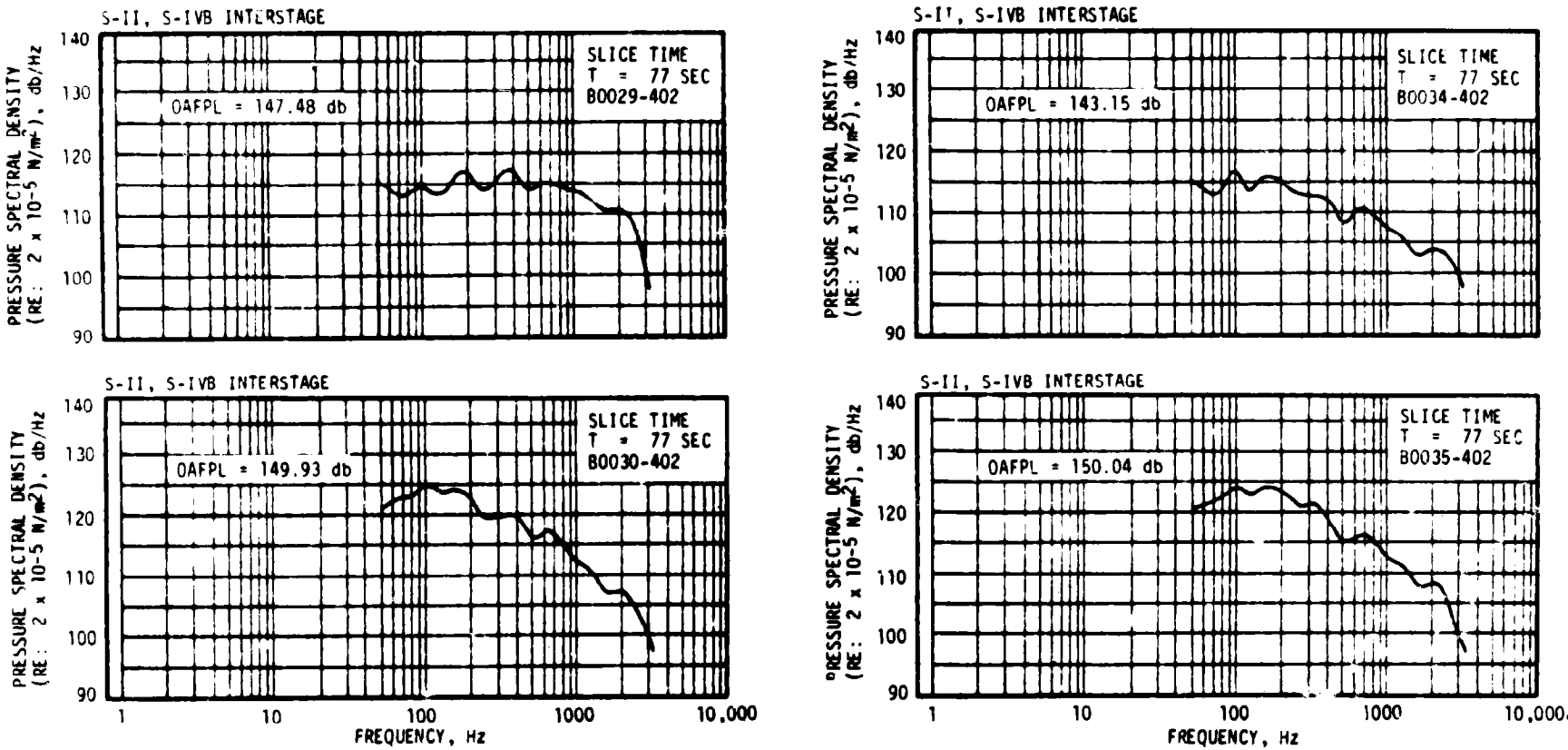

Figure 13-9. Vehicle External Fluctuating Pressure Spectral Densities (Sheet 1 of 2)

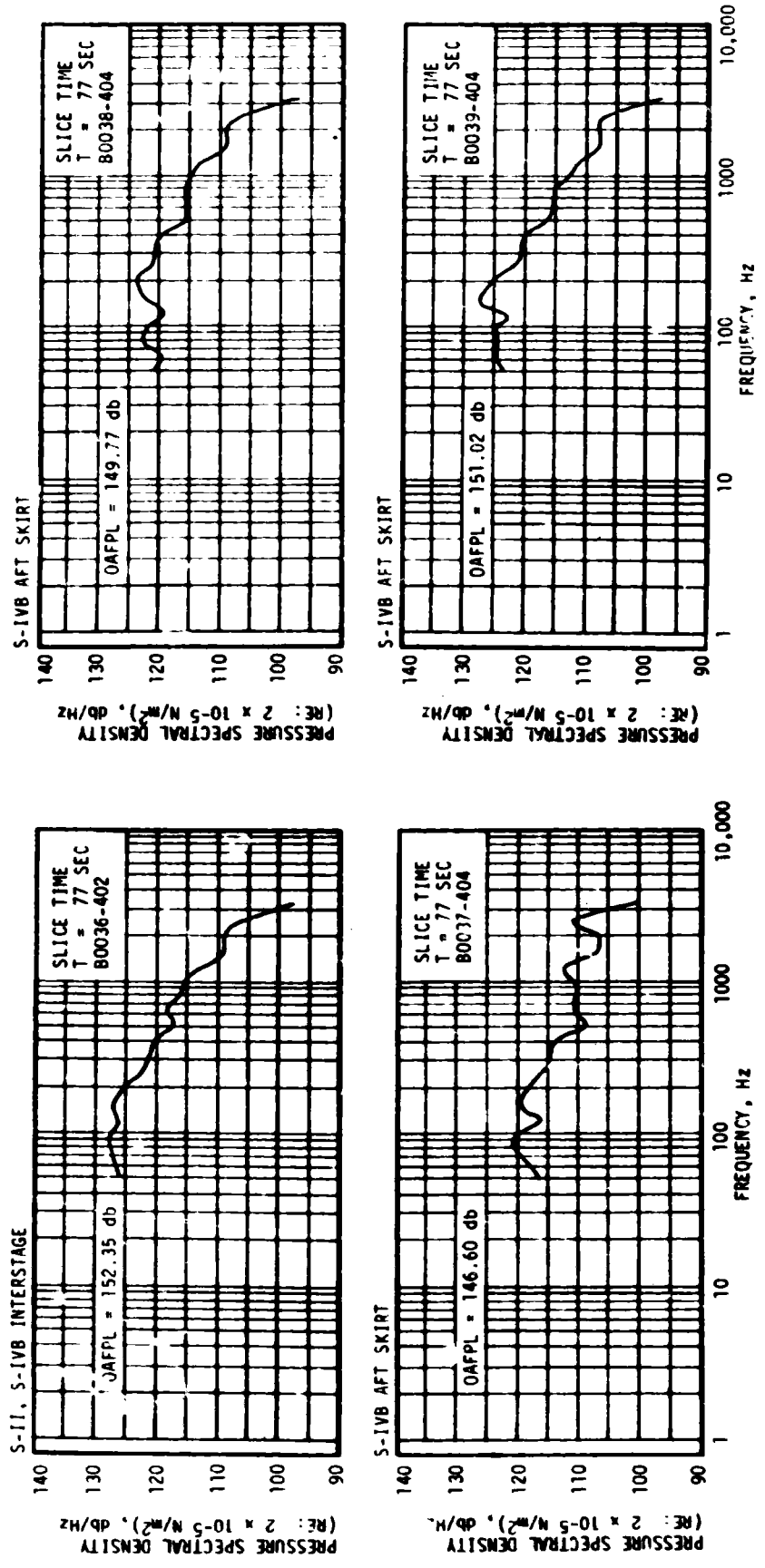

Figure 13-9. Vehicle External Fluctuating Pressure Spectral Densities (Sheet 2 of 2)

SECTION 14

VEHICLE THERMAL ENVIRONMENT

14.1 SUMMARY

The AS-507 S-IC base region thermal environments have similar magnitudes and trends as those measured during previous flights.

In general, base thermal environments on the S-II stage were similar to those measured on previous flights and were well below design limits. The total heating rate for the base heat shield on AS-507 was higher than corresponding values on previous flights. This was expected since the initial engine precant angle had been reduced from 2.3 to 1.3 degrees for AS-507.

Aerodynamic heating environments were not measured on AS-507.

14.2 S-IC BASE HEATING

Thermal environments in the base region of the S-IC stage were recorded by two total calorimeters and two gas temperature probes which were located on the base heat shield. Data from these instruments are compared with AS-506 flight data and presented in Figures 14-1 and 14-2. The AS-507 S-IC base heat shield thermal environments have similar magnitudes and trends as those measured during the previous flight. The maximum recorded total heating rate was 26.3 Btu/ft^2-s and occurred at 10.8 n mi, and the maximum recorded gas temperature of 1754°F occurred at 14 n mi. In general, Center Engine Cutoff (CECO) on AS-507 produced a spike in the thermal environment data with a magnitude and duration similar to previous flight data.

Ambient gas temperatures under the engine cocoons (monitored by C242-101 through -105) were within the range of previous flight data and within the predicted range. These temperatures are shown in Figure 14-3.

14.3 S-II BASE HEATING

Figure 14-4 presents total heating rate recorded by the calorimeter (C722-206) on the aft face of the base heat shield throughout S-II boost. The analytical prediction for this transducer and the AS-501 through AS-506 flight data are also shown in this figure for comparison. It is noted that the AS-507 total heating rate was higher than all other

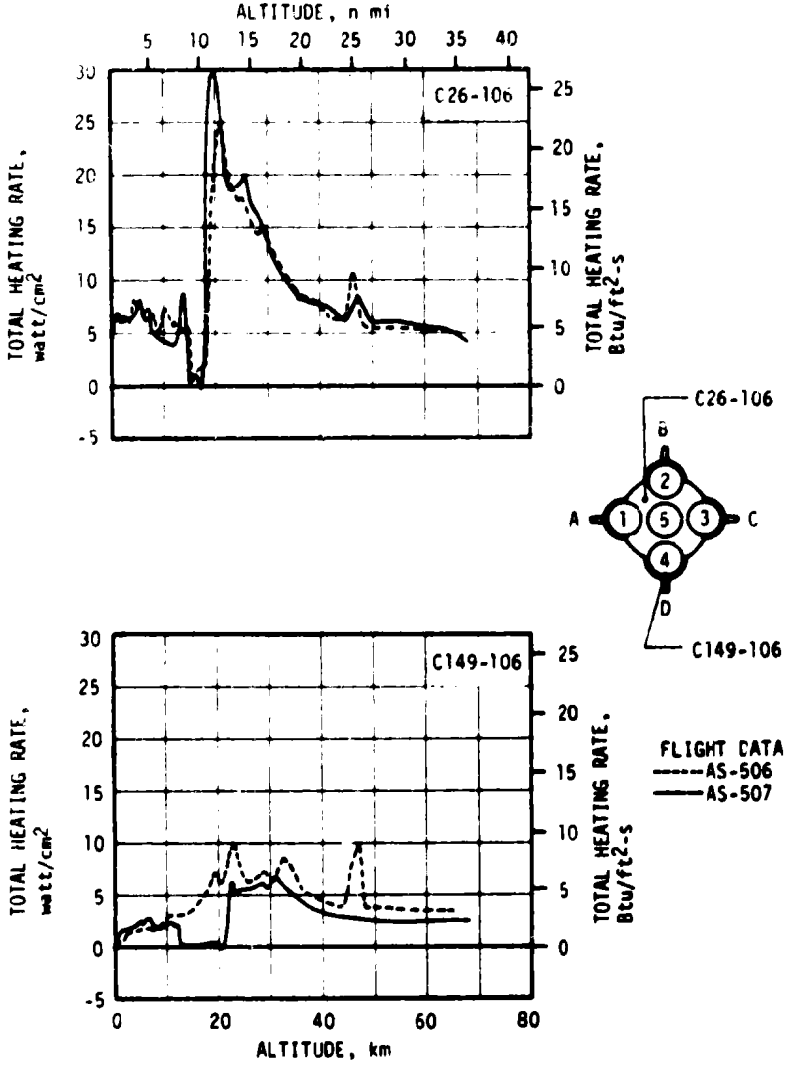

Figure 14-1. S-IC Base Heat Shield Total Heating Rate

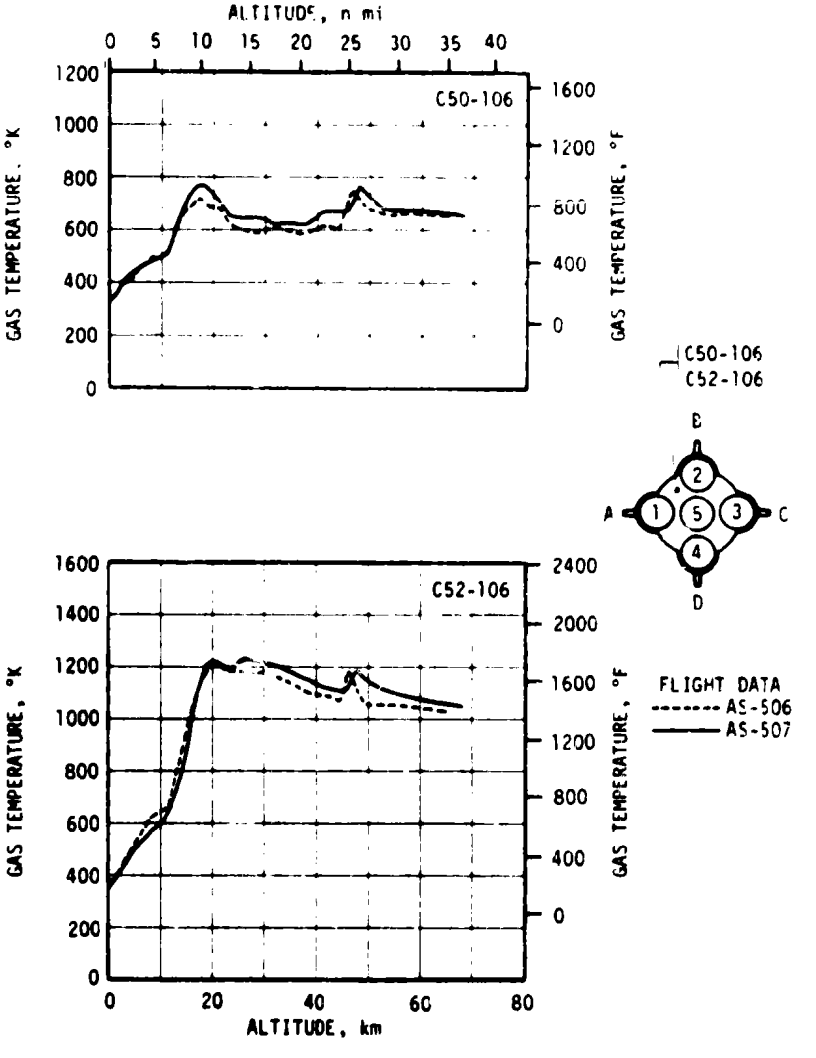

Figure 14-2. S-IC Base Region Gas Temperature

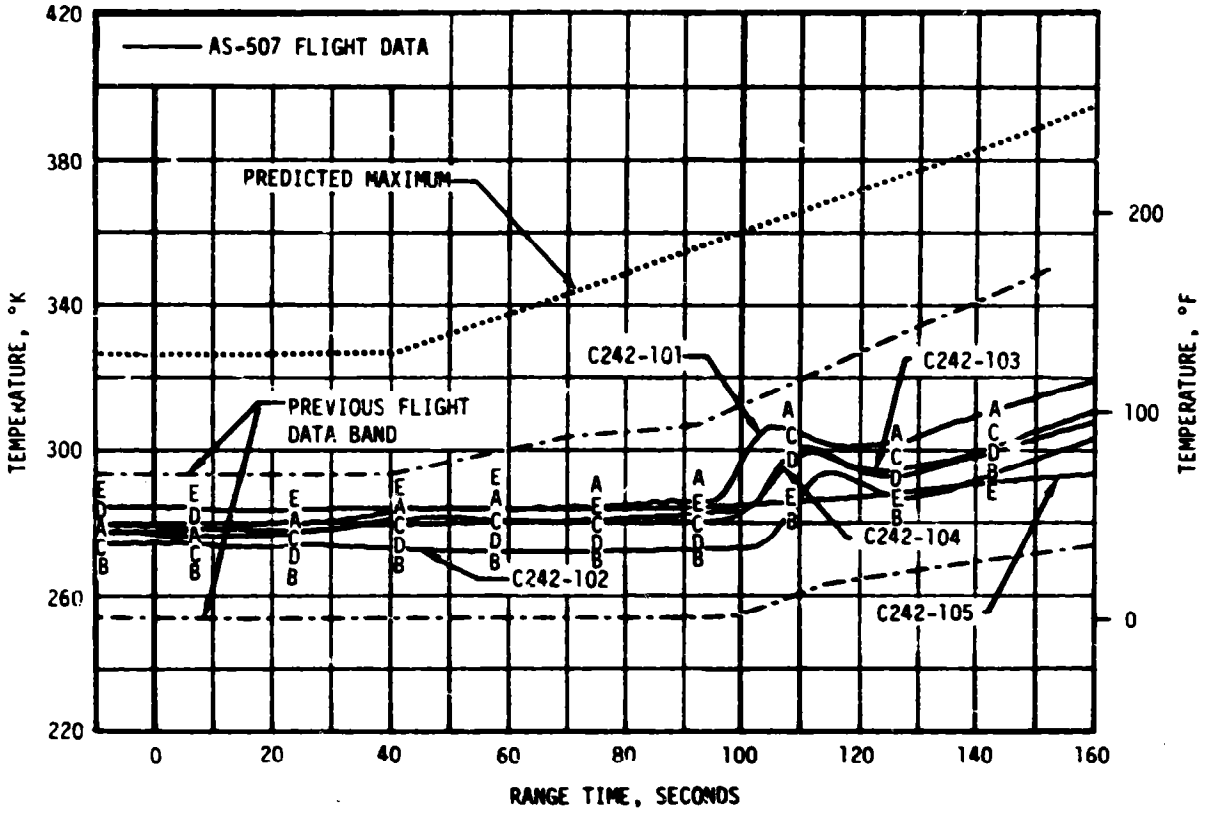

Figure 14-3. S-IC Base Heating Ambient Gas Temperature Under Engine Cocoon

corresponding values of the previous flight . This was expected since the initial engine precant angle had been reduced from 2.3 to 1.3 degrees on this stage. However, the increase was not as large as the predicted value which was based on test data. The effects of CECO on the aft face heating rate was determined from 1/25 scale model data.

Figure 14-5 shows the AS-507 flight and postflight prediction of the incident radiative heat flux to the base heat shield aft face surface. The previous flight data band is also shown for comparison.

Figure 14-6 shows the AS-507 flight and postflight prediction of the base region gas recovery temperature probe history. Also shown is the AS-503 through AS-506 flight data band.

The predicted gas recovery temperature is obtained by analysis using the measured total and radiative heating rates on the base heat shield aft surface and the probe temperature. Note that the flight values are the probe temperature and not the gas recovery temperatures.

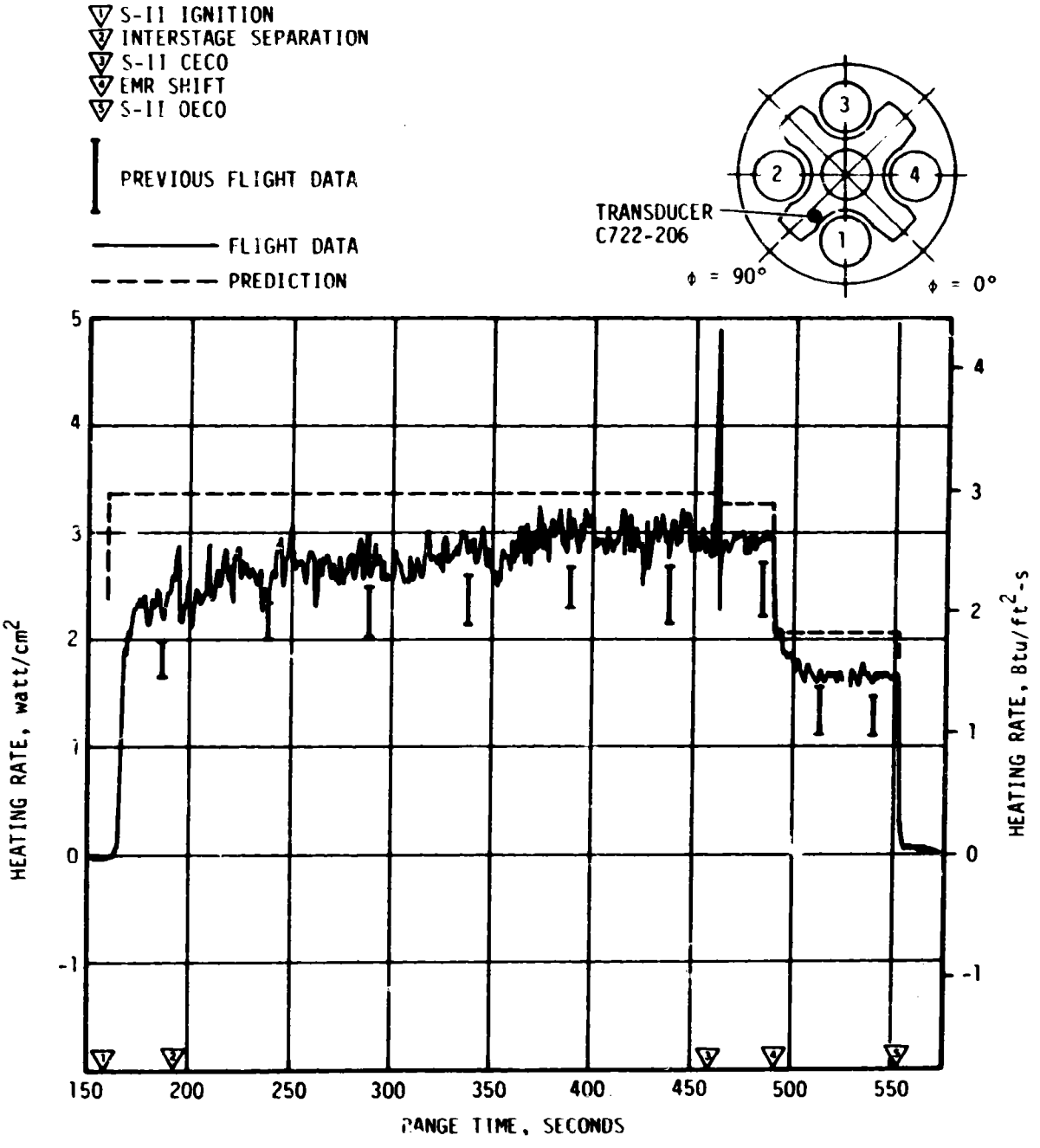

Figure 14-4. Heat Shield Aft Heat Rate

The probe and gas recovery temperatures were approximately 80°F higher than the corresponding AS-506 values prior to CECO. This was expected since the outboard engines are closer to the center engine during S-II boost due to reduced engine precant.

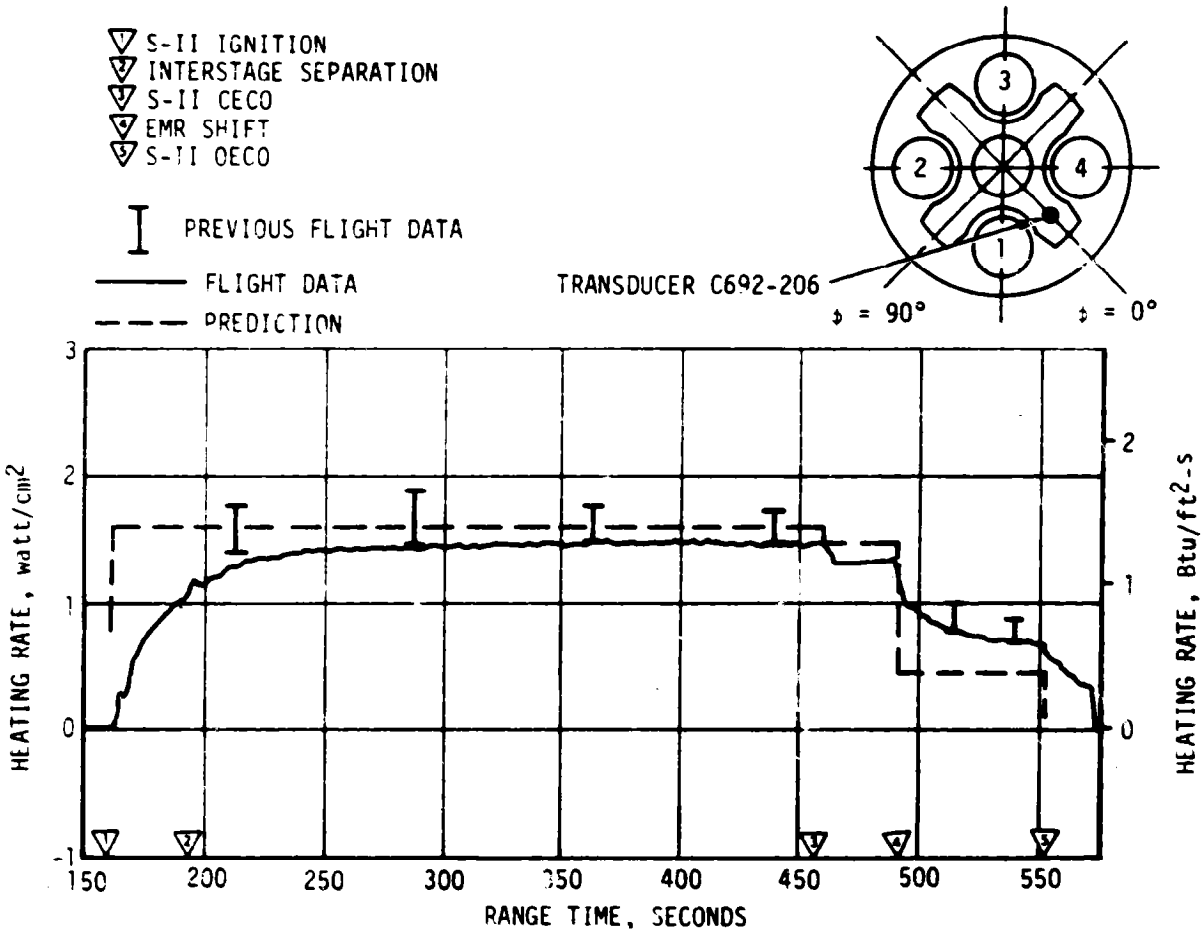

Figure 14-5. Heat Shield Aft Radiation Heat Rate

However, after CECO and EMR shift, the gas recovery temperature was approximately 90°F lower than the corresponding AS-506 value which was contrary to the expected trend. This contrary trend could be accounted for by the higher than normal measured radiation heating rate on AS-506 which analytically yielded a high gas recovery temperature.

There were no structural temperature measurements on the base heat shield and only three thrust cone forward surface temperature measurements for the base region. A maximum postflight predicted temperature was determined for the aft surface of the heat shield using base heating rates predicted for the AS-507 flight. This predicted temperature was 982°F which compared favorably with maximum postflight temperatures predicted for previous flights and was below the maximum design temperature of 1550°F. The maximum measured temperature on the thrust cone by any of the three forward surface temperature measurements was 26°F. The measured temperatures were below design values and in good agreement with postflight predictions.

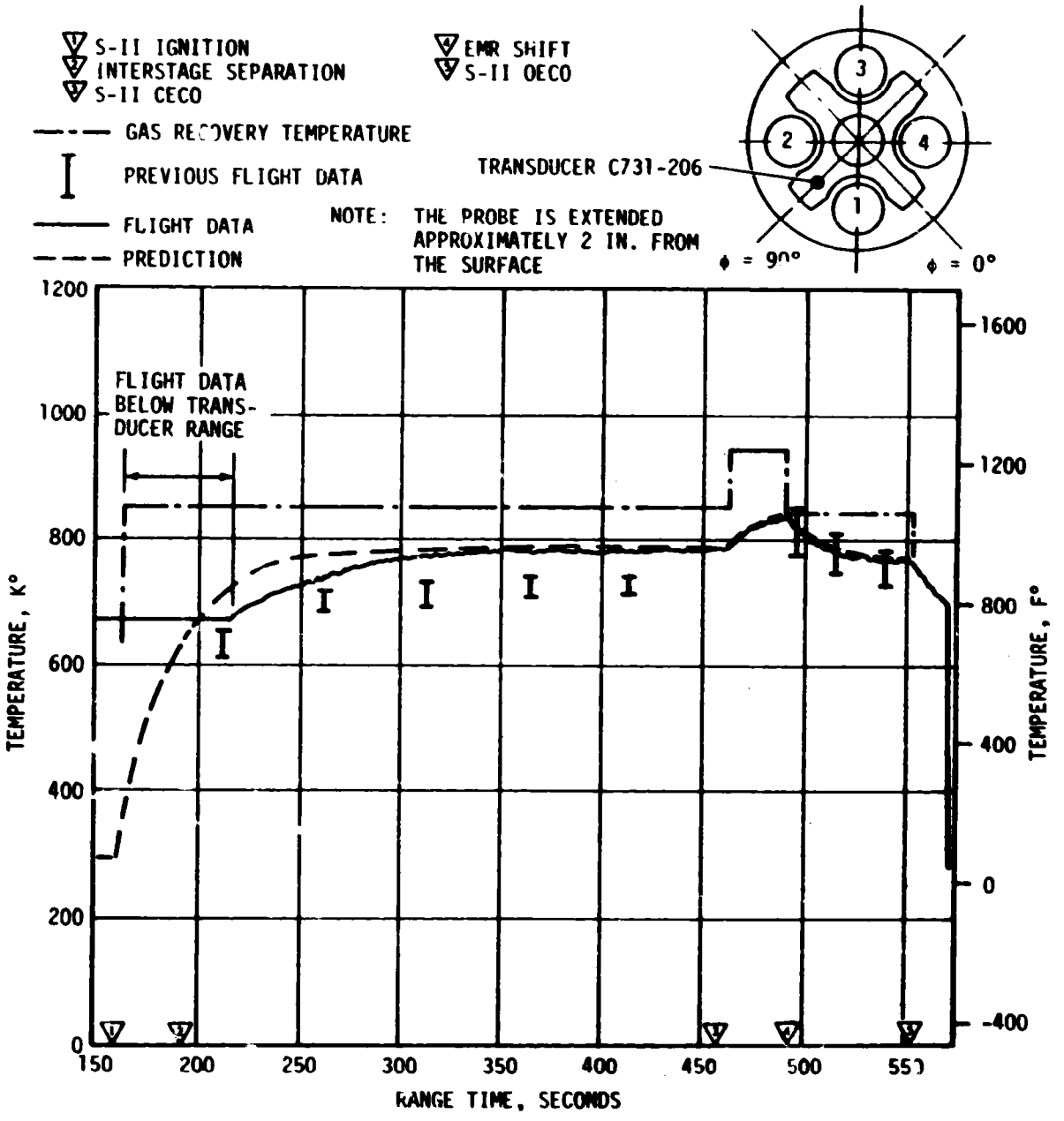

Figure 14-6. Heat Shield Recovery Temperature Probe

14.4 VEHICLE AEROHEATING THERMAL ENVIRONMENT

The aerodynamic heating environments were not measured on the AS-507 vehicle. Flight optical data on flow separation are not available for this flight.

Due to similarity in trajectory data, aerodynamic heating and flow separation heating environments are believed to be similar to that experienced by the AS-506 vehicle.

SECTION 15

ENVIRONMENTAL CONTROL SYSTEMS

15.1 SUMMARY

The S-IC forward compartment ambient temperatures were maintained above the minimum performance limit during the most severe phase of the AS-507 countdown. The aft compartment environmental conditioning system maintained the ambient temperature within design requirements during countdown.

The S-II thermal control and compartment conditioning system apparently performed satisfactorily since the ambients external to the containers were nominal, and there were no problems with the equipment in the containers.

The Instrument Unit (IU) Environmental Control System (ECS) performed satisfactorily for the duration of the IU mission. There was evidence of direct incidence solar heating near panel 20, through the open end of the IU, after spacecraft separation. Components located in this area showed an increase in temperature. However, none of the components cooled by the Thermal Conditioning System (TCS) showed performance degradation through 40,000 seconds of data, and all measurements were still within their operating limits , although solar heating did adversely affect the operation of components of the Command and Communications System (CCS). During this period of solar heating, the gas bearing differential pressure decreased below the expected lower limit because of temperature effects of the Gas Bearing Supply System (GBS) GN_2 pressure regulator. The performance of the ST-124M-3 platform was not affected by this decrease in pressure.

15.2 S-IC ENVIRONMENTAL CONTROL

The most severe forward compartment thermal environment occurs during J-2 engine chilldown. The lowest ambient temperature measured during AS-507 J-2 engine chilldown was -67°F at instrument location C206-120, which was above the minimum performance limit of -90°F. During flight, the lowest temperature measured was -140.8°F at instrument location C206-120.

The aft compartment environmental conditioning system maintained the ambient temperature within the design requirements during countdown. Prior to liftoff, the ambient temperatures ranged between 93.2°F at

measurement C107-115 and 75.2°F at measurement C203-115. During flight, the lowest temperature recorded was 57.2°F at instrument location C203-115.

15.3 S-II ENVIRONMENTAL CONTROL

The Engine Compartment Conditioning System maintained the ambient and thrust cone surface temperatures within design ranges throughout the launch countdown. The system also maintained an inert atmosphere within the compartment as evidenced by absence of H_2 or O_2 indications on the hazardous gas monitor.

There were no thermal control container temperature measurements; however, since the ambients external to the containers were satisfactory and there were no problems with the equipment in the containers, it is assumed that the thermal control systems performed adequately.

15.4 IU ENVIRONMENTAL CONTROL

15.4.1 Thermal Conditioning System

Performance of the Thermal Conditioning System (TCS) was satisfactory throughout the mission. The temperature of the Methanol Water (M/W) coolant was continuously maintained within the required 45 to 68°F temperature band.

Sublimator performance during ascent is shown in Figure 15-1. The water valve was opened at 181.9 seconds allowing water flow to the sublimator. The M/W coolant temperature began to decrease rapidly at about 500 seconds as full cooling from the sublimator was established. The low cooling rate during the first 300 seconds after the water valve opened is typical of a slow-starting sublimator and is not abnormal. At the first thermal switch sampling, the M/W coolant was still above the actuation point, and the water valve remained open. The second thermal switch sampling was at 781.4 seconds, and the water valve was closed.

Sublimator performance is shown in Figure 15-2 over the full time span for which data have been received. The data show normal M/W coolant temperature cycles up through 40,000 seconds of flight.

All component temperatures remained within their expected ranges throughout the primary mission as shown in Figure 15-3. The ST-124M-3 inertial gimbal temperature went below the operational temperature range (104°F) at about 8,600 seconds and leveled off at 103°F, which is close to the value observed on previous flights. The temperature followed almost exactly the curve of AS-505 until the Evasive Attitude Hold maneuver and then began a steady warming trend after 16,620 seconds. There was evidence of direct solar heating near panel 20, through the open end of the IU, after spacecraft separation (paragraph 16.4.4). The temperature of components located on IU panel 20 began increasing at about the same

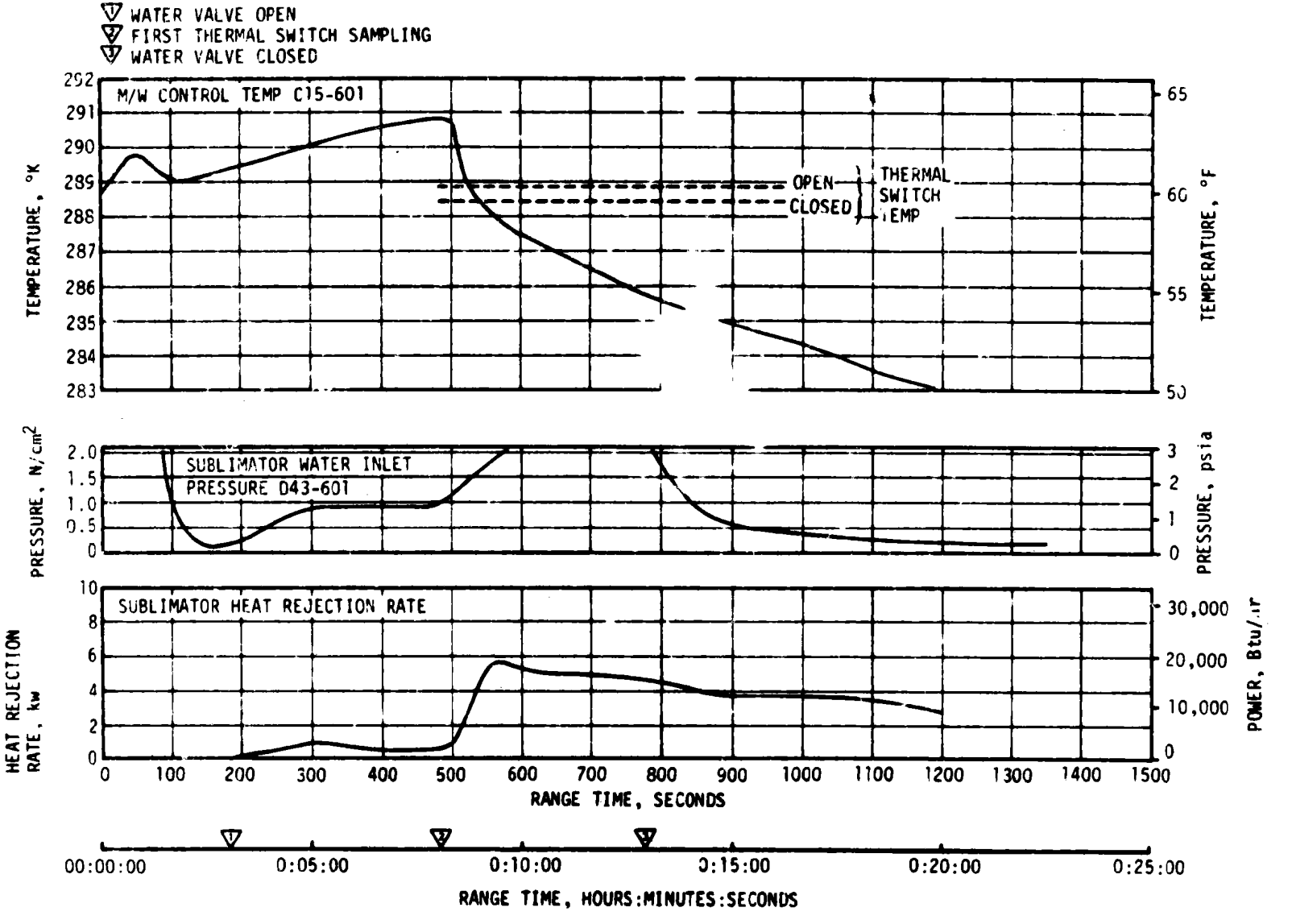

Figure 15-1. Sublimator Performance During Ascent

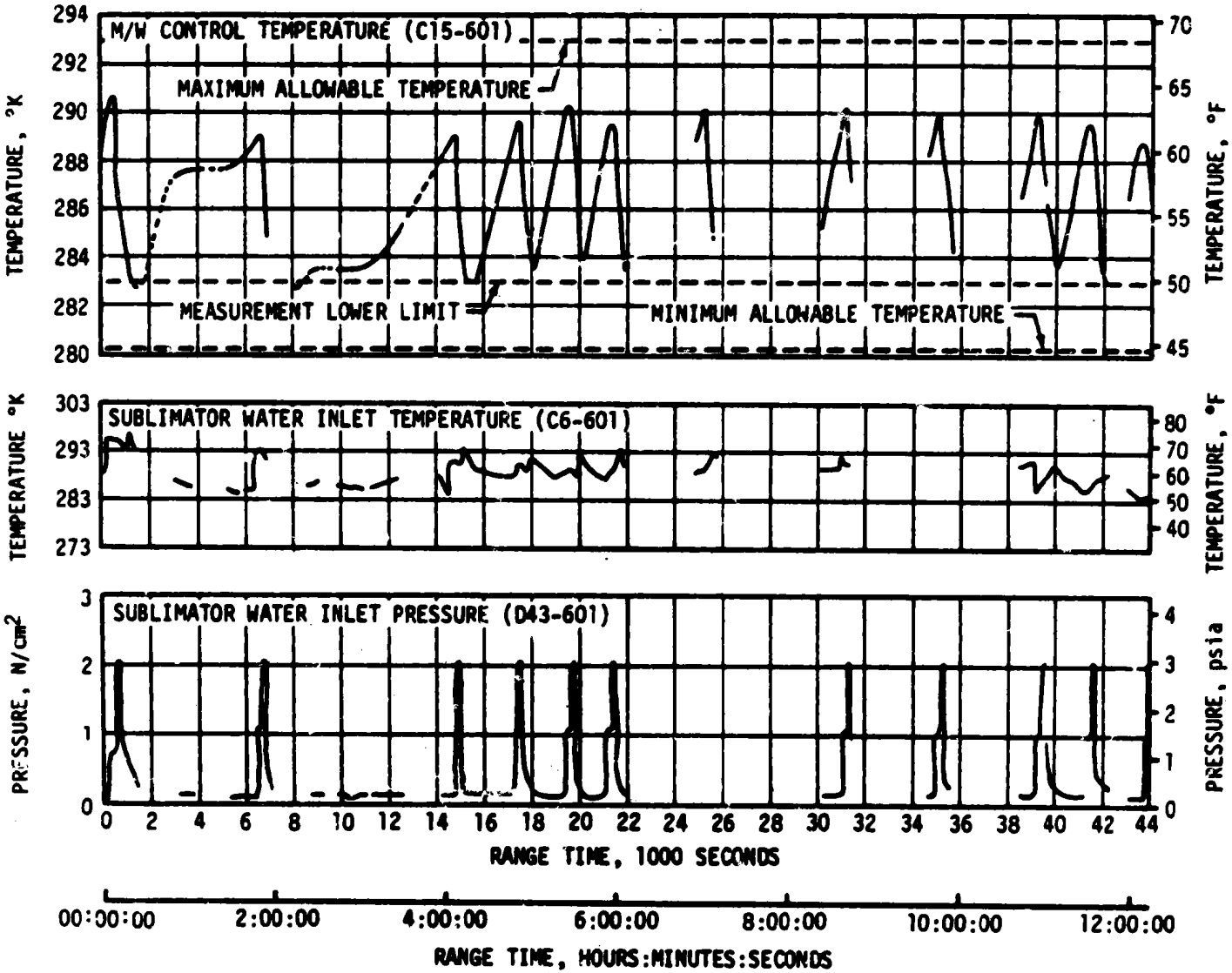

Figure 15-2. TCS Coolant Control Parameters

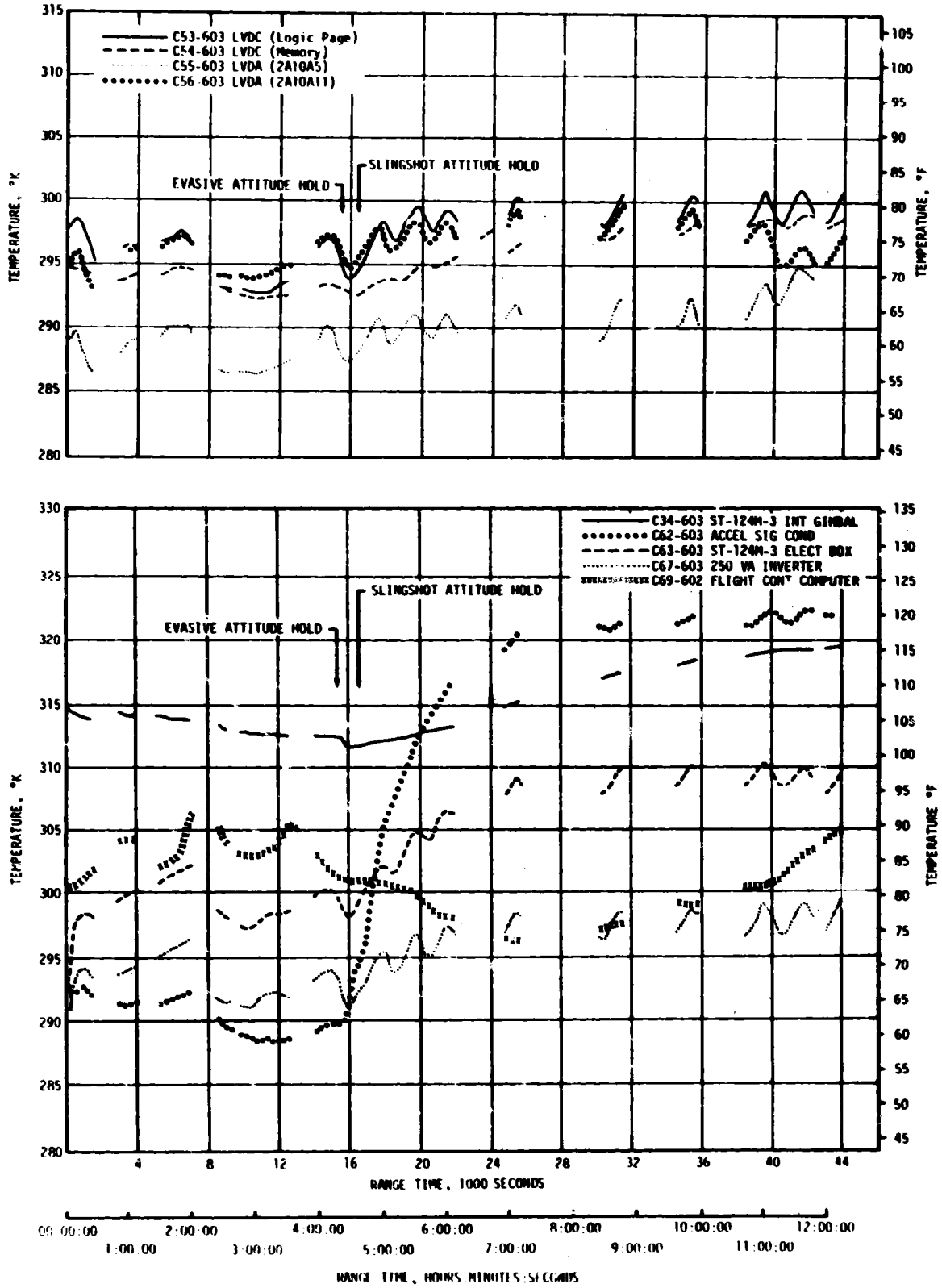

Figure 15-3. Selected Component Temperatures

time as the ST-124M-3 internal temperature. Also, the M/W control temperature and other sublimator parameters indicated an increase in activity, and therefore, an increase in heatload. None of the components cooled by the TCS showed performance degradation as a result of this heat load through 40,000 seconds of data, and all measurements were still within their operating limits. The ST-124M-3 internal gimbal temperature was at its upper operational value of 115°F. Effects of this solar heating on components of the CCS system are discussed in paragraph 16.4.4.

The TCS GN_2 supply sphere pressure decay was within the expected usage rate limits as shown in Figure 15-4. The change in slope from 15,000 to 17,000 seconds was due to the solar heating effects that occurred after spacecraft separation. There were no adverse effects on TCS performance as indicated by normal water accumulator and M/W accumulator pressures.

15.4.2 ST-124M-3 Gas Bearing System

Performance of the GBS was satisfactory throughout the primary mission.

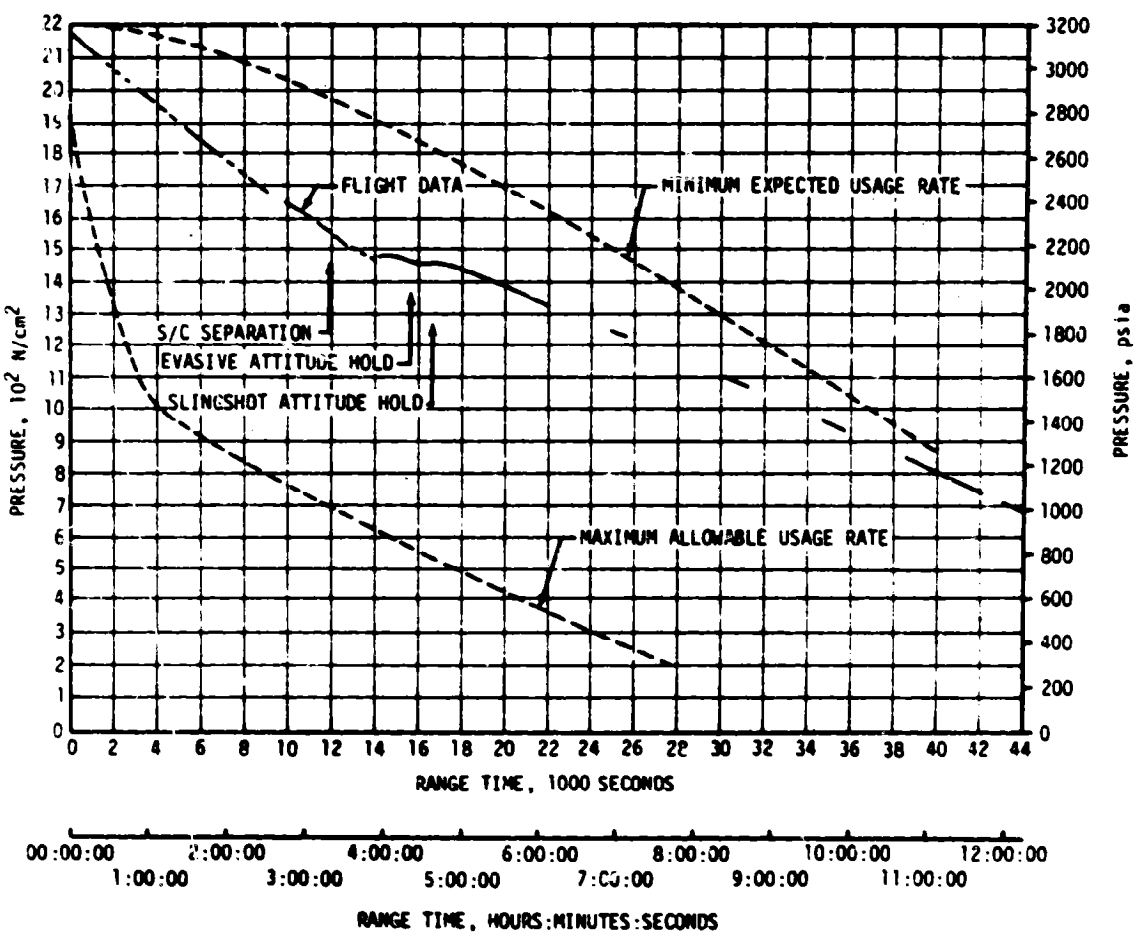

Figure 15-4. TCS GN_2 Sphere Pressure

The GBS GN_2 sphere pressure decay was nominal up to spacecraft separation as shown in Figure 15-5. After spacecraft separation, there was an increase in GBS GN_2 sphere pressure due to solar heating; however, there was no noticeable effect on platform performance.

The ST-124M-3 gas bearing differential pressure is shown in Figure 15-6. The gas bearing differential pressure decreased below the expected lower limit at about 18,400 seconds; however, the performance of the ST-124M-3 platform was not affected by this decrease in pressure. This decrease is attributed to an increase in the gas bearing regulator temperature caused by high incident solar heat rate. Previous component test data have shown that this is the expected performance of the regulator with an increase in component temperature. A modification is being considered on AS-508 to protect IU components from solar radiation through the open end of the IU. This modification consists of a thermal shroud and is discussed in paragraph 16.4.4.

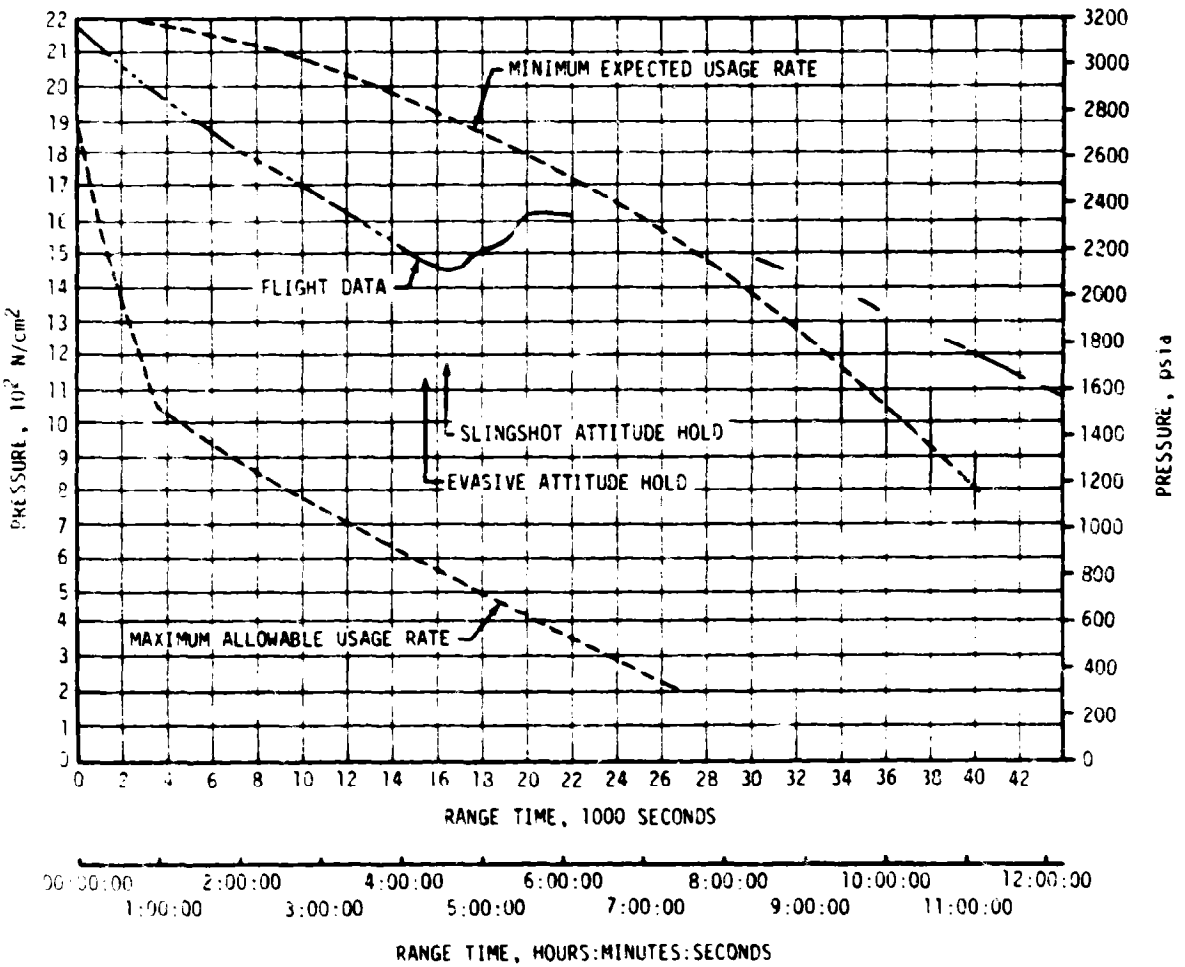

Figure 15-5. GBS GN_2 Sphere Pressure

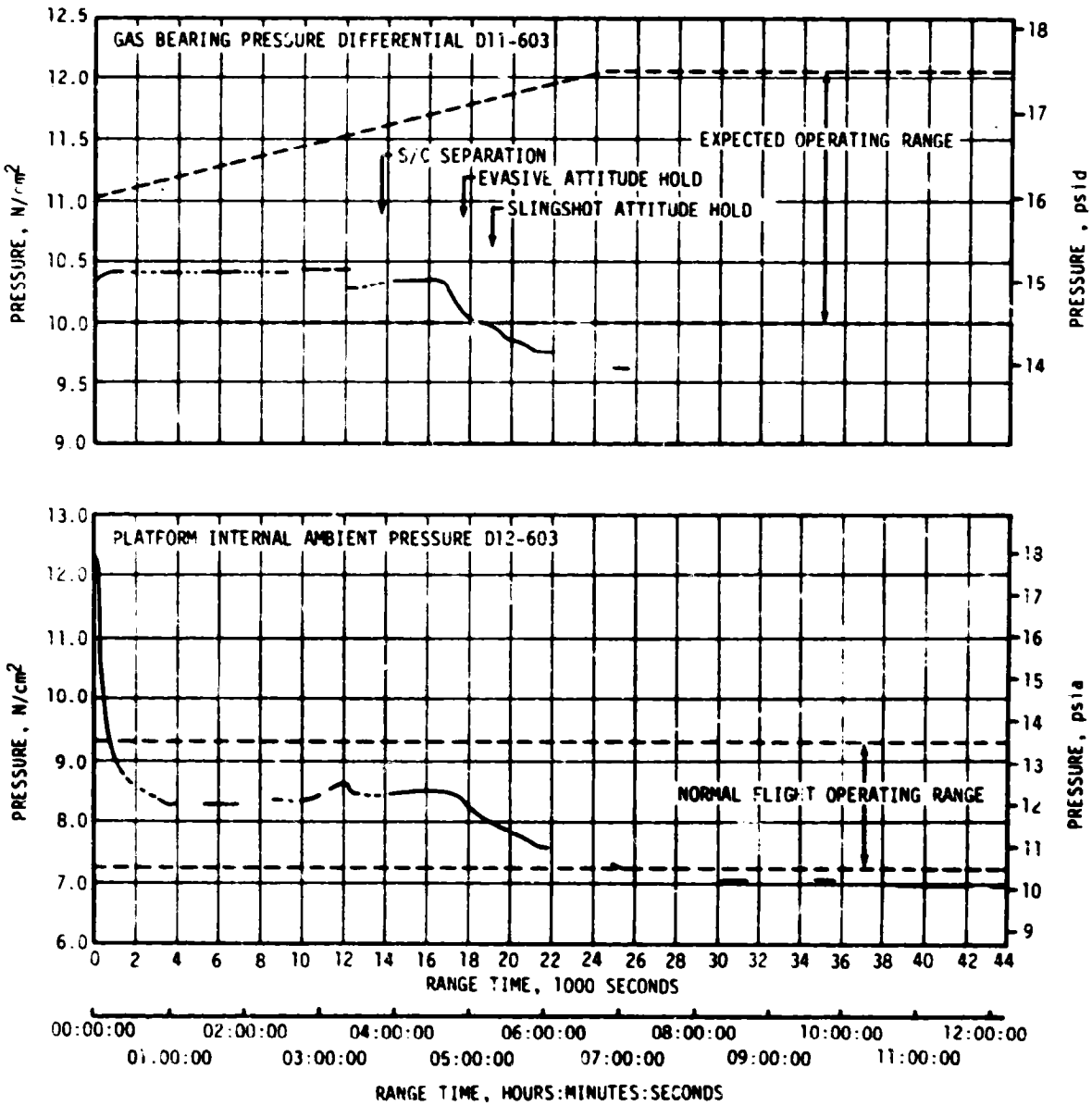

Figure 15-6. Inertial Platform GN_2 Pressures

SECTION 16

DATA SYSTEMS

16.1 SUMMARY

All elements of the data system performed satisfactorily throughout flight except the Command and Communication System (CCS). During translunar coast, the CCS omni downlink antenna system failed, and the CCS uplink signal dropped out sooner than expected.

Measurement performance was excellent, as evidenced by 99.9 percent reliability. This reliability is the same as on AS-506, when the highest reliability for any Saturn V flight was attained.

Telemetry performance was nominal. Very High Frequency (VHF) telemetry Radiofrequency (RF) propagation was generally good, though the usual problems due to flame effects and staging were experienced. Usable VHF data were received to 25,260 seconds (07:01:00). The Secure Range Safety Command Systems (SRSCS) on the S-IC, S-II, and S-IVB stages were ready to perform their functions properly on command if flight conditions during launch phase had required destruct. The system properly safed the S-IVB SRSCS on a command transmitted from Bermuda (BDA). The performance of the Command and Communications System (CCS) in the Instrument Unit (IU) was satisfactory, except for the uplink and downlink problems noted. Usable CCS data were received to 43,980 seconds (12:13:00).

Goldstone Wing Station (GDSX) received CCS signal carrier to 46,070 seconds (12:47:50). Good tracking data were received from the C-Band radar, with Merritt Island Launch Area (MILA) indicating final Loss of Signal (LOS) at 43,560 seconds (12:06:00).

The 71 ground engineering cameras provided good data during launch.

16.2 VEHICLE MEASUREMENT EVALUATION

The AS-507 launch vehicle had 1402 measurements scheduled for flight; five measurements were waived prior to start of the automatic countdown sequence leaving 1397 measurements active for flight. Of the waived measurements, one provided valid data during the flight.

A summary of measurement performance is presented in Table 16-1 for the total vehicle and for each stage. Measurement performance was exceptionally good, as evidenced by 99.9 percent reliability. This reliability is the same as on AS-506, when the highest reliability for any Saturn V flight was attained.

The waived measurements, totally failed measurements, and partially failed measurements are listed by stage in Tables 16-2 and 16-3. None of the listed failures had any significant impact on postflight evaluation.

16.3 AIRBORNE TELEMETRY SYSTEMS

Performance of the nine VHF Telemetry links was generally satisfactory with the minor exceptions noted. A brief performance summary of these links is shown in Table 16-4.

Data degradation and dropouts were experienced at various times during boost as on previous flights due to attenuation of RF transmission at these times, as discussed in paragraph 16.4.1.

Usable VHF telemetry data were received to 25,260 seconds (07:01:00) at Guaymas (GYM).

Performance of the CCS telemetry was generally satisfactory except for the period during translunar coast from 19,105.5 seconds (5:18:25.5) to 25,741.9 seconds (7:09:01.9). This problem is discussed in detail in paragraph 16.4.4. Usable CCS data were received at GDSX to 43,980 seconds (12:13:00).

16.4 RF SYSTEMS EVALUATION

16.4.1 Telemetry System RF Propagation Evaluation

The performance of the nine VHF telemetry links was excellent and generally agreed with predictions. Very high frequency telemetry link CS-1 was added on AS-507.

Moderate to severe signal attenuation was experienced at various times during boost due to main flame effects, S-IC/S-II and S-II/S-IVB staging, S-II ignition, and S-II second plane separation. Magnitude of these effects was comparable to that experienced on previous flights. S-IC main flame effects caused loss of VHF telemetry data on the S-IC and S-II stages. At S-IC/S-II staging, signal strength on all VHF telemetry links and on the CCS downlink dropped to threshold for approximately 1.0 and 12.5 seconds, respectively. Signal degradation due to S-II ignition and S-II flame effects was sufficient to cause loss of VHF telemetry data on the S-IC stage. Command and communication system data were lost during S-II second plane separation. S-II VHF data were lost during S-II/S-IVB separation. In addition, there were intervals during the launch phase

Table 16-1. AS-507 Measurement Summary

MEASUREMENTS CATEGORY	S-IC STAGE	S-II STAGE	S-IVB STAGE	INSTRUMENT UNIT	TOTAL VEHICLE
Scheduled	307	579	289	227	1402
Waived	3	0	2	0	5
Failures	1	0	0	0	1
Partial Failures	5	3	2	0	10
Reliability, Percent	99.7	100.0	100.0	100.0	99.9

Table 16-2. AS-507 Flight Measurements Waived Prior to Launch

MEASUREMENT NUMBER	MEASUREMENT TITLE	NATURE OF FAILURE	REMARKS
	S-IC STAGE		
C006-104	Temperature, Oxidizer Pump Bearing 1	Erratic - Cycled when bearing heaters were cycled	Rocketdyne transducer or cabling problem. KSC Waiver-I-B-507-3 (Open resistive element).
C009-103	Temperature, Engine Gimbal System Return Pitch Actuator	Amplifier driven negative	Open cable at transducer (Integral part of transducer) KSC Waiver-I-B-507-4.
L011-119	Segment Identification Fuel Discrete	Discrete 3 indicated wet at all times	Measurement provided valid data throughout powered flight. KSC Waiver I-B-507-1.
	S-IVB STAGE		
C022-406	Temperature, LOX Tank Diffuser Inlet Helium Gas	Measurement failed off-scale high at approximately -1178 seconds	Probable open transducer.
R0061-401	Miscellaneous Operational Telemetry (KIT) Reflected RF Power	Data were excessively high during the periods when the PCM transmitter was operating	This high reflected power was caused by improper isolation from PCM transmitter.

Table 16-3. AS-507 Measurement Malfunctions

MEASUREMENT NUMBER	MEASUREMENT TITLE	NATURE OF FAILURE	TIME OF FAILURE (RANGE TIME)	DURATION SATISFACTORY OPERATION	REMARKS
TOTAL MEASUREMENT FAILURES, S-IC STAGE					
D016-306	Pressure Differential, Heat Shield	Measurement pegged positive at 37 seconds	0 seconds	0 seconds	Possibly cap not removed from one port or sensor clogged
PARTIAL MEASUREMENT FAILURES, S-IC STAGE					
A001-118	Acceleration, Longitudinal	Positive transient of 3.5 Gpeak from -2 to 12 seconds.	-2 seconds	150 seconds	Installation problem
D004-304	Pressure, Fuel Pump Inlet 1	Very noisy - 30 percent double amplitude noise	0 seconds	Data usable entire flight	Transducer or connector problem
K037-115	Thrust OK Pressure Switch 2, Engine No. 2	Indicated OFF at 43.9, 61.2 and 77.7 seconds.	43.9, 61.2 and 77.7 seconds	Remainder of flight	
K062-118	Helium Flow Control Valve 4	Indicated erroneous CLOSE/OPEN at 140.9 seconds	140.9 seconds	Remainder of flight	
L002-119	LOX Level Position 11 Sensor Segment	Erratic counting between 4.39 and 3.809 seconds	-4.39 to 3.809 seconds	158 seconds	
PARTIAL MEASUREMENT FAILURES, S-II STAGE					
C001-203	Fuel Pump Discharge Temperature	Intermittent Transducer output	170 to 305 seconds	0 to 170 seconds and 305 seconds to end of S-II OECO	Data were saturated between 170 and 305 seconds.
C011-207	Fuel Turbine Inlet Temperature	Transducer Failure	300 seconds	300 seconds	Data usable in area of interest
C029-206	O_2 Pressure Regulator Outlet Temperature	Transducer Failure at Step Pressure	260 seconds	260 seconds	Partial data
PARTIAL MEASUREMENT FAILURES, S-IVB STAGE					
D021-415	Pressure - Ullage Control Chamber 2-4	Unbalance in DC amplifier	400 seconds	400 seconds	Slow upward drift of data from 400 seconds to end of data
D0104-403	Pressure - LH_2 Pressure Module Inlet	Cold-soak affect on transducer	During S-IVB second burn	Before and after S-IVB second burn	Gradual decrease of data during S-IVB second burn was invalid because of cold-soak affects on the transducer.

Table 16-4. AS-507 Launch Vehicle Telemetry Links

LINK	FREQUENCY (MHz)	MODULATION	STAGE	FLIGHT PERIOD (RANGE TIME, SEC)	PERFORMANCE SUMMARY
AF-1 AP-1	256.2 244.3	FM/FM PCM/FM	S-IC S-IC	422 422	Satisfactory Data Dropouts Range Time (sec) — Duration (sec) 136.7 — 2.1 162.8 — 1.0 166.0 — 1.3
BF-1 BF-2 BP-1	241.5 234.0 248.6	FM/FM FM/FM PCM/FM	S-II S-II S-II	772 772 772	Satisfactory Data Dropouts Range Time (sec) — Duration (sec) 131.4 — 6.0 162.6 — 1.0 553.2 — 3.7
CP-1 CS-1	258.5 253.8	PCM/FM SS/FM	S-IVB S-IVB	Flight Duration 724	Satisfactory Data Dropouts Range Time (sec) — Duration (sec) 162.6 — 1.0
DF-1 DP-1 DP-1B	250.7 245.3 2282.5	FM/FM PCM/FM PCM/FM	IU IU IU	Flight Duration Flight Duration 43,980	Satisfactory Data Dropouts Range Time (sec) — Duration (sec) 162.5 (VHF) — 1.0 162.0 — 12.5 193.5 — 2.0 19,105.5 — See 16.4.4 21,237.3 — See 16.4.4 (DP-1B only) 22,066.4 — See 16.4.4 (DP-1B only) 23,389.7 — See 16.4.4 (DP-1B only) 25,546.4 — See 16.4.4 (DP-1B only) 25,687.4 — See 16.4.4 (DP-1B only)

where some data were so degraded as to be unusable. Loss of these data, however, posed no problem since losses were of such short duration as to have little or no impact on flight analysis.

The performance of the S-IVB and IU telemetry systems was nominal during orbit, second burn, and final coast, except for the CCS problem discussed in paragraph 16.4.4.

Guaymas reported VHF LOS at 25,260 seconds (07:01:00), and GDSX reported CCS LOS at 46,070 seconds (12:47:50).

A summary of available VHF telemetry coverage showing Acquisition of Signal (AOS) and LOS for each station is shown in Figure 16-1.

16.4.2 Tracking Systems RF Propagation Evaluation

The C-Band radar operated satisfactorily during this flight, although several ground stations experienced some of the usual tracking problems.

The Cape Kennedy (CNV), MILA, Patrick Air Force Base (PAFB), and Grand Turk Island (GTK) stations experienced problems during launch caused by balance point shifts (erroneous pointing information caused by a sudden antenna null or a distorted beacon return). Similar problems have been experienced during previous flights. The ground stations momentarily switched to skin track when this problem was observed.

Cape Kennedy, MILA, and PAFB also experienced some dropouts during launch due to the adverse weather conditions. The only problems experienced during the second revolution occurred at the two BDA radar sites. The vehicle passed directly over the stations, and the resulting high azimuth rates at the maximum elevation angle (exceeded azimuth tracking rate capabilities of antennas) resulted in a 26-second dropout.

The MILA TPQ-18 and BDA FPQ-6 radars tracked the vehicle during the trans-lunar coast period. Bermuda reported two dropouts caused by low signal strength. This low signal strength was a result of the large slant range to the vehicle. Merritt Island launch area indicated final LOS at 43,560 seconds (12:06:00).

A summary of available C-Band radar coverage showing AOS and LOS for each station is shown in Figure 16-2.

There is no mandatory tracking requirement of the CCS; however, the CCS transponder has turnaround ranging capabilities and provided a backup to the Command and Service Module (CSM) transponder used for tracking in case of failure or desire for a cross check. Since the same transponder is used for all CCS functions, discussion of the tracking performance of this system is included in the general discussion of the CCS RF evaluation.

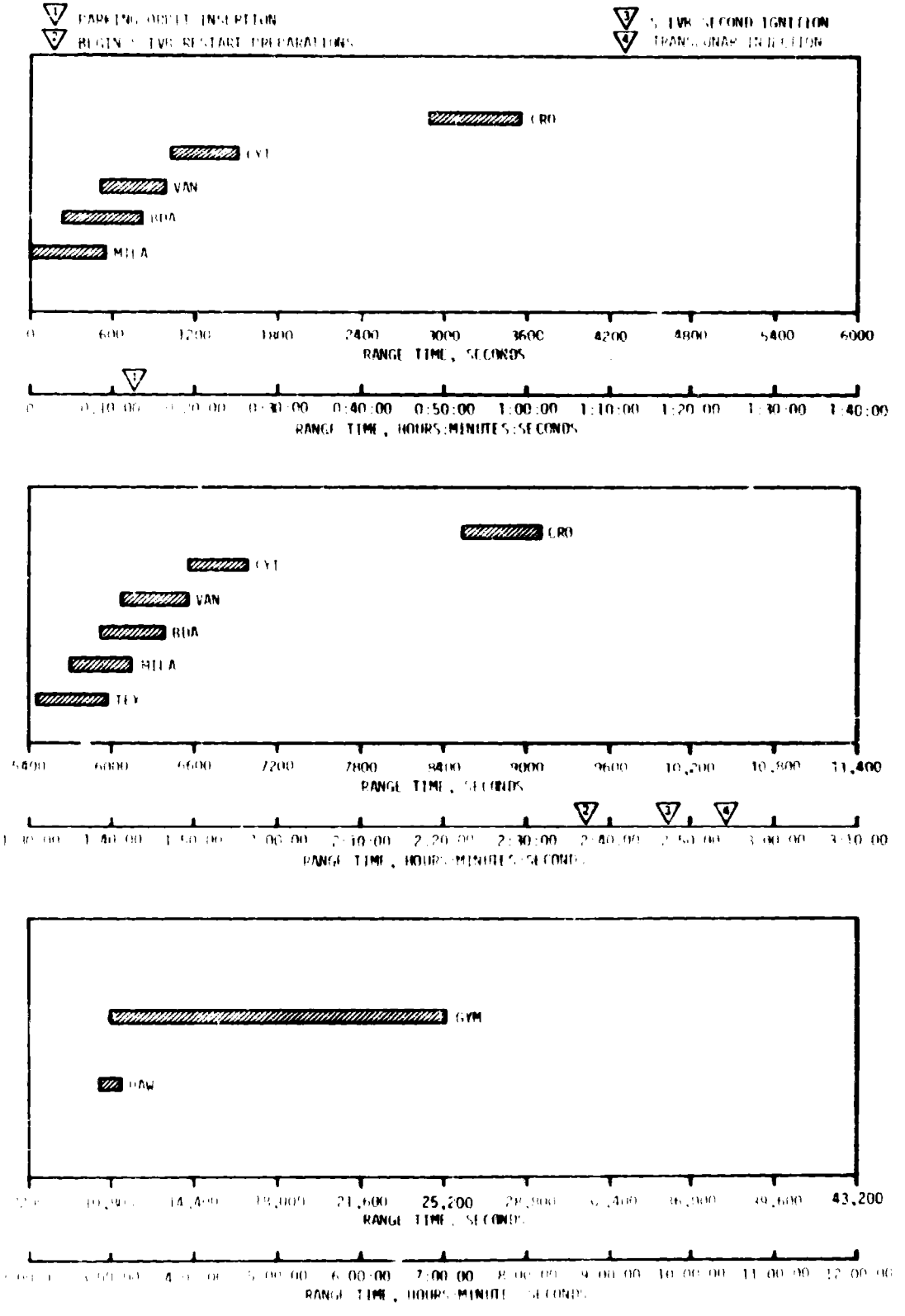

Figure 16-1. VHF Telemetry Coverage Summary

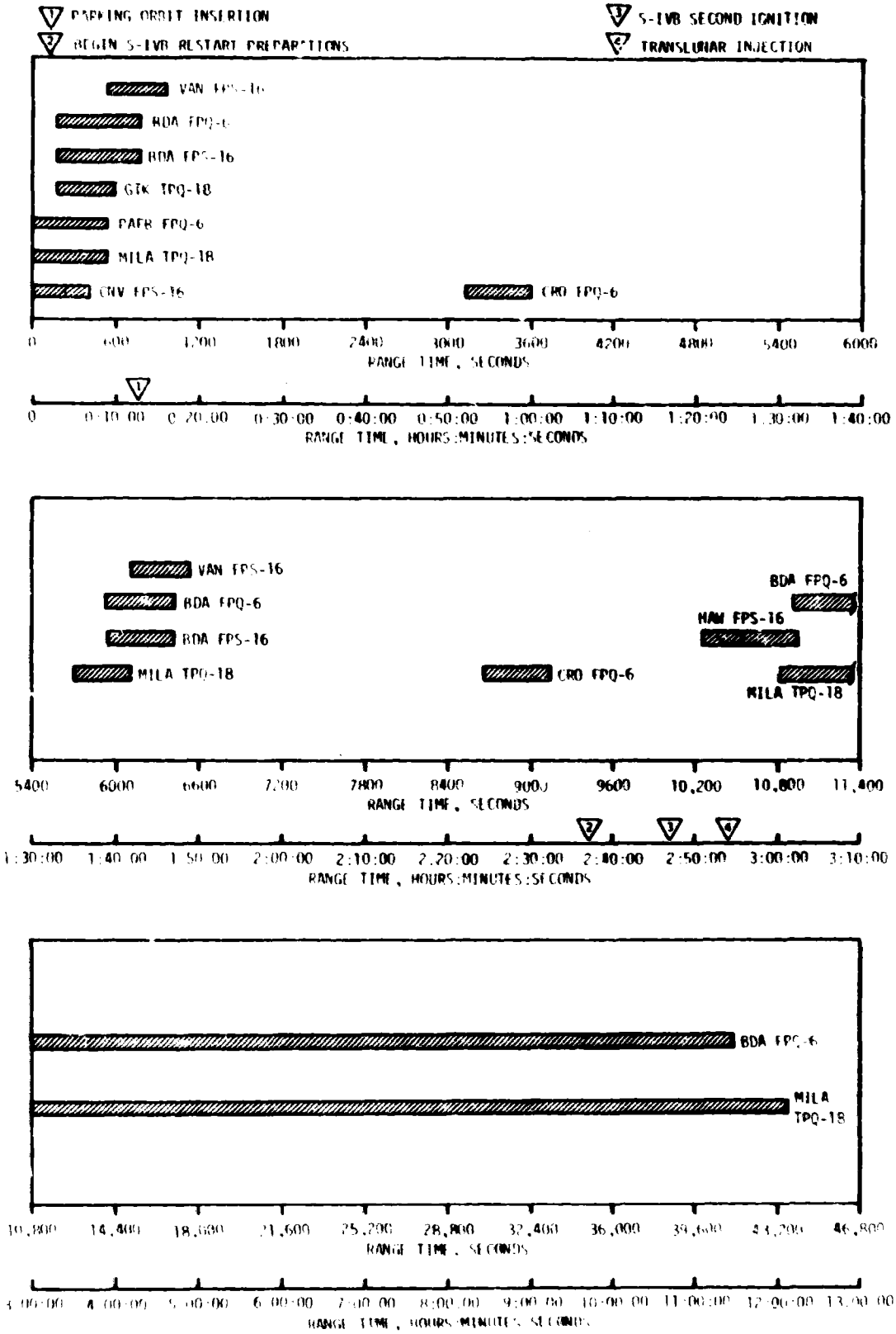

Figure 16-2. C-Band Radar Coverage Summary

16.4.3 Secure Range Safety Command Systems Evaluation

Telemetered data indicated that the command antennas, receivers/decoders, Exploding Bridge Wire (EBW) networks, and destruct controllers on each powered stage functioned properly during flight and were in the required state of readiness if flight conditions during the launch had required vehicle destruct. Since no arm/cutoff or destruct commands were required, all data except receiver signal strength remained unchanged during the flight. At approximately 120 seconds, a momentary dropout occurred on the receiver signal strength measurements, when the command station switched transmitting antennas. Power to the system was cut off at 708.2 seconds by ground command from BDA, thereby deactivating (safing) the system. Both S-IVB stage systems, the only systems in operation at this time, responded properly to the safing command.

16.4.4 Command and Communication System Evaluation

The command section of the CCS operated satisfactorily. Twenty-four commands were initiated by Mission Control Center-Houston (MCC-H) for transmission via three different ground stations, as shown in Table 16-5. The 24 commands consisted of 72 words. Of the 24 commands, 21 were accepted by the onboard equipment. Transmission of the three commands not received by the CCS occurred when the command subcarrier (70 kHz) or both the command subcarrier and the uplink carrier were out of lock.

The RF portion of the CCS performed satisfactorily during boost and parking orbit with minor exceptions. Downlink dropouts occurred during S-IC/S-II staging and at S-II second plane separation, as on previous flights. Station handovers were accomplished with very little data loss. Performance during second burn and during Translunar Injection (TLI) was nominal.

During translunar coast, the CCS RF performance was satisfactory until 19,105.5 seconds (5:18:25.5) when a downlink dropout occurred while operating on the omni antenna. Subsequent to this, the CCS downlink antennas were switched by ground command 16 times per planned tests. Each time the omni antenna was selected, there was a CCS downlink dropout as shown in Figure 16-3. The CCS downlink performance was nominal while on the low-gain and high-gain antennas. The loss of uplink signal to the CCS at 26,827 seconds (7:27:07) prevented any further commanding of the LVDC/LVDA via the command section of the CCS. Final CCS downlink LOS occurred at 46,070 seconds (12:47:50) as a result of battery depletion, while on low-gain antenna.

The above noted uplink and downlink problems may have been caused by the overheating of the CCS omni antenna coaxial cables. AS-507 data indicate there was an unusual temperature increase in the area of the omni antenna coaxial cables. Films taken by the astronauts and sur angle calculations indicate that the sun was shining into the open end of the IU after CSM/LM final separation. This temperature increase is shown in Figure 15-3 and

Table 16-5. Command and Communication System Commands History, AS-507

[illegible]	[illegible]	[illegible]	[illegible]	[illegible]	[illegible]
[illegible]	[illegible]	[illegible]	Set Unified S-Band Control Selector Switch	[illegible]	Accepted
[illegible]	[illegible]	[illegible]	Execute Maneuver	1	Accepted
[illegible]	[illegible]	[illegible]	Initiate Tape Recorder	1	Accepted
[illegible]	[illegible]	[illegible]	Set Antenna Low Gain	1*	Accepted
[illegible]	[illegible]	[illegible]	Ullage Engines ON	4	Accepted
[illegible]	[illegible]	[illegible]	Ullage Engines OFF	4	Accepted
[illegible]	[illegible]	[illegible]	Set Antenna High Gain	1	Accepted
[illegible]	[illegible]	[illegible]	Set Antenna Omni Directional	1	Accepted
[illegible]	[illegible]	[illegible]	Set Antenna Low Gain	3*	Accepted
[illegible]	[illegible]	[illegible]	Set Antenna High Gain	1	Accepted
[illegible]	[illegible]	[illegible]	Set Antenna Omni Directional	1	Accepted
[illegible]	[illegible]	[illegible]	Set Antenna Low Gain	2*	Accepted
[illegible]	[illegible]	[illegible]	Set Antenna High Gain	1	Not Received**
[illegible]	[illegible]	[illegible]	Set Antenna High Gain	1	Accepted
[illegible]	[illegible]	[illegible]	Set Antenna Omni Directional	1*	Accepted
[illegible]	[illegible]	[illegible]	Set Antenna Low Gain	1*	Accepted
[illegible]	[illegible]	[illegible]	Set Antenna High Gain	1	Accepted
[illegible]	[illegible]	[illegible]	Set Antenna Omni-Directional	1	Not Received ***
[illegible]	[illegible]	[illegible]	Set Antenna Omni-Directional	1*	Accepted
[illegible]	[illegible]	[illegible]	Set Antenna Low Gain	1*	Accepted
[illegible]	[illegible]	[illegible]	Set Antenna High Gain	1	Accepted
[illegible]	[illegible]	[illegible]	Set Antenna Omni-Directional	1	Accepted
[illegible]	[illegible]	[illegible]	Set Antenna Low Gain	1*	Accepted
[illegible]	[illegible]	[illegible]	Set Antenna High Gain	1	Not Received**

*One word is normally required to switch antennas. These commands were repeated because Address Verification Pulses (AVP's) and Computer Reset Pulses (CRP's) were not received due to telemetry dropouts.

**Command was not received because the uplink carrier was out of lock. The uplink carrier was out of lock because of low signal strength level at the input to the CSS receiver.

***Command was not received because the command subcarrier was out of lock. The command subcarrier was out of lock because of low signal strength level at the input to the CSS receiver.

the locations of the measurements with the most significant temperature increases are shown in Figure 16-4. All measurements in Figure 15-3 are moderated by Environmental Control System (ECS) conditioning. Calculated stabilization temperature for foamflex cable is approximately 375°F; calculated stabilization temperature for RG-214 cable is approximately 115°F. Neither cable is thermally protected, and will thus stabilize at these temperatures under direct sunlight impingement.

Thermal/vacuum tests on the omni antenna coaxial cables (Foamflex and RG-214) indicate that the AS-507 CCS problems may have been caused by solar heating of the coaxial cables. Heating tests of coaxial cables to approximately 263°F, minimum, caused the foamflex cable dielectric to soften, allowing the cable inner conductor to drift toward and finally short out on the outer conductor, and duplicate the flight failure mode. An artist reproduction of an X-ray showing a typical foamflex cable after a heating test is presented in Figure 16-5. The results of the coaxial cable tests are summarized in Table 16-6.

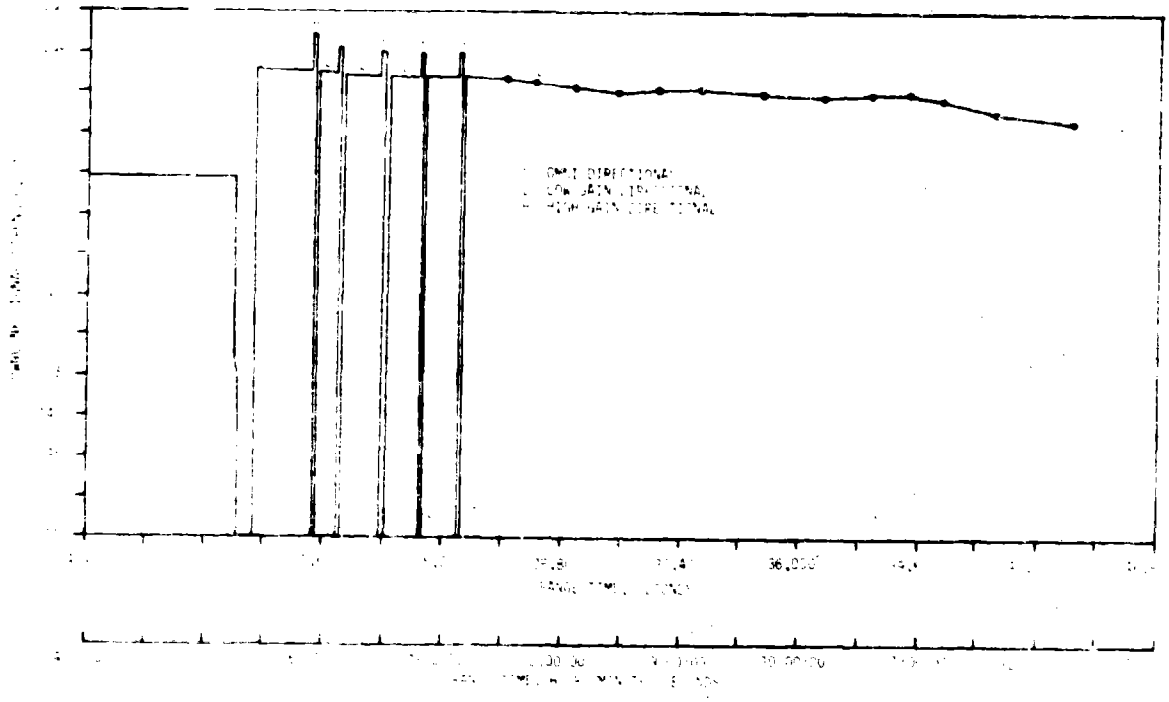

Figure 16-3. CCS Signal Strength at Goldstone Wing Station

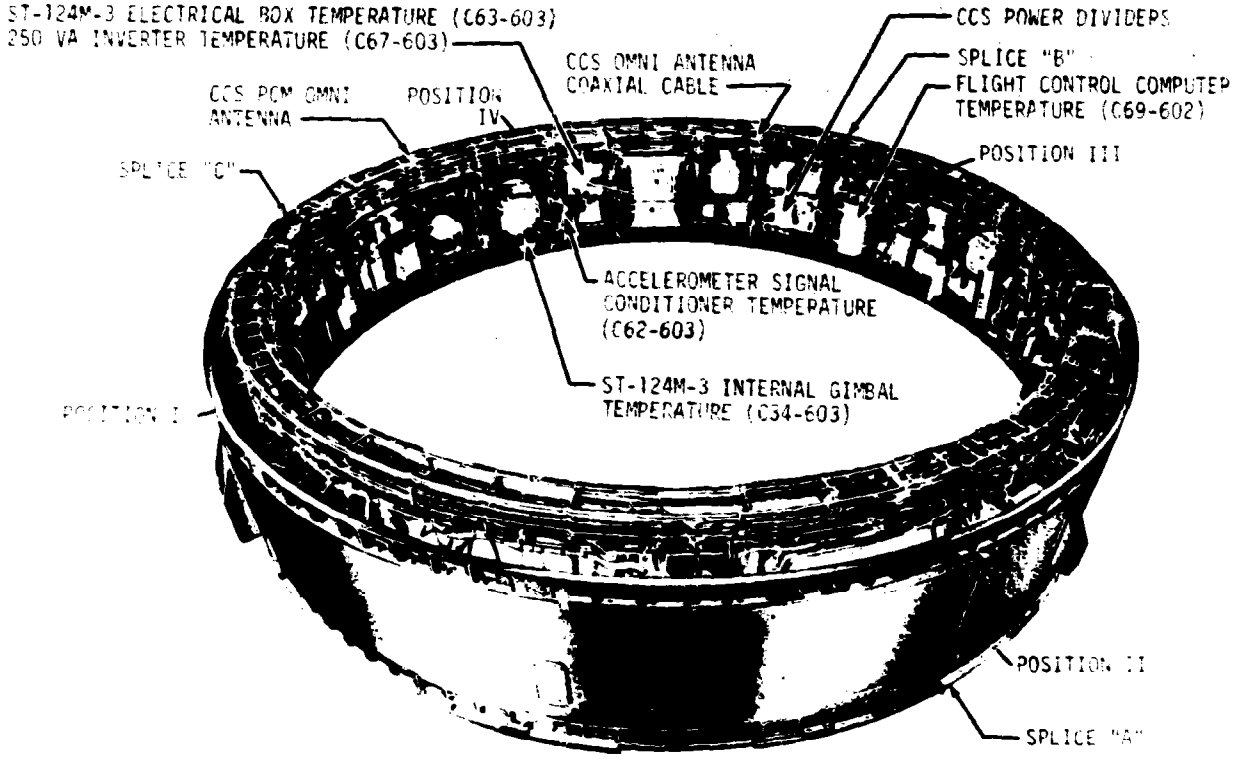

Figure 16-4. Instrument Unit

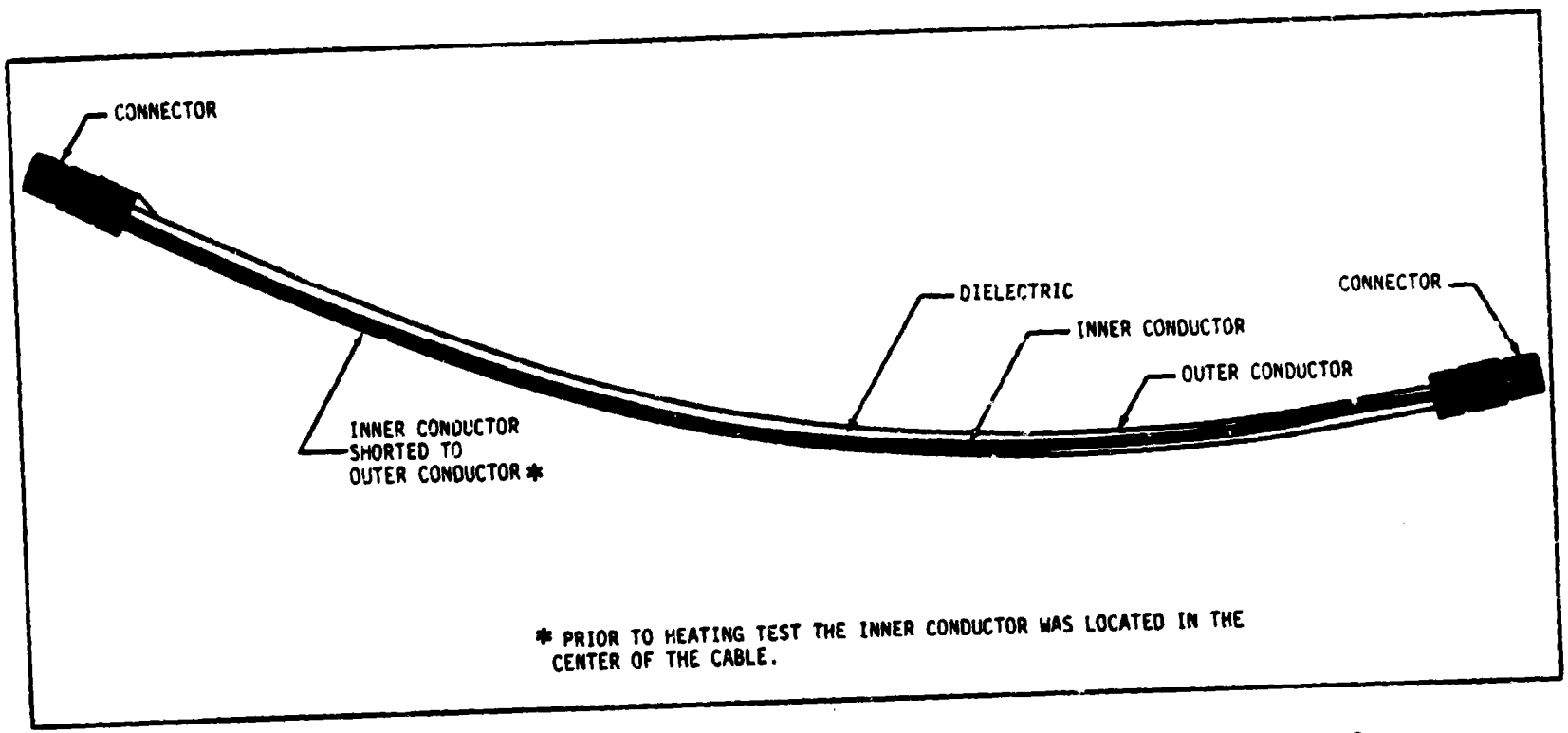

Figure 16-5. Artist Reproduction of X-Ray of a Typical Foamflex Cable After Heating Test

Table 16-6. Instrument Unit Coaxial Cable Test Summary

TEST	CABLE TYPE	LENGTH	BEND RADIUS	VSWR		FAILURE TEMP	INPUT HEAT
				BEFORE	AFTER		
*** 1	RG214/U Foamflex	40 in. 63.5 in.	5.56 in. 13.5 in.	- 1.26:1	1.75:1 Shorted	195°F 263°F	4.74 watts/ft 1.87 watts/ft
2	Foamflex	28 in.	11 ft	1.08:1	7.3:1	402°F	12.21 watts/ft*
3	RG214/U	37 in.	5.56 in.	1.1:1	Shorted	395°F	20.11 watts/ft**

* Slight recovery following rapid cooling
** PVC jacket expanded due to heat input
*** Foamflex failed. Test setup prohibited further test of RG-214.

An investigation is being conducted to determine if the AS-505 and AS-506 CCS problems can be attributed to the overheating of the coaxial cable, rather than the previously suspected leak in the coaxial switch (AS-507 had a new design coaxial switch). However, evidence of an overheated coaxial cable is purely circumstantial.

On AS-503, ECP 2319 will provide thermal shrouds to protect all IU components, including the affected coaxial cables, from direct solar heating. These shrouds will be made from "Kapton" sheeting with aluminum deposited on the side next to the components. This material will be reinforced with a glass cloth backing.

The addition of thermal shrouds should prevent any overheating caused by solar radiation. Therefore, a reoccurrence of a CCS malfunction on AS-508 would indicate that the cause is not thermal in nature.

A summary of CCS coverage showing AOS and LOS for each station is shown in Figure 16-6.

16.5 OPTICAL INSTRUMENTATION

In general, ground camera coverage was good. Seventy-one items were received from KSC and evaluated. Five cameras had bad timing, six cameras jammed or had no runs, and four cameras were extremely underexposed. As a result of these 15 failures, system efficiency was 79 percent. No tracking items were included in the 71 items or included in determining system efficiency since none were acquired because of low cloud coverage.

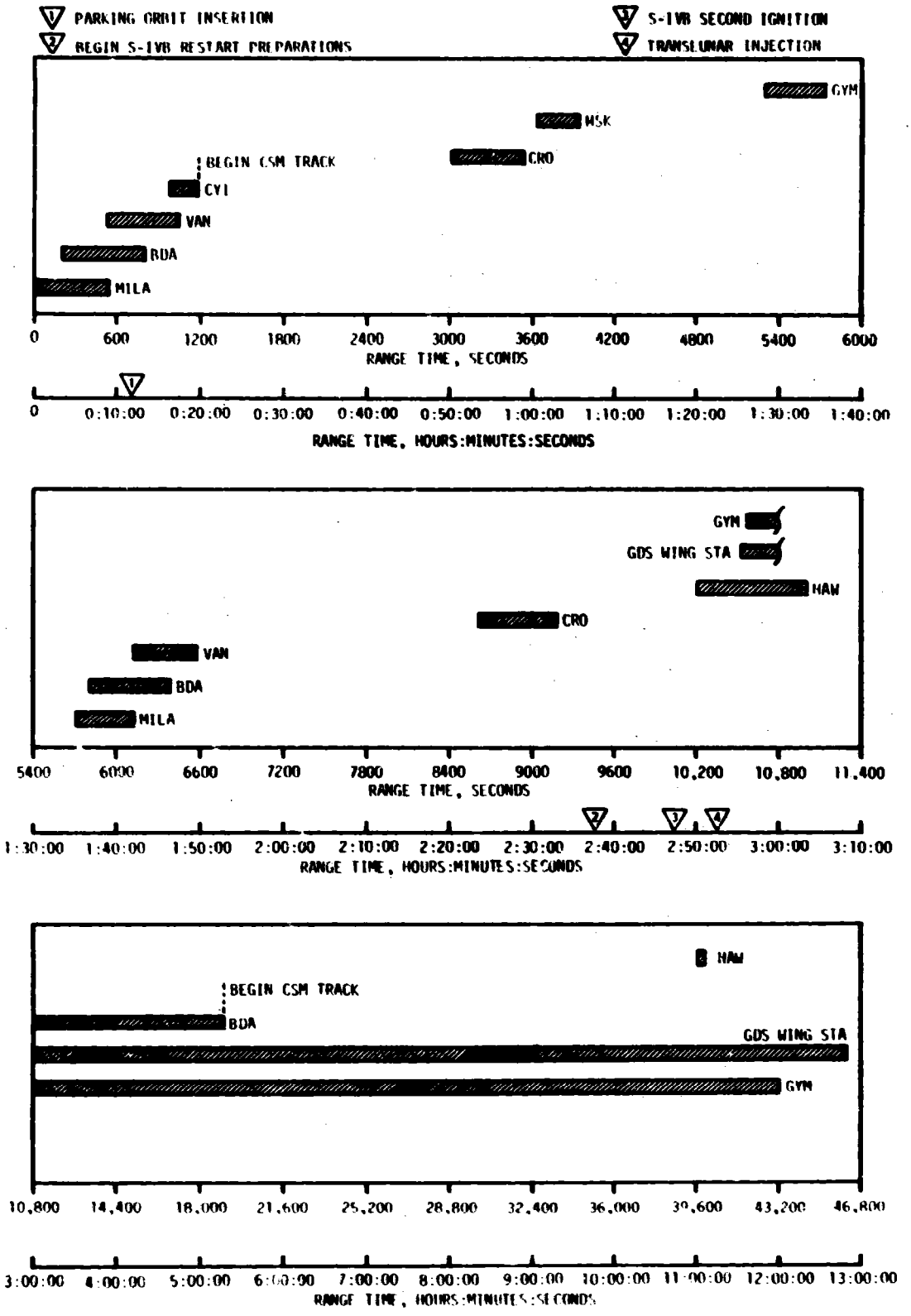

Figure 16-6. CCS Coverage Summary

SECTION 17

MASS CHARACTERISTICS

17.1 SUMMARY

Total vehicle mass determined from postflight analysis was within 0.80 percent of the prediction from ground ignition through S-IVB stage final shutdown. The small variations indicate that hardware weights, propellant loads and propellant utilization during powered flight were close to predicted.

17.2 MASS EVALUATION

Postflight mass characteristics are compared with final predicted mass characteristics (MSFC Memorandum S&E-ASTN-SAE-69-85) and the final operational trajectory (MSFC Memorandum S&E-AERO-FMT-188-69).

The postflight mass characteristics were determined from an analysis of all available actual and reconstructed data from S-IC stage ignition through S-IVB stage second burn cutoff. Dry weights of the launch vehicle are based on actual stage weighings and evaluation of the weight and balance log books (MSFC Form 998). Propellant loading and utilization was evaluated from propulsion system performance reconstructions. Spacecraft data were obtained from the Manned Spacecraft Center (MSC).

Deviations in dry weights of the inert stages and the loaded spacecraft were all within 0.40 percent of predicted, which was well within acceptable limits.

During S-IC powered flight, mass of the total vehicle was determined to be 3122 lbm or 0.05 percent higher than predicted at ignition, and 13,722 lbm or 0.76 percent higher at S-IC/S-II separation. These deviations are attributed to the mass of the upper stages and the S-IC stage propellant residuals at separation being greater than predicted. S-IC burn phase total vehicle mass is shown in Tables 17-1 and 17-2.

During S-II burn phase, the total vehicle mass varied from 6020 lbm or 0.41 percent higher than predicted at ignition to 2026 lbm or 0.43 percent higher at S-II/S-IVB separation. These deviations are due primarily to a greater than predicted S-II stage LOX load and a slight excess of upper stage mass. Total vehicle mass for the S-II burn phase is shown in Tables 17-3 and 17-4.

Total vehicle mass during both S-IVB burn phases, as shown in Tables 17-5 through 17-8, was within 0.53 percent of the prediction. A deviation of 1396 lbm (0.38 percent) from predicted at first burn ignition was due mainly to a heavier S-IVB propellant load and a larger spacecraft mass. The deviation at completion of second burn was 742 lbm (0.53 percent). Total vehicle mass at spacecraft separation was 601 lbm or 1.61 percent higher than predicted.

A summary of mass utilization and loss, actual and predicted, from S-IC stage ignition through completion of S-IVB second burn is presented in Table 17-9. A comparison of actual and predicted mass, center of gravity, and moment of inertia is shown in Table 17-10.

Table 17-1. Total Vehicle Mass - S-IC Burn Phase - Kilograms

EVENTS	GROUND IGNITION		HOLDDOWN ARM RELEASE		CENTER ENGINE CUTOFF		OUTBOARD ENGINE CUTOFF		S-IC/S-II SEPARATION	
	PRED	ACT	PRED	ACT	PRED	ACT	PRED	ACT	PRED	ACT
RANGE TIME--SEC	-6.50	-6.50	.25	.25	135.27	135.24	162.48	161.74	163.20	162.40
S-IC STAGE DRY	130567.	130588.	130567.	130589.	130567.	130588.	130567.	130588.	130567.	130589.
LOX IN TANK	1479759.	1480369.	1448732.	1448519.	198830.	194994.	958.	1261.	998.	998.
LOX BELOW TANK	21000.	21112.	21737.	21872.	21720.	21794.	16895.	17832.	14836.	16035.
LOX ULLAGE GAS	190.	169.	210.	211.	2590.	2664.	3090.	3357.	3096.	3362.
RP1 IN TANK	643806.	641734.	633691.	632752.	95347.	94767.	8541.	10513.	7461.	9433.
RP1 BELOW TANK	4313.	4311.	5996.	5994.	5996.	5994.	5958.	5957.	5958.	5957.
RP1 ULLAGE GAS	35.	73.	35.	76.	211.	226.	242.	249.	242.	250.
N2 PURGE GAS	36.	36.	36.	36.	20.	20.	20.	20.	20.	20.
HELIUM IN BOTTLE	289.	299.	289.	286.	113.	136.	82.	112.	81.	112.
FROST	635.	635.	635.	635.	340.	340.	340.	340.	340.	340.
RETROMOTOR PROP	1027.	1027.	1027.	1027.	1027.	1027.	1027.	1027.	1027.	1027.
OTHER	239.	239.	239.	239.	239.	239.	239.	239.	239.	239.
TOTAL S-IC STAGE	2281895.	2280583.	2243194.	2242236.	456999.	452790.	167998.	171496.	164865.	166362.
TOTAL S-IC/S-II IS	5200.	5220.	5200.	5220.	5200.	5220.	5200.	5220.	5166.	5187.
TOTAL S-II STAGE	480997.	483021.	480997.	483021.	480739.	482762.	480738.	482762.	480738.	482762.
TOT S-II/S-IVB IS	3645.	3639.	3645.	3638.	3645.	3638.	3645.	3638.	3645.	3638.
TOTAL S-IVB STAGE	117967.	118472.	117967.	118472.	117876.	118382.	117876.	118382.	117876.	118382.
TOTAL INSTRU UNIT	1940.	1940.	1940.	1940.	1940.	1940.	1940.	1940.	1940.	1940.
TOTAL SPACECRAFT	49732.	49915.	49732.	49915.	49732.	49915.	49732.	49915.	49732.	49915.
TOTAL UPPER STAGE	659479.	662207.	659479.	662207.	659130.	661858.	659130.	661858.	659097.	661825.
TOTAL VEHICLE	2941374.	2942790.	2902674.	2904443.	1116129.	1114648.	827129.	833353.	823962.	830187.

Table 17-2. Total Vehicle Mass - S-IC Burn Phase - Pounds Mass

EVENTS	GROUND IGNITION		HOLDDOWN ARM RELEASE		CENTER ENGINE CUTOFF		OUTBOARD ENGINE CUTOFF		S-IC/S-II SEPARATION	
	PRED	ACT	PRED	ACT	PRED	ACT	PRED	ACT	PRED	ACT
RANGE TIME--SEC	-6.50	-6.50	.25	.25	135.27	135.24	162.48	161.74	163.20	162.40
S-IC STAGE DRY	287850.	287898.	287850.	287898.	287850.	287898.	287850.	287898.	287850.	287898.
LOX IN TANK	3263309.	3263655.	3193309.	3193439.	438345.	428898.	2200.	2740.	2200.	2200.
LOX [illegible] TANK	46296.	46544.	47921.	48219.	47984.	48047.	37249.	39313.	32708.	35352.
LOX [illegible]	419.	372.	463.	466.	5710.	5874.	6911.	7400.	6925.	7413.
RP-1 IN TANK	1419348.	1419792.	1387050.	1394979.	210204.	208926.	19829.	23177.	16449.	20737.
RP-1 [illegible] TANK	3503.	3505.	13213.	13215.	13213.	13215.	13136.	13132.	13136.	13132.
RP-1 [illegible]	77.	161.	77.	168.	464.	498.	533.	550.	534.	551.
N2 PURGE [illegible]	80.	80.	80.	80.	43.	43.	43.	43.	43.	43.
HELIUM IN BOTTLE	636.	637.	636.	630.	249.	300.	180.	248.	179.	247.
FROST	1400.	1400.	1400.	1400.	750.	750.	750.	750.	750.	750.
PERFORMANCE PROP	2264.	2264.	2264.	2264.	2264.	2264.	2264.	2264.	2264.	2264.
OTHER	529.	529.	529.	528.	528.	528.	529.	528.	529.	528.
TOTAL S-IC STAGE	5030716.	5027926.	4945397.	4943235.	1007610.	999231.	370373.	379033.	363466.	371175.
TOTAL S-IC/S-II IS	11463.	11509.	11463.	11509.	11463.	11509.	11463.	11509.	11390.	11436.
TOTAL S-II STAGE	1060417.	1064878.	1060417.	1064878.	1059947.	1064308.	1059947.	1064308.	1059847.	1064308.
TOT S-II/S-IVB IS	8035.	8021.	8035.	8021.	8035.	8021.	8035.	8021.	8035.	8021.
TOTAL S-IVB STAGE	260072.	261197.	260072.	261197.	259972.	260997.	259972.	260997.	259872.	260997.
TOTAL INSTRU UNIT	4276.	4277.	4276.	4277.	4276.	4277.	4276.	4277.	4276.	4277.
TOTAL SPACECRAFT	103640.	110044.	103640.	110044.	103640.	110044.	103640.	110044.	103640.	110044.
TOTAL UPPER STAGE	1453303.	1453316.	1453303.	1453316.	1453133.	1453145.	1453133.	1453145.	1453060.	1453073.
TOTAL VEHICLE	6484620.	6481742.	6398300.	6396201.	2460643.	2452377.	1823506.	1832223.	1816526.	1824248.

Table 17-3. Total Vehicle Mass - S-II Burn Phase - Kilograms

EVENTS	S-IC IGNITION		S-II IGNITION		S-II MAINSTAGE		S-II ENGINE CUTOFF		S-II/S-IVB SEPARATION	
	PRED	ACT	PRED	ACT	PRED	ACT	PRED	ACT	PRED	ACT
RANGE TIME--SEC	-6.50	-6.50	164.90	164.20	166.90	166.40	550.99	552.34	551.90	553.20
S-IC/S-II IS SMALL	614.	614.								
S-IC/S-II IS LARGE	3969.	3996.	3969.	3996.	3969.	3996.				
S-IC/S-II IS PROP	617.	611.	313.	309.	0.	0.				
TOTAL S-IC/S-II IS	5200.	5220.	4281.	4305.	3969.	3996.				
S-II STAGE DRY	36387.	36394.	36387.	35334.	36397.	36334.	36397.	36394.	36387.	36394.
LOX IN TANK	371530.	373661.	371530.	373661.	371061.	373192.	659.	816.	545.	703.
LOX BELOW TANK	737.	737.	737.	737.	800.	900.	797.	787.	737.	797.
LOX ULLAGE GAS	187.	194.	187.	184.	189.	196.	2330.	2374.	2332.	2376.
LH2 IN TANK	71669.	71556.	71661.	71550.	71447.	71336.	1966.	1969.	1916.	1917.
LH2 BELOW TANK	105.	105.	111.	111.	128.	128.	123.	123.	123.	123.
LH2 ULLAGE GAS	77.	77.	77.	77.	77.	77.	709.	763.	710.	764.
INSULATION PURGE	54.	54.								
FROST	204.	204.								
START TANK GAS	14.	14.	14.	14.	2.	2.	2.	2.	2.	2.
OTHER	34.	34.	34.	34.	34.	34.	34.	34.	34.	34.
TOTAL S-II STAGE	480397.	483021.	480739.	482762.	480127.	482150.	42999.	43263.	42837.	43102.
TOT S-II/S-IVB IS	3645.	3639.	3645.	3639.	3645.	3639.	3645.	3639.	3645.	3639.
TOTAL S-IVB STAGE	117967.	118472.	117876.	118382.	117876.	118382.	117876.	118382.	117874.	118379.
TOTAL INSTRU UNIT	1940.	1940.	1940.	1940.	1940.	1940.	1940.	1940.	1940.	1940.
TOTAL SPACECRAFT	49732.	49915.	49732.	49915.	49732.	49915.	45695.	45850.	45695.	45850.
TOTAL UPPER STAGE	173283.	173966.	173192.	173875.	173192.	173875.	169155.	169810.	169153.	169807.
TOTAL VEHICLE	659479.	662207.	659212.	660943.	657289.	660028.	212154.	213073.	211990.	212909.

Table 17-4. Total Vehicle Mass - S-II Burn Phase - Pounds Mass

EVENTS	S-IC IGNITION		S-II IGNITION		S-II MAINSTAGE		S-II ENGINE CUTOFF		S-II/S-IVB SEPARATION	
	PRED	ACT	PRED	ACT	PRED	ACT	PRED	ACT	PRED	ACT
RANGE TIME--SEC	-6.50	-6.50	164.90	164.20	166.30	166.40	550.99	552.34	551.90	553.20
S-IC/S-II IS SMALL	1353.	1353.								
S-IC/S-II IS LARGE	8750.	8810.	8750.	8810.	8750.	8810.				
S-IC/S-II IS POOP	1360.	1346.	689.	682.	0.	0.				
TOTAL S-IC/S-II IS	11463.	11509.	9439.	9492.	8750.	8810.				
S-II STAGE DRY	80220.	80236.	80220.	80236.	80220.	80236.	80220.	80236.	80220.	80236.
LOX IN TANK	819083.	823781.	819083.	823781.	818050.	822745.	1452.	1800.	1202.	1550.
LOX BELOW TANK	1625.	1625.	1625.	1625.	1764.	1764.	1736.	1736.	1736.	1736.
LOX ULLAGE GAS	413.	405.	413.	405.	417.	409.	5136.	5233.	5141.	5238.
LH2 IN TANK	158000.	157755.	157986.	157741.	157513.	157268.	4335.	4338.	4223.	4226.
LH2 BELOW TANK	231.	231.	245.	245.	282.	282.	272.	272.	272.	272.
LH2 ULLAGE GAS	169.	169.	169.	169.	171.	171.	1564.	1683.	1565.	1684.
INSULATION PURGE	120.	120.								
FROST	450.	450.								
START TANK GAS	30.	30.	30.	30.	5.	5.	5.	5.	5.	5.
OTHER	76.	76.	76.	76.	76.	76.	76.	76.	76.	76.
TOTAL S-II STAGE	1060417.	1064879.	1059847.	1064309.	1058498.	1062959.	94796.	95379.	94440.	95023.
TOT S-II/S-IVB IS	8035.	8021.	8035.	8021.	8035.	8021.	8035.	8021.	8035.	8021.
TOTAL S-IVB STAGE	260072.	261187.	259872.	260987.	259872.	260987.	259872.	260987.	259867.	260982.
TOTAL INSTRU UNIT	4276.	4277.	4276.	4277.	4276.	4277.	4276.	4277.	4276.	4277.
TOTAL SPACECRAFT	109640.	110044.	109640.	110044.	109640.	110044.	100740.	101081.	100740.	101081.
TOTAL UPPER STAGE	382023.	383529.	381823.	383329.	381823.	383329.	372923.	374366.	372918.	374361.
TOTAL VEHICLE	1453903.	1459916.	1451109.	1457129.	1449071.	1455090.	467719.	469745.	467358.	469384.

Table 17-5. Total Vehicle Mass - S-IVB First Burn Phase - Kilograms

EVENTS	S-IC IGNITION		S-IVB IGNITION		S-IVB MAINSTAGE		S-IVB ENGINE CUTOFF		S-IVB END DECAY	
	PRED	ACT	PRED	ACT	PRED	ACT	PRED	ACT	PRED	ACT
RANGE TIME--SEC	-6.50	-6.50	555.00	556.60	557.50	559.10	689.96	693.91	690.10	694.10
S-IVB STAGE DRY	11362.	11369.	11339.	11346.	11339.	11346.	11278.	11284.	11279.	11284.
LOX IN TANK	85970.	86282.	85970.	86282.	85955.	86168.	61581.	61467.	61549.	61440.
LOX BELOW TANK	166.	166.	166.	166.	180.	180.	180.	180.	180.	180.
LOX ULLAGE GAS	18.	21.	18.	21.	20.	22.	94.	66.	94.	66.
LH2 IN TANK	19709.	19783.	19705.	19753.	19648.	19729.	14758.	14646.	14745.	14611.
LH2 BELOW TANK	22.	22.	26.	26.	26.	26.	26.	26.	26.	26.
LH2 ULLAGE GAS	20.	19.	20.	19.	20.	19.	61.	49.	61.	49.
ULLAGE MOTOR PROP	54.	54.	10.	8.	0.	0.	0.	0.	0.	0.
APS PROPELLANT	296.	298.	296.	298.	296.	299.	294.	298.	294.	298.
HELIUM IN BOTTLES	196.	205.	196.	205.	196.	204.	176.	184.	176.	184.
START TANK GAS	2.	2.	2.	2.	0.	0.	3.	3.	3.	3.
FROST	136.	227.	45.	136.	45.	136.	45.	136.	45.	136.
OTHER	25.	25.	25.	25.	25.	25.	25.	25.	25.	25.
TOTAL S-IVB STAGE	117967.	118472.	117809.	118297.	117642.	118153.	88513.	88365.	88469.	88303.
TOTAL INSTRU UNIT	1940.	1940.	1940.	1940.	1940.	1940.	1940.	1940.	1940.	1940.
TOTAL SPACECRAFT	45695.	45950.	45695.	45850.	45695.	45850.	45695.	45850.	45695.	45850.
TOTAL UPPER STAGE	47634.	47790.	47634.	47790.	47634.	47790.	47634.	47790.	47634.	47790.
TOTAL VEHICLE	165601.	166262.	165444.	166077.	165276.	165943.	136148.	136154.	136103.	136093.

Table 17-6. Total Vehicle Mass - S-IVB First Burn Phase - Pounds Mass

EVENTS	S-IC IGNITION		S-IVB IGNITION		S-IVB MAINSTAGE		S-IVB ENGINE CUTOFF		S-IVB END DECAY	
	PRED	ACT	PRED	ACT	PRED	ACT	PRED	ACT	PRED	ACT
RANGE TIME--SEC	-6.50	-6.50	555.00	556.60	557.50	559.10	689.86	693.91	690.10	694.10
S-IVB STAGE DRY	25050.	25064.	24999.	25013.	24999.	25013.	24864.	24878.	24864.	24878.
LOX IN TANK	189531.	190220.	189531.	190220.	184279.	189067.	135763.	135512.	135693.	135453.
LOX BELOW TANK	367.	367.	367.	367.	397.	397.	397.	397.	397.	397.
LOX ULLAGE GAS	39.	47.	39.	47.	44.	49.	203.	145.	208.	145.
LH2 IN TANK	43452.	43615.	43442.	43549.	43317.	43434.	32535.	32288.	32507.	32211.
LH2 BELOW TANK	48.	48.	58.	58.	59.	58.	58.	58.	58.	58.
LH2 ULLAGE GAS	43.	39.	43.	39.	44.	42.	135.	108.	135.	108.
ULLAGE MOTOR PROP	118.	118.	22.	17.	0.	0.	0.	0.	0.	0.
APS PROPELLANT	630.	657.	630.	657.	630.	657.	626.	656.	626.	656.
HELIUM IN BOTTLES	433.	451.	432.	451.	431.	449.	389.	406.	389.	406.
START TANK GAS	5.	5.	5.	5.	1.	1.	7.	7.	7.	7.
FROST	300.	500.	100.	300.	100.	300.	100.	300.	100.	300.
OTHER	56.	56.	56.	56.	56.	56.	56.	56.	56.	56.
TOTAL S-IVB STAGE	260072.	261197.	253725.	260779.	259356.	260493.	195138.	194811.	195040.	194675.
TOTAL INSTRU UNIT	4276.	4277.	4276.	4277.	4276.	4277.	4276.	4277.	4276.	4277.
TOTAL SPACECRAFT	100740.	101091.	100740.	101081.	100740.	101081.	100740.	101091.	100740.	101091.
TOTAL UPPER STAGE	105016.	105359.	105016.	105359.	105016.	105359.	105016.	105358.	105016.	105358.
TOTAL VEHICLE	365088.	366545.	358741.	366137.	364372.	365841.	300154.	300169.	300056.	300033.

Table 17-7. Total Vehicle Mass - S-IVB Second Burn Phase - Kilograms

EVENTS	S-IVB IGNITION		S-IVB MAINSTAGE		S-IVB ENGINE CUTOFF		S-IVB END DECAY		SPACECRAFT SEPARATION	
	PRED	ACT	PRED	ACT	PRED	ACT	PRED	ACT	PRED	ACT
RANGE TIME--SEC	10040.00	10042.70	10042.50	10045.20	10385.01	10383.89	10385.20	10384.20	15164.00	15180.90
S-IVB STAGE DRY	11278.	11284.	11278.	11284.	11278.	11284.	11279.	11284.	11278.	11294.
LOX IN TANK	61487.	61348.	61391.	61229.	2029.	1933.	1999.	1905.	1926.	1830.
LOX BELOW TANK	166.	166.	180.	180.	180.	180.	180.	180.	166.	166.
LOX ULLAGE GAS	152.	159.	153.	160.	245.	220.	245.	220.	45.	45.
LH2 IN TANK	13493.	13469.	13441.	13457.	943.	1124.	930.	1111.	548.	728.
LH2 BELOW TANK	26.	26.	26.	26.	26.	26.	26.	26.	22.	22.
LH2 ULLAGE GAS	185.	153.	185.	154.	307.	250.	307.	250.	64.	64.
ULLAGE MOTOR PROP	0.	0.	0.	0.	0.	0.	0.	0.	0.	0.
APS PROPELLANT	203.	256.	203.	256.	201.	254.	201.	254.	166.	233.
HELIUM IN BOTTLES	148.	169.	148.	169.	99.	114.	88.	113.	88.	113.
START TANK GAS	2.	2.	0.	0.	3.	3.	3.	3.	3.	3.
FROST	45.	136.	45.	136.	45.	136.	45.	136.	45.	136.
OTHER	25.	25.	25.	25.	25.	25.	25.	25.	25.	25.
TOTAL S-IVB STAGE	87212.	87196.	87077.	87077.	15372.	15550.	15328.	15509.	14378.	14650.
TOTAL INSTRU UNIT	1940.	1940.	1940.	1940.	1940.	1940.	1940.	1940.	1940.	1940.
TOTAL SPACECRAFT	45695.	45850.	45695.	45850.	45695.	45850.	45695.	45850.	626.	626.
TOTAL UPPER STAGE	47634.	47790.	47634.	47790.	47634.	47790.	47634.	47790.	2566.	2566.
TOTAL VEHICLE	134846.	134986.	134711.	134866.	63007.	63340.	62962.	63299.	16943.	17216.

Table 17-8. Total Vehicle Mass - S-IVB Second Burn Phase - Pounds Mass

EVENTS	S-IVB IGNITION		S-IVB MAINSTAGE		S-IVB ENGINE CUTOFF		S-IVB END DECAY		SPACECRAFT SEPARATION	
	PRED	ACT	PRED	ACT	PRED	ACT	PRED	ACT	PRED	ACT
RANGE TIME--SEC	10040.00	10042.70	10042.50	10045.20	10385.01	10383.89	10385.20	10384.20	15164.00	15180.90
S-IVB STAGE DRY	24864.	24878.	24864.	24878.	24864.	24878.	24864.	24878.	24864.	24878.
LOX IN TANK	135557.	135250.	135344.	134995.	4473.	4262.	4404.	4200.	4246.	4034.
LOX BELOW TANK	367.	367.	397.	397.	397.	397.	397.	397.	367.	367.
LOX ULLAGE GAS	336.	351.	333.	352.	541.	494.	541.	494.	100.	100.
LH2 IN TANK	29746.	29695.	29633.	29668.	2080.	2477.	2051.	2450.	1208.	1604.
LH2 BELOW TANK	59.	59.	59.	59.	58.	58.	59.	58.	48.	48.
LH2 ULLAGE GAS	407.	338.	408.	340.	676.	551.	676.	551.	141.	141.
ULLAGE MOTOR PROP	0.	0.	0.	0.	0.	0.	0.	0.	0.	0.
APS PROPELLANT	447.	564.	447.	564.	443.	561.	443.	561.	366.	513.
HELIUM IN BOTTLES	326.	373.	326.	372.	195.	251.	195.	250.	195.	250.
START TANK GAS	5.	5.	1.	1.	7.	7.	7.	7.	7.	7.
FROST	100.	300.	100.	300.	100.	300.	100.	300.	100.	300.
OTHER	56.	56.	56.	56.	56.	56.	56.	56.	56.	56.
TOTAL S-IVB STAGE	192269.	192235.	191971.	191971.	33890.	34282.	33792.	34192.	31698.	32298.
TOTAL INSTRU UNIT	4276.	4277.	4276.	4277.	4276.	4277.	4276.	4277.	4276.	4277.
TOTAL SPACECRAFT	100740.	101081.	100740.	101081.	100740.	101081.	100740.	101081.	1380.	1380.
TOTAL UPPER STAGE	105016.	105358.	105016.	105358.	105016.	105358.	105016.	105358.	5656.	5657.
TOTAL VEHICLE	297285.	297593.	296987.	297329.	138906.	139640.	138808.	139550.	37354.	37955.

Table 17-9. Flight Sequence Mass Summary

MASS HISTORY	PREDICTED KG	PREDICTED LBM	ACTUAL KG	ACTUAL LBM
S-IC STAGE, TOTAL	2281895.	5030716.	2290583.	5027826.
S-IC/S-II INTERSTAGE,TOTAL	5200.	11463.	5220.	11509.
S-II STAGE, TOTAL	480997.	1060417.	483021.	1064878.
S-II/SIIV3 INTERSTAGE	1645.	3635.	1638.	3621.
S-IVB STAGE, TOTAL	117967.	260072.	118472.	261187.
INSTRUMENT UNIT	1940.	4276.	1940.	4277.
SPACECRAFT INCLUDING LES	49732.	109640.	49915.	110044.
1ST FLT STG AT IGN	2941374.	6484520.	2942790.	6487742.
S-IC THRUST BUILDUP	-38700.	-85319.	-38347.	-84541.
1ST FLT STG HOLDDWN ARM REL	2902674.	6399300.	2904443.	6403201.
S-IC FROST	-295.	-650.	-295.	-650.
S-IC MAINSTAGE PROPELLANT	-2073916.	-4572202.	-2069456.	-4562370.
S-IC N2 PURGE	-17.	-37.	-17.	-37.
S-IC INBD ENGINE T.D. PROP	-793.	-1727.	-793.	-1727.
S-IC INBD ENG EXPENDED PROP	-185.	-408.	-190.	-419.
S-II INSULATION PURGE GAS	-54.	-120.	-54.	-120.
S-II FROST	-204.	-450.	-204.	-450.
S-IVB FROST	-91.	-200.	-91.	-200.
1ST FLT STAGE AT S-IC OECOS	827129.	1823506.	833353.	1837229.
S-IC OTBD ENGINE T.D. PROP	-3133.	-6907.	-3133.	-6909.
S-IC/S-II ULLAGE PKT PROP	-33.	-73.	-33.	-73.
1ST FLT STAGE AT SIC/SII SEP	823962.	1816526.	830187.	1830248.
S-IC STAGE AT SEPARATION	-168865.	-363468.	-168362.	-371175.
S-IC/S-II INTERSTAGE SMALL	-614.	-1353.	-614.	-1353.
S-IC/S-II ULLAGE PKT PROP	-83.	-184.	-83.	-184.
2ND FLT STAGE AT S-II SSC	659400.	1451523.	661127.	1457536.
S-II FUEL LEAD	3.	3.	3.	3.
S-IC/S-II ULLAGE PKT PROP	-189.	-414.	-185.	-407.
2ND FLT STAGE AT S-II IGN	659212.	1451109.	660943.	1457129.
S-II T.D. PROPELLANT	-601.	-1324.	-601.	-1325.
S-II START TANK	-11.	-25.	-11.	-25.
S-IC/S-II ULLAGE PKT PROP	-313.	-689.	-309.	-682.
2ND FLT STAGE AT MAINSTAGE	657298.	1449071.	660021.	1455099.
S-II MAINSTAGE + VENTING	-437070.	-963575.	-439829.	-969453.
LAUNCH ESCAPE SYSTEM	-4037.	-8900.	-4066.	-8963.
S-IC/S-II INTERSTAGE LARGE	-3969.	-8750.	-3996.	-8810.
S-II T.D. PROPELLANT	-58.	-127.	-58.	-127.
2ND FLT STAGE AT S-II C.O.S.	212154.	467719.	213073.	469745.
S-II T.D. PROPELLANT	-161.	-356.	-161.	-356.
S-IVB ULLAGE PROPELLANT	-2.	-5.	-2.	-5.
2ND FLT STG AT SII/SIVB SEP	211990.	467358.	212909.	469384.
S-II STAGE AT SEPARATION	-42837.	-94440.	-43102.	-95023.
S-II/S-IVB INTERSTAGE-DRY	-3164.	-6975.	-3156.	-6958.
S-II/S-IVB IS PROP	-481.	-1060.	-482.	-1063.
S-IVB AFT FRAME	-22.	-48.	-22.	-48.
S-IVB ULLAGE PROPELLANT	-1.	-3.	-1.	-3.
S-IVB DET PACKAGE	-1.	-3.	-1.	-3.
3RD FLT STG AT 1ST SSC	165484.	364829.	166145.	366296.
S-IVB ULLAGE PROPELLANT	-40.	-88.	-42.	-93.
S-IVB FUEL LEAD LOSS	-0.	-0.	-25.	-56.

Table 17-9. Flight Sequence Mass Summary (Continued)

MASS HISTORY	PREDICTED KG	PREDICTED LBM	ACTUAL KG	ACTUAL LBM
3RD FLT STG AT 1ST SIVB IGN	165444.	364741.	166077.	366137.
S-IVB ULLAGE PROPELLANT	-10.	-22.	-8.	-17.
S-IVB START TANK	-2.	-4.	-2.	-4.
S-IVB T.B. PROPELLANT	-155.	-342.	-125.	-275.
3RD FLT STG AT MAINSTAGE	165276.	364372.	165943.	365841.
S-IVB ULLAGE ROCKET CASES	-61.	-135.	-61.	-135.
S-IVB MAINSTAGE PROP	-29066.	-64079.	-29727.	-65536.
S-IVB APS PROPELLANT	-2.	-4.	-0.	-1.
3RD FLT STG AT 1ST SIVB COS	136149.	300154.	136154.	300169.
S-IVB T.D. PROPELLANT	-44.	-99.	-62.	-136.
3RD FLT STG AT END 1ST TD	136103.	300056.	136093.	300033.
S-IVB END PROP EXPENDED	-18.	-40.	-18.	-40.
S-IVB FUEL TANK LOSS	-1128.	-2486.	-986.	-2174.
S-IVB LOX TANK LOSS	-14.	-32.	-3.	-7.
S-IVB APS PROPELLANT	-81.	-179.	-42.	-92.
S-IVB START TANK	-1.	-2.	-1.	-2.
S-IVB O2/H2 BURNER	-7.	-16.	-7.	-16.
3RD FLT STG AT 2ND SSC	134853.	297301.	135035.	297702.
S-IVB FUEL LEAD LOSS	-7.	-15.	-49.	-109.
3RD FLT STG AT 2ND SIVB IGN	134846.	297285.	134986.	297593.
S-IVB START TANK	-2.	-4.	-2.	-4.
S-IVB T.B. PROPELLANT	-133.	-294.	-118.	-260.
3RD FLT STG AT MAINSTAGE	134711.	296997.	134866.	297329.
S-IVB MAINSTAGE PROP	-71703.	-158077.	-71525.	-157686.
S-IVB APS PROPELLANT	-2.	-4.	-1.	-3.
3RD FLT STG AT 2ND SIVB COS	63007.	138906.	63340.	139640.
S-IVB T.D. PROPELLANT	-44.	-99.	-40.	-89.
3RD FLT STG AT END 2ND TD	62962.	138808.	63299.	139550.
JETTISON SLA	-1170.	-2580.	-1170.	-2580.
COMMAND SERVICE MODULE	-28837.	-63574.	-28830.	-63559.
S-IVB STAGE LOSS	-650.	-1434.	-560.	-1234.
START OF TRANS/DOCKING	32305.	71220.	32739.	72177.
COMMAND SERVICE MODULE	28837.	63574.	28830.	63559.
S-IVB STAGE LOSS	0.	0.	0.	0.
END OF TRANS/DOCKING	61142.	134794.	61569.	135736.
COMMAND SERVICE MODULE	-28837.	-63574.	-28830.	-63559.
LUNAR MODULE	-15062.	-33206.	-15223.	-33562.
S-IVB STAGE LOSS	-299.	-660.	-299.	-660.
LAUNCH VEH AT S/C SEPARATION	16943.	37354.	17216.	37955.
SPACECRAFT NOT SEPARATED	-626.	-1380.	-626.	-1380.
INSTRUMENT UNIT	-1940.	-4276.	-1940.	-4277.
S-IVB STAGE AT SEPARATION	-14378.	-31698.	-14650.	-32298.

Table 17-10. Mass Characteristics Comparison

EVENT		MASS		LONGITUDINAL C.G. (X STA.)		RADIAL C.G.		ROLL MOMENT OF INERTIA		PITCH MOMENT OF INERTIA		YAW MOMENT OF INERTIA	
		KILO POUNDS	O/O DEV.	METERS INCHES	DELTA	METERS INCHES	DELTA	KG-M2 X10-6	O/O DEV.	KG-M2 X10-6	O/O DEV.	KG-M2 X10-6	O/O DEV.
S-IC STAGE DRY	PRED	130567.		9.364		0.0580							
		287850.		368.7		2.2847		2.585		16.656		16.581	
	ACTUAL	130588.		9.364	0.000	0.0580	0.0000						
		287898.	0.02	368.7	0.00	2.2847	0.0000	2.585	0.02	16.658	0.02	16.584	0.02
S-IC/S-II INTER-STAGE, TOTAL	PRED	5200.		41.622		0.1544							
		11463.		1638.7		6.0811		0.132		0.079		0.079	
	ACTUAL	5220.		41.628	0.005	0.1544	0.0000						
		11509.	0.40	1638.9	0.19	6.0811	0.0000	0.132	0.40	0.079	0.40	0.079	0.53
S-II STAGE, DRY	PRED	36387.		48.087		0.1761							
		80220.		1893.2		6.9354		0.602		2.017		2.030	
	ACTUAL	36394.		48.026	-0.060	0.1761	0.0000						
		80236.	0.02	1890.8	-2.40	6.9354	0.0000	0.602	0.02	1.979	-1.87	2.030	0.02
S-II/S-IVB INTER-STAGE, TOTAL	PRED	3645.		66.466		0.0589							
		8035.		2616.8		2.3194		0.064		0.044		0.044	
	ACTUAL	3638.		66.464	-0.002	0.0589	0.0000						
		8021.	-0.16	2616.7	-0.10	2.3194	0.0000	0.064	-0.16	0.043	-0.16	0.044	-0.16
S-IVB STAGE, DRY	PRED	11362.		72.562		0.2306							
		25050.		2856.8		9.0801		0.082		0.300		0.300	
	ACTUAL	11369.		72.562	0.000	0.2306	0.0000						
		25064.	0.06	2856.8	0.00	9.0801	0.0000	0.082	0.06	0.300	0.06	0.300	0.06
VEHICLE INSTRUMENT UNIT	PRED	1940.		82.415		0.3620							
		4276.		3244.7		14.2523		0.018		0.010		0.008	
	ACTUAL	1940.		82.417	0.002	0.3626	0.0006						
		4277.	0.02	3244.8	0.1014	2.2779	0.0255	0.018	0.02	0.010	0.02	0.008	0.02
SPACECRAFT, TOTAL	PRED	49732.		91.536		0.1106							
		109640.		3603.8		4.3566		0.091		1.582		1.583	
	ACTUAL	49915.		91.521	-0.015	0.1106	0.0000						
		110044.	0.37	3603.2	-0.60	4.3566	0.0000	0.091	0.37	1.591	0.55	1.594	0.64

Table 17-10. Mass Characteristics Comparison (Continued)

EVENT		MASS		LONGITUDINAL C.G. (X STA.)		RADIAL C.G.		ROLL MOMENT OF INERTIA		PITCH MOMENT OF INERTIA		YAW MOMENT OF INERTIA	
		KILO POUNDS	O/O DEV.	METERS INCHES	DELTA	METERS INCHES	DELTA	KG-M2 X10-6	O/O DEV.	KG-M2 X10-6	O/O DEV.	KG-M2 X10-6	O/O DEV.
		2941374.		30.312		0.0039							
	PRED	6484620.		1193.3		0.1565		3.698		873.729		873.697	
1ST FLIGHT STAGE AT IGNITION		2942791.		30.343	0.031	0.0039	0.0000						
	ACTUAL	6487744.	0.05	1194.6	1.22	0.1565	0.0000	3.702	0.13	875.597	0.21	875.524	0.21
		2902674.		30.256		0.0039							
1ST FLIGHT STAGE AT HOLDDOWN ARM RELEASE	PRED	6399301.		1191.2		0.1565		3.733		874.661		874.629	
		2904444.		30.282	0.025	0.0039	0.0000						
	ACTUAL	6403203.	0.06	1192.2	0.98	0.1565	0.0000	3.738	0.13	876.666	0.23	876.634	0.23
		827129.		46.403		0.0136							
1ST FLIGHT STAGE AT OUTBOARD ENGINE CUTOFF SIGNAL	PRED	1823506.		1826.9		0.5385		3.718		440.722		440.693	
		833353.		46.281	-0.121	0.0136	-0.0000						
	ACTUAL	1837229.	0.75	1822.1	-4.79	0.5371	-0.0013	3.724	0.16	445.395	1.20	445.966	1.20
		823963.		46.543		0.0136							
1ST FLIGHT STAGE AT SEPARATION	PRED	1816526.		1832.4		0.5385		3.716		436.457		436.428	
		830187.		46.417	-0.125	0.0136	-0.0000						
	ACTUAL	1830248.	0.76	1827.4	-4.94	0.5371	-0.0013	3.722	0.17	441.902	1.25	441.873	1.25
		658400.		55.816		0.0182							
2ND FLIGHT STAGE AT START SEQUENCE COMMAND	PRED	1451523.		2197.4		0.7199		0.991		135.232		135.245	
		661128.		55.813	-0.003	0.0182	0.0000						
	ACTUAL	1457536.	0.41	2197.3	-0.11	0.7200	0.0000	0.993	0.24	135.694	0.34	135.747	0.37
		657288.		55.829		0.0182							
2ND FLIGHT STAGE AT MAINSTAGE	PRED	1449071.		2198.0		0.7199		0.979		135.111		135.124	
		660021.		55.825	-0.004	0.0182	0.0000						
	ACTUAL	1455096.	0.42	2197.8	-0.15	0.7200	0.0000	0.981	0.26	135.576	0.34	135.628	0.37
		212154.		71.067		0.0544							
2ND FLIGHT STAGE AT CUTOFF SIGNAL	PRED	467719.		2797.9		2.1433		0.877		44.637		44.649	
		213072.		71.046	-0.021	0.0541	-0.0002						
	ACTUAL	469744.	0.43	2797.1	-0.83	2.1333	-0.0099	0.879	0.20	44.903	0.60	44.955	0.68

Table 17-10. Mass Characteristics Comparison (Continued)

EVENT		MASS		LONGITUDINAL C.G. (A STA.)		RADIAL C.G.		ROLL MOMENT OF INERTIA		PITCH MOMENT OF INERTIA		YAW MOMENT OF INERTIA	
		KILO POUNDS	O/O DEV.	METERS INCHES	DELTA	METERS INCHES	DELTA	KG-M2 X10-6	O/O DEV.	KG-M2 X10-6	O/O DEV.	KG-M2 X10-6	O/O DEV.
2ND FLIGHT STAGE AT SEPARATION	PRED	211990.		71.087		0.0544							
		467358.		2798.7		2.1433		0.877		44.530		44.542	
	ACTUAL	212909.		71.065	-0.022	0.0541	-0.0004						
		469383.	0.43	2797.8	-0.87	2.1333	-0.0099	0.879	0.20	44.795	0.60	44.847	0.69
3RD FLIGHT STAGE AT 1ST START SEQUENCE COMMAND	PRED	165484.		77.160		0.0394							
		364829.		3037.8		1.5520		0.198		13.400		13.398	
	ACTUAL	166145.		77.159	-0.000	0.0387	-0.0006						
		366286.	0.40	3037.7	-0.02	1.5269	-0.0251	0.200	0.88	13.419	0.14	13.418	0.15
3RD FLIGHT STAGE AT 1ST IGNITION	PRED	165444.		77.156		0.0394							
		364740.		3037.6		1.5520		0.198		13.400		13.397	
	ACTUAL	166077.		77.155	-0.001	0.0387	-0.0006						
		366137.	0.38	3037.6	-0.05	1.5268	-0.0251	0.200	0.88	13.418	0.14	13.418	0.15
3RD FLIGHT STAGE AT 1ST MAINSTAGE	PRED	165276.		77.158		0.0394							
		364372.		3037.7		1.5520		0.198		13.397		13.395	
	ACTUAL	165943.		77.157	-0.000	0.0387	-0.0006						
		365841.	0.40	3037.6	-0.02	1.5268	-0.0251	0.200	0.88	13.418	0.15	13.417	0.17
3RD FLIGHT STAGE AT 1ST CUTOFF SIGNAL	PRED	136148.		78.022		0.0476							
		300153.		3071.7		1.8762		0.197		12.621		12.618	
	ACTUAL	136154.		78.035	0.012	0.0470	-0.0005						
		300169.	0.01	3072.2	0.49	1.8543	-0.0219	0.199	0.89	12.625	0.04	12.625	0.05
3RD FLIGHT STAGE AT 1ST END THRUST DECAY, START COAST	PRED	136103.		78.023		0.0476							
		300055.		3071.8		1.8762		0.197		12.619		12.617	
	ACTUAL	136093.		78.036	0.012	0.0470	-0.0005						
		300033.	-0.00	3072.3	0.49	1.8543	-0.0219	0.199	0.89	12.625	0.04	12.624	0.06
3RD FLIGHT STAGE AT 2ND START SEQUENCE COMMAND	PRED	134853.		78.031		0.0477							
		297300.		3072.0		1.8815		0.196		12.616		12.614	
	ACTUAL	135035.		78.041	0.010	0.0472	-0.0005						
		297702.	0.13	3072.5	0.41	1.8593	-0.0222	0.198	1.21	12.624	0.06	12.623	0.07

Table 17-10. Mass Characteristics Comparison (Continued)

EVENT		MASS		LONGITUDINAL C.G. (X STA.)		RADIAL C.G.		ROLL MOMENT OF INERTIA		PITCH MOMENT OF INERTIA		YAW MOMENT OF INERTIA	
		KILO POUNDS	O/O DEV.	METERS INCHES	DELTA	METERS INCHES	DELTA	KG-M2 X10-6	O/O DEV.	KG-M2 X10-6	O/O DEV.	KG-M2 X10-6	O/O DEV.
		134846.		78.031		0.0475							
	PRED	297285.		3072.0		1.8730		0.196		12.617		12.615	
3RD FLIGHT STAGE AT 2ND IGNITION		134986.		78.041	0.009	0.0472	-0.0003						
	ACTUAL	297593.	0.10	3072.4	0.39	1.8593	-0.0137	0.198	1.20	12.624	0.06	12.624	0.07
		134711.		78.034		0.0477							
	PRED	296997.		3072.2		1.8815		0.196		12.615		12.613	
3RD FLIGHT STAGE AT 2ND MAINSTAGE		134866.		78.040	0.011	0.0472	-0.0005						
	ACTUAL	297329.	0.12	3072.6	0.46	1.8593	-0.0222	0.198	1.20	12.621	0.05	12.621	0.06
		63007.		85.768		0.1004							
3RD FLIGHT STAGE AT 2ND CUTOFF SIGNAL	PRED	138905.		3376.7		3.9553		0.195		5.270		5.268	
		63340.		85.737	-0.031	0.0993	-0.0011						
	ACTUAL	139640.	0.53	3375.4	-1.22	3.9118	-0.0434	0.198	1.23	5.291	0.40	5.290	0.43
		62962.		85.779		0.1004							
3RD FLIGHT STAGE AT 2ND END THRUST DECAY	PRED	138807.		3377.1		3.9553		0.195		5.259		5.257	
		63299.		85.748	-0.031	0.0993	-0.0011						
	ACTUAL	139550.	0.53	3375.9	-1.24	3.9118	-0.0434	0.198	1.23	5.281	0.42	5.280	0.45
		32305.		78.873		0.0854							
	PRED	71219.		3105.2		3.3655		0.139		1.654		1.649	
CSM SEPARATED		32739.		78.871	-0.001	0.0896	0.0042						
	ACTUAL	72177.	1.34	3105.1	-0.07	3.5311	0.1656	0.142	2.36	1.668	0.86	1.665	0.94
		61141.		85.335		0.1321							
	PRED	134793.		3359.6		5.2034		0.186		4.621		4.615	
CSM DOCKED		61569.		85.288	-0.046	0.1331	0.0009						
	ACTUAL	135736.	0.70	3357.8	-1.84	5.2413	0.0379	0.189	1.36	4.654	0.71	4.648	0.73
		16943.		73.652		0.1651							
	PRED	37353.		2899.6		6.5012		0.109		0.603		0.600	
SPACECRAFT SEPARATED		17216.		73.669	.17	0.1692	0.0041						
	ACTUAL	37955.	1.61	2900.3	0.6	6.6640	0.1627	0.112	2.01	0.607	0.72	0.604	0.62

SECTION 18

MISSION OBJECTIVES ACCOMPLISHMENT

Table 18-1 presents the MSFC Mandatory Objectives and Desired Objectives as defined in the Saturn V Mission Implementation Plan, "H" Series Missions, Apollo 12, 13, 14 and 15; MSFC Document PM-SAT-8010.5 (Revision B), dated August 29, 1969. An assessment of the degree of accomplishment of each objective is shown. Discussion supporting the assessment can be found in other sections of this report as shown in Table 18-1.

Table 18-1. Mission Objectives Accomplishment

NO.	MSFC MANDATORY OBJECTIVES (MO) AND DESIRABLE OBJECTIVES (DO)	DEGREE OF ACCOMPLISHMENT	DISCREPANCIES	PARAGRAPH IN WHICH DISCUSSED
1	Launch on a flight azimuth between 72 to 96 degrees and insertion of S-IVB/IU/SC into a circular earth parking orbit (MO).	Complete	None	4.1, 4.3.2, 10.3
2	Restart the S-IVB during either the second or third revolution and injection of the S-IVB/IU/SC onto the planned translunar trajectory (MO).	Complete	None	4.1, 4.3.3, 10.3, 11.4
3	Provide the required attitude control for the S-IVB/IU/SC during the TD&E maneuver (MO).	Complete	None	11.4.4, 11.5
4	Use S-IVB APS burn to execute a LV evasive maneuver after ejection of CSM/LM from S-IVB/IU (DO).	Complete	None	11.4.4
	Use residual S-IVB propellants and APS to maneuver to a trajectory that utilizes lunar gravity to insert the expended S-IVB/IU into a solar orbit (slingshot) (DO).	Not accomplished	S-IVB/IU failed to achieve solar orbit	4.3.5, 10.2.3
5	Venting and dumping of all remaining gases and liquids to safe the S-IVB/IU (DO).	Complete	None	7.13

SECTION 19

SPACECRAFT SUMMARY

The Apollo 12 mission provided a wealth of scientific information in this initial significant step of detailed lunar exploration. The emplaced experiments with a central transmitting station will enable scientific observation to be made for approximately 1 year of expected equipment operation. These experiments will provide scientists with a greater understanding of the lunar surface environment, perturbations to its structure, and characteristic energy release. This mission will yield more lunar scientific data than all previous manned space missions, as well as unmanned lunar missions. Scientists estimate that our lunar knowledge will be advanced many orders of magnitude after a complete examination of the information obtained.

The space vehicle, with a crew consisting of astronauts Charles Conrad, Jr., Commander; Richard F. Gordon, Jr., Command Module (CM) Pilot; and Alan L. Bean, Lunar Module (LM) Pilot; was launched from Kennedy Space Center, Florida, at 11:22:00 A.M. Eastern Standard Time on November 14, 1969. The activities during earth orbit checkout, translunar injection, and translunar coast were similar to those of Apollo 11, except for the special attention given to verifying the LM and command and service module systems as a result of the potential electro-static discharges at 36.5 and 52 seconds. As planned, only one mid-course correction, applied at about 31 hours to place the spacecraft on a non-free-return trajectory, was required prior to lunar orbit insertion. Initial checkout of LM systems during translunar coast and in lunar orbit was satisfactory. The Commander and the LM Pilot entered the LM for descent at about 104 hours.

The two spacecraft were undocked at about 108 hours, and descent orbit insertion was performed at approximately 109.5 hours. One hour later, the mission objective of achieving a precision landing was accomplished using the automatic guidance system, with small manual corrections applied in the final phase of descent. The spacecraft touched down at 110:32:34 in the Ocean of Storms only 600 feet from the Surveyor III spacecraft. The landing coordinates were 3.2 degrees south latitude and 23.4 degrees west longitude.

Two hours after landing, the crewmen configured the LM cabin for depressurization and completed preparations for egress. As the Commander descended to the surface, he deployed the modularized equipment storage assembly, which permitted transmission of color television pictures. The television

camera, however, subsequently failed. The first extravehicular activity period began at 115.25 hours. After assisting the Commander with transfer of a contingency sample to the LM, the LM Pilot descended to the surface and erected the solar wind composition foil. The crew then deployed the Apollo lunar surface experiments package, which included a cold cathode ion gage, a lunar surface magnetometer, a passive seismometer, a solar wind spectrometer, a dust detector, and a suprathermal ion detector. On the return traverse, the crew collected a core-tube soil specimen and additional surface samples. The duration of the first extravehicular activity period was 4 hours.

Following a 7 hour rest period, the second extravehicular activity period began at 131.5 hours with preparation for the geology traverse. Documented samples, core-tube samples, trench site samples, and gas analysis samples were collected on the traverse to the Surveyor III spacecraft. The crew photographed the Surveyor and from it retrieved a cable, a painted tube, an unpainted tube, the television camera, and the scoop. Following the return traverse, the solar wind composition foil was retrieved. The second extravehicular activity period was terminated at 135.25 hours for a duration of 3.75 hours. Crew mobility and portable life support system operation, as in Apollo 11, were excellent throughout the total 7 hour 46 minute extravehicular period.

The ascent stage lifted off the lunar surface at 142 hours. Firing of the ascent engine placed the vehicle into a 62- by 9 n mi-orbit. The ascent engine burned about 1.2 seconds longer than planned, and subsequent nulling of the overburn by the crew returned the orbit to the planned orbit of 45 by 9 n mi. After a nominal rendezvous sequence, the two spacecraft were docked at 145.5 hours. The ascent stage was jettisoned following crew transfer and was maneuvered remotely to impact on the lunar surface: impact occurred at 150 hours approximately 40 n mi from the descent stage.

After a period of extensive landmark tracking and photography, transearth injection was accomplished with the service propulsion engine during the 45th lunar orbit revolution at 172.5 hours. The lunar orbit photography was conducted using a 500 MM longrange lens to obtain mapping and training data for Apollo 13. During transearth coast, two midcourse corrections were required, and the entry sequence was normal. The CM landed in the Pacific Ocean at 244.5 hours. The landing coordinates, as determined from the onboard computer, were 15 degrees 47 minutes south latitude and 165 degrees 11 minutes west longitude.

APPENDIX A

ATMOSPHERE

A.1 SUMMARY

This appendix presents a summary of the atmospheric environment at launch time of the AS-507. The format of these data is similar to that presented on previous launches of Saturn vehicles to permit comparisons. Surface and upper winds, and thermodynamic data near the launch time are given.

A.2 GENERAL ATMOSPHERIC CONDITIONS AT LAUNCH TIME

A cold front was moving slowly southward through the central section of Florida and was near the pad at launch time. This cold front produced the rain showers and overcast conditions that existed over the pad at launch time.

Discussion of the atmospheric electrical discharge to the AS-507 Apollo-Saturn vehicle is included in the general discussion of the lightning phenomena in Section 12A.

A.3 SURFACE OBSERVATIONS AT LAUNCH TIME

At launch time clouds were 10/10 stratocumulus with bases estimated at 0.6 kilometer (2100 ft). Cloud tops were observed by aircraft before launch to be 5.8 to 6.1 kilometers (19,000 to 20,000 ft) altitude. No solar radiation data is available to present here due to overcast conditions. Surface observations at launch time are summarized in Table A-1.

A.4 UPPER AIR MEASUREMENTS

Data were used from three of the upper air wind systems to compile the final meteorological tape. Table A-2 summarizes the data systems used.

A.4.1 Wind Speed

The wind speed was 6.8 m/s (13.3 knots) at the surface, and increased to a peak of 47.6 m/s (92.5 knots) at 14.23 kilometers (46,570 ft). The wind speed then decreased to 4.9 m/s (9.5 knots) at 23.38 kilometers (76,690 ft). Above this altitude the wind speed continued to increase again as shown in Figure A-1.

Table A-1. Surface Observations at AS-507 Launch Time

LOCATION	TIME AFTER T-0 (MIN)	PRESSURE N/CM² (PSIA)	TEMPERATURE °K (°F)	DEW POINT °K (°F)	VISIBILITY KM (STAT MI)	AMOUNT (TENTHS)	SKY COVER TYPE	HEIGHT OF BASE METERS (FEET)	WIND SPEED M/S (KNOTS)	WIND DIR (DEG)
Kennedy Space Center, Florida	0	10.081 (14.62)	293.2 (68.0)	291.5 (65.0)	6 (4)	10	Strato-cumulus	640- (2100)-	2.6 (5.0)	230
Cape Kennedy Rawinsonde Measurements*										
Pad 39A Lightpole SE 18.3 m (60.0 ft)**	0	--	--	--	--	--	--	--	6.8 (13.3)	280

*No values given here due to the fact that rawinsonde data was obtained at 312 minutes.
**Above natural grade.
-Estimated.

Table A-2. Systems Used to Measure Upper Air Wind Data for AS-507

TYPE OF DATA	RELEASE TIME		PORTION OF DATA USED			
			START		END	
	TIME (UT)	TIME AFTER T-0 (MIN)	ALTITUDE M (FT)	TIME AFTER T-0 (MIN)	ALTITUDE M (FT)	TIME AFTER T-0 (MIN)
FPS-16 Jimsphere	1650	28	0	28	14,975 (49,130)	78
Rawinsonde	2045	263	15,000 (49,215)	312	25,000 (82,020)	345
Loki Dart	1808	106	54,750 (179,625)	106	25,250 (82,840)	127

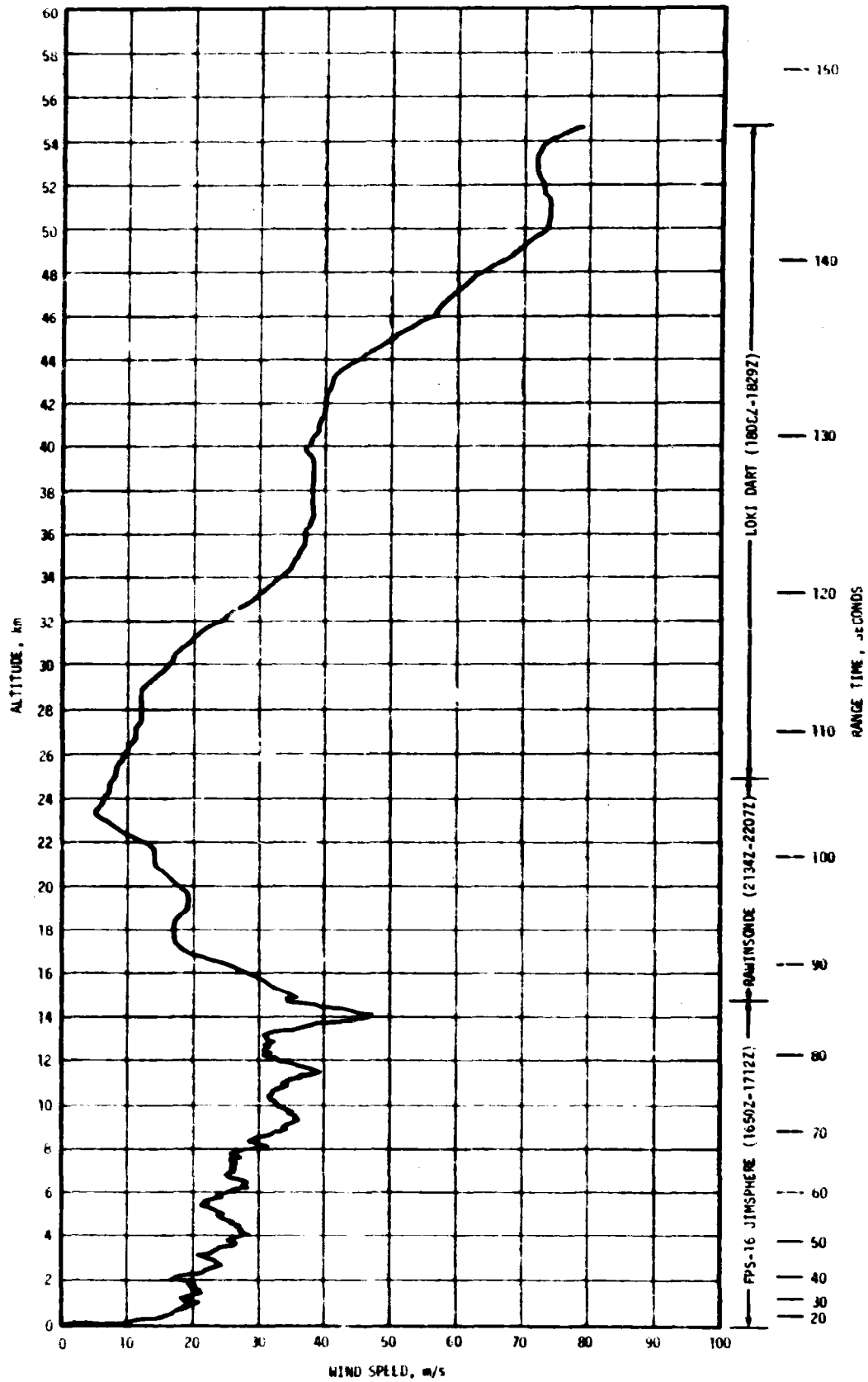

Figure A-1. Scalar Wind Speed at Launch Time of AS-507

A.4.2 Wind Direction

At launch time the surface wind direction was from the west and stayed approximately westerly with altitude as shown in Figure A-2. The surface wind speed and surface wind direction values, shown in Figures A-1 and A-2, disagree with the surface values due to the fact that the cold front had not yet passed the FPS-16 jimsphere release station at release time.

A.4.3 Pitch Wind Component

The surface pitch wind speed component was a tail wind of 3.8 m/s (7.4 knots). A maximum tail wind of 47.2 m/s (91.7 knots) was observed at 14.23 kilometers (46,670 ft) altitude. See Figure A-3.

A.4.4 Yaw Wind Component

The yaw wind speed component at the surface was a wind from the right of 5.9 m/s (11.4 knots). The peak yaw wind speed was a wind from the right of 19.5 m/s (37.9 knots) at 13.65 kilometers (44,780 ft) altitude. See Figure A-4.

A.4.5 Component Wind Shears

The largest component wind shear (Δh = 1000 m) in the altitude range of 8 to 16 kilometers (26,247 to 52,493 ft) was a pitch shear of 0.0183 sec^{-1} at 14.3 kilometers (46,750 ft). The largest yaw wind shear, in the lower levels, was 0.0178 sec^{-1} at 14.6 kilometers (47,820 ft). See Figure A-5.

A.4.6 Extreme Wind Data in the High Dynamic Region

A summary of the maximum wind speeds and wind components is given in Table A-3. A summary of the extreme wind shear values is given in Table A-4.

A.5 THERMODYNAMIC DATA

Comparisons of the thermodynamic data taken at AS-507 launch time with the Patrick Reference Atmosphere, 1963 (PRA-63) for temperature, density, pressure, and Optical Index of Refraction are shown in Figures A-6 and A-7 and discussed in the following paragraphs.

A.5.1 Temperature

Atmospheric temperature deviations were small, being less than 5 percent deviation from the PRA-63. From the surface up to 14.8 kilometers (48,560 ft) the air temperature was colder than the PRA-63. Above this altitude the temperature at most levels was warmer than the PRA-63. See Figure A-6.

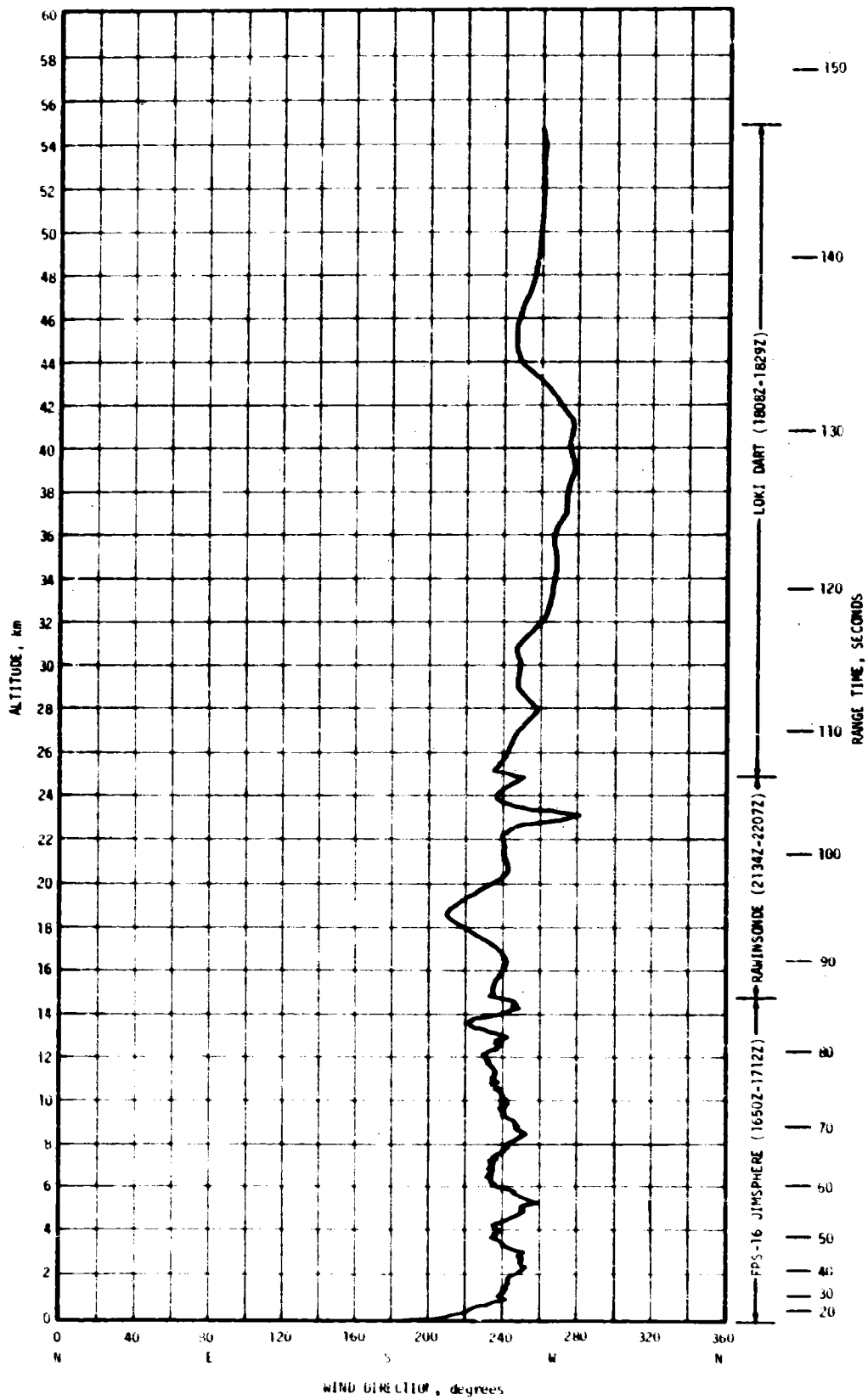

Figure A-2. Wind Direction at Launch Time of AS-507

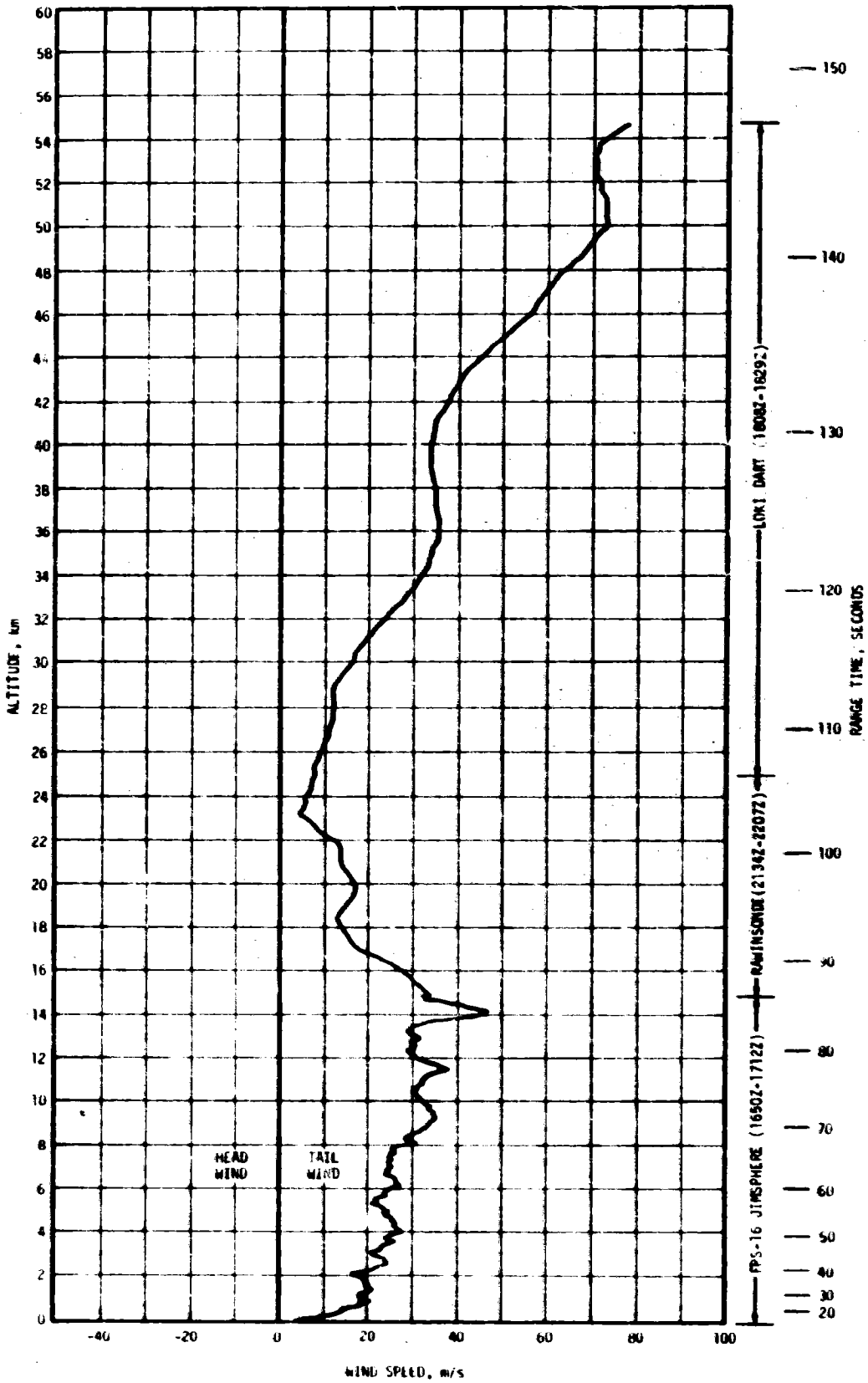

Figure A-3. Pitch Wind Speed Component (W_X) at Launch Time of AS-507

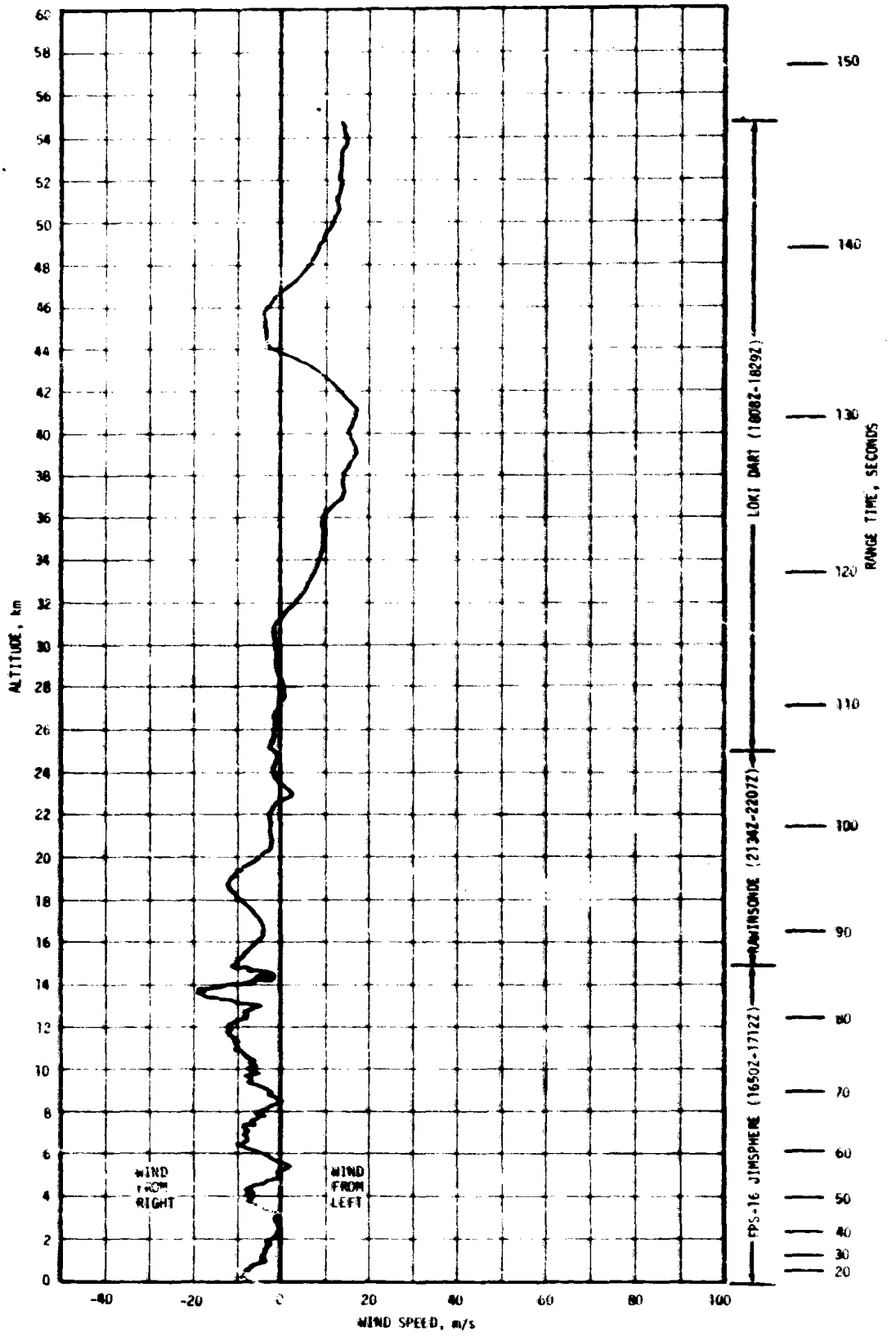

Figure A-4. Yaw Wind Speed Component (W_z) at Launch Time of AS-507

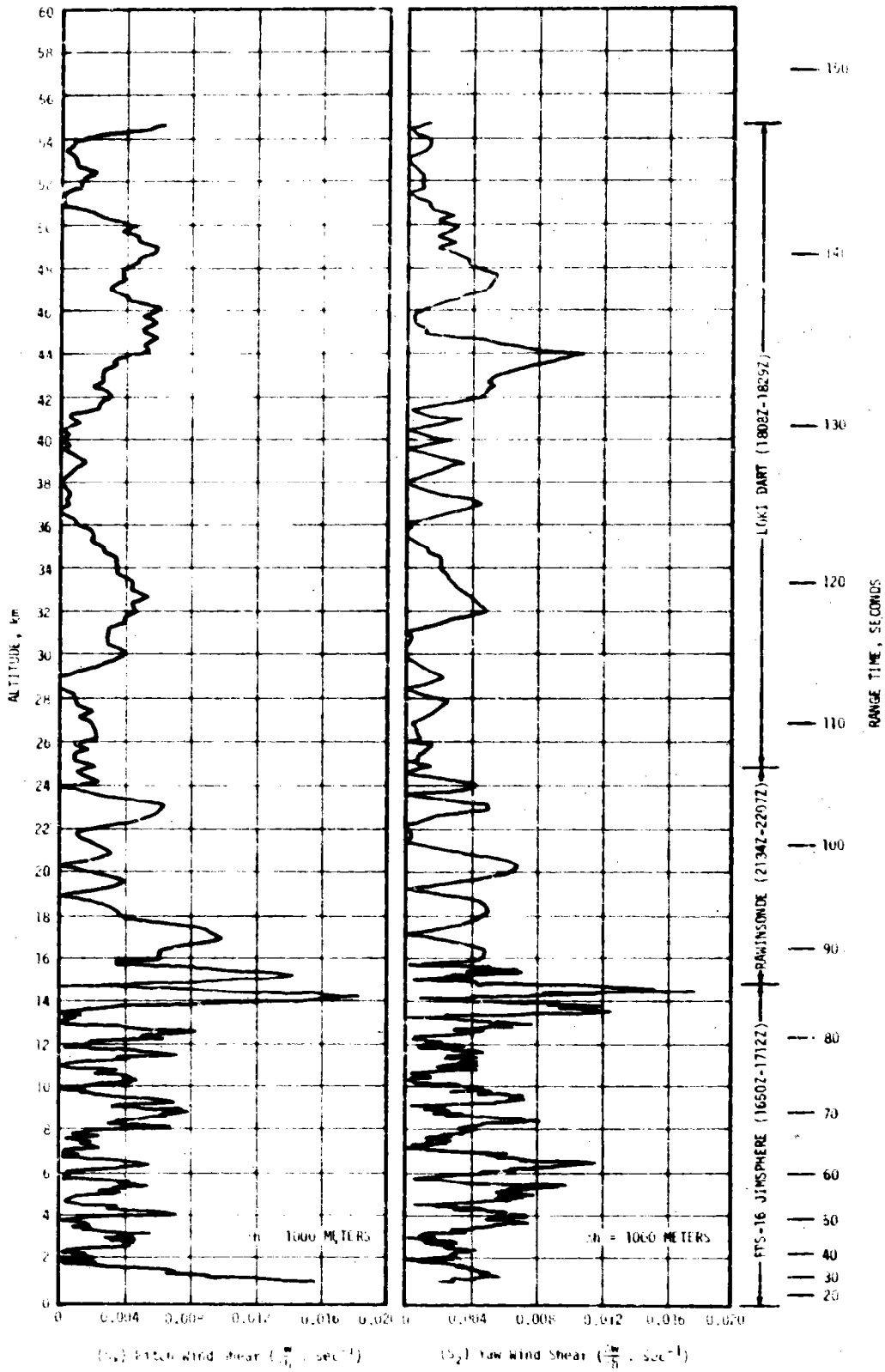

Figure A-5. Pitch (S_X) and Yaw (S_Z) Component Wind Shears At Launch Time of AS-507

Table A-3. Maximum Wind Speed in High Dynamic Pressure Region for Apollo/Saturn 501 through Apollo/Saturn 507 Vehicles

VEHICLE NUMBER	MAXIMUM WIND			MAXIMUM WIND COMPONENTS			
	SPEED M/S (KNOTS)	DIR (DEG)	ALT KM (FT)	PITCH (W_X) M/S (KNOTS)	ALT KM (FT)	YAW (W_Z) M/S (KNOTS)	ALT KM (FT)
AS-501	26.0 (50.5)	273	11.50 (37,700)	24.3 (47.2)	11.50 (37,700)	12.9 (25.1)	9.00 (29,500)
AS-502	27.1 (52.7)	255	12.00 (42,600)	27.1 (52.7)	12.00 (42,600)	12.9 (25.1)	15.75 (51,700)
AS-503	34.8 (67.6)	284	15.22 (49,900)	31.2 (60.6)	15.10 (49,500)	22.6 (43.9)	15.80 (51,800)
AS-504	76.2 (148.1)	264	11.73 (38,480)	74.5 (144.8)	11.70 (38,390)	21.7 (42.2)	11.43 (37,500)
AS-505	42.5 (82.6)	270	14.18 (46,520)	40.8 (79.3)	13.80 (45,280)	18.7 (36.3)	14.85 (48,720)
AS-506	9.6 (18.7)	297	11.40 (37,400)	7.6 (14.8)	11.18 (36,680)	7.1 (13.8)	12.05 (39,530)
AS-507	47.6 (92.5)	245	14.23 (46,670)	47.2 (91.7)	14.23 (46,670)	19.5 (37.9)	13.65 (44,780)

A.5.2 Atmospheric Density

Positive atmospheric density deviations were small, being less than 3 percent of the PRA-63 for all altitudes. The largest negative deviation of density was -8.4 percent at 17.0 kilometers (55,770 ft) altitude. See Figure A-6.

A.5.3 Atmospheric Pressure

Atmospheric pressure deviations were less than 6 percent from the PRA-63 pressure values at all altitudes as shown in Figure A-7.

A.5.4 Optical Index of Refraction

At the surface, the Optical Index of Refraction was 5.5×10^{-6} units lower than the corresponding value of the PRA-63. The deviation became less negative with altitude, becoming a maximum positive deviation of 1.1×10^{-6} units greater than the corresponding value of the PRA-63 at 10.5 kilometers (34,450 ft). Above this altitude the Optical Index of Refraction was less than the corresponding PRA-63 value and then it approximates the PRA-63 at high altitudes. See Figure A-7.

Table A-4. Extreme Wind Shear Values in the High Dynamic Pressure Region for Apollo/Saturn 501 through Apollo/Saturn 507 Vehicles

(Δh = 1000 m)				
VEHICLE NUMBER	PITCH PLANE		YAW PLANE	
	SHEAR (SEC^{-1})	ALTITUDE KM (FT)	SHEAR (SEC^{-1})	ALTITUDE KM (FT)
AS-501	0.0066	10.00 (32,800)	0.0067	10.00 (32,800)
AS-502	0.0125	14.90 (48,900)	0.0084	13.28 (43,500)
AS-503	0.0103	16.00 (52,500)	0.0157	15.78 (51,800)
AS-504	0.0248	15.15 (49,700)	0.0254	14.68 (48,160)
AS-505	0.0203	15.30 (50,200)	0.0125	15.53 (50,950)
AS-506	0.0077	14.78 (48,490)	0.0056	10.30 (33,790)
AS-507	0.0183	14.25 (46,750)	0.0178	14.58 (47,820)

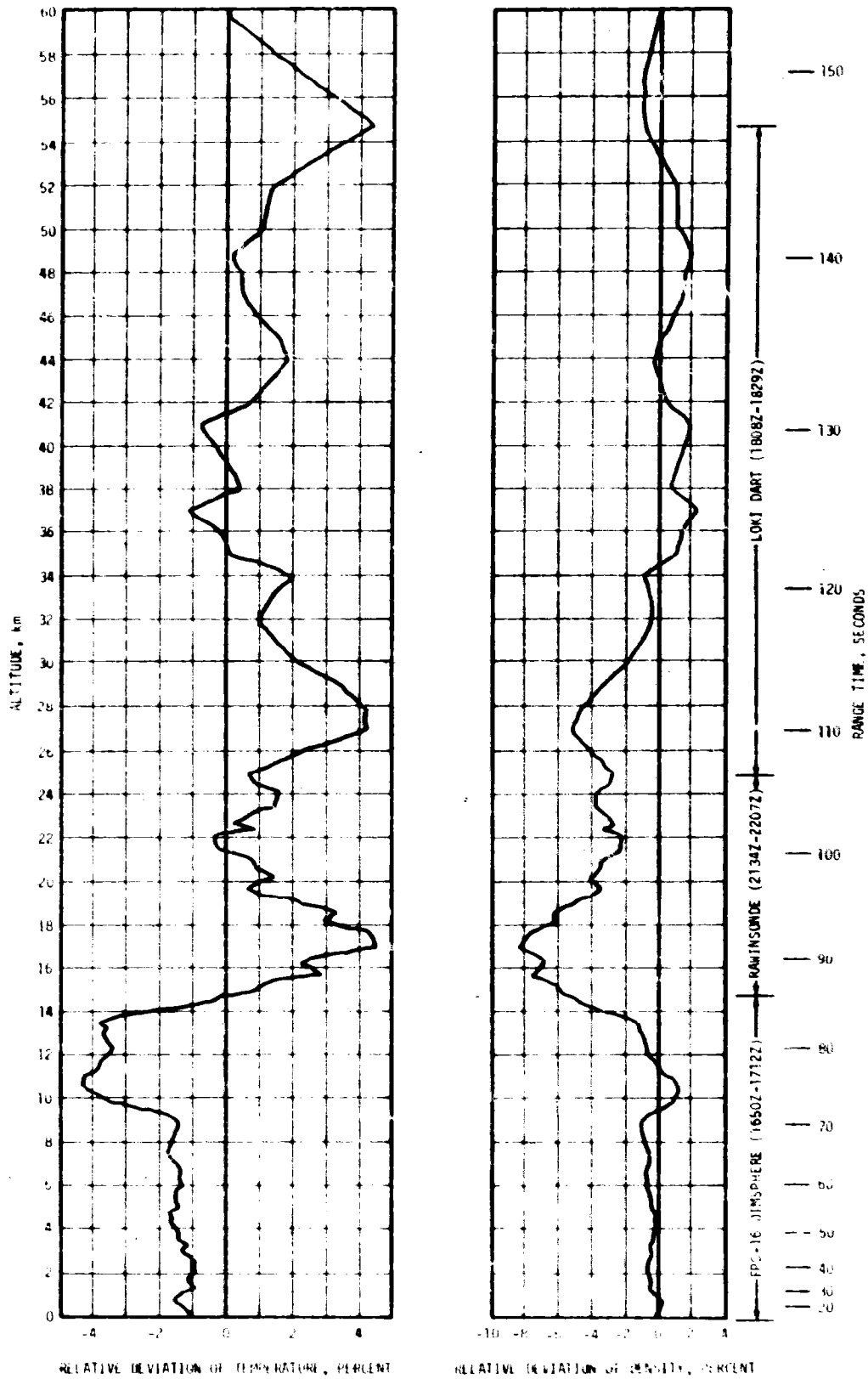

Figure A-6. Relative Deviation of Temperature and Density From the PRA-63 Reference Atmosphere, AS-507

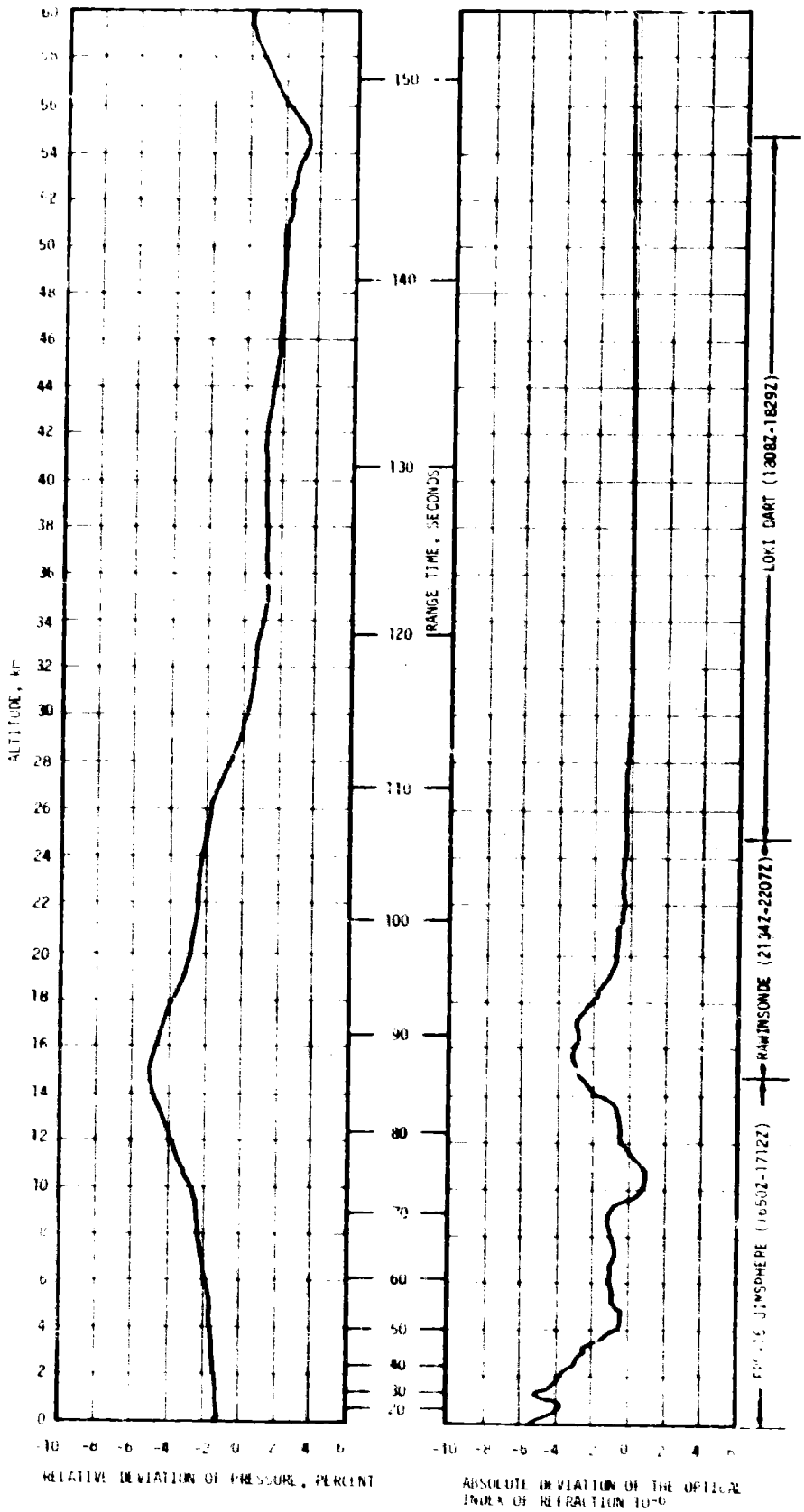

Figure A-7. Relative Deviation of Pressure and Absolute Deviation of the Index of Refraction From the PRA-63 Reference Atmosphere, AS-507

A.6 COMPARISON OF SELECTED ATMOSPHERIC DATA FOR SATURN V LAUNCHES

A summary of the atmospheric data for each Saturn V launch is shown in Table A-5.

Table A-5. Selected Atmospheric Observations for Apollo/Saturn 501 Through Apollo/Saturn 507 Vehicle Launches at Kennedy Space Center, Florida

VEHICLE NUMBER	VEHICLE DATA			SURFACE DATA						INFLIGHT CONDITIONS		
	DATE	TIME NEAREST MINUTE	LAUNCH COMPLEX	PRESSURE N/CM²	TEMPERATURE °C	RELATIVE HUMIDITY PERCENT	WIND* SPEED M/S	WIND* DIRECTION DEG	CLOUDS	MAXIMUM WIND IN 8-16 KM LAYER ALTITUDE KM	MAXIMUM WIND IN 8-16 KM LAYER SPEED M/S	MAXIMUM WIND IN 8-16 KM LAYER DIRECTION DEG
AS-501	9 Nov 67	0702 EST	39A	10.261	17.6	55	8.9	70	1/10 cumulus	11.50	26.0	273
AS-502	4 Apr 68	0600 EST	39A	10.200	20.9	83	5.4	132	5/10 stratocumulus, 1/10 cirrus	13.00	27.1	255
AS-503	21 Dec 68	0751 EST	39A	10.207	15.0	88	1.0	360	4/10 cirrus	10.22	34.8	284
AS-504	3 Mar 69	1100 EST	39A	10.095	19.6	61	6.9	160	7/10 stratocumulus, 10/10 altostratus	11.73	76.2	264
AS-505	18 May 69	1249 EDT	39B	10.190	26.7	75	8.2	125	4/10 cumulus, 2/10 altocumulus, 10/10 cirrus	14.18	42.5	270
AS-5	16 Jul 69	0932 EDT	39A	10.203	29.4	75	3.3	175	1/10 cumulus, 2/10 altocumulus, 9/10 cirrostratus	11.40	9.6	297
AS-507	14 Nov 69	1122 EST	39A	10.081	23.0	92	6.8	280	10/10 stratocumulus with rain	14.23	47.6	285

*Instantaneous readings from charts at T-0 from anemometers on launch pad at 10.1 m (60.0 ft) on launch complex 39 (A&B). Heights of anemometers are above natural grade.

APPENDIX B

AS-507 SIGNIFICANT CONFIGURATION CHANGES

B.1 INTRODUCTION

AS-507, seventh flight of the Saturn V series, was the fifth manned Apollo Saturn V vehicle. The AS-507 launch vehicle configuration was essentially the same as the AS-506 with significant exceptions shown in Tables B-1 through B-3. (There were no significant configuration changes on the S-IC stage.) The basic AS-507 Apollo 12 spacecraft structure and components were unchanged from the AS-504 Apollo 9 configuration except Lunar Module (LM) crew provisions were accompanied by portable life support systems and associated controls required to accommodate extra vehicular surface activity, similar to AS-506, Apollo 11. The basic vehicle description is presented in Appendix B of the Saturn V Launch Vehicle Flight Evaluation Report AS-504, Apollo 9 Mission, MPR-SAT-FE-69-4.

Table B-1. S-II Significant Configuration Changes

SYSTEM	CHANGE	REASON
Structure	Change in J-2 engine pre-cant angle from 2.3 degrees to 1.3 degrees.	To reduce the thrust cone heating rate during the interstage-on portion of flight by 25 percent thereby allowing the mission to continue to S-II stage propellant depletion in the event of an actuator failure hardover-outboard occurring either prior to or after S-II stage/interstage separation (i.e., eliminates flight mission rule 6-8A).
Propellant Utilization	Addition of parallel wire to PU computer.	To supply rated voltage at computer interface under all stage bus normal limits.
Instrumentation	Addition of three new pressure measurements, three new vibration measurements, and re-channelization of three pressure measurements.	To provide data for evaluation of low frequency oscillations at end of S-II boost period.
Launch Vehicle Ground Support Equipment (LVGSE)	Change S7-41 start tank pressurizing regulator range setting from 1175 ±15 psia to 1225 ±25 psia.	To provide greater margin for Ground Support Equipment (GSE) to satisfy liftoff redlines.

Table B-2. S-IVB Significant Configuration Changes

SYSTEM	CHANGE	REASON
Instrumentation	Added one SS/FM link. Added 12 acoustic, 5 vibration and 2 miscellaneous measurements.	To better define the low frequency vibration which occurred on AS-505 and to investigate the acoustic environment on the S-II/S-IVB interstage below the protruding APS module.

Table B-3. IU Significant Configuration Changes

SYSTEM	CHANGE	REASON
Environmental Control	The preflight air/GN_2 purge duct was modified at locations 19 and 23. Ducting, brackets, and nozzles similar to those used on S-IU-505 were installed on S-IU-507.	Additional ducts were routed to the Radio Isotope Thermo-Electrical Generator (RTG) fuel cask located in the LM descent stage to provide preflight cooling.
	The MFCV will be driven to zero bypass prior to liftoff.	Increase ECS reliability by driving Modulating Flow Control Valve (MFCV) to zero bypass prior to going into the flight mode.
	Thermal switch settings for S-IU-507 Environmental Control System (ECS). Open: 59.6°F Close: 60.3°F	These settings determined from preflight test data.
	Second source ECS pump will be flown as primary on S-IU-507.	This pump is being flown as part of its flight qualification program.
Instrumentation and Communications	New design Command and Communications System (CCS) coaxial switch flown on S-IU-507.	The switches flown on S-IU-501 through S-IU-506 were subject to failure if the switch lost internal pressure. Failures occurred on S-IU-505 and S-IU-506 resulting in loss of CCS downlink.
	Two S-IVB vibration measurements added to the DF-1 telemetry link. Added Measurements: E99-411 Bending Mode Vibration, Pitch Forward E100-411 Bending Mode Vibration, Yaw Forward	Added to monitor low frequency structural vibrations.

Table B-3. IU Significant Configuration Changes (Continued)

SYSTEM	CHANGE	REASON
Networks	Additional cables and modifications to the measuring distributor and DF-1 TM assembly.	Modifications were required to add two S-IVB vibration measurements to the DF-1 telemetry system.
	Cable modified to interchange INT 2 and DIN 17 functions.	Provide an interrupt to the LVDA indicating spacecraft commanded S-IVB ECO and a discrete input for S-IC center engine out A.
	Coolant pump filter not in IU networks on S-IU-507.	Second-source (vendor) coolant pump has an internal filter.
Special Equipment	Four underwater location devices added to the IU.	These are self contained devices attached to IU cold-plates to assist in locating the LM RTG fuel cask in the event of an over the water abort.
Flight Programs	First generalized flight program to be flown.	Facilitates easier program modification and promotes economical utilization of LVDC core memory.
	S-II two engine out detection capability.	Prior to this, only one S-II engine out could be detected by the program.

APPROVAL

SATURN V LAUNCH VEHICLE FLIGHT EVALUATION REPORT

AS-507, APOLLO 12 MISSION

By Saturn Flight Evaluation Working Group

The information in this report has been reviewed for security classification. Review of any information concerning Department of Defense or Atomic Energy Commission programs has been made by the MSFC Security Classification Officer. The highest classification has been determined to be unclassified.

Stanley L. Fragge
Security Classification Officer

This report has been reviewed and approved for technical accuracy.

George H. McKay, Jr.
Chairman, Saturn Flight Evaluation Working Group

Herman K. Weidner
Director, Science and Engineering

Roy E. Godfrey
Saturn Program Manager

DISTRIBUTION

MSFC:

Dr. Von Braun, DIR
Mr. Foster, DIR
Dr. Rees, DEP-T
Mr. Cook, DEP-M
Dr. Stuhlinger, AD-S

E

Mr. Maus, E-DIR
Mr. Smith, E-S

PA

Mr. Slattery, PA-DIR

PD

Dr. Lucas, PD-DIR
Mr. Williams, PD-DIR (2)
Mr. Mrazek, PD-DIR
Mr. Thomason, PD-DO-DIR
Mr. Goerner, PD-DO-DIR
Mr. Nicaise, PD-DO
Mr. Jean, PD-RV
Mr. Digesu, PD-DO-E
Mr. Palaoro, PD-SS
Mr. Blumrich, PD-DO-SL

PM

Mr. L. James, PM-DIR
Mr. Andressen, PM-PR-MGR
Mr. Huff, PM-SAT-E
Dr. Speer, PM-MO-MGR (4)
Mr. Belew, PM-AA-MGR
Mr. Braun, PM-EP-MGR
Mr. Smith, PM-EP-J
Mr. Norman, PM-MO
Mr. Boffola, PM-EP-F
Mr. Godfrey, PM-SAT-MGR
Mr. R. Smith, PM-SAT-MGR
Mr. Burns, PM-SAT-T
Mr. Bell, PM-SAT-E
Mr. Moody, PM-SAT-Q
Mr. Webb, PM-SAT-P
Mr. Urlaub, PM-SAT-S-IB/S-IC
Mr. Lahatte, PM-SAT-S-II
Mr. Meyers, PM-SAT-S-IVB
Mr. Duerr, PM-SAT-IU
Mr. Smith, PM-SAT-G
Col. Montgomery, PM-KM
Mr. Peters, PM-SAT-S-IVB
Mr. Weir, PM-SAT-IU
Mr. Ferrell, PM-EP-EJ
Mr. Stamy, PM-MA-MGR
Mr. Riemer, PM-MA-QP
Mr. Balch, PM-MT-MGR
Mr. Auter, PM-MT-T
Mr. Sparks, PM-SAT-G
Mr. Haley, PM-SAT-S-IB/S-IC
Mr. Higgins, PM-SAT-S-IVB
Mr. Odom, PM-SAT-S-II
Mr. Stover, PM-SAT-S-II
Mr. Reaves, PM-SAT-Q
Mr. Wheeler, PM-EP-F
Mr. Johnson, PM-SAT-T
Mr. Cushman, PM-SAT-T (10)
Mr. Marchese, PM-MA-QR

S&E

Mr. Weidner, S&E-DIR
Mr. Richard, S&E-DIR
Dr. Johnson, S&E-R
Mr. Hamilton, MSC-RL

S&E-AERO

Dr. Geissler, S&E-AERO-DIR
Mr. Horn, S&E-AERO-DIR
Mr. Dahm, S&E-AERO-A (2)
Mr. Holderer, S&E-AERO-A
Mr. Dunn, S&E-AERO-ADV
Mr. Elkin, S&E-AERO-AT
Mr. Wilson, S&E-AERO-AT
Mr. Jones, S&E-AERO-AT
Mr. Reed, S&E-AERO-AC
Mr. Guest, S&E-AERO-AL
Mr. Ryan, S&E-AERO-DO
Mr. Cremin, S&E-AERO-M
Mr. Lindberg, S&E-AERO-M (16)
Mr. Baker, S&E-AERO-G
Mr. Jackson, S&E-AERO-P
Mr. Cummings, S&E-AERO-T
Mr. O. E. Smith, S&E-AERO-Y
Mr. J. Sims, S&E-AERO-P
Dr. Lovingood, S&E-AERO-D
Mr. Vaughan, S&E-AERO-Y

S&E-CSE

Dr. Haeussermann, S&E-CSE-DIR
Mr. Hoberg, S&E-CSE-DIR
Mr. Mack, S&E-CSE-DIR
Dr. McDonough, S&E-CSE-A
Mr. Aberg, S&E-CSE-S
Mr. Fichtner, S&E-CSE-G
Mr. Vann, S&E-CSE-GA
Mr. Hammers, S&E-CSE-I
Mr. Wolfe, S&E-CSE-I
Mr. E. May, S&E-CSE-L
Mr. McKay, S&E-CSE-LF
Mr. R. L. Smith, S&E-CSE-V
Mr. Brooks, S&E-CSE-V
Mr. Hagood, S&E-CSE-M (3)

S&E-ASTR

Mr. Moore, S&E-ASTR-DIR
Mr. Stroud, S&E-ASTR-SC
Mr. Robinson, S&E-P-ATM (4487)
Mr. Dale, S&E-ASTR-SCC
Mr. Erickson, S&E-ASTR-SE
Mr. Darden, S&E-ASTR-SBC
Mr. Justice, S&E-ASTR-SDA
Mr. Vallely, S&E-ASTR-SDC
Mr. George, S&E-ASTR-SDI
Mr. Jones, S&E-ASTR-SI
Mr. Mandel, S&E-ASTR-G
Mr. Ferrell, S&E-ASTR-GS
Mr. Powell, S&E-ASTR-I
Mr. Boehm, S&E-ASTR-M
Mr. Laminack, S&E-ASTR-GMF
Mr. Taylor, S&E-ASTR-R

S&E COMP

Dr. Hoelzer, S&E-COMP-DIR
Mr. Prince, S&E-COMP-DIR
Mr. Fortenberry, S&E-COMP-A
Mr. Cochran, S&E-COMP-R
Mr. Houston, S&E-COMP-RR
Mr. Craft, S&E-COMP-RR

S&E-ME

Mr. Siebel, S&E-ME-DIR
Mr. Muenscher, S&E-ME-DIR
Mr. Orr, S&E-ME-A
Mr. Franklin, S&E-ME-T

S&E-ASTN

Mr. Heimburg, S&E-ASTN-DIR
Mr. Kingsbury, S&E-ASTN-DIR
Mr. Hellebrand, S&E-ASTN-DIR
Mr. Edwards, S&E-ASTN-DIR
Mr. Sterett, S&E-ASTN-A
Mr. Schwinghamer, S&E-ASTN-M
Mr. Earle, S&E-ASTN-P
Mr. Reilmann, S&E-ASTN-P
Mr. Thompson, S&E-ASTN-E
Mr. Fuhrmann, S&E-ASTN-EM
Mr. Cobb, S&E-ASTN-PP (2)
Mr. Black, S&E-ASTN-PPE
Mr. Wood, S&E-ASTN-P
Mr. Hunt, S&E-ASTN-A
Mr. Beam, S&E-ASTN-AD
Mr. Riquelmy, S&E-ASTN-SDF
Mr. Katz, S&E-ASTN-SER
Mr. Showers, S&E-ASTN-SL
Mr. Frederick, S&E-ASTN-SS
Mr. Furman, S&E-ASTN-AA
Mr. Green, S&E-ASTN-SVM
Mr. Grafton, S&E-ASTN-T
Mr. Lutonsky, S&E-ASTN-VAH
Mr. Devenish, S&E-ASTN-VMP (2)
Mr. Sells, S&E-ASTN-VDD
Mr. Schulze, S&E-ASTN-V (2)
Mr. Rothe, S&E-ASTN-XA
Mr. Griner, S&E-ASTN-KSJ
Mr. Boone, S&E-ASTN-KEK

S&E-QUAL

Mr. Grau, S&E-QUAL-DIR
Mr. Chandler, S&E-QUAL-DIR
Mr. Henritze, S&E-QUAL-A
Mr. Rushing, S&E-QUAL-PI
Mr. Klauss, S&E-QUAL-J
Mr. Hughes, S&E-QUAL-P
Mr. Landers, S&E-QUAL-PC (3)
Mr. Peck, S&E-QUAL-F
Mr. Brien, S&E-QUAL-Q
Mr. Wiltmann, S&E-QUAL-T
Mr. Davis, S&E-QUAL-F

S&E-SSL

Mr. Heller, S&E-SSL-DIR
Mr. Sieber, S&E-SSL-S

MS

MS-H
MS-I
MS-IP
MS-IL (8)
MS-D (2)

CC-P

Mr. Hofford, CC-P

KSC

Dr. Debus, CD
Dr. Gruene, LV
Mr. Rigell, LV-ENG
Mr. Sendler, IN
Mr. Mathews, AP
Dr. Knothe, EX-SCI
Mr. Edwards, LV-INS
Mr. Fannin, LV-MEC
Mr. Youmans, LV-ORD-3
Mr. Pickett, LV-TMD
Mr. Rainwater, LV-TMD
Mr. Bell, LV-TMD-3
Mr. Lealman, LV-GDC
Mr. Preston, DE
Mr. Mizell, LV-PLN-12
Mr. O'Hara, LV-TMD
Mr. Braam, AP-SVO-3
Mr. Smith, AP-SVO

EXTERNAL

Headquarters, National Aeronautics & Space Administration
Washington, D. C. 20546

Mr. Mathews, M
Dr. Petrone, MA
Gen. Stevenson, MO (3 copies)
Mr. Schneider, MO-2
Capt. Freitag, MC
Capt. Holcomb, MAO
Mr. White, MAR (2 copies)
Mr. King, MAT (10 copies)
Mr. Watkinson, MAR
Mr. Seabat, MAP
Mr. Wagner, MAS (2 copies)
Mr. Anderson, MR
Mr. Mathews, MT (3 copies)
Mr. [illegible], MT
Mr. [illegible], MY

Director, Ames Research Center: Dr. H. Julian Allen
National Aeronautics & Space Administration
Moffett Field, California 94035

Director, Flight Research Center: Paul F. Bikle
National Aeronautics & Space Administration
P. O. Box 273
Edwards, California 93523

Goddard Space Flight Center
National Aeronautics & Space Administration
Greenbelt, Maryland 20771
Attn: Herman LaGow, Code 300

John F. Kennedy Space Center
National Aeronautics & Space Administration
Kennedy Space Center, Florida 32899
Attn: Technical Library, Code RT-42
Mrs. L. B. Russell

Director, Langley Research Center: Dr. Floyd L. Thompson
National Aeronautics & Space Administration
Langley Station
Hampton, Virginia 23365

Lewis Research Center
National Aeronautics & Space Administration
21000 Brookpark Road
Cleveland, Ohio 44135
Attn: Dr. Abe Silverstein, Director
Robert Washko, Mail Stop 86-1
E. F. Jonash, Centaur Project Mgr.

Manned Spacecraft Center
National Aeronautics & Space Administration
Houston, Texas 77058
Attn: Director, Dr. Robert R. Gilruth, AA
Mr. McDivitt, PA
Mr. Arabian, ASPO-PT (15 copies)
Mr. Paules, PC-5
J. Hamilton, PF (MSFC Resident Office)
G. F. Prude, CF-33 (3 copies)

Director, Wallops Station: R. L. Krieger
National Aeronautics & Space Administration
Wallops Island, Virginia 23337

Director, Western Operations Office: Robert W. Kamm
National Aeronautics & Space Administration
150 Pico Blvd.
Santa Monica, California 90406

Scientific and Technical Information Facility
P. O. Box 5700
Bethesda, Maryland 20014
Attn: NASA Representative (S-AK/RKT) (25 copies)

Jet Propulsion Laboratory
4800 Oak Grove Drive
Pasadena, California 91103
Attn: Irl Newlan, Reports Group (Mail 111-122)
H. Levy, TCMIA (Mail 179-203) (4 copies)

Office of the Asst. Sec. of Defense for Research and Engineering
Room 3E1065
The Pentagon
Washington, D. C. 20301
Attn: Tech Library

Director of Guided Missiles
Office of the Secretary of Defense
Room 3E131
The Pentagon
Washington, D. C. 20301

Central Intelligence Agency
Washington, D. C. 20505
Attn: OCR/DD/Publications (5 copies)

Director, National Security Agency
Ft. George Meed, Maryland 20755
Attn: C3/TDL

U. S. Atomic Energy Commission, Sandia Corp.
University of California Radiation Lab.
Technical Information Division
P. O. Box 808
Livermore, California 4551
Attn: Clovis Craig

U. S. Atomic Energy Commission, Sandia Corp.
Livermore Br, P. O. Box 969
Livermore, California 94551
Attn: Tech Library

Commander, Armed Services Technical Inf. Agency
Arlington Hall Station
Arlington, Virginia 22212
Attn: TIPCR (Transmittal per Cognizant Act Security Instruction) (5 copies)

Commanding General
White Sands Missile Range,
New Mexico 88002
Attn: RE-L (3 copies)

Chief of Staff, U. S. Air Force
The Pentagon
Washington, D. C. 20330
1 Cpy marked for DCS/D AFDRD
1 Cpy marked for DCS/D AFDRD-EK

Headquarters SAC (DPLBS)
Offutt AFB, Nebraska 68113

Commander
Arnold Engineering Development Center
Arnold Air Force Station, Tennessee 37389
Attn: Tech Library (2 copies)

Commander
Air Force Flight Test Center
Edwards AFB, California 93523
Attn: FTOTL

Commander
Air Force Missile Development Center
Holloman Air Force Base
New Mexico 88330
Attn: Tech Library (SRLT)

Headquarters
6570th Aerospace Medical Division (AFSC)
U. S. Air Force
Wright-Patterson Air Force Base, Ohio 45433
Attn: H. E. Wonjerke

Systems Engineering Group (RTD)
Attn: SEPIR
Wright-Patterson, AFB, Ohio 45433

AFETR (ETLLG-1)
Patrick AFB, Florida 32925

EXTERNAL (CONT.)

Director
U. S. Naval Research Laboratory
Washington, D. C. 20390
Attn: Code 2027

Chief of Naval Research
Department of Navy
Washington, D. C. 20390
Attn: Code 463

Chief, Bureau of Weapons
Department of Navy
Washington, D. C. 20390
1 Cpy to RESI, 1 Cpy to SP,
1 Cpy to AD3, 1 Cpy to RUW3

Commander
U. S. Naval Air Missile Test Center
Point Mugu, California 93041

AMSMI-RSLD, RSIC (3 copies)
Bldg. 4484
Redstone Arsenal, Alabama 35809

Aerospace Corporation
Reliability Dept.
P. O. Box 95085
Los Angeles, California 90045
Attn: Don Herzstein

Bellcomm, Inc.
1100 Seventeenth St. N. W.
Washington, D. C. 20036
Attn: Miss Scott, Librarian

The Boeing Company
P. O. Box 1680
Huntsville, Alabama 35807
Attn: S. C. Krausse, Mail Stop AD-60
(20 copies)
F. B. Williams, Mail Stop JA-51
(1 copy)

The Boeing Company
P.O. Box 58747
Houston, Texas 77058
Attn: H. J. McClellan, Mail Stop HH-05
(2 copies)

The Boeing Company
P. O. Box 29100
New Orleans, Louisiana 70129
Attn: F. R. Malthesen, Mail Stop LS-05
(10 copies)

Mr. Norman Sissenwine, CREW
Chief, Design Climatology Branch
Aerospace Instrumentation Laboratory
Air Force Cambridge Research Laboratories
L. G. Hanscom Field
Bedford, Massachusetts 01731

Lt/Col. H. P. Montague
Det. 11, 4th Weather Group
Eastern Test Range
Patrick Air Force Base, Florida 32964

Mr. W. Davidson
NASA Resident Management Office
Mail Stop 8890
Martin Marietta Corporation
Denver Division
Denver, Colorado 80201

Chrysler Corporation Space Division
Huntsville Operation
1312 N. Meridian Street
Huntsville, Alabama 35807
Attn: J. Fletcher, Dept. 4830 (2)

McDonnell Douglas Astronautics Company
Missile & Space Systems Division/SSC
5301 Bolsa Avenue
Huntington Beach, California 92646
Attn: G. J. Soldat (40 copies)

Grumman Aircraft Engineering Corp.
Bethpage, Long Island, N. Y. 11714
Attn: NASA Resident Office
John Johansen

International Business Machine
Mission Engineering Dept. F103
150 Sparkman Dr. NW
Huntsville, Alabama 35805
Attn: C. W. Hansen (15 copies)

Martin Company
Space Systems Division
Baltimore, Maryland 21203
Attn: W. P. Sommers

North American Rockwell/Space Division
12214 South Lakewood Boulevard
Downey, California 90241
Attn: D. P. Binns (35 copies)

Radio Corporation of America
Defense Electronic Products
Data Systems Division
8500 Balboa Blvd.
Van Nuys, California 91406

Rocketdyne
6633 Canoga Avenue
Canoga Park, California 91303
Attn: T. L. Johnson (10 copies)

Foreign Technology Division
FTD (TDPSL)
Wright-Patterson Air Force Base, Ohio 45433

Mr. George Mueller
Structures Division
Air Force Flight Dynamics Laboratory
Research and Technology Division
Wright-Patterson Air Force Base, Ohio 45433

Mr. David Hargis
Aerospace Corporation
Post Office Box 95085
Los Angeles, California 90045

Mr. H. B. Tolefson
DLD-Atmospheric Physics Branch
Mail Stop 240
NASA-Langley Research Center
Hampton, Virginia 23365

Mr. Chasteen
Sperry Rand
Dept. 223
Blue Spring Road
Huntsville, Ala.

EXTERNAL (CONT.)

J. L. Trader
NASA Resident Manager's Office
McDonnell Douglas Astronautics Corp.
5301 Balsa Avenue
Huntington Beach, California 92646

L. C. Curran
NASA Resident Manager's Office
North American Rockwell Space Division
12214 Lakewood Blvd.
Downey, California [illegible]

L. M. McBride
NASA Resident Manager's Office
North American Rockwell Rocketdyne
6633 Canoga Avenue
Canoga Park, California [illegible]

L. M. Norton
NASA Resident Manager's Office
International Business Machines
150 Sparkman Drive
Huntsville, Alabama [illegible]

N. G. Futral
NASA Resident Manager's Office
North American Rockwell Space Division
69 Bypass NE
McAllester, Oklahoma [illegible]

C. Flora
McDonnell Douglas Astronautics Corp.
Sacramento Test Center
11505 Douglas Avenue
Rancho Cardova, California [illegible]

W. Klaburde
Northrop
6025 Technology Drive
Huntsville, Alabama 35804

David L. Christensen
UAH, P. O. Box 1247
Huntsville, Alabama 35807

A. T. Ackerman
MAS-BELLCOM

END

DATE

FILMED

APR 1 1970